ADVANCES IN PHYSICS, 2003, VOL. 52, NO. 4, 219–342

Taylor & Francis
Taylor & Francis Group

Glassy dynamics of kinetically constrained models

F. RITORT[1] and P. SOLLICH[2*]

[1]Department of Physics, Faculty of Physics, University of Barcelona, Diagonal 647, 08028 Barcelona, Spain

[2]Department of Mathematics, King's College London, Strand, London WC2R 2LS

[Received 17 October 2002]

Abstract

We review the use of kinetically constrained models (KCMs) for the study of dynamics in glassy systems. The characteristic feature of KCMs is that they have trivial, often non-interacting, equilibrium behaviour but interesting slow dynamics due to restrictions on the allowed transitions between configurations. The basic question which KCMs ask is therefore how much glassy physics can be understood without an underlying 'equilibrium glass transition'. After a brief review of glassy phenomenology, we describe the main model classes, which include spin-facilitated (Ising) models, constrained lattice gases, models inspired by cellular structures such as soap froths, models obtained via mappings from interacting systems without constraints, and finally related models such as urn, oscillator, tiling and needle models. We then describe the broad range of techniques that have been applied to KCMs, including exact solutions, adiabatic approximations, projection and mode-coupling techniques, diagrammatic approaches and mappings to quantum systems or effective models. Finally, we give a survey of the known results for the dynamics of KCMs both in and out of equilibrium, including topics such as relaxation time divergences and dynamical transitions, nonlinear relaxation, ageing and effective temperatures, cooperativity and dynamical heterogeneities, and finally non-equilibrium stationary states generated by external driving. We conclude with a discussion of open questions and possibilities for future work.

Contents

* Author for correspondence. e-mail: peter.sollich@kcl.ac.uk

Advances in Physics ISSN 0001–8732 print/ISSN 1460–6976 online
http://www.tandf.co.uk/journals
DOI: 10.1080/0001873031000093582

1. Introduction

After many decades of research our theoretical understanding of the glass transition remains substantially incomplete. Ideally, a comprehensive theory should explain all thermodynamic and kinetic properties of glasses, both at the macroscopic and the mesoscopic level. It should also be consistent with the wealth of experimental data which has been accumulated in the past century, and to which ongoing work is continuing to add.

Theoretical approaches to the glass transition range between two extremes. At one end of the spectrum are microscopic theories, which start from first principles (e.g. Newton's equations for classical particles). To arrive at predictions that can

be compared to experiment, rather drastic mathematical approximations are then required, whose physical meaning can be difficult to assess. One of the most successful theories of this kind is the mode-coupling theory (MCT, see references at the end of this introduction), which predicts a dynamical arrest in sufficiently supercooled liquids that arises from the nonlinear interaction of density fluctuations. On the other extreme are phenomenological theories which incorporate a set of basic ingredients chosen on the grounds of physical intuition as most relevant for glass transition dynamics. Predictions are normally easier to derive from such theories, and conceptual ideas can be tested relatively directly. This flexibility is also a disadvantage, however: phenomenological theories can be difficult to disprove if they can always be extended or modified to account for new data. Among the best-known theories in this group are the free volume theories developed by Flory and Cohen, the entropic theories due to Adam, Gibbs and Di Marzio and the energy landscape approach introduced by Stillinger and Weber.

The models we discuss in this review have a character intermediate between these two extremes. Similarly to the phenomenological approaches, they use effective variables which are normally of mesoscopic character, e.g. averages of particle density over suitably small coarse-graining volumes, and are chosen on an intuitive basis as most directly responsible for glassy dynamics. On the other hand, as in the microscopic theories, a Hamiltonian (or energy function) and appropriate dynamical evolution equations are explicitly defined, and one attempts to predict the behaviour of the model on this basis, without further approximation if possible.

The above category of models is still rather rich. The basic variables can be discrete or continuous, for example, and the energy function may contain pairwise potentials or higher-order interactions. The dynamics are normally constrained only to obey detailed balance with respect to the specified energy function, and this leaves considerable freedom when defining a model. The energy function may even include quenched disorder, and it has been shown that e.g. appropriate spin-glass models can reproduce much of the phenomenology of structural glasses such as window glass. As expected, the more complicated the energy function, the more complicated also the static (equilibrium) behaviour of the resulting models; spin-glass models, for example, exhibit non-trivial ergodicity breaking transitions at low temperature.

The philosophy of the *kinetically constrained models* (KCMs) which we discuss in this review is to simplify the modelling approach further by considering models with essentially trivially equilibrium behaviour; the simplest models of this type in fact have energy functions without any interactions between the mesoscopic variables considered. In other words, KCMs ask the question: how much glassy physics can we understand without relying on non-trivial equilibrium behaviour? Instead, KCMs attempt to model glassy dynamics by introducing 'kinetic constraints' on the allowed transitions between different configurations of the system, while preserving detailed balance. (As we will see in detail below, the easiest method of implementing this is to forbid transitions between certain pairs of configurations.) Since it is now widely recognized that the glass transition is a dynamical phenomenon, such a focus on dynamics certainly makes sense. Of course, the simplicity of the energy function of KCMs means that one would not expect them to reproduce the behaviour of supercooled liquids and glasses under all conditions; instead, they should capture those aspects of their behaviour which are predominantly caused by dynamical slowing-down. One obvious aspect ignored by KCMs is crystallization: real glass-forming liquids can crystallize if cooled sufficiently slowly through the melting point.

However, it is widely believed that the existence of a crystalline phase is not crucial for the behaviour of glasses and supercooled liquids; this view is supported by the fact that spin-glass models, where the analogue of an ordered crystalline phase is suppressed through quenched disorder in the energy function, nevertheless display many features characteristic of glasses. By disregarding crystallization effects, the KCM approach therefore avoids unnecessary complications in glass modelling and focuses on the key dynamical mechanisms for glassy behaviour.

It is worth addressing already at this point another possible objection to the KCM approach. By construction, since all the 'interesting' features of KCMs arise from the dynamical rules, a relatively minor change in these rules can alter the resulting behaviour quite dramatically; we will see examples of this below in the difference between models with directed and undirected constraints. This lack of 'robustness' may appear undesirable, and contrasts with models with more complicated energy functions where the location and character of *equilibrium* phase transitions is normally unaffected by the precise dynamics chosen. However, as explained above, KCMs should be regarded as effective mesoscopic models which encode in their dynamics the complex interactions of an underlying microscopic model (see section 3.6 for simplified instances of this kind of mapping). In this view, a change in the dynamical rules corresponds to a non-trivial modification of the underlying microscopic model, e.g. by adding new interaction terms to the energy function, and it makes sense that this should have a significant effect on the resulting behaviour.

Initially introduced in the early 1980s by Fredrickson and Andersen, KCMs have recently seen a resurgence in interest. Due to their simplicity, many questions can be answered in detail, either analytically or by numerical simulation, and so KCMs form a useful testbed for our understanding of the key ingredients of glassy dynamics. We feel it is time now to gather the existing results, to analyse what we have learnt from recent work on KCMs, and to assess the successes and drawbacks of the KCM approach. The topics that we discuss will be inspired both by experimental issues surrounding the glass transition, and by theoretical questions that have wider relevance to the field of non-equilibrium statistical mechanics.

The scope of this review is as follows. The core KCMs are the spin-facilitated Ising models pioneered by Fredrickson and Andersen, and the kinetically constrained lattice gases introduced by Kob and Andersen, and Jäckle and coworkers. We have attempted to be comprehensive in our coverage of the literature on these and closely related models, up to a cutoff date around the end of 2001. Nevertheless, omissions will undoubtedly have occurred, and we apologize in advance to any colleagues whose work we may have overlooked. There is also a range of models which do not strictly speaking belong in the KCM category but which we felt were sufficiently closely related to merit inclusion. For these models we have only tried to give a representative cross-section of publications. Finally, to the vast literature in the general area of glassy dynamics we can only give a few pointers here. A summary of early experiments and theories of glasses can be found in e.g. [1–7]. The state of the art in theory and experiment as of 1995 is reviewed in a series of papers [8–12]; [13–15] give more recent accounts. Moving on to more specific topics, there are a number of reviews of MCT, e.g. [16–19], while [20] contains a good overview of the more phenomenological glass theories. For some of the earliest work on ageing [21] is a good resource; a very recent review of fluctuation–dissipation theorem violations in ageing systems can be found in [22]. Reference [23] provides an in-depth discussion

of modern theories of disordered systems and spin glasses and their relation to 'older' glass theories, and [24] gives a recent and wide-ranging overview of theoretical approaches to glassy dynamics. The topic of dynamical heterogeneities in glasses is reviewed in [25, 26]; and [27] surveys the energy landscape approach to glassy dynamics. Finally, on KCMs in particular, the reviews [20, 28, 29] provide excellent guides to work on these models done up to the end of the 1980s. The proceedings of a recent workshop on KCMs [30] complement this with surveys of current work, and we will refer below to a number of articles from this volume as useful sources of further detail.

We wrote this review with two groups of readers in mind: 'quick' readers, who may be new to the field of KCMs and want to get an overview of the most important models, results and open questions; and 'experts' who already work on aspects of KCMs but are interested in a comprehensive survey of other research in the area. Accordingly, there are two different routes through this review. Quick readers could read section 2, where we give some background on glass phenomenology and important topics in glassy dynamics; section 3, where we define the various KCMs and related models and summarize the most important results; and section 6, which contains our conclusions and an outlook towards open questions for future work. Expert readers, on the other hand, may only need to refer to section 2 to acquaint themselves with our notation, and to browse section 3 for the definitions of the models we discuss. For them, the more detailed sections that follow should be of most interest: in section 4 we review the broad range of numerical and analytical techniques that have been used to study KCMs, while section 5 provides a comprehensive survey of the results obtained.

2. Basics of glassy dynamics

In this section we outline some basic issues in glassy dynamics to set the scene for the questions that have been studied using KCMs. Section 2.1 contains a sketch of important experimental phenomena, including the all-important pronounced slow-down in the dynamics as temperature is lowered. In section 2.2 we review how dynamics in the stationary regime—where a liquid is already supercooled past its melting point, but still in metastable equilibrium—can be characterized using correlation and response functions. Section 2.3 generalizes this to the glass regime, where equilibrium is no longer reached on accessible timescales; correlation and response then become two-time quantities because of ageing effects, and can be useful for defining so-called effective temperatures. In section 2.4 we review the energy landscape approach to understanding glassy dynamics, whose usefulness for KCMs has recently been investigated in some detail. Section 2.5 introduces the issues of dynamical lengthscales and heterogeneities, and in section 2.6 we briefly mention some other systems exhibiting glassy dynamics.

2.1. *Some experimental phenomena*

The standard experimental procedure for generating a glass is to take a liquid well above its melting temperature and cool it down quickly enough to avoid crystallization. On cooling through the melting temperature T_m, the liquid is initially in a metastable equilibrium state—the true equilibrium state being the crystal—and therefore referred to as supercooled. On timescales much shorter than those required for crystallization processes to occur, the properties of the supercooled liquid at a

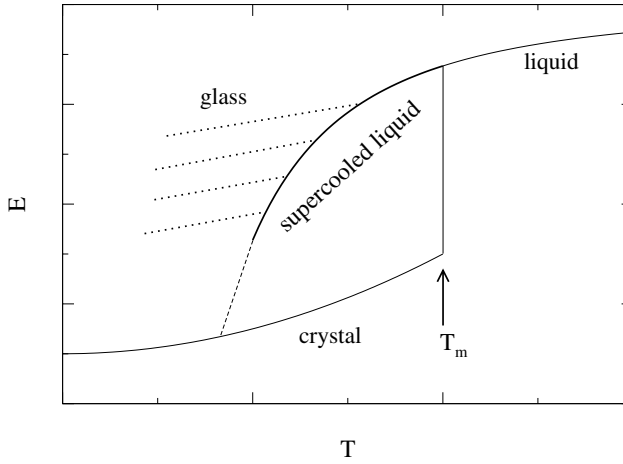

Figure 1. Schematic plot of energy E versus temperature T, showing the liquid line continued into the supercooled regime; no singularities appear at the melting temperature T_m. Also shown are, for four different cooling rates, the deviations which occur as the system falls out of equilibrium at a cooling-rate dependent glass transition temperature T_g. A naive extrapolation of the supercooled liquid line, shown by the dashed line, could suggest a thermodynamic glass transition at a lower (Kauzmann) temperature.

given temperature are stationary, i.e. independent of time. They are also smoothly related to those of the genuine equilibrium liquid above T_m, so that a plot of, e.g. the energy of a supercooled liquid against temperature would show no unusual behaviour as T_m is crossed (see figure 1).

As cooling proceeds, the dynamics in the supercooled liquid slows down, often very rapidly. At some temperature T_g, the longest relaxation timescales of the supercooled liquid therefore begin to exceed the experimental timescale set by the inverse $1/r$ of the cooling rate r. The system then falls out of its (metastable) equilibrium and becomes a glass proper, whose properties evolve slowly with time even at constant temperature; the plot of, e.g. energy versus temperature begins to deviate markedly from the supercooled line at T_g (see figure 1). As defined, it is clear that the glass transition temperature T_g depends on the cooling rate, being the temperature where the longest relaxation times τ are of order $1/r$. In line with the expectation that the dynamics slow down as temperature is lowered, T_g is observed to decrease when the cooling rate r is reduced. The actual dependence $T_g(r)$ is generally logarithmic, corresponding to an exponential temperature variation of relaxation timescales; see below.

One of the most striking experimental manifestations of the dynamical slow-down in supercooled liquids is the temperature dependence of the viscosity η. One can write $\eta = G\tau$, where G is the shear modulus and τ is the relaxation time (more precisely, the integrated relaxation time for shear stress relaxation; see section 2.2). Since G is only weakly temperature dependent, η therefore gives a direct measure of a typical relaxation timescale τ in supercooled liquids. The point where η reaches the value 10^{13} Poise ($= 10^{12}$ Pa s) is often used to define the glass transition temperature T_g operationally; given typical values of G, this corresponds to relaxation timescales τ of the order of hundreds of seconds or more. In so-called *strong* liquids, of which

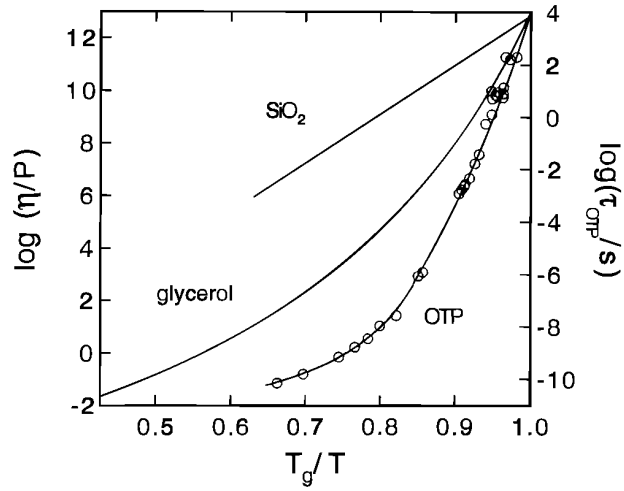

Figure 2. Angell plot of log-viscosity (essentially log-relaxation time, see right axis) against T_g/T. In this representation, strong glass-formers such as SiO_2 with their Arrhenius dependence of timescales on temperature give straight lines, while the super-Arrhenius divergence of timescales in fragile glasses (e.g. glycerol) leads to curved plots. Reproduced with permission from [13]. Copyright 1996 American Chemical Society.

silica (SiO_2) is an example, τ as determined from viscosity measurements increases according to an *Arrhenius* law

$$\tau \sim \exp\left(\frac{B}{T}\right) \tag{1}$$

which corresponds to thermal activation over a—possibly effective—barrier B; here and throughout we set $k_B = 1$. In an 'Angell plot' of log-viscosities against T_g/T, as shown in figure 2, this gives a straight line. A more pronounced timescale increase is referred to as super-Arrhenius or superactivated—we use both terms interchangeably—and occurs in the so-called *fragile* supercooled liquids. They can show a dramatic growth in τ, of up to 15 orders of magnitude, over a temperature interval as narrow as 10% of T_m. This increase is commonly fitted by the Vogel–Tamman–Fulcher (VTF) law [31–33]

$$\tau \sim \exp\left(\frac{A}{T - T_0}\right). \tag{2}$$

This suggests a divergence of τ at some non-zero temperature T_0, though it has been argued that this is difficult to justify from microscopic models [34]. An exponential inverse temperature square (EITS) law

$$\tau \sim \exp\left(\frac{A}{T^2}\right) \tag{3}$$

which exhibits no such divergence can provide an equally good fit to data for many systems [35, 36]. In its most general form, one can write the relaxation time increase of fragile supercooled liquids as an Arrhenius law with an effective barrier $B(T)$ that increases as T decreases,

$$\tau \sim \exp\left(\frac{B(T)}{T}\right). \tag{4}$$

Over the experimental time window, with longest accessible times of the order of hours or days, $B(T)$ then increases by at most a factor of around five while τ itself increases by many orders of magnitude. This limited range of $B(T)$ makes it clear why it is almost impossible to distinguish, on the basis of experimental data, between the VTF and EITS laws or indeed other possible superactivated fitting forms for $\tau(T)$. Theories have been proposed to link the drastic slowing-down in fragile supercooled liquids to (near-) singularities in their thermodynamic properties; an early and still hotly debated example is the proposal by Adam and Gibbs [37] that the effective activation barrier scales as the inverse of the entropy of the configurational degrees of freedom. We will not dwell on this point here, but return to the issue of how configurational entropies can be defined in section 2.4.

Within the supercooled regime discussed above one can define a further characteristic temperature T_c at which relaxation processes begin to take place in two temporally separated stages, with relaxation functions developing shoulders that eventually grow into plateaux (see section 2.2). The longest relaxation timescales τ in this regime, of order 10^{-6} s, are already large compared to their values in the liquid but still small relative to the timescales at T_g. In this temperature region the growth of $\tau(T)$ can often be fitted with an apparent power-law divergence at non-zero temperature, as suggested by MCT [16–19].

At the transition from the supercooled liquid to the glass, one observes experimentally a drop in the specific heat over a narrow temperature interval; the location of this drop defines the so-called calorimetric glass transition temperature. Intuitively, the change in specific heat corresponds to the effective freezing of those slow degrees of freedom which fall out of equilibrium at the glass transition. In a plot of energy versus temperature, it corresponds to a change in slope from a larger value in the supercooled regime to a rather smaller value for the glass. (Superficially, the specific heat jump resembles the behaviour at second-order phase transitions with vanishing specific heat exponent α, but in this latter case the specific heat actually *increases* as T is lowered.) Notice that our terminology above is appropriate for systems at constant volume; we use this since all models discussed below are of this type. Experiments are normally carried out at constant pressure. Instead of energy, the relevant thermodynamic potential whose temperature derivative gives the specific heat is then the enthalpy. For simplicity, we will continue to refer to the constant-volume situation below.

Further experimental illustration of the non-equilibrium nature of the glass state is provided by interesting hysteresis effects in heating–cooling cycles. As explained above, on cooling the energy will initially follow the supercooled line but then depart from it at T_g, with a concomitant drop in the specific heat. On further cooling, the energy remains above the supercooled line. If the system is then heated back up through T_g, however, the energy increases initially very slowly and actually crosses below the supercooled line, rejoining it by a steep increase at a temperature slightly above the original T_g (see figure 3). In the specific heat this increase shows up as a pronounced peak. The crossing of the energy below the supercooled line is a characteristic non-equilibrium effect which reveals that the glass retains a strong memory of its temperature history.

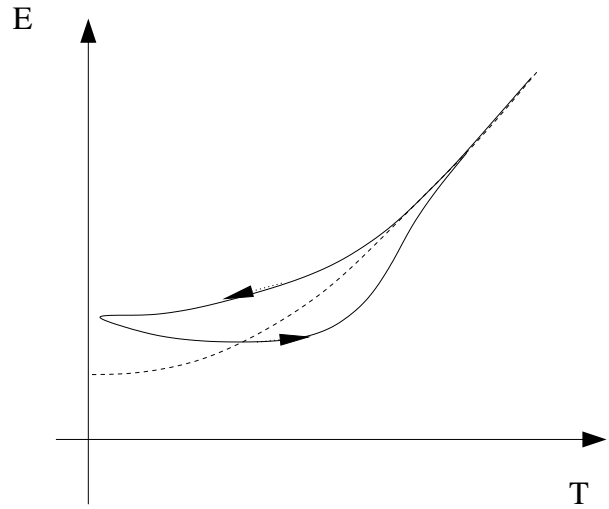

Figure 3. Schematic hysteresis plot for a heating–cooling cycle. On cooling, E remains above the supercooled line (dashed) as the system falls out of equilibrium; on reheating, E remains low and crosses underneath the supercooled line before rejoining it in a steep rise.

To rationalize the complexities of non-equilibrium behaviour, it is tempting to look for a description of glasses in terms of a few effective thermodynamic parameters. For example, the dynamics in a glass at fixed low temperature can be so slow that quantities such as the energy are effectively constant. One could then experimentally define a 'fictive temperature' [38] as that for which the (extrapolated) energy of the supercooled liquid has the value measured in the glass. However, the same procedure applied to a different experimental quantity, such as density, will not necessarily give the same fictive temperature (see e.g. [7]), so that the physical meaning of such assignments remains unclear. More recently, it has been argued [39] that two-time correlation and response functions may be more appropriate for defining effective temperatures; this proposal is discussed in more detail in section 2.3.

2.2. *Stationary dynamics: correlation and response*

We next describe some of the correlation and response or relaxation functions that can be used to probe the stationary (i.e. equilibrium, though metastable) behaviour of supercooled liquids. Many of these correspond to experimentally measurable quantities, and are therefore key quantities which one would like to predict from theoretical models.

Let us denote by $\phi(t)$ any observable quantity which can evolve in time after applying a given perturbation $h(t)$. For instance, ϕ could be the polarization of a supercooled liquid and the corresponding perturbation h the electric field, or ϕ could be the volume and the perturbation h a change in pressure. Suppose the system is in equilibrium at $t = 0$, i.e. $\phi(0) = \phi_{\mathrm{eq}}$, from which time a perturbation h is applied and held constant. For small h, the deviation of $\phi(t)$ from its equilibrium value then defines the linear response function to a step perturbation,

$$\chi(t) = \frac{\phi(t) - \phi_{\mathrm{eq}}}{h}. \tag{5}$$

The long-time limit $\chi_{\rm eq} = \chi(t \to \infty)$ of this then also gives the equilibrium susceptibility. Thinking of the response as the relaxation from an original perturbed state to a new equilibrium state, one can also define the relaxation function

$$\psi(t) = 1 - \frac{\chi(t)}{\chi_{\rm eq}} \tag{6}$$

which is normalized to one at $t = 0$ and decays to zero for $t \to \infty$. Analogues of χ and ψ also exist for large perturbations which drive the system far from equilibrium. An extreme example would be a sudden lowering ('quench') of temperature from the supercooled into the glass regime, with the corresponding nonlinear relaxation function describing the out-of-equilibrium relaxation of the energy.

Equally relevant for experiments are correlation functions of fluctuating quantities; density fluctuations, for example, can be measured by scattering techniques. The equilibrium autocorrelation function of observable ϕ is defined as

$$C(t) = \langle \phi(t)\phi(0) \rangle - \phi_{\rm eq}^2 \tag{7}$$

and obeys $C(t) = C(-t)$ from time-translation invariance (TTI). It is related to the linear response function $\chi(t)$ by the fluctuation–dissipation theorem (FDT) [40], which states that for $t > 0$

$$\frac{\partial}{\partial t}\chi(t) = R(t) = -\frac{1}{T}\frac{\partial}{\partial t}C(t). \tag{8}$$

Here $R(t)$ is the impulse response, i.e. the response of $\phi(t)$ to a perturbation $h\delta(t)$. In integrated form the FDT reads $C(t) = T[\chi_{\rm eq} - \chi(t)]$. Equation (6) then shows that $C(t) = C(0)\psi(t)$ with $C(0) = T\chi_{\rm eq}$, so that the relaxation function also gives the time evolution of the correlations: in equilibrium, fluctuations decay with the same time-dependence whether occurring spontaneously or induced by an applied perturbation.

The FDT can also be expressed in the frequency domain, where it relates the linear response to oscillatory perturbations to the power spectrum of equilibrium fluctuations. The time- and frequency-dependent quantities can of course be expressed in terms of each other; experimentally, the latter are often more easily accessible, while theoretical work tends to focus on the former. From linearity, the response to a small oscillatory perturbation $h(t) = \Re[h\exp(\mathrm{i}\omega t)]$ is $\phi(t) = \int_{-\infty}^{t} \mathrm{d}t'\, R(t-t')h(t')$ with $R(t) = \partial\chi(t)/\partial t$ the impulse response as before. After an integration by parts one then has $\phi(t) = \Re[\hat{\chi}(\omega)h\exp(\mathrm{i}\omega t)]$ with

$$\hat{\chi}(\omega) = \mathrm{i}\omega\int_0^\infty \mathrm{d}t\ \chi(t)\mathrm{e}^{-\mathrm{i}\omega t} = \chi_{\rm eq} - \mathrm{i}\omega\chi_{\rm eq}\int_0^\infty \mathrm{d}t\ \psi(t)\mathrm{e}^{-\mathrm{i}\omega t}. \tag{9}$$

(Formally, an infinitesimal negative imaginary part should be added here to ω to make all integrals convergent; physically this corresponds to a very slow switching on of the oscillatory perturbation.) The complex susceptibility $\hat{\chi}(\omega)$ can be written as $\hat{\chi}(\omega) = \hat{\chi}'(\omega) - \mathrm{i}\hat{\chi}''(\omega)$ where $\hat{\chi}'$ is the in-phase or reversible part of the response and $\hat{\chi}''$ is the out-of-phase or dissipative part. The related fluctuation quantity is the power spectrum, which gives the amplitude of fluctuations of frequency ω and can be expressed as the temporal Fourier transform of the correlation function

$$S(\omega) = \int_{-\infty}^{\infty} \mathrm{d}t\ C(t)\mathrm{e}^{-\mathrm{i}\omega t}. \tag{10}$$

The FDT (8) together with $C(t) = C(-t)$ then relates the power spectrum of fluctuations to the dissipative part of the response, according to

$$S(\omega) = 2T\hat{\chi}'(\omega)/\omega. \tag{11}$$

At high temperatures, relaxation functions are often simple ('Debye') exponentials, $\psi(t) = \exp(-t/\tau)$, giving a dissipative response $\hat{\chi}''(\omega) = \chi_{\rm eq}\omega\tau/(1+\omega^2\tau^2)$ with a single maximum at the peak frequency $\omega = 1/\tau$, and a power spectrum $S(\omega) \sim 1/(1+\omega^2\tau^2)$ of Lorentzian shape. It was already observed in 1854 by Kohlrausch [41], and later by Williams and Watts, that relaxation functions decay non-exponentially in supercooled liquids at low temperatures, and can often be fitted by a stretched exponential or Kohlrausch–William–Watts (KWW) function

$$\psi(t) = \exp(-at^b) \tag{12}$$

with a stretching parameter $b < 1$. This can be thought of as a superposition of exponential relaxations with a broad spectrum of relaxation timescales; in the frequency domain, the corresponding dissipative response $\hat{\chi}''(\omega)$ therefore shows a broad maximum. The value of the stretching exponent b typically decreases with temperature, reaching values around 0.5 at $T_{\rm g}$. The value of a decreases rapidly with T, corresponding to a large increase in the typical relaxation time. It should be noted that fits to experimental data, which cover a limited range of timescales where $\psi(t)$ is often not yet small compared to unity, cannot exclude a cross-over to simple exponential behaviour for much longer times. Nevertheless, the ubiquity of stretched exponential relaxation in supercooled liquids suggests that this is a generic feature of glassy dynamics which theory needs to be able to predict. An interesting issue is whether the observed stretching arises from an average over a heterogeneous spatial structure, with different local regions having very different relaxation times, or whether the relaxation dynamics is intrinsically non-exponential but homogeneous; we return to this point in section 2.5.

We have already hinted that one can obtain a relaxation time τ from the relaxation function $\psi(t)$. A number of different definitions have been used; broadly one would hope that they give qualitatively similar values, though we will see counter-examples below. Common procedures for defining τ are:

- The *instantaneous relaxation time*, defined as the time at which the relaxation function has decayed to 1/e of its initial value, $\psi(t = \tau) = 1/{\rm e}$. This time is simple to measure and therefore favoured by experimentalists.
- The *integrated relaxation time*, defined as $\tau = \int_0^\infty {\rm d}t\, \psi(t)$. This is mostly used in theoretical analysis; its use in experiment would require a fit for the long-time behaviour to carry out the time-integration.
- The *fitting time*, which is defined as the timescale parameter appearing in an appropriate fit of the relaxation function. For a KWW fit (12), for example, one can write $\psi(t) = \exp[-(t/\tau)^b]$ with $\tau = a^{-(1/b)}$.

Notice that all definitions coincide for an exponential relaxation function, $\psi(t) = \exp(-t/\tau)$.

Many relaxation functions in supercooled liquids actually display behaviour more complicated than described above, requiring the definition of several relaxation times. For example, the relaxation of density fluctuations (as defined further below) proceeds in two stages in supercooled liquids. The initial decay of $\psi(t)$ is to a non-zero plateau value. Physically, this *β-relaxation* process is thought to correspond to

the localized motion of particles in the structural 'cages' formed by their neighbours; the corresponding relaxation time τ_β normally increases in an Arrhenius fashion as T is decreased. On a much longer timescale τ_α, the relaxation function then decays from the plateau to zero, and only the long-time part of this α-*relaxation* is well described by a stretched exponential. The α-relaxation dominates the integral $\int_0^\infty \mathrm{d}t\, \psi(t)$ of the relaxation time, so that the integrated relaxation time τ is of the same order as τ_α. It is this timescale that increases strongly as temperature is lowered, with the temperature dependence discussed in section 2.1. (MCT in fact predicts that τ_α genuinely diverges at some non-zero temperature [16–19].) In the frequency domain, the presence of two relaxation processes with widely separated timescales means that the dissipative response $\hat{\chi}''(\omega)$ has two maxima around the inverses of the α- and β-relaxation times.

We finish this section by mentioning two important examples of correlation functions. In a system consisting of a number of particles with position vectors $\mathbf{r}_a$, the Fourier component with wavevector $\mathbf{k}$ of the local density is $\phi_\mathbf{k} = \sum_a \exp(\mathrm{i}\mathbf{k}\cdot\mathbf{r}_a)$, up to a constant prefactor which we ignore. As long as the system remains ergodic, particles are equally likely to be anywhere inside the system volume at equilibrium, so that $\phi_\mathbf{k}^{\mathrm{eq}} = 0$ for non-zero $\mathbf{k}$. The correlation function of $\phi_\mathbf{k}$ is therefore, using the obvious generalization of (7) to complex observables,

$$C(\mathbf{k},t) = \langle \phi_\mathbf{k}(t)\phi^*_{-\mathbf{k}}(0)\rangle = \sum_{ab} \langle \mathrm{e}^{i\mathbf{k}\cdot[\mathbf{r}_a(t)-\mathbf{r}_b(0)]}\rangle. \tag{13}$$

This 'coherent' correlation function (also known as the dynamic structure factor or intermediate scattering function) can be measured using dynamic light scattering experiments, for example. On large lengthscales, i.e. for small $\mathbf{k}$, and for long times, density fluctuations should relax diffusively and so one expects $C(\mathbf{k},t) \sim \exp(-D\mathbf{k}^2 t)$. This relation can be used to deduce from knowledge of $C(\mathbf{k},t)$ for small $\mathbf{k}$ and large t the value of the *collective diffusion* constant D controlling the relaxation of long-wavelength density fluctuations. A self-correlation analogue of $C(\mathbf{k},t)$ can also be defined, as the sum of correlation functions for the single-particle observables $\exp(\mathrm{i}\mathbf{k}\cdot\mathbf{r}_a)$,

$$C_\mathrm{s}(\mathbf{k},t) = \sum_a \langle \mathrm{e}^{i\mathbf{k}\cdot[\mathbf{r}_a(t)-\mathbf{r}_a(0)]}\rangle. \tag{14}$$

For small $\mathbf{k}$ and long t this correlation function, referred to as the intermediate self-scattering function, should again behave as $C_\mathrm{s}(\mathbf{k},t) \sim \exp(-D_\mathrm{s}\mathbf{k}^2 t)$. Since $C_\mathrm{s}(\mathbf{k},t)$ only measures correlations of each particle with itself, however, the diffusion constant D_s entering here is the one for *self-diffusion*, and determines the long-time mean-square displacement of individual particles according to $\langle[\mathbf{r}_a(t) - \mathbf{r}_a(0)]^2\rangle = 6D_\mathrm{s}t$. Notice that $C_\mathrm{s}(\mathbf{k},t)$ is the Fourier transform of the so-called self-part of the van Hove correlation function,

$$G_\mathrm{s}(\mathbf{r},t) = \sum_a \langle \delta(\mathbf{r}_a(t) - \mathbf{r}_a(0) - \mathbf{r})\rangle. \tag{15}$$

The latter is conventionally normalized by dividing by the total number of particles, so that $G_\mathrm{s}(\mathbf{r}, t=0) = \delta(\mathbf{r})$; the second moment $\int \mathrm{d}\mathbf{r}\, \mathbf{r}^2 G_\mathrm{s}(\mathbf{r},t)$ then gives the mean-square particle displacement as a function of time t.

2.3. *Out-of-equilibrium dynamics: two-time quantities and effective temperatures*

When supercooled liquids are cooled to sufficiently low temperatures, their longest relaxation times will become comparable and eventually exceed experimental timescales. The system is then referred to as a glass. It no longer reaches (metastable) equilibrium on accessible timescales and instead *ages*: its properties depend on the waiting time t_w elapsed since the glass was prepared, e.g. by a temperature quench. We review in this section how correlation and response functions are generalized to two-time quantities in the ageing regime. We also discuss how out-of equilibrium correlation and response can be used for defining effective temperatures. This suggestion first appeared in the context of mean-field spin-glass models but has since found much wider application; see e.g. [23] for a review.

The two-time autocorrelation function of an observable ϕ is defined, in a natural generalization of (7), as

$$C(t, t_w) = \langle \phi(t)\phi(t_w)\rangle - \langle \phi(t)\rangle\langle \phi(t_w)\rangle. \tag{16}$$

Similarly, one can define a two-time impulse response function

$$R(t, t_w) = \left.\frac{\delta\langle \phi(t)\rangle}{\delta h(t_w)}\right|_{h=0}$$

which gives the linear response of $\phi(t)$ to a small impulse $h(t) = h\delta(t - t_w)$ in the conjugate perturbation at time t_w. The step response is then given by

$$\chi(t, t_w) = \int_{t_w}^{t} \mathrm{d}t'\, R(t, t') \tag{17}$$

and tells us how ϕ responds to a small constant field switched on at time t_w.

Now, in *equilibrium*, $C(t, t_w) = C(t - t_w)$ by time-translation invariance (TTI); the same will be true of R and χ and FDT (8) holds. A parametric 'FDT plot' of χ

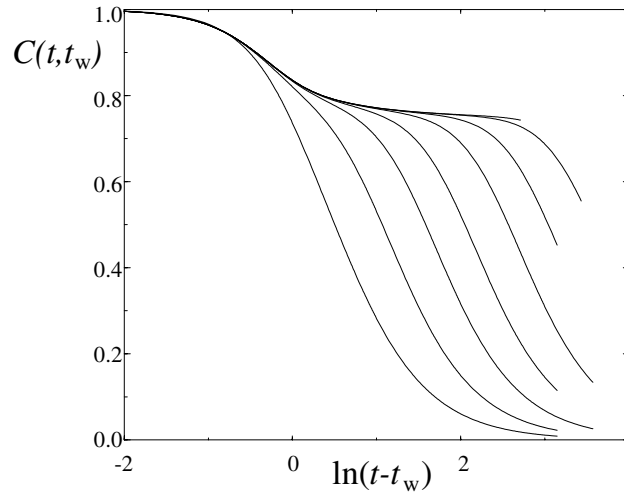

Figure 4. Typical shape of a two-time correlation function, plotted as a function of $t - t_w$ (in log-scale) with system age t_w increasing from left to right. Notice the two separate relaxation processes: the short-time part of the relaxation is independent of t_w and obeys time-translation invariance while the long-time decay from the plateau takes place on a timescale growing with t_w.

versus C is thus a straight line of slope $-1/T$. In an ageing system such as a glass, on the other hand, correlation and response functions will be non-trivial functions of both their arguments. A generic scenario for the behaviour of the correlation function is depicted in figure 4: the initial (β-) part of the relaxation takes place on a timescale which—for large enough t_w—is independent of the age t_w. In this regime $C(t, t_w)$ is a function of $t - t_w$ only and thus obeys TTI. The long-time (α-)relaxation, on the other hand, takes part on 'ageing timescales' growing with t_w; the most straightforward case where $\tau_\alpha \sim t_w$ is often referred to as simple ageing.

The out-of-equilibrium, two-time correlation and response functions are not expected to obey FDT; to quantify this one can define an FDT violation factor $X(t, t_w)$ through [42, 43]

$$-\frac{\partial}{\partial t_w}\chi(t, t_w) = R(t, t_w) = \frac{X(t, t_w)}{T}\frac{\partial}{\partial t_w}C(t, t_w). \tag{18}$$

One may wonder why derivatives with respect to t_w are used here rather than t; in equilibrium the two choices are equivalent since all functions depend only on $t - t_w$. However, derivatives with respect to t would make rather less sense in the out-of-equilibrium regime, since only the t_w-derivative of $\chi(t, t_w)$ is directly related to the impulse response $R(t, t_w)$; physically, this corresponds to causality of the response. Adopting therefore the definition (18), one sees that values of X different from unity mark a violation of FDT. In glasses, these can persist even in the limit of long times, indicating strongly non-equilibrium behaviour even though one-time observables of the system—such as energy and entropy—may be evolving only extremely slowly.

Remarkably, the FDT violation factor for several *mean field* models [42, 43] assumes a special form at long times: taking $t_w \to \infty$ and $t \to \infty$ at constant $C = C(t, t_w)$, $X(t, t_w) \to X(C)$ becomes a (non-trivial) function of the single argument C. If the equal-time correlator $C(t, t)$ also approaches a constant C_0 for $t \to \infty$, it follows that

$$\chi(t, t_w) = \frac{1}{T}\int_{C(t,t_w)}^{C_0} \mathrm{d}C\, X(C). \tag{19}$$

Graphically, this limiting non-equilibrium FDT relation is obtained by plotting χ versus C for increasingly large times; from the slope $-X(C)/T$ of the limit plot, an *effective temperature* [39] can be defined as $T_{\mathrm{eff}}(C) = T/X(C)$. Typical FDT plots are shown in figure 5.

In the most general ageing scenario, a system displays dynamics on several characteristic timescales, one of which may remain finite as $t_w \to \infty$, while the others diverge with t_w; the case with one finite timescale and one growing with t_w is illustrated in figure 4. If these different timescales become infinitely separated as $t_w \to \infty$, they form a set of distinct 'time sectors'; in mean field, $T_{\mathrm{eff}}(C)$ can then be shown to be *constant* within each such sector [43]. In the short time sector ($t - t_w = O(1)$), where $C(t, t_w)$ decays from C_0 to some plateau value, one generically has quasi-equilibrium with $T_{\mathrm{eff}} = T$, giving an initial straight line with slope $-1/T$ in the FDT plot. The further decay of C (on ageing timescales $t - t_w$ that grow with t_w) gives rise to one of three characteristic shapes: (i) In models which statically show one step replica symmetry breaking (RSB), e.g. the spherical p-spin model [42], there is only one ageing time sector and the FDT plot exhibits a second straight line, with $T_{\mathrm{eff}} > T$ (see figure 5). (ii) In models of coarsening and domain growth, e.g. the $O(n)$

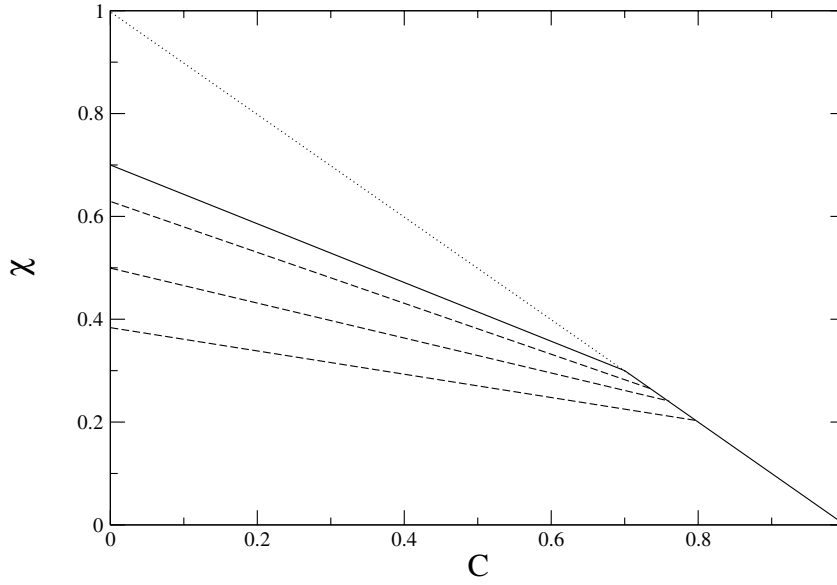

Figure 5. Schematic FDT plots of step response χ versus correlation C in glassy systems. The dotted line shows the equilibrium slope of $-1/T$. The FDT plot first follows this line as the correlation function decays from its initial value, but then crosses over to a non-equilibrium part, as shown by the dashed lines for a series of increasing waiting times t_w (bottom to top). The (negative inverse) slope of this part of the plot can be used to define an effective temperature T_{eff}, which in this example is greater than T and decreases as the system ages. In some exactly solvable mean-field models a non-trivial limiting plot is approached for long times (solid line).

model at large n, this second straight line is flat, and hence $T_{\text{eff}} = \infty$ [44]. (iii) In models with an infinite hierarchy of time sectors (and infinite step RSB in the statics, e.g. the SK model) the FDT plot is instead a continuous curve [43].

T_{eff} has been interpreted as a timescale-dependent non-equilibrium temperature, and within mean field has been shown to display many of the properties associated with a thermodynamic temperature [39]. For example (within a given time sector), it is the reading which would be shown by a thermometer tuned to respond on that timescale. Furthermore—and of crucial importance to its interpretation as a temperature—it is independent of the observable ϕ used to construct the FDT plot [39]. While this picture is theoretically well established only in mean-field models, non-trivial FDT plots have recently also been found in many non-mean-field systems including KCMs. A number of open questions remain, however, over whether these FDT relations can be used to define meaningful effective temperatures (see section 5.4.3 for details). A unique T_{eff} may not result for arbitrary observables ϕ, for example, and one may have to restrict attention to a suitable class of 'neutral' observables. Also, in some cases the slope of the FDT plot is not constant in a given time sector but changes when $t - t_w$ is changed by a factor of order one, while a meaningful T_{eff} should be insensitive to such changes.

We finish this section with a brief discussion of the most appropriate representation of FDT plots in non-mean-field systems, which can be somewhat subtle [45]. For mean field systems the existence of a limiting relation (19) between response χ and

correlation C ensures that parametric plots of χ versus C converge, for long times, to a limiting FDT plot whose negative slope directly gives $X(C)/T$. Equation (19) implies that the plots can be produced either with t as the curve parameter, holding the earlier time t_w fixed, or vice versa. The first version is more convenient and therefore normally preferred [42, 43]. In general, however, the definition (18) ensures a slope of $-X(t,t_w)/T$ for a parametric χ-C plot *only* if t_w is used as the parameter, with t being fixed. If the equal-time correlator $C(t,t)$ varies with t, then 'raw' FDT plots at increasing t may also grow or shrink in scale, indefinitely if $C(t,t) \to 0$ or $\to \infty$. It is therefore helpful to 'attach' the plots to a specific point, either by showing $\chi(t,t_w)$ versus $\Delta C(t,t_w) = C(t,t) - C(t,t_w)$ [46] to get a plot through the origin, or by plotting the normalized values $\tilde{\chi}(t,t_w) = \chi(t,t_w)/C(t,t)$ and $\tilde{C}(t,t_w) = C(t,t_w)/C(t,t)$ to get curves passing through $(\tilde{C}=1, \tilde{\chi}=0)$ [45]. If a limiting plot exists for $t \to \infty$, this then means that X becomes a function of only ΔC or $\tilde{C}$ in the limit. Either t or t_w can be used as the curve parameter in such a situation, but the reference value of the correlator must still be $C(t,t)$ rather than $C(t_w,t_w)$ to maintain the link between $X(t,t_w)$ and the slope of the FDT plot.

2.4. *Energy landscape paradigms*

An interesting take on glassy behaviour is provided by viewing the dynamics 'topographically', as an evolution in a very rugged $3N$-dimensional (if there are N particles) potential energy landscape [47]. This point of view was taken up in the early 1980s by Stillinger and Weber (SW) [48] and has since been further developed [12, 27, 49]; for a selection of references on successful applications of the framework to Lennard-Jones glasses see also [50]. The basic idea of SW was to split configuration space into the basins (or valleys, or inherent structures (IS)) of the energy landscape. Each basin can be defined as the set of configurations that map onto the same configuration in a steepest descent (zero-temperature) dynamics on the energy; because this mapping is deterministic, it splits configuration space into non-overlapping basins. Each one can be labelled by a representative configuration, taken as the one of minimum energy e_{IS} (per particle, say) within the basin. The number density of basins as a function of e_{IS} will be exponential in system size, $\mathcal{N}(e_{IS}) = \exp[N s_c(e_{IS})]$, and by doing the sum over configurations $\mathcal{C}$ basin by basin the partition function can be written as ($\beta = 1/T$)

$$Z = \sum_{IS} \sum_{\mathcal{C} \in IS} e^{-\beta E(\mathcal{C})} = \int de_{IS}\, \exp\{N[s_c(e_{IS}) - \beta e_{IS} - \beta \Delta f(\beta, e_{IS})]\}. \tag{20}$$

Here the term

$$\Delta f(\beta, e_{IS}) = -\frac{T}{N} \ln \sum_{\mathcal{C} \in IS} e^{-\beta[E(\mathcal{C}) - N e_{IS}]} \tag{21}$$

effectively measures the width of a given basin, being a within-basin free energy relative to the bottom e_{IS} of the basin. We have assumed that $\Delta f(\beta, e_{IS})$ is the same for all basins with the same e_{IS}; otherwise a more general definition would be needed in place of (21). We have also written discrete sums over configurations $\mathcal{C}$, rather than integrals as would be appropriate for classical particle systems, in anticipation of the discrete configuration spaces of most KCMs. The above description naturally introduces the concept of configurational entropy or complexity of inherent structures, $s_c(e_{IS})$, and this has been argued to be more relevant to glassy dynamics

than the standard thermodynamic entropy over all configurations originally contemplated by Adam, Gibbs and Di Marzio [37, 51]. The reason is that s_c as defined above excludes all 'trivial' contributions to the entropy arising from local excitations within a given basin. In a supercooled liquid these would correspond to small vibrations of the particles around their average positions. Assuming that these vibrations are similar in the supercooled liquid and the crystal, one can alternatively view s_c as the difference between the entropies of a supercooled liquid and of a crystal at the same temperature.

Looking ahead, we note that in models for glassy dynamics where configuration space is discrete (which includes most KCMs) the dynamics remains stochastic even at zero-temperature: there can be many equivalent directions in configuration space that lead to the same energy decrease. The boundaries between basins in configuration space determined by the $T = 0$ dynamics then become 'soft', and would need to be specified in terms of the probability of a given configuration being assigned to a specific basin. This complicates the calculation of the within-basin free energies Δf. However, the 'bottom' of each basin remains unambiguous and corresponds to a configuration which will not evolve at $T = 0$, so that the configurational entropy $s_c(e_{IS})$ can be defined and calculated as before.

A promising recent refinement of the SW approach is to define the configurational entropy by counting basins with the same *free energy* $f = e_{IS} + \Delta f$ rather than the same e_{IS} [52]. This makes sense because the equilibrium weight of each basin is $\exp(-\beta f)$ rather than $\exp(-\beta e_{IS})$; the additional factor $\exp(-\beta \Delta f)$ correctly accounts for the different weight of narrow and wide basins. (In mean-field spin glasses, equal weight is similarly assigned to basins of equal free energy [53]. In this case the division of configuration space is more clear cut, however, since the different basins are separated by energy barriers that diverge in the thermodynamic limit and thus correspond to genuine thermodynamic states. See [54, 55] for further discussion.) Since the effective width Δf of a basin depends on temperature, so does the configurational entropy $s_c(f, \beta)$ defined in this way.

Developing the SW approach in a different direction, one may wonder about the rationale for splitting configuration space according to basins defined by steepest-descent dynamics. For example, if two adjacent basins are separated by a low-energy barrier then at non-zero temperature it will make more sense to regard them as a single basin which the system will explore on short timescales. Biroli and Kurchan [56] proposed that one should therefore replace the notion of basins with metastable states, i.e. collections of configurations within which the system equilibrates on a given timescale t_* (and at a given temperature T). This leads to a *timescale-dependent* definition of the configurational entropy, which is physically very plausible: e.g. on infinite timescales t_* the system must equilibrate over the whole of configuration space and so the configurational entropy must vanish. To get a meaningful result for the configurational entropy, the timescales for equilibration *inside* metastable states and for transitions *between* such states must be well separated, with t_* chosen to lie between them. (As explained above, in mean-field systems the metastable states are normally genuine thermodynamic states with transition times between them that diverge in the thermodynamic limit; a non-trivial configurational entropy is thus obtained even for $t_* \to \infty$. For further discussion of these and related issues see [22, 57, 58].)

Closely related to inherent structures are ideas that have arisen out of attempts to describe the dynamics of granular media under external tapping or vibration (see

section 2.6) by an effective equilibrium statistical mechanics. Edwards (see e.g. [59]) proposed that an appropriate statistical ensemble would be a flat (microcanonical) distribution over all *blocked* (or 'jammed') configurations of a granular system with given volume or energy, etc. The logarithm of the number of such configurations then defines an 'Edwards entropy', from which analogues of, e.g. temperature and pressure can be derived [59]. The connection to IS follows from the fact that after a tap on its container, a granular material relaxes to some blocked configuration where no particle can move further; since thermal energies are irrelevant in granular materials (see section 2.6), this corresponds to the steepest-descent or $T = 0$ dynamics used to define IS. Biroli and Kurchan [56] proposed that the notion of an Edwards measure could be extended to generic glassy systems, where e.g. non-zero temperature will play a role, by generalizing it to a flat distribution over metastable states of a given lifetime t_*. One intriguing, and largely open, question is under what circumstances the effective temperatures derived from Edwards measures (or analogously from configurational entropies) match those used to rationalize out-of-equilibrium fluctuation–dissipation violations (see section 2.3).

2.5. *Dynamical lengthscales, cooperativity and heterogeneities*

An obvious question to ask about glassy dynamics is whether the dramatic slow-down of the dynamics is correlated with a corresponding increase in an appropriately defined lengthscale. Critical slowing-down around second-order phase transitions, for example, is correlated with the divergence of a static correlation length. In supercooled liquids, the consensus is that there is no growing *static* lengthscale, since e.g. the static structure—as measured by the amplitude of density fluctuations—changes only negligibly while relaxation timescales grow by orders of magnitude. (KCMs take this insight to extremes, by assuming that static correlations are entirely absent.) Any growing lengthscale in glassy dynamics must therefore be of *dynamic* origin, and as such rather more difficult to define unambiguously.

One route to the definition of a dynamical lengthscale is via the idea of cooperative motion, which goes back to at least Adam and Gibbs [37]. In a system of densely packed (spherical, say) particles, for example, motion of one particle over a distance comparable to its diameter should require many of its neighbours to move in concert in order to create a space big enough for the particle to move into. There is support for this theoretically appealing idea. In simulations of particles interacting via Lennard-Jones potentials [60, 61], for example, the most mobile particles were found to 'follow each other around' along string-like clusters. Limitations on computer time mean that such simulations only probe the temperature regime where relaxation timescales are still relatively short compared to those at T_g. Experiments, however, allow longer timescales to be accessed. For example, recent work [62] on colloidal glasses (dense suspensions of spherical colloid particles) found that the most mobile particles—defined as having moved furthest on an appropriately chosen timescale—form extended clusters, with neighbouring fast particles moving predominantly in parallel directions, i.e. cooperatively. The cluster size distribution was observed to be broad, so that a precise definition of a cooperativity lengthscale would have been difficult, but typical clusters sizes were found to be on the order of tens of particles. (There was also some evidence that the structure of the largest clusters was fractal, with fractal dimension ≈ 2.)

The above results show that the idea of cooperativity is closely linked to the appearance of dynamical heterogeneities, i.e. the existence of local regions in a

material with very different relaxation timescales. The existence of such heterogeneities is also suggested by the non-exponential character of relaxation functions in supercooled liquids and glasses, though the alternative of intrinsically non-exponential but homogeneous dynamics is equally possible (see section 2.2). Standard experimental quantities such as the intermediate scattering function (13) measure spatial averages and so do not directly reveal heterogeneities. However, more refined experimental techniques such as multidimensional nuclear magnetic resonance [63, 64], photobleaching [65, 66] and dielectric measurements [67] do give access to local quantities and provide support for the existence of dynamical heterogeneities; for a recent review see [25]. The size of the heterogeneities, i.e. of local regions with a well-defined relaxation timescale, provides an alternative definition of a dynamical lengthscale. How this is related to the cooperativity length is not obvious, however; Ediger [25] argues that the latter must be smaller than the size of the heterogeneous regions, on the grounds that cooperativity makes sense only among particles relaxing on comparable timescales. In addition to a lengthscale, heterogeneities also define a timescale: in an ergodic system, every local region must eventually sample the whole ensemble of local relaxation times. Thus, heterogeneities must have a certain finite lifetime, over which the local relaxation time remains approximately constant before switching to a new value. Of particular interest is the ratio Q [68] of this lifetime to the typical relaxation timescales within a local region. In order for the local relaxation time to be well defined, one expects $Q \geq 1$. Some experiments (see, e.g. [25] for review) do indeed give Q of order unity, suggesting that the time in which slow local structures lose memory of their relaxation time is of the order of the relaxation time itself. More recently, values of Q orders of magnitude larger have also been found, however. Experimental results on the rotation of probe molecules in supercooled polymer melts [69], for example, show heterogeneities persisting for times much longer than typical relaxation times. The switching of local relaxation times was interpreted as due to rare, large-scale, cooperative rearrangements of heterogeneities; interestingly, this suggests that the associated cooperativity length is actually *larger* than the size of heterogeneities, contrary to Ediger's argument [25].

It is clear even from the brief sketch above that the existence of heterogeneities and dynamical lengthscales induced by, e.g. cooperativity remains an intriguing open problem in glassy dynamics. We will see in section 5.5 that KCMs can provide considerable insight in this area, allowing different definitions of dynamical lengthscales to be compared and cooperativity effects to be investigated in detail.

2.6. *Glassy dynamics in other systems*

So far in this overview of glassy dynamics we have focused on glasses which are produced by the conventional route of cooling appropriate 'glass-forming' liquids; essentially all liquids fall into this category though the poorer glass-formers may require very high cooling rates [20]. Glassy dynamics is a much more widespread phenomenon, however; we have already mentioned polymer melts, which become glassy at sufficiently low temperatures, and suspensions of colloid particles, where glassy effects are induced by compression to sufficiently large densities. The glass transition has indeed been viewed as a special case of a more general 'jamming transition' (see, e.g. [70]) which occurs in a variety of systems including, e.g. dense granular materials such as sand. We highlight the latter case here because KCMs have recently also been used as models of such granular materials. As reviewed in, e.g. [71, 72], these materials display a number of 'glassy' features. An interesting

difference to conventional glasses is that thermal excitation effects are negligible since $k_B T$ at room temperature is negligible compared to the energy required to lift a grain of sand by its own diameter. Effectively, one therefore has $T = 0$ and the dynamics is driven by external excitations such as vibrations or vertical tapping of the container. Increasing or decreasing the tapping intensity then corresponds to changing temperature, and hysteresis effects appear in the density of the material when the tapping intensity is modified cyclically. The temporal increase of density at constant tapping intensity has also received much attention, and is experimentally observed to have a very slow, logarithmic dependence on time that is referred to as logarithmic compaction.

3. Overview of models

In this section we collect all KCMs and related models that are covered in this review. The 'core' KCMs are the spin-facilitated models (section 3.1), which have inspired a number of variations (section 3.2), and the constrained lattice gases discussed in section 3.3. Closely related are some models defined on hierarchical structures (section 3.4); inspired by cellular structures such as froths (section 3.5); or obtained via mappings from models with unconstrained dynamics (section 3.6). All models covered in these subsections have stochastic, Markovian dynamics obeying detailed balance with respect to a trivial energy function, and as their key ingredient explicit constraints forbidding some local transitions between configurations. In the final section 3.7, we gather other models which are not strictly speaking KCMs according to this classification, but merit inclusion because they share a number of features with KCMs.

3.1. *Spin-facilitated Ising models*

Spin-facilitated Ising models (SFM) were introduced in the early 1980s in the seminal work of Fredrickson and Andersen [73, 74]. They can be formulated in terms of $N = L^d$ two-state variables $n_i = 0, 1$ on a d-dimensional lattice, normally chosen as cubic with side length L. Physically, an up-spin $n_i = 1$ represents a mobile, low-density region of a supercooled liquid or glass, while $n_i = 0$ models a less mobile region of higher density. A generic energy function with nearest-neighbour (n.n.) interactions is then the Ising Hamiltonian,

$$E = -J \sum_{(i,j)} (2n_i - 1)(2n_j - 1) + \sum_i n_i. \tag{22}$$

The coefficient of the linear ('magnetic field') term has been set to unity and fixes the temperature scale, and its sign is chosen in line with the intuition that at low temperatures most regions should be of high density, $n_i = 0$. The sum in the interaction term runs over all distinct n.n. pairs. For $J > 0$ this term favours neighbouring regions to be in the same state, but we will see shortly that this effect is unimportant, with most work on the model focusing on the case $J = 0$. The model with the energy function (22) has no equilibrium phase transition due to the presence of the non-zero field term, and at low temperatures the concentration $c = \langle n_i \rangle$ of up-spins or mobile regions tends to zero.

The key idea of Fredrickson and Andersen was that rearrangements in any given region of the material should be possible only if there are enough mobile low-density regions in the neighbourhood that can *facilitate* the rearrangement. In the language

of spins, a rearrangement from low to high density or vice versa corresponds to a spin-flip, and the facilitation constraint is formalized by requiring that a spin can flip only if at least $f \geq 1$ of its n.n.s are in the mobile state $n_i = 1$. In line with much—though unfortunately not all—notation in the literature we will call the resulting model the f, d-SFM: the spin-facilitated (Ising) model on a d-dimensional cubic lattice, with f facilitating up-spins required for spin-flips. Mathematically, its dynamical evolution is governed by a master equation for the time-dependent probability $p(\mathbf{n}, t)$ of being in a given configuration $\mathbf{n} = (n_1 \dots n_N)$,

$$\frac{\partial}{\partial t} p(\mathbf{n}, t) = \sum_{\mathbf{n}'} w(\mathbf{n}' \to \mathbf{n}) p(\mathbf{n}', t) - \sum_{\mathbf{n}'} w(\mathbf{n} \to \mathbf{n}') p(\mathbf{n}, t). \tag{23}$$

Here $w(\mathbf{n} \to \mathbf{n}')$ is the *rate* for a transition from $\mathbf{n}$ to $\mathbf{n}'$ ($\neq \mathbf{n}$), defined such that in a small time interval $\mathrm{d}t$ the probability for this transition is $w(\mathbf{n} \to \mathbf{n}')\,\mathrm{d}t$. The only allowed transitions in the f, d-SFM are spin-flips. *Without the kinetic constraint*, the rates for these would be given by

$$w(n_i \to 1 - n_i) = w_0(\Delta E). \tag{24}$$

Here ΔE is the change of the energy (22) in the transition from n_i to $1 - n_i$, and $w_0(\Delta E)$ is a transition rate that obeys detailed balance with respect to E. The Metropolis rule $w_0(\Delta E) = \min(1, \exp(-\beta \Delta E))$ and Glauber dynamics $w_0(\Delta E) = 1/[1 + \exp(\beta \Delta E)]$ are the most common choices; we set $\beta = 1/T$ throughout. We also adopt the convention that rates for any transitions that are not explicitly listed are zero. The full set of transition rates defined by (24) is therefore

$$w(\mathbf{n} \to \mathbf{n}') = \sum_i \delta_{\mathbf{n}', F_i \mathbf{n}} w(n_i \to 1 - n_i) \tag{25}$$

with F_i the operator that flips spin i, $F_i \mathbf{n} = (n_1 \dots 1 - n_i \dots n_N)$. Finally, in (23) we have used a continuous-time formulation which is convenient for theoretical work. A discrete-time version would be as follows. Advance time in discrete steps $1/N$. At each step, randomly select one of the N spins, n_i say, for a possible spin-flip. Accept this proposed 'move' with probability proportional to $w(n_i \to 1 - n_i)$, otherwise reject it. In the thermodynamic limit $N \to \infty$, this discrete-time algorithm leads to the same results as its continuous-time counterpart, i.e. it gives the same evolution of $p(\mathbf{n}, t)$ up to possibly a trivial rescaling of time (see section 4.2).

Having set up the general framework for the dynamics, we now need to incorporate the kinetic constraints. Define f_i to be the number of up-spin neighbours of spin n_i; Fredrickson and Anderson then proposed to implement the kinetic constraint by modifying the transition rates from (24) to

$$w(n_i \to 1 - n_i) = f_i(f_i - 1) \cdots (f_i - f + 1) w_0(\Delta E). \tag{26}$$

The new factor forces the rate to be zero whenever $f_i < f$. For $f = 1$, for example, this factor is simply f_i, which is zero for $f_i = 0$ but non-zero for $f_i \geq 1$; for $f = 2$ the kinetic constraint factor $f_i(f_i - 1)$ vanishes for $f_i = 0$ or $f_i = 1$ but is non-zero for $f_i \geq 2$. Importantly, the fact that some rates are zero due to the kinetic constraint does not break detailed balance, since a transition and its reverse transition are always forbidden together. It is also clear that the main effect of the kinetic constraint factor $f_i(f_i - 1) \cdots (f_i - f + 1)$ is to set some rates to zero and thus rule out the corresponding transitions. Its precise value for *allowed* transitions should not

affect the results qualitatively, and one could equally define it so that it always equals unity for allowed transitions [75–78]. An advantage for theoretical treatment of the form (26) is that the constraint factor can be written relatively simply in terms of the neighbouring spin variables,

$$w(n_i \to 1 - n_i) = \sum_{j_1 \neq \cdots \neq j_f} n_{j_1} \cdots n_{j_f} w_0(\Delta E) \tag{27}$$

where the site indices $j_1, \ldots, j_f$ are summed over the n.n. sites of spin i.

The origin of glassy dynamics in the f, d-SFM is easy to understand intuitively. From the energy function (22) we see that at low temperatures the equilibrium concentration $c_{\mathrm{eq}} = \langle n_i \rangle$ of up-spins, i.e. mobile regions, becomes small; for $T \to 0$, $c_{\mathrm{eq}} \to 0$ since the field-term in the energy function forces all spins to point down. Only a very small number of spins will then have f or more up-spin neighbours, while all other spins will be effectively frozen until enough of their neighbours flip up. The kinetic constraint thus creates a dynamical bottleneck, which becomes more pronounced as the number f of facilitating spins is increased.

We should stress that the variables $n_i = 0, 1$ in SFMs do not correspond to particles, but merely to high and low values of an appropriately coarse-grained density. This will be different in the lattice gas models discussed in section 3.3, where $n_i = 0$ and $n_i = 1$ correspond to a particle and a hole, respectively, and $\sum_i n_i$ represents the total particle number, a conserved quantity. Notice also that in the lattice gases the glassy 'jammed' regime of high density corresponds to $c = \langle n_i \rangle$ close to one, whereas for SFMs c represents the concentration of mobile regions and glassy features occur when c becomes small. Finally, it is worth pointing out that SFMs have often been formulated in terms of spin variables taking the values -1 and $+1$ rather than 0 and 1. We find the latter more convenient, especially since in SFMs the up- and down-states do not represent equivalent physical states related by symmetry.

It is clear from the above discussion that glassy dynamics in SFMs will occur whenever the concentration of up-spins is small. As anticipated above, the interaction term in the energy function (22) is not necessary for this effect to occur, and therefore most studies of the f, d-SFM have focused on the case of the non-interacting energy function

$$E = \sum_i n_i. \tag{28}$$

Compared to (22) this produces completely trivial thermodynamics, corresponding to free spins in a field. The equilibrium concentration of up-spins is therefore

$$c_{\mathrm{eq}} = 1/(1 + \mathrm{e}^{\beta}) \tag{29}$$

and, as expected, becomes very small in the low-temperature limit of large β. The energy change ΔE entering the unconstrained transition rates $w_0(\Delta E)$ then also simplifies to $\Delta E = 1 - 2n_i$, and Glauber transition rates take the simple form

$$w_0(\Delta E) = (1 - c_{\mathrm{eq}})n_i + c_{\mathrm{eq}}(1 - n_i). \tag{30}$$

Unless $J \neq 0$ is specified explicitly, we will always mean the non-interacting case $J = 0$ when referring to the f, d-SFM in the following. From (29), either temperature or the up-spin concentration c_{eq} can then be used to specify the equilibrium state of the system.

More recently, versions of SFMs with *directed constraints* (sometimes also called asymmetric constraints) have been introduced, mainly by Jäckle and coworkers, and have proved to be very useful in adding to our understanding of the original SFMs. The new feature of models with directed constraints is that only n.n. spins in specific lattice directions can act as facilitators. Two such models have been considered in some detail. The simplest is the *East model*, first proposed in [79] and later rediscovered [80]. The model is defined in dimension $d = 1$, with a spin allowed to flip only if the nearest neighbour on the left is up. (The name 'East model' derives from the fact that in the original formulation of the model [79] the opposite convention was chosen for the direction of the constraint, with facilitating neighbours assumed to be on the right, i.e. to the East.) The transition rates for spin-flips in the East model are $w(n_i \to 1 - n_i) = n_{i-1} w_0(\Delta E)$, which for the trivial energy function (28) and Glauber dynamics (30) becomes

$$w(n_i \to 1 - n_i) = n_{i-1}[(1 - c_{\mathrm{eq}})n_i + c_{\mathrm{eq}}(1 - n_i)]. \tag{31}$$

The model is the directed version of the $1,1$-SFM; in the latter, an up-spin neighbour either to the left or right can facilitate a spin-flip, while in the East model a spin can never flip if its left neighbour is down, whatever the state of its right neighbour. This seemingly innocent modification actually has profound effects on the dynamics; see the summary of results in section 3.1.2. On a square lattice one can similarly define the directed analogue of the $2,2$-SFM, called the North-East model, by requiring that a spin can flip only if both its neighbours to the North and East are up [81]. A weaker directionality constraint had earlier been proposed by Reiter [82], who considered a model where a spin can flip if at least two neighbours in orthogonal directions—e.g. North and West, or South and West—are up.

For the East model and the $1,1$-SFM, a model which interpolates between the two extreme cases of fully directed and undirected constraints has also been considered very recently [55, 83, 84]. The transition rates can be chosen as, for example

$$w(n_i \to 1 - n_i) = (n_{i-1} + a n_{i+1})[(1 - c_{\mathrm{eq}})n_i + c_{\mathrm{eq}}(1 - n_i)]. \tag{32}$$

For $a = 0$ and 1 this gives the East model and the $1,1$-SFM, respectively; for intermediate values of the parameter a one has an 'asymmetric $1,1$-SFM' where spins with an up-spin neighbour on the right are able to flip but only with a rate reduced by the factor a.

Finally, models with directed constraints have also been defined on more abstract structures, e.g. Cayley trees [81]. Starting from a root node, at each node the tree branches into $a - 1$ nodes on the next level down, so that each node is connected to a others, one above and $a - 1$ below. Figure 16 below shows an example with three levels and $a = 4$. The directed (a,f)-Cayley tree model is then defined by the constraint that spins can only flip if f of the $a - 1$ spins below them are up. An undirected version of this model could also be contemplated, by allowing spins to flip whenever *any* f of their a neighbours, whether above or below, are up. To make sure that the root node also has a neighbours, it is then sensible to consider a Bethe lattice, i.e. a set of a Cayley trees linked together at a common root node. It has been argued [81], however, that this undirected variant has features very similar to the directed Cayley tree model—with e.g. blocking transitions, where a finite fraction of spins are permanently frozen, occurring at the same up-spin concentration—so we do not consider it further in the following.

3.1.1. *Interlude: reducibility and ergodicity*

So far, we have naively assumed that the equilibrium behaviour of KCMs—such as SFMs and their directed analogues—is described by the usual Boltzmann distribution. In the presence of kinetic constraints, this is not completely trivial, and one has to consider the possibility that the dynamics might be *reducible*. We pause in our overview of KCMs to discuss this issue, contrasting it with the closely related though distinct question of ergodicity.

Recall that the Boltzmann distribution $p_{\rm eq}(\mathbf{n}) \sim \exp[-\beta E(\mathbf{n})]$ is guaranteed to describe the unique equilibrium state, i.e. the long-time limit of $p(\mathbf{n}, t)$ for a finite system, under two conditions: that the dynamics obeys detailed balance with respect to the energy function E, and that the dynamics is irreducible. Irreducibility means that the system can pass from any configuration to any other by some finite number of 'allowed' transitions, i.e. transitions with non-zero rates. Pictorially, there must be a path in configuration space from any one configuration to any other. Notice that the definition of irreducibility refers to a finite system, and only addresses the existence of paths and not the (possibly very long) time it would take the system to traverse a given path.

In systems without kinetic constraints and at non-zero temperature, irreducibility is normally trivial. For example, in Ising models with the unconstrained spin-flip rates (24), any spin-flip is an allowed transition, and one can get from any configuration to any other with at most N spin-flips. In KCMs, on the other hand, the presence of the kinetic constraints can cause the dynamics to be *reducible*, with configuration space splitting into mutually inaccessible *partitions*. A partition can be constructed by starting from some configuration $\mathbf{n}$, adding all configurations that are accessible from $\mathbf{n}$ via allowed transitions, and iterating until no new configurations are found. All configurations in the partition are then mutually accessible: detailed balance ensures that if there are paths from $\mathbf{n}$ to $\mathbf{n}_1$ and $\mathbf{n}_2$, then the reverse path from $\mathbf{n}_1$ back to $\mathbf{n}$ also exists and can be followed from there to $\mathbf{n}_2$. On the other hand, no paths exist that connect configurations in different partitions. Thus, if the system is started off in a configuration in a given partition, it will equilibrate to the Boltzmann distribution in *that partition* only, while the probability of being in states in other partition remains zero for all time.

A simple example of reducibility, with only two partitions, is provided by the $1, d$-SFM. Clearly, the configuration with all spins down, $n_i = 0$, allows no transitions at all to other configurations since no facilitating up-spins exist; it forms a partition on its own. On the other hand, starting in any other configuration, one can flip up the n.n.s of all up-spins and continue this process until all spins are up. All these configurations are therefore connected to the all-up configuration and form a single partition which—since it contains the all-up state—is normally referred to as the high-temperature partition in the context of SFM. (This is somewhat of a misnomer, since for the energy function (28) the equilibrium state with $c_{\rm eq} = \langle n_i \rangle = 1$ corresponds formally to $\beta = -\infty$, rather than $\beta = 0$.) The reducibility in this case is thus of a rather trivial nature: the dominant high-temperature partition contains all configurations except for a fraction 2^{-N} which vanishes for $N \to \infty$. One can thus proceed to calculate equilibrium properties as if the Boltzmann distribution extended over all configurations, and we can call the system *effectively irreducible*.

To formulate the requirement for effective irreducibility more generally, consider again SFMs with the trivial energy function (28). The partition function for the high-temperature partition can then be written down as [85]

$$Z = \sum_{E=0}^{N} \frac{N!}{E!(N-E)!} p(E/N, N) e^{-\beta E} \tag{33}$$

with $p(c, N)$ the fraction of configurations with up-spin concentration $c = E/N$ that are in the high-temperature partition. The naive partition function calculated over all states has the same form but with $p(E/N, N)$ replaced by 1. The two procedures for calculating Z will give the same answers in the thermodynamic limit if $p(c, N) \to 1$ for $N \to \infty$ at the naive equilibrium up-spin concentration $c = 1/(1 + e^{\beta})$ (see (29)). For effective irreducibility we would like this to hold at any non-zero temperature, and will therefore define a system to be effectively irreducible if $p(c, N) \to 1$ for $N \to \infty$ at any fixed $c > 0$. Two comments are in order here. First, effective irreducibility does not say anything about the total *number* of configuration space partitions, which in fact generically grows exponentially with system size; it merely requires that the fraction of total configuration space *volume* taken up by partitions other than the dominant (high-temperature) partition must shrink to zero in the thermodynamic limit. Second, the function $p(c, N)$ can exhibit strong finite-size effects. As explained in more detail in section 4.1, if one defines a threshold up-spin concentration $c_*(N)$ above which a finite system is effectively irreducible because $p(c, N) \approx 1$, then this will often converge to zero only very slowly, e.g. logarithmically in N. One then has to be careful not to assume naive equilibrium results to hold for arbitrarily low c and finite N; the results for $p(c, N)$ for the 2, 2-SFM shown in figure 6 illustrate this.

We stress once more that (effective) irreducibility, and the existence of the corresponding (effectively) unique Boltzmann equilibrium distribution, are static

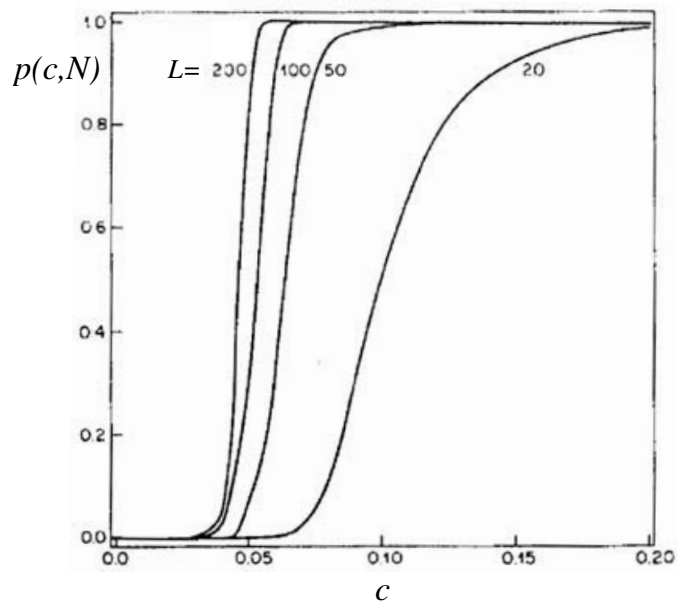

Figure 6. Probability $p(c, N)$ for states with up-spin concentration c to belong to the high-temperature partition in the 2, 2-SFM, for different values of $L = N^{1/2}$ as indicated. Notice that the value $c_*(N)$ above which $p(c, N)$ is close to one and the system thus effectively irreducible decreases to zero only very slowly with N (in fact logarithmically; see section 5.1). From [85]. Copyright American Institute of Physics.

notions that tell us nothing about the timescales involved. Since they relate only to the existence of paths in configuration space, but not to the time it would take the system to traverse these paths, time is effectively always taken to infinity for finite N, i.e. before the thermodynamic limit is invoked. This contrasts with *ergodicity*: we will call a system ergodic if any two configurations—with the exception of possibly a vanishingly small fraction of configuration space—remain mutually accessible on timescales that remain *finite* in the limit $N \to \infty$. Of course, reducibility implies non-ergodicity, but the reverse is not true. Another way of putting this is to say that irreducibility is concerned with the existence of configuration space paths, whereas ergodicity focuses on whether these paths retain sufficient statistical weight in the thermodynamic limit [86]. A simple example is the Ising ferromagnet in zero field and with unconstrained Glauber dynamics. As explained above, the dynamics is then irreducible for any $T > 0$, but ergodicity is broken below the critical temperature T_c, with states of positive and negative magnetization mutually inaccessible on finite timescales. The ergodicity breaking occurs here (as it does in general, though not for KCMs; see below) at an equilibrium phase transition; at T_c, a singular change in the equilibrium properties of the system occurs, and the two ergodic components into which configuration space splits have genuine meaning as different physical phases of the system. This should be contrasted with the concept of reducibility, for which temperature is irrelevant—the value of T never changes an allowed transition into a forbidden one, as long as $T > 0$—and where the different mutually inaccessible partitions of configuration space have no interpretation as thermodynamic phases.

As reviewed in section 5.1 below, most of the KCMs we will consider in this review are effectively irreducible; the exceptions are the Cayley tree and the North-East models, which become strongly reducible below a critical value c_* of the up-spin concentration. For the effectively irreducible models, equilibrium properties can be calculated in the naive way, and the trivial energy functions used ensure that there are no equilibrium phase transitions. An intriguing question then poses itself: can these models nevertheless show *dynamical transitions* where ergodicity is broken even though there is no underlying thermodynamic transition? Such a transition could be caused by a divergence of a relaxation time at non-zero temperature, for example; see [87] for a detailed discussion. This effect occurs in some mean-field spin glasses (see, e.g. the review [23]) and is also predicted by approximations for supercooled liquids such as MCT [16–19]. For most KCMs the evidence points towards the absence of a true dynamical transition; we defer a detailed discussion of this point to section 5.2 below.

We end this section with a suggestion advanced in [88] that reducibility in KCMs may not be as important as it seems: one could consider a weaker form of kinetic constraints where the notionally forbidden transitions take place with a very small rate $1/\tau_0$. As long as τ_0 is finite, the connectivity of configuration space is the same as that for an unconstrained model and so the dynamics is trivially irreducible. On the other hand, the dynamical evolution of the system should be independent of τ_0 for times $t \ll \tau_0$, so that the weakening of the constraint is irrelevant for the behaviour on *finite* timescales.

3.1.2. *Some results for spin-facilitated models*

Having clarified the issue of reducibility, we now return to our discussion of spin-facilitated models (SFMs). In this section we give an illustrative overview of some of

the key ideas and results for SFMs, primarily for 'quick' readers who do not wish to delve too deeply into the details; 'expert' readers can find the latter in section 5.

To start with, it is important to note that SFMs can be classified into two broad families. In models with undirected constraints and $f = 1$ (one-spin facilitated models), relaxation occurs primarily by the *diffusion of defects*, which in this case are isolated up-spins, and there are close links to other defect-diffusion models, e.g. [89–92]. All other models—i.e. the f, d-SFMs with $f > 1$ and the models with directed constraints—require *cooperative* processes for relaxation to occur. This distinction is important because the dynamical effects of the kinetic constraints are very different in the two model families: we will see that the models with diffusing defects show strong glass behaviour, i.e. an Arrhenius temperature dependence of relaxation times, while the cooperative models exhibit much more pronounced relaxation time increases resembling those in fragile glasses. To understand the origin of this difference, consider an $f, 2$-SFM in equilibrium at low up-spin concentration $c = 1/(1 + \mathrm{e}^{\beta}) \approx \mathrm{e}^{-\beta}$; we write c instead of c_{eq} here for brevity. We can then think of the up-spins as defects in the ground state configuration with all spins down. Because c is small, a typical defect is surrounded by down-spins as illustrated in figure 7. Let us focus on the relaxation of the central defect, which proceeds by different mechanisms depending on whether $f = 1$ or $f \geq 2$.

If $f = 1$, the central defect can facilitate an up-flip of any of its neighbouring down-spins. From (26) and (30), the rate for this is $w_0(\Delta E) = c$, with a corresponding Arrhenius timescale $1/c \approx \mathrm{e}^{\beta}$. Once a neighbouring spin points up, two different transitions can happen, both with rate $w_0(\Delta E) = 1 - c \approx 1$: either the new up-spin flips back down, or the original up-spin flips down. In the latter case, the defect has effectively moved to the neighbouring site, and the effective rate for this process is $c/2$ for small c. (The down-flips do not contribute to this because they only take time of order one, while the factor $1/2$ arises because the original defect will only move if it flips down before the newly created up-spin does.) By a repetition of this process, the defect can then move *diffusively* through the whole lattice, with effective diffusion constant $D_{\mathrm{eff}} = c/2$ if the lattice constant is fixed to one; the same argument applies to $1, d$-SFMs in any dimension d. The longest relaxation time in these models can be estimated as the timescale on which diffusing defects encounter each other. With typical distances between defects of order $l \sim c^{-1/d}$ this gives

$$\tau \sim l^2/D_{\mathrm{eff}} \sim c^{-1-2/d} \approx \exp[(1 + 2/d)\beta] \tag{34}$$

demonstrating the Arrhenius temperature dependence of relaxation times anticipated above. Depending on the precise definition of the relaxation time, Arrhenius behaviour with different effective activation energies may result; see section 5.3 for details. The *integrated* relaxation time, for example, is estimated to scale as $\sim \exp(2\beta)$ in $d = 1$, diverging less slowly than the longest relaxation time (34); figure 8 shows results for the former quantity in the $1, 1$-SFM. Notice that the diffusive character of the dynamics in the SFMs with diffusing defects is also visible in the out-of-equilibrium dynamics. After a quench from equilibrium at high temperature, for example, the average distance between up-spins increases with the characteristic power law $l(t) \sim t^{1/2}$; see figure 21 below.

Now contrast the above analysis for $f = 1$ with the cooperative case $f > 1$. Due to the stronger kinetic constraint, the central defect in figure 7 cannot now on its own facilitate up-flips of its neighbouring down-spins. It therefore remains itself unable to move until a region of up-spins further away manages to flip up spins in its

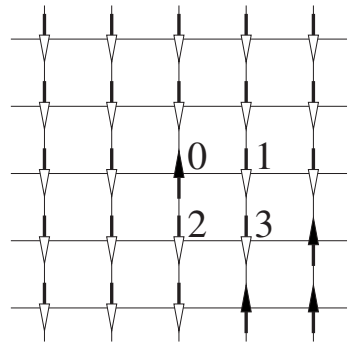

Figure 7. An example configuration of a small region of an $f,2$-SFM. The spin in the centre, labelled by 0, is in the up-state ($n = 1$) and can flip to $n = 0$ in different ways depending on the value of f. If $f = 1$, all four n.n.s of spin 0 are mobile and spin 0 itself can flip down after any one of these has flipped up. If $f = 2$, on the other hand, spin 0 can only be flipped down in a more cooperative process, with the sequence of spin-flips $3 \to 2 \to 1 \to 0$ or $3 \to 1 \to 2 \to 0$.

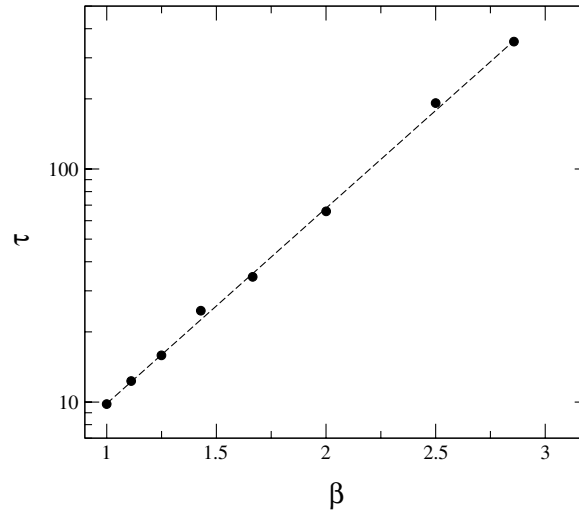

Figure 8. Integrated relaxation time τ as a function of $\beta = 1/T$ in the 1,1-SFM. The straight line fit is given by $\tau = 1.43\exp(1.93\beta)$, close to the theoretically expected behaviour $\tau \sim \exp(2\beta)$ for low T (see section 5.3). From [55]. Copyright American Institute of Physics.

neighbourhood and to propagate this up-spin 'wave' until it reaches the central up-spin. The example in figure 7 shows that this can be a highly cooperative process, requiring a significant number of spin-flips to take place in the right order. While no simple scaling argument for the relaxation time τ exists in this case, it is clear that τ cannot scale as a fixed inverse power of c, since the number of up-flips involved in the cooperative process grows as c decreases and the distance between defects increases. Correspondingly, as a function of temperature one has a superactivated timescale increase. Exemplary results from [77, 78] are shown in figure 9; the curvature in the plot of log-relaxation time versus $1/T$ clearly demonstrates the non-Arrhenius behaviour (and should be contrasted with figure 8). Beyond the general recognition

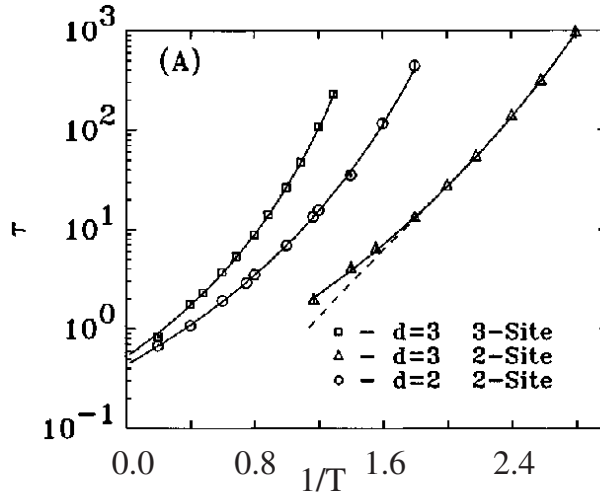

Figure 9. Relaxation times in cooperative f, d-SFMs as a function of $1/T$. Three cases are shown from left to right: $(f = d = 3)$, $(f = d = 2)$, $(f = 2, d = 3)$. From [78]. Copyright American Physical Society.

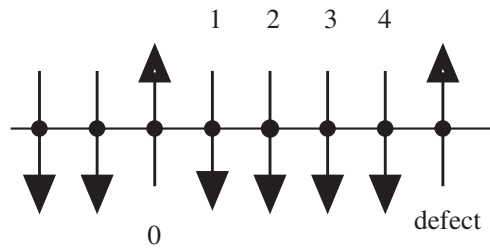

Figure 10. Typical configuration of the East model at low temperatures, where up-spins are separated by large domains of down-spins. The up-spin labelled 0 can progressively activate (flip up) spins 1, 2, 3 and 4 until the defect on the right can be relaxed, i.e. flipped down. At low T, the relaxation proceeds via the route with the smallest activation energy, i.e. the smallest number of spins that are simultaneously up. This is achieved by creating 'anchor' spins (see text for details): in this example, spin 1 can be flipped down once spin 2 has been flipped up, and the relaxation can proceed from there with spin 2 as the anchor.

that the cooperative SFMs behave like fragile glasses, very little is known about the precise form of the timescale increase at low temperature; some studies have suggested that it might in fact be doubly exponential, $\tau \sim \exp[A \exp(1/T)]$ (see section 5.5).

One example of a cooperative model where relaxation times *can* be deduced by relatively simple arguments is the East model. A typical equilibrium configuration at low c is shown in figure 10. The defect on the left can progressively flip up its neighbours to the right, and thus eventually relax the defect on the right. One may suspect that this process requires all intermediate spins to be flipped up, suggesting a relaxation rate $\tau \sim (1/c)^{l-1} \approx \exp[(l-1)\beta]$ for defects a distance l apart; the factor $l-1$ in the exponent just gives the energy barrier arising from the additional up-spins that need to be created. In fact, one can show that the relaxation process can be made more efficient if some spins are flipped back down once 'anchoring' spins

between the two defects have been flipped up. This process proceeds in a hierarchical fashion, with anchors created successively at distances 1, 2, 4, ... to the right of the original defect, and requires a maximum number of $k \approx \ln l / \ln 2$ up-spins at any one time; see section 4.6 for details. With typical distances between defects of order $l \sim 1/c \approx \exp(\beta)$, this gives a relaxation time $\tau \sim \exp(k\beta) \sim \exp(\beta^2/\ln 2) = \exp[1/(T^2 \ln 2)]$. This is an EITS law (3) and gives the very strong increase of τ at low temperatures that is typical of fragile glasses.

Due to the cooperative nature of the dynamics, f, d-SFMs with $f \geq 2$ also show rather complex relaxation functions in their **equilibrium dynamics**. Stretched exponential behaviour has been found in spin autocorrelation functions, for example; in the East model there is evidence that the stretching may become extreme at low temperatures, with the stretching exponent tending to 0 for $T \to 0$ (see section 5.3). The out-of-equilibrium dynamics is also rather more intricate than in the models with diffusing defects ($f = 1$); the East model again provides a simple example, with the up-spin concentration after a quench decaying as an anomalous power law $\sim t^{-T \ln 2}$ with a temperature-dependent exponent (see section 5.4.1).

Work on **out-of-equilibrium correlation and response functions** of SFMs and their variants is rather more recent, and we do not yet have a coherent picture of fluctuation–dissipation theorem (FDT) violations in these models and the corresponding effective temperatures; see section 5.4 for details. One complication is that response functions in these models can be non-monotonic. In the 1, 1-SFM, for example, only spins that are next to an up-spin are mobile and can contribute to the response to an applied field; after a quench the number of such spins decreases in time with the total up-spin concentration. The response for any *given* spin increases with time after the field has been switched on, but the decrease in the number of spins that can respond makes the overall response non-monotonic. In an appropriate representation, FDT plots for some observables can nevertheless be well-behaved; a recent study for the 1, 1-SFM found, surprisingly, that even trivial equilibrium FDT plots can result [46] (though subtleties remain; see section 5.4.3). Whether FDT relations can be used to define physically meaningful effective temperatures in these models remains largely an open questions; static definitions of an effective temperature (e.g. via configurational entropies, see section 5.6) do not appear to be useful.

SFMs have also yielded insights into the cooperative nature of glassy dynamics, and the existence of **dynamical heterogeneities**, with most work having been done on the 2, 2-SFM (see section 5.5). Simulations have confirmed [93, 94] the intuitive scenario described above, showing regions of inactive sites which remain frozen until 'mobility is propagated' to them via a cooperative sequence of spin flips from active sites, i.e. mobile spins, elsewhere in the lattice. See figure 27 below. A number of definitions for dynamical lengthscales have also been investigated, one of them being the typical distance between the (only vaguely defined) active sites referred to above. Relaxation timescales were found to increase as a power law with this lengthscale to good approximation, with a large exponent, giving very long timescales even for modest dynamical lengths. Future work on SFMs should help to identify more precise definitions of dynamical lengthscales and shed more light on the role of dynamical heterogeneities in glassy dynamics.

We mention finally that a number of recent studies have considered SFMs as abstract models for **granular dynamics**, studying the behaviour under a sequence of 'taps' (modelled by evolution at $T > 0$, for example, followed by relaxation at

$T = 0$). This approach has yielded insights into logarithmic compaction (see section 5.7). In some circumstances the resulting non-equilibrium stationary states can also be described in terms of effective equilibrium using Edwards measures, but much remains to be done to rationalize when and why this approach works.

3.2. *Variations on spin-facilitated models*

SFMs have inspired a number of variations, which we review in the present section.

A variation of the SFMs with added 'mean-field' facilitation was introduced in [95]: spins can flip if either at least f of their neighbours are up, *or* if the overall concentration of up-spins in the system is greater than some threshold c_{th}. If the model without the added facilitation is reducible, such as in the case of the 2, 1-SFM, then the extended model has a sharp dynamical transition when the concentration of up-spins reaches c_{th}; for lower concentrations (i.e. lower T) the chain splits into segments consisting of frozen and mobile spins, respectively. A more detailed analysis of the dynamics has not been performed, however; the model also goes somewhat against the philosophy of KCMs by introducing a global restriction instead of a local one. (Global constraints arise in some other models related to KCMs, but are then motivated by global conservation laws; see section 3.7.)

Variations on SFMs involving quenched disorder have also been considered. Schulz and Donth [96], for example, considered a $2,2$-SFM with locally varying quenched couplings J_{ij} and fields h_i. This gives corresponding locally varying timescales for spin flips, thus broadening out the spectrum of the faster β-processes which involve only a few spin flips. For the slow α-processes, on the other hand, which rely on cooperative flips of a large number of spins, the local timescale variations tend to average out and so a single dominant α-timescale is retained. Willart *et al*. considered an SFM in $d = 2$ with $f = 1.5$, defined by assigning $f = 1$ to a randomly chosen set of half the lattice sites, and $f = 2$ to the remaining sites [97]; again, these assignments are quenched, i.e. fixed during the course of a simulation.

Schulz, Schulz and Trimper considered a model with two species coupled together, spins and 'ion concentrations' [98]. The motivation comes from the so-called mixed mobile ion effect, a strong nonlinear dependence of the conductivity in strong covalently bonded glasses (such as SiO_2) on the composition ratio of two different species of alkali ions included. In this model there are two two-state variables at each lattice site, $n_i = 0, 1$ for immobile and mobile regions as before and r_i for the two types of cations. Introducing a kinetic constraint for the r_i similar to that for the n_i, which forbids diffusion of ions in a locally homogeneous environment, the authors indeed found the expected strong variation of the diffusivity with the composition ratio of cations.

Schulz and Reineker [99] considered a variation on $2,2$-SFMs that allows, beyond $n_i = 0, 1$, a third state at each lattice site to model local 'vacancies'. These vacancies are introduced to allow fast local relaxation processes, and so are postulated to lift the kinetic constraint on all their neighbours; vacancies are also allowed to diffuse through the lattice at some constant rate by changing place with neighbouring up-spins. At low temperatures the unconstrained relaxation near vacancies, with its almost temperature-independent timescale, is faster than the highly cooperative dynamics that does not rely on vacancies. This fast process—whose existence can also be deduced from simple mean-field approximations [100]—produces a plateau in correlation functions and can be likened to the β-relaxation

observed in structural glasses [99]. A disadvantage is that also the long-time ('α') behaviour loses its cooperative aspects and becomes dominated by the diffusion of vacancies through the lattice, with relaxation times exhibiting simple Arrhenius behaviour [99].

For ferromagnetic spin systems, many different kinds of kinetic constraints have been considered, mainly for the Ising chain in zero field with energy function $E = -J \sum_i \sigma_i \sigma_{i+1}$ in terms of conventional spins $\sigma_i = \pm 1$. In fact, already Kawasaki dynamics, where the only allowed transitions are the exchange of neighbouring spins with opposite orientation and the up-spin concentration is therefore conserved, can be thought of as a kind of kinetic constraint. It does give rise to some glassy features, e.g. freezing into non-equilibrium domain structures when the system is cooled sufficiently rapidly [101]. Skinner [102], in the context of an abstract model for polymer dynamics, considered Glauber dynamics with the constraint that spins can flip only if they have exactly one up and one down neighbour. This is equivalent to evolution at constant energy, leading to a random walk of a fixed number of domain walls that can neither cross nor annihilate. Because of the fixed energy restriction, the model cannot be used to study out-of-equilibrium relaxation, but Skinner [102] predicted using an approximate calculation that the spin–spin autocorrelation function in equilibrium at low temperatures should have a stretched exponential decay $\sim \exp(-t^b)$ with exponent $b = 1/2$. The value of the exponent, which was later obtained rigorously as the true asymptotic behaviour [103], is related to the diffusive motion of the domain walls and also appears in similar defect-diffusion models [89, 90]. (Intuitively, the exponent $b = 1/2$ arises since a given spin relaxes within time t if there are initially domain walls present within the diffusion distance $d \sim t^{1/2}$, and the probability for this to be the case decays exponentially with d.) The model can be extended by relaxing the constraint; spins with two identical neighbours can then flip but at a reduced rate. Numerical results again show a stretched exponential decay, but with stretching exponent $b > 1/2$ [104].

In Skinner's [102] model, spins are constrained to be immobile if their two neighbours are either both up or both down. Recently, Majumdar *et al.* [105] considered a weaker constraint where only spins with two *up-spin* neighbours are prevented from flipping. While the energy function is still that of an Ising chain in zero field, the kinetic constraint breaks the symmetry between up- and down-spins and this has interesting consequences for the coarsening behaviour at low temperatures which are described in section 5.4.1.

An approach opposite to that of Skinner has also been taken, by considering an Ising chain where spin flips which do *not* change the energy are forbidden; only spins with two equal neighbours can flip. In the $T = 0$ limit the only allowed transitions are then those which lower the energy, i.e. flips of up-spins sandwiched between two down-spins or vice versa [106–109]. This 'falling' dynamics has also been considered on more complicated structures such as ferromagnets on random graphs where each spin is linked to a fixed number of randomly chosen neighbours [107]. Even at $T > 0$, the constraint that the energy must change in a move is strong enough to make the dynamics reducible; a domain of an even number of up-spins surrounded by all down-spins, for example, can never be eliminated. The main interest in these models therefore arises when the falling dynamics is coupled with periodic excitations (e.g. 'tapping' by random spin flips) that restore an element of ergodicity; see section 5.7.

3.3. *Lattice gas models*

The spin-facilitated models discussed so far do not conserve the number of up-spins, which model mobile low-density regions in the material. But in structural glasses the overall particle number and hence density is conserved. To model this situation more directly, lattice gases with kinetic constraints have been defined. Here particles occupy the sites of a finite-dimensional lattice and can move to nearest neighbour sites according to some dynamical rules; each site can be occupied by at most one particle. In some sense these are the simplest KCMs because all allowed configurations have the same energy and the same Boltzmann weight so the energy landscape is trivial. Kob and Andersen (KA) [88] introduced the simplest of these models, originally for particles on a cubic lattice. Particles move to empty nearest neighbour sites with unit rates, subject to the condition that the particle has fewer than m occupied neighbour sites both *before and after* the move. (The parameter m as defined here is larger by one than that of [88]; our choice has the advantage that the same m appears in the bootstrap percolation problem closely related to the irreducibility of the KA model.) The restriction on the number of neighbours after the move is necessary to ensure detailed balance. The choice of m determines the strength of the kinetic constraint. For $m = 6$, the model is unconstrained while for $m = 3$ it would clearly be strongly reducible: any set of eight particles occupying the sites of a $2 \times 2 \times 2$ cube could never move, all particles having at least three neighbours whether or not sites around the cube are occupied. KA chose the smallest value, $m = 4$, which does not produce such obvious reducibility effects, and this defines the standard KA model. The intuition behind the kind of kinetic constraint imposed is that if particles are 'caged in' by having too many neighbours, they will not be able to move. KA originally proposed the model to test the MCT for supercooled liquids [16–19], which is based mainly on this caging effect, but found surprisingly poor agreement. The model has nevertheless been intensively studied, with several variants proposed recently as reviewed below.

It is worth pointing out that if we let $n_i = 1$ for sites i that are occupied by a particle and $n_i = 0$ for those that are not, then the KA model with $m = 4$ is actually very similar to a 3, 3-SFM with Kawasaki dynamics; the exchange of neighbouring up- and down-spins is equivalent to moving a particle. Notice however that the facilitating states are now the 'holes' $n_i = 0$, corresponding to down-spins rather than up-spins. (A second distinction is that in order to preserve detailed balance, motion is allowed if the up-spin of the pair to be exchanged has at least $6 - m + 1 = 3$ down-spin neighbours and if the down-spin has at least two down-spin neighbours.) Due to the facilitation by holes, the glassy regime in the KA model occurs at high particle density $c = \langle n_i \rangle \approx 1$, while in the SFMs it corresponds to $c \approx 0$. Finally, if a configuration in the KA model is described using the n_i, it is clear that the particles are treated as indistinguishable; this is appropriate for studying the behaviour of density fluctuations, for example. However, for observables related to self-diffusion, concerning e.g. the average displacement of a given particle over some time interval, particles need to be distinguished one from the other and a configuration is then specified by giving the position vector (or site number) for each particle.

In the KA model as described above the total number of particles is conserved, and since we have a lattice model so is therefore the particle density. This makes it difficult to study ageing effects where the density evolves with time. One might wish to study, for example, the behaviour following an instantaneous quench (or better

crunch) to a higher density of particles. An extension of the KA model for this purpose was introduced in [110]. (See also [111] for a related model with a global kinetic constraint.) Here particle exchange with a reservoir is allowed in one designated plane of the lattice. This can be thought of as the 'surface', although periodic boundaries are maintained so that one effectively has a slab of material between two parallel surfaces in contact with the reservoir. The rates for eliminating and introducing a particle in this layer are $e^{-\mu}$ and 1, respectively, corresponding to a reservoir at chemical potential μ (with the inverse temperature fixed to $\beta = 1$). The dynamics obeys detailed balance with respect to the energy function $E = -\mu \sum_i n_i$, and the equilibrium particle density is

$$c_{\mathrm{eq}} = 1/(1 + e^{-\mu}). \tag{35}$$

A crunch can be obtained by increasing μ; to have meaningful results for a bulk system one then needs to check, however, that the density does not exhibit strong inhomogeneities. This grand canonical version of the KA-model can alternatively be thought of as canonical [112], with $1/\mu$ and $1/c$ respectively corresponding roughly to temperature T and energy E in a system that is brought into the glassy region by lowering temperature. A recent overview of relevant results for the grand canonical KA model can be found in [112]. An attractive feature of allowing particle exchange with a reservoir is that many more configurations become mutually accessible, if necessary by first removing particles one by one and then reinserting them; this significantly weakens reducibility effects (see section 5.1).

A model similar to the KA lattice gas, on a two-dimensional triangular lattice, was considered by [113]; reviews of the main results for this model, as well as the hard-square lattice gas (see section 3.7) can be found in [86, 114]. The constraint here is that the two sites which are nearest neighbours of both the departure and the arrival site—in other words, the sites adjoining the 'hop path'—are empty; see figure 11. This two-vacancy assisted hopping model, called a triangular lattice gas

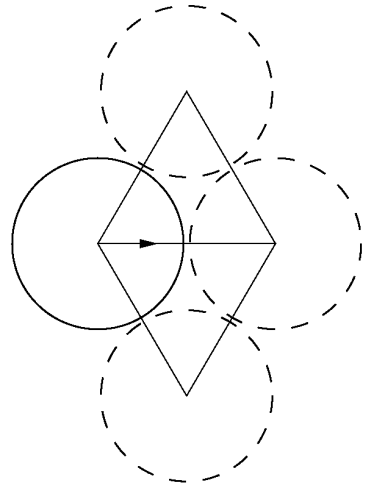

Figure 11. Hop path in the triangular (two-vacancy-assisted) lattice gas. The particle indicated by the full-line circle can hop to the neighbouring site along the path indicated by the arrow only if the three sites surrounded by the dashed circles are free. From [86]. Copyright Institute of Physics Publishing.

below for short, was found to display typical glassy features. However, if the constraint is relaxed from two vacancies to one, these largely disappear [113]: pairs of vacancies can then diffuse freely even in an otherwise fully occupied lattice, since each vacancy in a pair can rotate around the other one. A generalization of two-vacancy assisted hopping to a three-dimensional face-centred cubic lattice has also been suggested [113]; hopping is again between nearest neighbour sites and vacancies are required on all four sites adjoining the hop path. Since the hop path and two of the vacancies are within a triangular lattice plane, in crystallographic (111) orientation, the constraint includes the one for the two-dimensional model and so would be expected to lead to even more pronounced glassy effects. Finally, for the two-dimensional two-vacancy assisted model an extension to particles with orientational degrees of freedom has been proposed [115]. The rules for translational motion are as before. The kinetic restriction on rotational motion can best be visualized if one thinks of the particles as 'lemons', i.e. hard discs with small noses on opposite sides; a rotation of one such lemon by $\pi/3$ is allowed only if the two neighbouring sites located along the direction between the old and the new orientation are empty (otherwise the noses would get stuck). Orientations are randomly distributed in equilibrium, but the kinetic constraint couples orientational fluctuations to the translational motion.

A model similar to one-vacancy assisted hopping, but on a d-dimensional hypercubic lattice, was studied in [116]. There, the hopping rate was taken to be proportional to the number of vacancies on the n.n. sites surrounding the hop path; hops are therefore allowed only if at least one such vacancy is present. Unfortunately the analysis of this model given in [116] was flawed since it involved an approximation which violates conservation of particle number.

Finally, the KA model has recently been generalized to include the effects of gravity [117]. Here the energy of a configuration is (setting particle mass and gravitational acceleration to unity)

$$E = \sum_i h_i n_i \tag{36}$$

with h_i the height of site i. The kinetic constraints are of the same kind as in the KA model—in [117], for example, a b.c.c. (body-centred cubic) lattice with $m = 5$ was used—but the non-zero transition rates now take energy changes into account when particles move up or down. Such models are particularly useful for studying glassy effects in granular materials, where gravity is important in driving phenomena such as compaction. As explained in section 2.6, the temperature T used in this context is not the thermodynamic one but should rather be regarded as representing some external excitation of the material, e.g. by vibration or vertical tapping.

3.3.1. *Some results for lattice gas models*

This section is again intended for quick readers and summarizes important results for the constrained lattice gas models. Details can be found in section 5.

The KA model has been studied mainly on cubic lattices in $d = 3$, with the constraint parameter set to $m = 4$ (so that particles with four or more neighbours are unable to move). As in the case of spin-facilitated models (see section 3.1.1), one has to be careful with **reducibility effects** in finite-sized systems. The analogue of a configuration belonging to the high-temperature partition is, in a lattice gas, that all particles should be able to move throughout the whole lattice eventually, i.e. that no

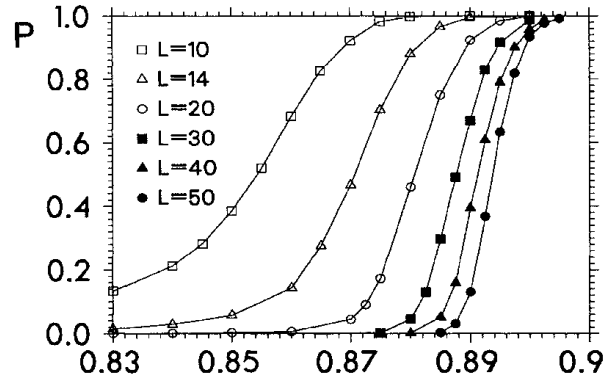

Figure 12. Plot of the probability that a randomly chosen configuration of the KA model has a backbone of frozen particles, against particle density c for a range of linear lattice sizes L as shown. From [88]. Copyright American Physical Society.

particles are permanently blocked. KA [88] suggested that one could define a 'backbone' of frozen particles by iteratively removing particles from the system until all remaining particles are frozen; this in principle only gives a lower bound on the number of frozen particles in the system but in fact turns out to be an accurate approximation (see section 5.1). An example of a backbone would be a 2×2 tube of particles that stretches across a finite system and, due to periodic boundary conditions, connects back onto itself; there could also be several such tubes with 'bridges' between them, etc. Figure 12 shows the probability $p = p(c, L)$ for a random configuration of density c on a lattice of linear size L to contain a backbone. One sees that linear sizes of $L \approx 20$ are sufficient to have negligible reducibility effects up to $c = 0.86$, but that even for slightly larger densities (e.g. $c = 0.89$) much larger systems are needed. This is consistent with theoretical estimates. These are based on the close link between the iterative process that defines the backbone and so-called bootstrap percolation (see section 4.1) and predict that the threshold density $c_*(L)$ for which $p(c, L) = 1/2$ converges to one only as $1 - c_*(L) \sim 1/\ln(\ln L)$ or even more slowly; conversely, the system size L required for effective irreducibility diverges as a *double* exponential of $1/(1 - c)$ for $c \to 1$.

To investigate the slowing down of the (equilibrium) dynamics with increasing density, KA calculated the self-diffusion constant D_s from the measured mean-squared displacement of particles as a function of time; see after (14). The results are shown in figure 13 and suggest that D_s vanishes at $c_{dyn} \simeq 0.881$ according to a power law $D_s \sim (c_{dyn} - c)^{\phi}$ with $\phi \simeq 3.1$. Data for D_s in the triangular lattice gas could also be fitted with the same functional form [113], though there an alternative form $D_s \sim \exp[-A/(1 - c)]$ which predicts no dynamical transition at any $c < 1$ also provided a good fit; see section 5.2.

Equilibrium relaxation functions have also been studied for constrained lattice gases. KA [88] considered an analogue of the intermediate self-scattering function C_s (14), modified suitably to take into account the lattice symmetry. The modification consists in replacing $\exp(i\mathbf{k} \cdot \Delta\mathbf{r})$ in (14) (where $\Delta\mathbf{r} \equiv \mathbf{r}_a(t) - \mathbf{r}_a(0)$ for short) by $(1/3)[\exp(ik\Delta x) + \exp(ik\Delta y) + \exp(ik\Delta z)]$; in the corresponding van Hove correlation function (15) this means that particle displacements are measured in terms of the number of lattice planes traversed in the x-, y- or z-direction. Typical results for the

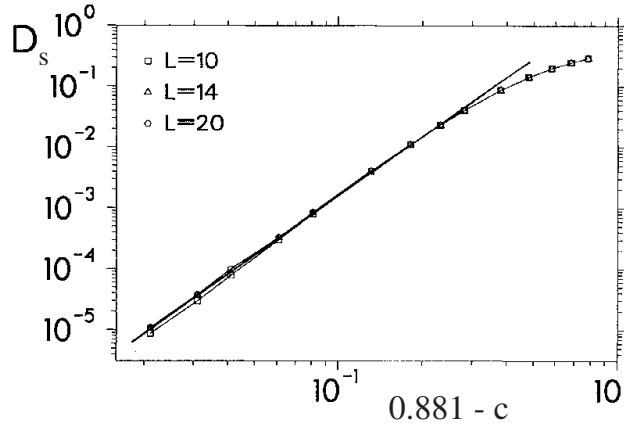

Figure 13. Self-diffusion constant D_s in the KA model as a function of $c_{dyn} - c$, for system sizes L as shown. From [88]. Copyright American Physical Society.

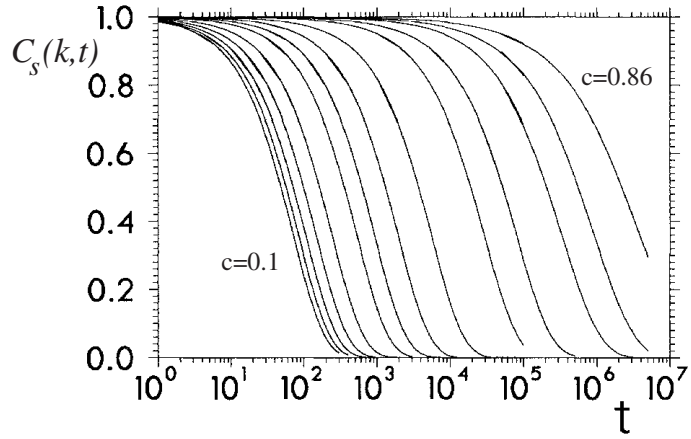

Figure 14. Self-intermediate scattering function in the KA model plotted against time, for the smallest possible 'wavevector' $k = 2\pi/L$ and a range of densities c. Notice the absence of a two-step relaxation with intermediate plateau even at high density. From [88]. Copyright American Physical Society.

shortest 'wavevector' $k = 2\pi/L$ are shown in figure 14 for a range of densities; KA found that for the higher densities the long-time decay is well described by a stretched exponential. At shorter times, the absence of an intermediate plateau, and thus of a clear separation into β- and α-relaxation, is notable; KA argued that the β relaxation was either absent or very weak (giving a plateau too close to the initial value to be visible) because in the KA model particles either diffuse or are completely stuck, rather than initially 'rattling' in cages formed by their neighbours. (Intriguingly, the *triangular* lattice gas *does* exhibit two-step relaxations [118]; see section 5.3.) The density dependence of the relaxation time τ extracted from the self-intermediate scattering function depends on the wavevector k. KA [88] found that for the largest $k = \pi$, corresponding to distances of the order of the lattice spacing, τ diverged as a power law $\tau \sim (c_{dyn} - c)^{-\phi'}$, with a value of $c_{dyn} \simeq 0.88$ compatible

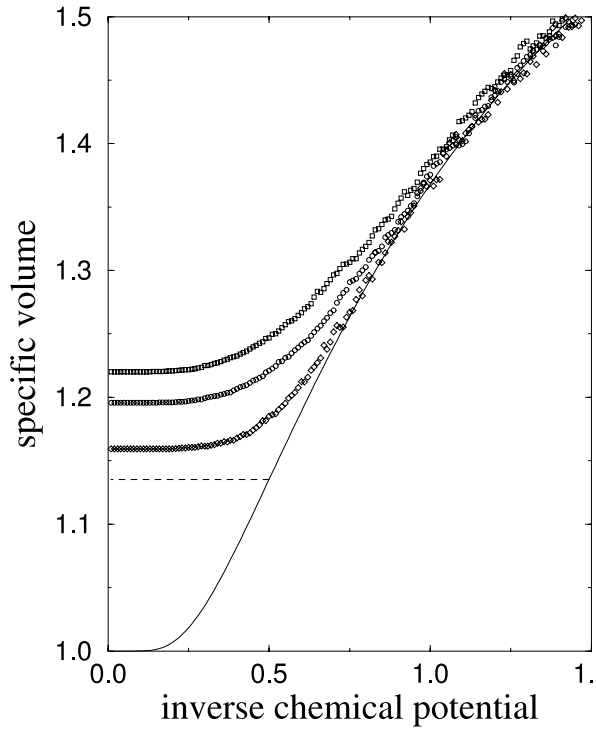

Figure 15. Density as a function of chemical potential in the grand canonical KA model. (Plotted is the inverse density, i.e. the specific volume, versus the inverse chemical potential, to emphasize the analogy with plots of E versus T.) The analogue of a cooling run is shown, where the chemical potential of the particle reservoir is increased gradually over time; the curves from top to bottom correspond to decreasing 'cooling' rates. Notice that the system falls out of equilibrium when the inverse density approaches $1/c_{\mathrm{dyn}} \approx 1/0.881 \approx 1.135$ (dashed line). From [110].

with that estimated from the self-diffusion constant but with a different exponent $\phi' \simeq 5$.

More recently, **out-of-equilibrium effects** in constrained lattice gases have also been investigated (see section 5.4 for details), using the versions of the KA model where either particle exchange with a reservoir is allowed or the particle density can change under the influence of gravity. Typical glassy features are observed. For example, the analogue of cooling rate effects have been investigated in the grand canonical model by gradually increasing the reservoir chemical potential [110]. Typical results are shown in figure 15; as the system becomes more compressed, the density appears to get stuck around c_{dyn} even though the chemical potential is increased further, demonstrating that the system falls out of equilibrium. Cyclical compression and decompression then also lead to hysteresis effects. Sudden 'crunches', i.e. increases in chemical potential, have been studied as well and result in slow power-law relaxation of the density. If during this relaxation mean-square particle displacements and the conjugate two-time response function are measured, one finds the remarkable result that the FDT plot has a simple 'mean field' form, consisting of two straight line segments; and the slope of the out-of-equilibrium part can be understood on the basis of an appropriate flat Edwards measure over frozen

configurations (see section 5.6). These exciting results are only a beginning, however, and much remains to be done to understand the origin of such apparent mean-field behaviour.

3.4. *Constrained models on hierarchical structures*

Almost simultaneously with the first proposal of SFMs by Fredrickson and Andersen, Palmer *et al.* introduced the idea of a whole *hierarchy* of kinetic constraints, in a paper [119] that has been instrumental in establishing the conceptual basis of the field of KCMs.

In the model of [119] the microscopic degrees of freedom are represented by spins that live on a hierarchical tree (figure 16) containing N_l spins at levels numbered by $l = 0, 1, \ldots$; N_l decreases as one moves up in the hierarchy with increasing l. Although initially devoid of any microscopic interpretation the spins can be thought of as representing cooperative regions in a glass of lengthscales increasing with l, with the bottom level 0 corresponding to the dynamics of single spins or particles. The relaxation time of large regions should depend on that of smaller ones, and this is modelled by assuming that a spin in level $l+1$ can relax only if a given set of μ_l facilitating spins in level l are in one particular configuration out of the 2^{μ_l} possible ones. If the spins are assumed to be up or down with equal probability, the typical relaxation time for the spins in level $l+1$ is

$$\tau_{l+1} = 2^{\mu_l}\tau_l \tag{37}$$

which gives

$$\tau_l = \tau_0 \exp\left[(\ln 2)\sum_{k=0}^{l-1}\mu_k\right]. \tag{38}$$

If N is the total number of spins and $w_l = N_l/N$ is the fraction at level l, then the equilibrium correlation function can be estimated by averaging the autocorrelation over all spins, i.e. over all levels, giving

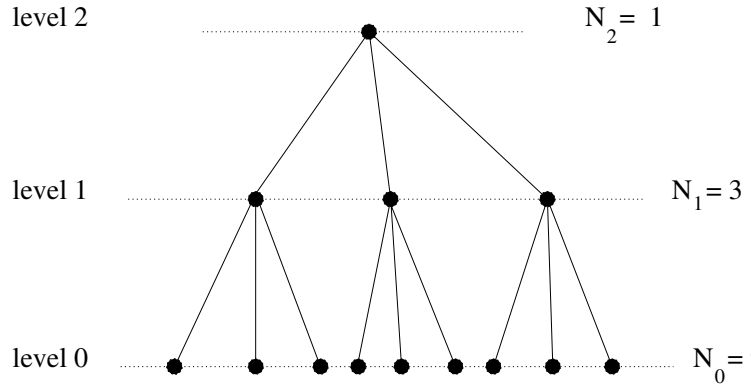

Figure 16. A hierarchical tree with three levels $n = 0, 1, 2$ containing $N_0 = 9$, $N_1 = 3$ and $N_2 = 1$ spins respectively. The spins on level 0 have a short relaxation time τ_0. Spins on level 1 relax more slowly because each is constrained by the configuration of $\mu_0 = 3$ specific spins in the level below, as indicated by the solid lines. The top spin on level 2 is similarly constrained by the $\mu_1 = 3$ spins in level 1. The connectivity shown here is that of a Cayley tree; Palmer *et al.* [119] also allowed for more general cases where a given spin can act as facilitator for more than one spin in the next level above.

$$C(t) = \sum_{l=0}^{\infty} w_l \exp(-t/\tau_l) \tag{39}$$

for a hierarchy with infinitely many levels. (A formally similar solution was also found by Ogielski and Stein in a model of particle hopping on hierarchical structures [120].) Palmer *et al.* [121] argued that since realistic systems are not expected to have the assumed sharp partitioning into discrete levels, one could equally or better regard l as a continuous variable and replace the sum in (39) by an integral; see also [122]. They investigated the asymptotic behaviour of the correlation function for different choices of w_l and μ_l [119]. In particular, assuming $\mu_l = \mu_0/l^p$ and $w_l = w_0/\lambda^l$ (with $\lambda > 1$) they found stretched exponential behaviour for the correlation function. The maximum relaxation time, obtained from (38) for $l \to \infty$, is $\tau_{\max} = \tau_0 \exp[(\mu_0 \ln 2)/(p-1)]$ which is reminiscent of the VTF law (2) if p depends on temperature and vanishes linearly with T in the vicinity of T_0. If one instead assumes that $\mu_l \propto w_l$ at all levels, then the correlation function shows a slow logarithmic decay in an intermediate time regime, independently of the precise l-dependence of w_l [123]. The effects of heating and cooling cycles have also recently been investigated in an appropriate generalization [124] of the hierarchical model.

The models discussed above have been very influential conceptually, in emphasizing that glassy dynamics could be caused by kinetic constraints linking a hierarchy of degrees of freedom. However, the large number of parameters μ_l and w_l, which are difficult to assign on physical grounds, is a drawback if one wants to make quantitative statements about the behaviour of these models. We will therefore omit them from further discussion. One interesting special case that we will cover, however, is the $(a, a-1)$ Cayley tree model discussed in section 3.1. This can be regarded as a concrete realization of the hierarchical scenario discussed above: in the Cayley tree there is a finite number of levels $l = 0 \ldots L$, with $N_l = (a-1)^{L-l}$, $\mu_l = a - 1$, and the sets of spins in each level that facilitate the relaxation of different spins in the level above are chosen so that they do not overlap each other. Notice however that the approach by Palmer *et al.* effectively fixes the up-spin concentration to $c_{\mathrm{eq}} = 1/2$ (corresponding to infinite temperature), while this is normally regarded as an important tunable parameter in the Cayley tree models.

3.5. *Models inspired by cellular structures*

Kinetically constrained models have also been inspired by the study of soap froths and other cellular patterns. These models incorporate topological constraints as kinetic restrictions in the transition rules. (They also have some similarities with tiling models, see section 3.7.5 but, especially in the lattice versions discussed below, are more amenable to analytical investigation.) The simplest cellular pattern in the plane is a hexagonal tiling, comprising only six-sided cells that have six neighbours each. However, most cellular structures in nature, such as froths and biological tissue, are disordered. Aste and Sherrington [125] proposed a model which only keeps track of the topology of the cellular structure, i.e. of which cells are neighbours to each other; see figure 17(a). If cell i has n_i sides, then the average value of n_i is six from the Euler theorem; in the perfect hexagonal arrangement, one even has $n_i = 6$ for each individual cell. The deviation from this arrangement can be characterized by an energy function

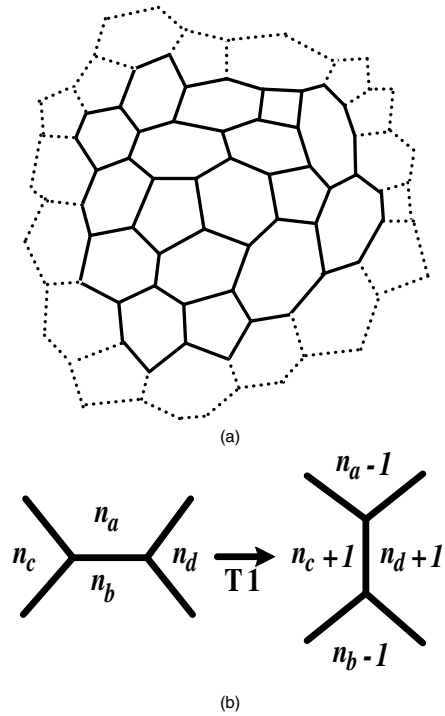

Figure 17. (a) A topological froth. (b) A T1 or neighbour-switching move, in which two cells gain one edge and two others lose one edge. From [125]. Copyright Institute of Physics Publishing.

$$E = \sum_i (n_i - 6)^2 \tag{40}$$

which contains no interactions. The kinetic constraint arises from the fact that the only allowed transitions are so-called T1 moves, where four cells exchange neighbours; see figure 17(b). Two cells thus gain an edge, while the other two lose an edge, and a proposed move is accepted with the usual Glauber probability $1/[1 + \exp(\beta \Delta E)]$. For high temperatures, the equilibrium structure of the cellular pattern is disordered, with many cells with $n_i \neq 6$. As $T \to 0$, on the other hand, only a small number of pentagonal ($n_i = 5$) and heptagonal ($n_i = 7$) cells, effectively defects in a hexagonal structure, are present. There are then very few moves which do not increase the energy, and the dynamics becomes dominated by activated processes. The only freely diffusing defect structures are in fact 5-7 pairs of cells [126], which can annihilate when they meet or be absorbed by isolated pentagons or heptagons.

The topological froth model discussed above has the complication that its equilibrium behaviour is non-trivial to work out, requiring a sum over all possible topological arrangements of cells. The situation is clearer in a lattice analogue which has genuinely trivial equilibrium behaviour. In this lattice model, three-state spins $\sigma_i \in \{-1, 0, 1\}$ occupy the cells of a hexagonal lattice [127, 128]. The σ_i correspond to the local deviations $n_i - 6$ from the optimal hexagonal structure in the off-lattice model. The energy is therefore defined as

$$E = \sum_i \sigma_i^2. \tag{41}$$

The initial configuration is chosen so that $\sum_i \sigma_i = 0$ (in analogy with $\langle n_i \rangle = 6$). The kinetic constraint is modelled on that of the off-lattice model: the only allowed transitions are those in which the spins in two neighbouring cells are increased by one and the spins in their two common neighbours decreased by one, or vice versa. Moves that would produce spins outside the range $-1, 0, 1$ are of course forbidden. At low temperatures in this model, 'dimers' composed of a $+1$-spin and a -1-spin can diffuse (in a zig-zag motion) across a background of largely 0-spins. These are the analogues of the 5-7 pairs of the topological model. They come in six different possible orientations, and can annihilate with an 'anti-dimer' of the opposite orientation when they meet, or be absorbed by isolated defects, i.e. ± 1-spins. Dimer diffusion dominates the fast dynamics of the model. On longer, activated timescales, isolated defects themselves can diffuse by creating freely diffusing dimers at an energy cost of $\Delta E = 2$. Overall, the model produces glassy phenomena similar to the original off-lattice version. A variant with $E = -\sum_i \sigma_i^2$ has also been considered; this is still non-interacting but has a highly degenerate ground state, leading to subtle modifications of the low-temperature behaviour detailed in [127]. Finally, the model can be further simplified by using a square rather than hexagonal lattice, without qualitatively changing the behaviour [128].

It is clear from this overview that the above models inspired by cellular structures can all be understood by mappings to defects which can diffuse and 'react' with each other; this reaction–diffusion behaviour gives rise to characteristic power-laws in the relaxation functions. The timescales involved are activated, so that these KCMs are appropriate for modelling strong glasses. As explained for the model (41), two separate timescales can be involved and give two-step relaxations, as well as ageing effects when the longest timescale exceeds the experimental or simulation time window.

3.6. *Models with effective kinetic constraints*

Recently it has been realized that there exists a class of models which are conventionally formulated in terms of non-trivial energy functions and unconstrained dynamics, but which can be mapped to non-interacting defects with constrained dynamics; see [129] for a review. The simplest example is a Glauber Ising chain, with energy function

$$E = -J \sum_i \sigma_i \sigma_{i+1} \tag{42}$$

in terms of conventional spins $\sigma_i = \pm 1$. One can introduce defect variables $n_i = (1 - \sigma_i \sigma_{i+1})/2$, with $n_i = 0$ and $n_i = 1$ corresponding to the absence and presence of a domain wall, respectively. Importantly, the mapping from the σ_i to the n_i is one-to-one—subject to appropriate boundary conditions, e.g. an open chain with the left spin fixed—so that either set of variables can be used to specify a configuration. The mapping to defect variables has two consequences. On the one hand, the energy becomes $E = 2J \sum_i n_i$ up to a constant, so that the defects are non-interacting. On the other hand, while the dynamics is simple in terms of spin flips, it is effectively constrained in terms of the n_i since only simultaneous changes of pairs of neighbouring n_i's are allowed.

More interesting than the trivial Ising chain example are higher-dimensional models. In $d = 2$, there are two cases where a one-to-one mapping to defects is possible, subject again to appropriate boundary conditions [129]. The 'triangle model' has spins on a triangular lattice with triplet interactions in the *downward* pointing triangles only [130, 131]

$$E = -J \sum_{ijk \in \bigtriangledown} \sigma_i \sigma_j \sigma_k. \tag{43}$$

The defect variables $n_i = (1 - \sigma_i \sigma_j \sigma_k)/2$ live on the centres of the downward triangles, which themselves form a dual triangular lattice that is isomorphic to the original one; the energy is again $E = 2J \sum_i n_i$ up to a constant. Spin flip dynamics in the original model implies that the only allowed transitions between defect configurations are the inversions of three n_i at the corners of any *upward* pointing elementary triangle of the dual lattice. At low temperatures, where most defects ($n_i = 1$) are isolated, this constraint slows the dynamics: flipping any triangle of defect variables then leads to a state with an additional defect, and requires an activation over the energy barrier $2J$. In fact, one can show that there is a whole hierarchy of energy barriers, and an associated hierarchy of slow timescales, arising from the relaxation of defects arranged in the corners of equilateral triangles with side length a power of two. As discussed in detail in section 5.4.1, the situation is in fact very similar to that in the East model, and the longest relaxation timescale exhibits an EITS divergence characteristic of fragile glasses.

A second model in $d = 2$ has plaquette interactions on a square lattice [132, 133]

$$E = -J \sum_{ijkl \in \square} \sigma_i \sigma_j \sigma_k \sigma_l \tag{44}$$

with defect variables $n_i = (1 - \sigma_i \sigma_j \sigma_k \sigma_l)/2$ sitting on the dual square lattice, and elementary moves being the simultaneous flipping of four defects around a plaquette of the dual lattice. The seemingly innocent change of lattice structure from the triangle model has a profound effect on the dynamics: two neighbouring defects along one of the lattice directions can now diffuse freely along the orthogonal direction, and the diffusion of these defect-pairs gives the model strong glass characteristics, with timescales growing only in an Arrhenius fashion as temperature is lowered.

In three dimensions, models similar to those above could be constructed on, e.g. an f.c.c. (face-centred cubic) lattice with four-spin interactions on downward-pointing tetrahedra, or a cubic lattice with eight-spin interactions between spins around the elementary cubes [129]. We note in passing that closely related to the $d = 2$ plaquette model are the so-called gonihedric spin models, which normally include additional two-spin interactions and exhibit some glassy features as well as interesting metastability effects [134–137].

In terms of the defect variables, the static equilibrium behaviour of the above models is of course trivial. In the following, we always assume that the coupling J in the original model is chosen so that $E = \sum_i n_i$ in terms of the defect variables, giving again $c = \langle n_i \rangle = 1/(1 + e^{\beta})$. The equilibrium properties of the underlying spin system can be worked out from that of the n_i. In particular, one finds that $\langle \sigma_i \rangle = 0$ and that spin correlation functions are non-vanishing only if they can be expressed as a product of a finite number of defects (or, more precisely, of the variables $2n_i - 1 \in \{-1, +1\}$). In the triangle model, for example, the simplest non-

vanishing correlation function is that of the three spins at the corners of an elementary downward triangle [131].

It is clear that, in the description in terms of defect variables, the triangle and plaquette models are quite similar to the lattice versions of the topological froth described in the previous section: only certain groups of the elementary variables are allowed to flip together. An advantage is that these kinetic constraints are not imposed ad hoc, but result naturally from the dynamics of the underlying spin system. For uniformity of terminology, we will normally refer to the defect variables n_i as spins when no confusion with the variables σ_i of the underlying unconstrained spin system is possible.

3.7. *Related models without explicit kinetic constraints*

This section gives an overview of some models which do not strictly have kinetic constraints but which in many cases share some features of KCMs. In some cases the thermodynamics of these models may not be trivial, in other cases it is very simple although the system may present a critical point, for instance at zero-temperature. A simplifying feature of the models discussed in this section is that the dynamics is normally trivially irreducible.

3.7.1. *Ordinary Ising models*

Ordinary Ising models with ferromagnetic nearest-neighbour interactions and Glauber dynamics are the 'baseline' models for SFMs. In spite of the absence of kinetic constraints, they display some features associated with glassy dynamics, especially when quenched to low temperatures near or below their critical points; see, e.g. [138] for a recent overview. The simplest example is the one-dimensional Glauber chain, for which many exact results were already found by Glauber himself [139]; in fact a fully exact diagonalization of the master equation can be obtained via a mapping to free fermions [140]. The critical point is at $T_c = 0$, where the model coarsens by diffusion and annihilation of domains walls, with the typical domain size growing as $l(t) \sim t^{1/2}$. Two-time correlation and response functions obey simple scaling with t_w/t, or equivalently with $l(t_w)/l(t)$ (see, e.g. [141–143]) as expected from general arguments for coarsening models [144]. A non-trivial FDT plot is obtained in the limit of long times [142, 143] but is non-trivially dependent on the observable considered [45, 145]. In equilibrium at low but non-zero temperatures, relaxation functions also show stretched exponential behaviour at intermediate times [146]; hysteresis effects are found when the system is heated and cooled cyclically (see section 5.4.2). In higher dimensions, finally, coarsening at $T = T_c > 0$ and below T_c need to be distinguished and give different scaling relations for two-time quantities [138, 147].

3.7.2. *Urn models*

This category of models has recently received considerable attention. Urn models do not contain local kinetic constraints; instead a conservation law acts as a global constraint leading to cooperative behaviour. Their equilibrium properties are very simple and usually independent of the dimensionality. Like KCMs—and in contrast to other models with standard second-order phase transitions, such as the Ising models discussed above—they do not have a large equilibrium correlation length at low temperatures. Instead, they show a condensation transition, at either zero or non-zero T.

Urn models generally are comprised of a number M of urns or boxes and N particles distributed among these boxes. A configuration is specified through the occupancies n_r in the boxes $r = 1, \ldots, M$. Each set of such occupation numbers has assigned to it a degeneracy factor which encodes whether the particles are regarded as distinguishable or indistinguishable. The original urn model, introduced by Ehrenfest [148] at the beginning of the twentieth century to prove that thermal equilibrium in the microcanonical ensemble corresponds to the maximum entropy state, has $M = 2$ urns and a large number N of particles. The Backgammon model [149], which stimulated renewed interest in urn models, instead considers the limit $N, M \to \infty$ with $N/M = \rho$ held constant; cooperative glassy behaviour then appears if the energy function is defined appropriately. Many other aspects of the model and a number of variations have since been studied [150–164].

In the most general formulation, the energy function of urn models is written as

$$E = \sum_{r=1}^{M} F(n_r) \tag{45}$$

where $F(x)$ is an arbitrary function subject only to the condition that it must yield a well-defined thermodynamics. To show the type of global constraint present in this type of model it is useful to work out the partition function in the canonical ensemble,

$$Z_{\mathrm{c}}(N, M) = \sum_{\{n_r\}} D(\{n_r\}) \exp\left[-\beta \sum_{r=1}^{M} F(n_r)\right] \delta\left(\sum_{r=1}^{M} n_r - N\right) \tag{46}$$

where $D(\{n_r\})$ is the degeneracy factor $D = \prod_{r=1}^{M} d(n_r)$, with $d(n_r) = 1/n_r!$ for distinguishable particles and $d(n_r) = 1$ for indistinguishable ones. The interesting aspect of (46) is the fact that, although the energy function (45) is non-interacting, particle conservation as expressed through the (discrete) delta function makes the thermodynamics non-trivial and allows phase transitions to occur. To actually work out the partition function, one switches to the grand canonical ensemble to eliminate the global constraint, which yields

$$Z_{\mathrm{gc}} = \sum_{N=0}^{\infty} z^N Z_{\mathrm{c}}(N, M) = \mathrm{e}^{MG(\beta, z)} \tag{47}$$

with $z = \exp(\beta\mu)$ the fugacity and $G(\beta, z)$ given by

$$G(\beta, z) = \ln \sum_{n=0}^{\infty} z^n d(n) \exp[-\beta F(n)]. \tag{48}$$

The equation of state in this type of model relates the three variables T, z, and the density $\rho = N/M$ by

$$\rho = \frac{\langle N \rangle}{M} = \frac{\partial G(\beta, z)}{\partial \ln z}. \tag{49}$$

The equilibrium properties discussed up to now are the same in the canonical and grand canonical ensembles. Non-equilibrium properties differ substantially, on the other hand, and we are interested only in the canonical case where the global constraint induces cooperativity.

The allowed transitions in the dynamics of urn models are moves of individual particles from a 'departure' to an 'arrival' box; move proposals are accepted according to the conventional Metropolis rule which depends on the energy change ΔE in the move. (We discuss the dynamics here in the framework of a discrete-time Monte Carlo simulation.) To fully define the dynamics one still needs to specify how departure and arrival boxes are chosen. For the case of distinguishable particles, a departure box is picked with probability proportional to its occupation number n_r; this is equivalent to choosing a *particle* to move at random. For indistinguishable particles, each box has the same probability of being chosen as the departure box. Godrèche and Luck [162, 163] called these two types of dynamics 'Ehrenfest class' and 'Monkey class', respectively. The arrival box is always picked at random from all boxes connected to the departure box; which boxes are connected defines the geometry of the model. Simplest is the mean-field geometry, where all boxes are connected to each other. It can yield exactly solvable models and has been the focus of most recent work. More complicated is the short-range case, where boxes are located on a finite-dimensional lattice and particles can be moved between neighbouring boxes only.

In summary, urn models are defined by specifying (a) the energy function F, (b) whether particles are distinguishable or not, corresponding to Ehrenfest class and Monkey class dynamics respectively, and (c) the geometry of connections between boxes. The resulting behaviour is very rich, and even a change in only one of the features (a)–(c) can change the dynamics completely. Two specific urn models which lead to interesting glassy dynamics are as follows.

1. The Backgammon model has mean-field geometry, particles are distinguishable and $F(n) = -\delta_{n,0}$ so that the local energy is either -1 or 0 depending on whether the box is empty or not. This model shows a $T = 0$ condensation transition—where all particles gather in one box—and typical relaxation timescales increasing in Arrhenius fashion as T is lowered. The interesting feature of this model is that the system can evolve without having to surmount energy barriers: relaxation can always proceed by moves (those which move particles into boxes that are already occupied) which do not increase the energy. Instead there are entropy barriers, created by a bottleneck in the number of such escape 'directions' from a given configuration. This bottleneck appears because at low T only a few boxes are occupied; moves where a particle lands in an occupied box are then very rare.
2. Zeta-urn models also have mean-field geometry, but particles are indistinguishable (Monkey class dynamics) and $F(n) = \ln(n+1)$. This model shows a $T > 0$ condensation transition with a $T - \rho$ phase diagram where a critical line separates regions of different dynamical behaviour. Much effort has gone into the analytical description of the dynamics along this critical line.

Urn models are schematic approaches which allow a number of general questions about non-equilibrium dynamics to be investigated explicitly. In particular, the Backgammon model and its variants are cases where slow dynamics is determined by the presence of entropy barriers that slow down the dynamics (see above): the system has to attempt many moves before finding a downhill direction in energy. The main difference to models dominated by energy barriers is that the latter arrest completely at $T = 0$ after short-time relaxations are complete, whereas models with entropy barriers relax even at $T = 0$; this relaxation dominates also the dynamics at $T > 0$

until a cross-over at long times where activation effects come into play. Interestingly, the configurational bottleneck created by the entropy barriers induces a typical relaxation time [149] of activated (Arrhenius) character. Much work remains to be done on urn models with non-trivial spatial structure, to understand for example whether they might display cooperative effects reminiscent of those found in real glasses (resulting in, e.g. fragile behaviour of relaxation timescales).

3.7.3. *Oscillator models*

Another family of models which share some similarities with kinetically constrained models are oscillator models. These are mean-field models comprising an ensemble of uncoupled linear oscillators with Monte Carlo dynamics. These models have neither local nor global kinetic constraints. Nevertheless, they share some similarities with KCMs in that there is no interaction among oscillators—making the thermodynamics trivial, with no phase transition even at zero-temperature—while the dynamics is glassy due to the dynamical rules. In this respect they are simpler than the urn models discussed above where, in some cases, a condensation transition may take place due to the effective interaction induced by particle conservation. The slow-down in the dynamics at low temperatures and long times is caused by the low rate at which proposed Monte Carlo moves are accepted; this low acceptance rate could loosely be viewed as a kinetic 'constraint' generated by the dynamics itself.

Originally, oscillator models were introduced indirectly in the analysis of the Monte Carlo dynamics of the spherical Sherrington–Kirkpatrick model, which can be mapped to a set of disordered harmonic oscillators [165, 166]. The 'oscillator model' proper is obtained by simplifying this to an ensemble of identical harmonic oscillators [167]. It is defined by the energy function

$$E = \frac{K}{2} \sum_i x_i^2 \tag{50}$$

where the x_i are the real-valued displacement variables of the N oscillators and $K > 0$ is a Hooke constant. The equilibrium properties are trivial due to the absence of interactions, but the Monte Carlo dynamics couples the oscillators in a non-trivial way. Moves are proposed according to

$$x_i \to x_i' = x_i + \frac{r_i}{\sqrt{N}} \tag{51}$$

where the r_i are Gaussian random variables with zero mean and variance Δ^2, and are accepted according to the usual Metropolis rule. Each move is a parallel update of the whole set of oscillators. Both the energy function (50) and the dynamics as defined by (51) are invariant under rotations in the N-dimensional space of the x_i. This symmetry makes the dynamics exactly solvable, so that questions about, e.g. ageing, effective temperatures and FDT violations can be answered analytically.

At low temperatures the oscillator model displays slow dynamics, as can be easily understood from the following argument. For small T the equilibrium energy, which from equipartition is $E = NT/2$, is very small. Correspondingly, equilibrium configurations are located in a small sphere around the point $x_i = 0$, with radius of order $R = (NT/K)^{1/2}$. This sphere shrinks to zero as $T \to 0$, so that the vast majority of new configurations proposed according to (51) fall outside, producing very small Metropolis acceptance probabilities $\exp(-\beta \Delta E)$. In fact, at $T = 0$ the

system never reaches equilibrium, and the radius of the configuration space sphere explored by the system shrinks to zero logarithmically in time.

Some of the main known results for the oscillator model (see, e.g. [168]) are as follows. The relaxation time shows Arrhenius behaviour at low temperatures; as in KCMs, this occurs even though there are no static interactions. At low temperatures ageing effects occur, with correlation functions and responses showing simple ageing scaling with $(t - t_w)/t_w$ up to subdominant logarithmic corrections. The effective temperature defined via the fluctuation–dissipation ratio (section 2.3) can be computed analytically. Surprisingly, even in the out-of-equilibrium dynamics at $T = 0$ it is linked to the time-dependent value of the energy by the equipartition relation $E(t_w) = NT_{\rm eff}(t_w)/2$.

A number of variants of the oscillator model have been considered, all sharing the feature that oscillators do not interact. For example, Nieuwenhuizen and coworkers [169–171] studied a model with (spherical) spin variables in addition to oscillators. The new variables are used to mimic fast relaxation processes not contained in the original formulation; this imposed separation into slow and fast degrees of freedom mimics the α- and β-relaxation processes in supercooled liquids. We will not detail results for this model below, but refer to [172] for a recent overview.

3.7.4. *Lattice gases without kinetic constraints*

We discussed in section 3.3 the KA model, a lattice gas with a trivial energy function but glassy dynamics produced by local kinetic constraints. The converse approach, where glassy behaviour results from unconstrained dynamics but non-trivial interactions between the particles, has of course also been explored. A simple example is the so-called hard-square lattice gas, where particles moving on a square lattice are not allowed to occupy n.n. sites. This interaction results naturally if the particles are visualized as hard squares oriented at 45° to the lattice axes and with side length $\sqrt{2}a$, a being the lattice constant. This model has a non-trivial equilibrium phase transition at particle density ≈ 0.37, above which particles are located preferably on one of two sublattices. As the maximum density of $1/2$ is approached, the dynamics becomes very slow and shows glassy features. Since we focus in this review on models with essentially trivial thermodynamics, we will only touch on results for the hard-square lattice gas occasionally and refer the interested reader to [173] and the recent review [86] for details.

The unconstrained baseline version of the KA model, a lattice gas without interactions—except for the standard hard-core repulsion that allows at most one particle per site—and without kinetic constraints has been studied under the name of 'sliding block model'. The name arises from the children's puzzle, where blocks can be slid around only by moving them into a neighbouring hole. The interesting limit is normally that of very low vacancy concentration; the vacancies then just perform random walks. The movement of the particles, however, is non-trivial, and the typical displacement of a given particle shows a stretched exponential increase with time at short times. We refer to [174] for simulations and references to earlier theoretical work on this type of model.

3.7.5. *Tiling models*

For completeness we now discuss tiling models. This is a slight departure from our overall philosophy since in these models the energy function chosen leads to non-

trivial equilibrium behaviour. Nevertheless, the following attractive features make them worthy of a brief mention: (a) crystalline phases can be included in addition to amorphous ones, (b) irreducibility is trivial to establish and (c) the idea of a cooperative lengthscale is included right from the beginning. We focus on the j-tiling model introduced by Stillinger and Weber [175] and developed in detail by Weber, Fredrickson and Stillinger [176].

Tiling models are systems made up of non-overlapping square tiles, which can fragment into smaller tiles or, conversely, be joined together into a larger one. Consider a square lattice with $N = L^2$ sites and periodic boundary conditions, covered without gaps by non-overlapping square tiles of all possible side lengths $j = 1, \ldots, L$. Let n_j denote the number of squares of size $j \times j$; these numbers satisfy the global constraint

$$\sum_{j=1}^{L} j^2 n_j = N. \tag{52}$$

The ideal amorphous packing of particles is represented by a single tile of size L, while between smaller tiles it is assumed that there is a strain energy cost proportional to the contact length, arising from a mismatch in the particle packing in neighbouring tiles. This gives the energy function

$$E = 2\lambda \sum_{j=1}^{L} j n_j. \tag{53}$$

A crystal phase can be added by designating tiles of a certain size $j_0 \times j_0$ as crystalline and adding a term $-\mu n_{j_0}$ to E. The equilibrium behaviour of this model cannot be solved exactly even at infinite temperature, but a perturbation expansion around $\beta\lambda = -\infty$ gives a first-order phase transition to the configuration with a single macroscopic tile around $\beta\lambda_c = 0.27 \pm 0.1$. This is confirmed by series expansions and mean-field Flory approximations [175] and transfer matrix calculations and upper bound estimates [177].

The dynamics of tiling models is made interesting by kinetic constraints on the possible fragmentation and aggregation processes. One possibility ('minimal aggregation') is to allow tiles of side length pq to divide into p^2 tiles of side length q if and only if p is the smallest prime factor (larger than 1) of pq. The corresponding rule applies to the reverse aggregation process. Aggregation and fragmentation rates are given by the standard Metropolis rule; in addition, however, a slowing down of the dynamics for large tiles is implemented by including an additional factor of $\alpha^{2pq(p-1)}$ in the rates, with $\alpha \leq 1$. In an alternative version of the dynamics ('boundary shift'), tiles of side length $(p+1)$ fragment into a tile of side length p and an L-shaped band of $(2p+1)$ unit tiles [178]. Both types of dynamics are trivially irreducible since all configurations can be transformed into the one with all unit tiles. It is not clear, however, which dynamical rules are most appropriate for modelling glasses, and this may be one reason why tiling models have received much less attention than SFMs. Some generic glassy features have nevertheless been found [176, 178]. Energy–energy autocorrelation functions in equilibrium, for example, can be fitted to stretched exponentials (but progressively cross over to power-law decays at long times as the glassy regime is approached). Typical relaxation times derived from these correlation functions show superactivated temperature dependences; cooling rate effects on the

energy have also been observed. Beyond this brief overview, we do not consider tiling models further in this review; nonetheless, as explained at the beginning of this section, they have some attractive features which may make them worth revisiting in future work.

There are a number of extensions of the j-tiling models in the literature. For example, Bhattacharjee [179] (see also [180]) considered the equilibrium behaviour of a model with an additional term of the form $\sum_j j^\alpha n_j$ in the energy function. Random tiling models [181–185] or Wang tiles for quasi-crystals have also been studied, though again with a focus on equilibrium; an exception for the latter case is the analysis of the dynamics without kinetic constraints in [186].

3.7.6. *Needle models*

Models of thin needle-shaped particles interacting only via hard (excluded-volume) interactions and subject to Newtonian or diffusive Brownian dynamics may not appear related to KCMs at first sight. They do have interesting glassy dynamics accompanied by trivial equilibrium behaviour, however, and are therefore included here.

Frenkel and Maguire [187, 188] investigated the Newtonian dynamics of a gas of infinitely thin, hard rods of length L at number densities $\sim 1/L^3$. Since the average excluded volume for rods of zero diameter is zero, all static properties of the system are those of an ideal gas. The equilibrium dynamics are non-trivial, but diffusion constants and autocorrelation functions vary smoothly with density even at large normalized densities $L^3\rho$, so that the model does not present pronounced glassy features. Edwards, Evans and Vilgis [189, 190] considered the same model at finite but still small needle diameter $D \ll L$, and larger densities ρ of order $1/(DL^2) \gg 1/L^3$. They argued that in this regime the rotational diffusion of needles is so strongly suppressed that they can effectively only translate along their axis. Because of the non-zero D, other needles will impede this one-dimensional diffusive motion, however; each needle can only move if enough of its neighbours move out of the way. A self-consistency argument then suggests that the diffusion constant decreases to zero at some finite value of $DL^2\rho$, and that on approaching this value relaxation times should diverge [189]; a more sophisticated version of the theory can also reproduce a VTF-like divergence of the inverse diffusion constant. Unfortunately, in roughly the same density regime an equilibrium phase transition occurs to a state of nematic ordering [191], where the needles align with each other rather than being randomly oriented as assumed in the calculation. The glassy phenomena predicted by Edwards *et al.* would therefore be observable only after a sufficiently fast density increase which avoids this transition.

To eliminate the possibility of equilibrium phase transitions, other models postulate that the needles are fixed to a crystal lattice so that only rotational motion is allowed. A number of variants have been considered, including attaching the midpoints of the needles to an f.c.c. [192] or b.c.c. [193] lattice, or their endpoints to a cubic or square lattice [194]; in the last case the motion of the needles was assumed to take place in the (three-dimensional) half-space to one side of the lattice plane. In the limit of vanishing needle diameter, assumed throughout, equilibrium properties are again trivial. The dynamics can become glassy, however, for ratios L/a of needle length and lattice constant above order one: the motion of each needle is then restricted by those around it, leading to 'orientational caging'.

3.7.7. *Models without detailed balance*

Since our main concern is with models with trivial equilibrium behaviour but interesting dynamics, we will not discuss models without detailed balance, for which the nature of any stationary state can be highly non-trivial. A recent review of some models of this type can be found in [195]. Here we only give a few examples that are closely related to KCMs. In SFMs for example, detailed balance will be broken if the kinetic constraint only operates on spin flips in one direction, e.g. for flipping an up-spin down, while the reverse transition is unconstrained. Stationary states are then determined by the competition between the constraints and the structure of the energy function [196]. Halpern [197, 198] introduced a 'cluster-facilitated' variant of SFMs, where the kinetic constraint is that the cluster containing the spin to be flipped and its nearest neighbours must contain at least f up-spins. This means that up-spins require only $f-1$ facilitating up-spin neighbours, while down-spins need f. Again, this asymmetry destroys detailed balance; for $f=1$, for example, the only stationary distribution is the one which assigns probability one to the configuration with all spins down. However, at sufficiently high temperatures long-lived metastable states with non-zero up-spins concentrations can exist.

Schulz and Reineker also considered a model for the irreversible growth of a crystalline phase into a glass [199]. With $n_i = 0, 1$ to represent immobile and mobile regions as before, the model of [199] effectively introduces a third spin state $n_i = -1$ into the $2,2$-SFM, to model regions with local crystalline ordering. The kinetic constraint remains as before (at least two up-spin neighbours are required for a spin to flip, $n_i = 0 \leftrightarrow n_i = 1$) but an additional irreversible process $n_i = 1 \rightarrow n_i = -1$ subject to the same constraint is postulated to model crystallization. Crystal formation from immobile regions, $n_i = 0$, is not allowed. One can now consider an equilibrium configuration of the $2,2$-SFM at some up-spin concentration c_{eq}, on a lattice with periodic boundary conditions in the x-direction (say). If this configuration is 'seeded' with a crystalline surface by setting all spins with vertical coordinate $y = 0$ to $n_i = -1$, then this crystalline phase will grow irreversibly into the 'glass' phase at $y > 0$. At long times the average height of the interface will grow linearly with time; the crystal phase behind the interface is not homogeneous but contains inclusions of liquid- and solid-like regions. The fluctuations of the interface height across the sample also define a roughness, whose scaling behaviour can be used to define a characteristic lengthscale of cooperative behaviour. The results agree broadly with those found for the conventional $2,2$-SFM using other definitions; see section 5.5.

Finally, many non-detailed balance variations of Glauber dynamics in the one-dimensional ferromagnetic Ising chain have been studied. A recent example is [200], where detailed balance is broken by imposing transition rates that only depend on the left neighbour of the spin to the flipped.

4. Techniques

In this section we review the various techniques that have been used to study KCMs. Effective irreducibility is important for KCMs to ensure that equilibrium properties can be predicted from the naive Boltzmann distribution over all configurations; we sketch some techniques for proving this in section 4.1. As far as the dynamics of KCMs is concerned, numerical simulations (section 4.2) are often a convenient starting point, and sometimes the only possible method of attack. Some

properties are, however, amenable to exact analytical solution (section 4.3). Where this is not the case, a number of approximation techniques can be used, ranging from mean-field-like decoupling schemes and adiabatic approximations to special techniques for one-dimensional models; see sections 4.4–4.6. Mode-coupling approximations derived within the projection formalism (section 4.7) and closely related diagrammatic techniques (section 4.8) have also been employed, and mappings to quantum systems offer scope for further analytical work (section 4.9). Finally, mappings to effective models can be helpful to understand the low-temperature dynamics of KCMs as outlined in section 4.10.

4.1. *Irreducibility proofs*

The problem of the reducibility of the Markov chains that formally define KCMs has been tackled by many authors. In general, different types of models require different kinds of analytical or numerical techniques to check whether reducibility effects are significant; in this section, we sketch some of the more common approaches.

Much effort has gone into establishing the irreducibility or otherwise of the f, d-**SFMs**. One starts by defining what is called the high-temperature partition (see section 3.1.1). This partition comprises the configuration with all spins pointing up and all other configurations that can be reached from there; the latter are also called nucleating configurations [74, 82]. Clearly, the configuration with all spins down $n_i = 0$ can never belong to the high-temperature partition. This trivial reducibility is not necessarily significant, however; as explained in section 3.1.1 we only require for 'effective irreducibility' that a typical configuration with given energy (or equivalently up-spin concentration, if we consider the standard SFMs without ferromagnetic interactions) belongs to the high-temperature partition with probability one in the limit of infinite system size.

Now consider a random configuration of the f, d-SFM at up-spin configuration c. To find out whether this configuration belongs to the high-temperature partition, one first flips up all mobile down-spins. This may mobilize further down-spins, so one iterates the procedure until a configuration with no mobile down-spins is reached. If this final configuration has all spins up, the original configuration belongs to the high-temperature partition. This cellular automaton-style rule of flipping down-spins recursively has been studied under the name of diffusion percolation [201], although there one normally asks whether the final configuration contains a spanning cluster of up-spins, rather than *only* up-spins. Diffusion percolation in turn is closely related to bootstrap percolation (BP) [202]; for a review see [203]. The relation is via a simple mapping that exchanges the roles of up- and down-spins. From the original configuration with a fraction c of up-spins, reverse all spins to get a configuration with up-spin concentration $1 - c$. Interpreting sites with the new up-spins (i.e. $n_i = 1$) as occupied by particles, m-BP is defined by recursively removing all particles which have fewer than m occupied neighbouring sites. In spin language, this means flipping down all up-spins that have fewer than m up-spin neighbours, i.e. on a cubic lattice in d dimensions at least $2d - m + 1$ down-spin neighbours. Reversing all spin directions again, this is just the diffusion percolation algorithm for the f, d-SFM, with $f = 2d - m + 1$. Thus, a configuration with up-spin concentration c belongs to the high-temperature partition of the f, d-SFM exactly when m-BP with $m = 2d + 1 - f$ gives an empty lattice when started with the corresponding reversed configuration that has a fraction $1 - c$ of sites

occupied. As an aside, we note that if instead of the probability of reaching an empty lattice one considers the probability for an infinite spanning cluster of particles in the final configuration, then m-BP clearly becomes a generalization of ordinary percolation, which is included as the special case $m = 0$. For $m = 1$ only isolated particles are removed compared to ordinary percolation, while for $m = 2$ isolated particles plus dangling ends of clusters of particles are removed.

Consider now a configuration of an f, d-SFM on a d-dimensional (hyper-)cubic lattice of size L, with each of the $N = L^d$ spins chosen as up with probability c. Let $p(c, L)$ be the probability that such a configuration belongs to the high-temperature partition, i.e. that the inverted configuration leads to an empty lattice in BP with $m = 2d + 1 - f$. (In section 3.1.1 we had written the size-dependence of $p(c, L)$ in terms of $N = L^d$ rather than L, but this should not cause confusion.) Some trivial cases are easily understood. For the $1, d$-SFM, all spins can be flipped up as long as there is a single up-spin in the original configuration, so $p(c, L) = 1 - (1 - c)^L$ and for any $c > 0$ the model is effectively irreducible since $p(c, L \to \infty) = 1$. On the other hand, for $f > d$ it is easy to see that $p(c, L \to \infty) = 0$ for any $c < 1$ and thus these models have significant reducibility effects. The $3, 2$-SFM is a simple example: any 2×2 square of down-spins can never be flipped up whatever the state of the neighbouring spins, and for $c < 1$ the probability that such squares exist tends to one for $L \to \infty$. In the regime $2 \leq f \leq d$, it turns out that the models are effectively irreducible. The proofs rely on the existence of what are called, in the corresponding BP problem, large void instabilities [204]; in our context they are large clusters of up-spins starting from which the whole system can eventually be covered with up-spins. Taking the $2, 2$-SFM as an example, we paraphrase here an analogous argument for hard-square lattice gases by Jäckle *et al.* [205, 206]. Consider an $l \times l$ square of all up-spins. A little thought shows that this can be grown outwards—by flipping up mobile down-spins—into an $(l + 2) \times (l + 2)$ square at least if there is one up-spin in each of the four rows of length l bordering the square. The probability for this is $p_l = [1 - (1 - c)^l]^4$. With increasing l this converges to one so quickly that the probability

$$p_{l\to\infty} = \prod_{k\geq 0} p_{l+2k} = \exp\left\{4 \sum_{k\geq 0} \ln[1 - (1 - c)^{l+2k}]\right\} \tag{54}$$

for the process to continue to infinity is non-zero. Once a sufficiently large cluster (or 'critical droplet' [207]) of up-spins has been established, this probability is in fact very close to one, since for large l one can approximate

$$p_{l\to\infty} \approx \exp\left[-4 \sum_{k\geq 0} (1 - c)^{l+2k}\right] = \exp[-4(1 - c)^l/(2c - c^2)] \tag{55}$$

so that clusters of size above $l = \ln(2c - c^2)/\ln(1 - c)$, i.e. $l \approx (-\ln c)/c$ for small c, are unstable in the sense that they will continue to grow to infinity with high probability. Returning now to (54), the probability of reaching the all up-spin configuration from a single up-spin 'nucleation site', $p_{1\to\infty}$, can be estimated by replacing the sum over k by an integral [207], giving

$$p_{1\to\infty} \approx \exp\left\{2 \int_0^\infty \mathrm{d}u \ln[1 - (1 - c)^u]\right\} = \exp\left\{-\frac{2}{\ln(1 - c)} \int_0^\infty \mathrm{d}v \ln[1 - e^{-v}]\right\} \tag{56}$$

which scales as $p_{1\to\infty} \sim \exp(-\text{const}/c)$ for small c. The fact that $p_{1\to\infty} > 0$ is sufficient to guarantee that in an infinite system at least one such nucleation site will exist; hence the original configuration belongs to the high-temperature partitions with probability $p(c, L \to \infty) = 1$.

An important proviso regarding such proofs of effective irreducibility is whether the thermodynamic limit behaviour is reached in systems of realistic size. To quantify finite-size effects, one can consider $p(c, L)$ as a function of c. For sufficiently large L this increases steeply from zero to one in a narrow region around some value $c_*(L)$—see figure 6 above—which one could define, e.g. by the condition $p(c_*(L), L) = 1/2$. If a system is effectively irreducible then necessarily $c_*(L \to \infty) = 0$, but the rate of this approach can be very slow. In the example of the 2, 2-SFM above one can estimate how large L needs to be to have $p(c, L) = \mathcal{O}(1)$, using the condition $cL^2 p_{1\to\infty} \approx 1$ that there is of order one nucleation site in the system. Using (56) this gives $L \sim \exp(\text{const}/c)$ to leading order, and inverting one has an up-spin concentration $c_*(L) \sim 1/\ln L$ above which a finite system will be essentially irreducible. For the 3, 3-SFM, one finds an even slower convergence, $c_*(L) \sim 1/\ln(\ln L)$ [208]. In this case it is clear that even for a macroscopic $L = 10^{10}$ (say) the thermodynamic limit is not yet reached and the system will show strong reducibility effects below some non-zero $c_*(L)$.

Spin models with **directed kinetic constraints** can have non-zero thresholds $c_* \equiv c_*(L \to \infty) > 0$ even for an infinite system and are then effectively irreducible only for up-spin concentrations $c > c_*$. This is most easily seen for models on Cayley trees, where these thresholds can be calculated by a simple recursion. Take the $(3, 2)$-Cayley tree, where a spin is mobile if both of its neighbours on the level below in the tree are up. We follow the arguments of [81]; see also [202] for closely similar reasoning regarding bootstrap percolation on Bethe lattices. Start with a tree of $L + 1$ levels, with up-spins assigned randomly with probability c. Beginning with the bottom layer, where the spins are frozen since they have no facilitating neighbours, move upwards through the tree and flip up all down-spins that are mobile. Call $p(c, L)$ the probability that the spin at the top node is up at the end of this procedure. This can happen either because the spin was originally up (probability c) or, if it was originally down, because the two spins below have ended up in the up state. Since these two spins have independent trees of depth L below them, one has the recursion

$$p(c, L) = c + (1 - c)p^2(c, L - 1). \tag{57}$$

For large tree depth L, $p(c, L)$ thus tends to a stable fixed point $p(c, L \to \infty)$ of this recursion; which one is determined by the starting value $p(c, 0) = c$. This gives $p(c, L \to \infty) = 1$ for $c \geq c_* = 1/2$ and $p(c, L \to \infty) = c/(1 - c)$ for $c < c_*$. The fraction of permanently frozen spins near the top of the tree, $1 - p^2(c, L \to \infty)$, thus increases smoothly from zero as c decreases below c_*. Above c_*, on the other hand, one has $p(c, l) \approx 1$ in all layers l of the tree except for a finite number at the bottom. This means that the configuration with all up-spins can be reached with probability close to one and (this part of) the system is effectively irreducible.

For **kinetically constrained lattice gas models** (section 3.3), the question of irreducibility is normally cast somewhat differently: one asks whether there are any particles that remain permanently blocked in their initial positions in all configurations that are accessible via any sequence of allowed transitions, i.e. in all configurations within the relevant partition of configuration space. The dynamics can then be defined as effectively irreducible if the fraction of typical configurations

that contain blocked particles vanishes in the thermodynamic limit. The triangular lattice gas [113] and the hard-square lattice gas [173, 205, 206] have in fact been proved to be effectively irreducible in this sense, by techniques similar to the ones outlined above.

A subtlety in determining which particles in a lattice gas are permanently blocked is that a particle may be blocked by a sufficiently large number of neighbouring particles which themselves are *not* permanently blocked. One therefore often focuses on a subset of blocked particles, the so-called 'backbone' [88]. This contains all particles which are permanently frozen by *other frozen* particles. Particles in the backbone remain frozen even when all mobile particles are removed; the backbone can therefore be determined simply by iteratively removing all mobile particles from the system. For the KA model this procedure is closely related to bootstrap percolation; see section 5.1 for further details. One may of course be concerned that the backbone 'misses' a significant number of permanently blocked particles, but simulations for the triangular lattice gas [113] suggest that this is not so: the number of particles in the backbone was found to be a very good approximation to the number of particles that remained blocked in long simulations of the actual dynamics.

4.2. *Numerical simulations*

As defined in section 3.1, the dynamics of most KCMs can be described by a Markovian dynamics in continuous time as expressed by the master equation (23). While it is possible to simulate this directly (see below), for a 'quick and dirty' simulation it is often convenient to have an equivalent discrete-time formulation. We start by outlining how the two are related. To be concrete, consider f, d-SFMs where the only possible transitions between configurations are spin flips. The transition rates can then be written in the general form $w(\mathbf{n} \to \mathbf{n}') = \sum_i w_i(\mathbf{n}) \delta_{\mathbf{n}', F_i\mathbf{n}}$ where $w_i(\mathbf{n}) \equiv w(\mathbf{n} \to F_i\mathbf{n})$ and F_i is the operator that flips spin i, $F_i\mathbf{n} = (n_1, \ldots, 1 - n_i, \ldots, n_N)$. The master equation (23) then reads

$$\frac{\partial}{\partial t} p(\mathbf{n}, t) = \sum_i [w_i(F_i\mathbf{n}) p(F_i\mathbf{n}, t) - w_i(\mathbf{n}) p(\mathbf{n}, t)]. \tag{58}$$

If any of the spin-flip rates $w_i(\mathbf{n})$ are greater than one, let κ be the inverse of the largest rate, otherwise set $\kappa = 1$; the rescaled rates then obey $0 \leq \kappa w_i(\mathbf{n}) \leq 1$. Now consider the following discrete-time Monte Carlo dynamics where time is advanced in steps of κ/N. At each step one of the N possible transitions out of the current configuration $\mathbf{n}$ is chosen randomly; since we are dealing with spin-flips, this just means picking a random spin to flip, n_i say. The proposed transition is accepted with probability $\kappa w_i(\mathbf{n})$, while with probability $1 - \kappa w_i(\mathbf{n})$ it is rejected and the system remains in its current configuration $\mathbf{n}$. The Markov equation for this process is

$$p(\mathbf{n}, t + \kappa/N) = \frac{1}{N} \sum_i \{\kappa w_i(F_i\mathbf{n}) p(F_i\mathbf{n}, t) + [1 - \kappa w_i(\mathbf{n})] p(\mathbf{n}, t)\}$$

or

$$\frac{N}{\kappa} [p(\mathbf{n}, t + \kappa/N) - p(\mathbf{n}, t)] = \sum_i [w_i(F_i\mathbf{n}) p(F_i\mathbf{n}, t) - w_i(\mathbf{n}) p(\mathbf{n}, t)]. \tag{59}$$

For $N \to \infty$ this becomes equivalent to (58), so that the discrete and continuous time descriptions can be used interchangeably. In general, the discrete time dynamics is obtained by randomly selecting, at each step, one of the possible transitions—spin flips, or moves of a particle to a neighbouring site in the lattice gas models of section 3.3—and accepting the proposed move with probability proportional to the continuous time rate for the transition.

A standard Monte Carlo simulation in discrete time is very simple to set up, and often useful for initial exploration of the dynamics of KCMs. At low temperatures, where relaxation timescales can become very large, such an approach quickly runs into problems and more sophisticated approaches are necessary [209–211]. The key difficulty is that in KCMs many of the transitions that are possible in principle are forbidden by the kinetic constraints, so that a standard Monte Carlo simulation would reject almost all proposed moves. One way around this problem is a technique known variously as rejection-free, continuous-time, faster-than-the-clock or Bortz–Kalos–Lebowitz [212] simulation. In a continuous-time description, let $w_i \equiv w_i(\mathbf{n})$ be the rates for all possible transitions out of the current configuration $\mathbf{n}$. It is then easy to show that the time interval Δt to the next transition is exponentially distributed with a rate equal to the sum $w_{\text{tot}} = \sum_i w_i$ of all rates, i.e. $P(\Delta t) = w_{\text{tot}} \exp(-w_{\text{tot}} \Delta t)$. Values of Δt from this distribution can easily be sampled, so that one can go directly to the next 'successful' transition. It then remains to be determined which transition actually occurs; one easily derives that the probability for the first transition to be the one with rate w_i is w_i/w_{tot}. Sampling from this distribution can be the rate-limiting step in the algorithm, and so it is often useful to devise efficient methods for this. An example is provided by recent simulations of the East model [213]: here the positions of all mobile spins in the chain were stored in a binary tree which can be quickly searched to determine which particular spin should be flipped in any given transition.

4.3. *Exact solutions*

In this section we give examples of techniques that have been used to solve aspects of the dynamics of KCMs exactly. In the cases discussed, the simplifying feature that makes such exact solutions possible is either a restriction to dynamics at $T = 0$, or the mean-field character of the dynamics as in the Backgammon and oscillator models.

One of the models whose zero-temperature dynamics can be solved exactly is the 1, 1-SFM [214, 215]. If the system is quenched at $t = 0$ from some initial state to one with equilibrium up-spin concentration $c_{\text{eq}} = 1/(1 + \mathrm{e}^{\beta})$, the Glauber dynamics transition rates for $t > 0$ are, from (27) and (30)

$$w(n_i \to 1 - n_i) = (n_{i-1} + n_{i+1})[(1 - c_{\text{eq}})n_i + c_{\text{eq}}(1 - n_i)]. \tag{60}$$

Now, from the master equation (23), one easily deduces that the average of a general observable $\phi(\mathbf{n})$ evolves in time according to

$$\frac{\partial}{\partial t}\langle \phi(\mathbf{n}) \rangle = \sum_i \langle w(n_i \to 1 - n_i)[\phi(F_i\mathbf{n}) - \phi(\mathbf{n})] \rangle \tag{61}$$

where $F_i\mathbf{n}$ is the configuration $\mathbf{n}$ with spin n_i flipped to $1 - n_i$. Applying this to the $(k + 1)$-spin correlation functions $D_k = (1/N) \sum_j \langle n_j \cdots n_{j+k} \rangle$ one finds, in the zero-temperature limit where $c_{\text{eq}} \to 0$, the closed hierarchy

$$\frac{\partial}{\partial t} D_k = -2(kD_k + D_{k+1}) \tag{62}$$

which can be solved by introducing the generating function $G(x) = \sum_{k=0}^{\infty} D_k x^k / k!$. Not surprisingly, since the $T = 0$ dynamics is strongly reducible—up-spins that are isolated at $t = 0$ can never flip, for example—the results for $t \to \infty$ depend strongly on the initial conditions. For a given initial up-spin concentration c_0 one finds, for example, that $c(t) \equiv D_0(t)$ converges to $c_0 \exp(-c_0)$ for $t \to \infty$, rather than to the equilibrium value $c_{\rm eq} = 0$. It was later shown [55] that exactly the same solution applies to the asymmetric 1, 1-SFM with transition rates (32), except that the factor 2 in (62) is replaced by $1 + a$. This has also been confirmed [109] via a mapping to equivalent models of (random or cooperative) sequential adsorption [216]. Looking back at (60), one sees that the $T \to 0$ limit corresponds to neglecting processes occurring with rates $c_{\rm eq}$; the above solution for the dynamics will therefore also give the correct results for *non-zero* temperatures on timescales shorter than $1/c_{\rm eq} \approx \exp(\beta)$.

A hierarchy very similar to (62) has been used to solve exactly [108] the $T = 0$ dynamics of a Glauber Ising chain in zero field, when spin flips that leave the energy unchanged are forbidden [106]. The only possible flips are then those causing two neighbouring domain walls to annihilate. After a mapping to domain wall variables via $n_i = (1 - \sigma_i \sigma_{i+1})/2$, such moves correspond to two neighbouring up-spins ($n_i = 1$) flipping down simultaneously, and the correlation functions D_k as defined above obey closed equations that differ only by numerical factors from (62). In particular, the domain wall concentration $c = \langle n_i \rangle$ converges to $c_0 \exp(-2c_0)$ from an initial equilibrium state with $c = c_0$. This result can also be obtained from a mean-field approach which becomes exact in one dimension [107].

The exact solution of the $T = 0$ dynamics of the asymmetric 1, 1-SFM, described above, can actually be pushed further to calculate exactly the probability $P(c, T)$ that the system will end up in a metastable configuration with up-spin concentration c if quenched to zero-temperature from an equilibrium state at some non-zero T. From this an appropriately defined entropy of metastable configurations can be obtained since for large systems $P(c, T)$ will be exponential, $P(c, T) \sim \exp[N\pi(c, T)]$. In [55] the quadratic expansion of $\pi(c, T)$ around its maximum with respect to c was obtained, corresponding to a Gaussian approximation to $P(c, T)$; more recently the full form of $\pi(c, T)$ has also been found [109]. As before, the analysis also applies to the extreme limits of the asymmetric 1, 1-SFM, the East model and the conventional 1, 1-SFM.

Another example where dynamical equations can be exactly solved is the Backgammon model [150–153] introduced in section 3.7.2. Most calculations have focused on the case where the number of boxes is equal to the number of particles, $M = N$. One defines $P_k(t)$ as the probability that a randomly selected box contains k particles. For models such as Backgammon which are in the Ehrenfest class, this probability depends on time through a dynamical equation of the form

$$\frac{\partial P_k(t)}{\partial t} = f(P_k, P_{k+1}, P_{k-1}, P_0) \tag{63}$$

where f is a linear function of its arguments with coefficients depending on P_0. This set of equations constitutes a closed hierarchy of nonlinear equations, the non-

linearity appearing only through the time-dependent coefficient $P_0(t)$. For instance, the equation for the energy $E/M = -P_0$ is given by

$$\frac{\partial P_0(t)}{\partial t} = P_1(1 - P_0) - \mathrm{e}^{-\beta} P_0(1 - P_0). \tag{64}$$

The full hierarchy can be solved by defining a generating function $G(x, t) = \sum_{k=0}^{\infty} x^k P_k(t)$ and solving the resulting partial differential equation [152]. At $T = 0$ one finds [153]

$$-P_0(t) = \frac{E(t)}{M} = -1 + \frac{1}{\ln t + \ln(\ln t)} \tag{65}$$

up to subdominant corrections; this solution can also be obtained using an adiabatic approximation [150] (see section 4.5) which becomes exact for long times and at $T = 0$. At small but non-zero temperature, the energy relaxation crosses over to exponential behaviour on a timescale whose dominant dependence on T is an Arrhenius (activated) law. Similar generating function techniques have generally been very useful for urn models, e.g. in the calculation of correlation and response functions [152–155, 160]. A hierarchy similar to (63) has also been derived in a simplified version of the Backgammon model [158].

Closed hierarchies of dynamical equations can also be derived for oscillator models. For the spherical Sherrington–Kirkpatrick model [165, 166] the technique is very similar to that for the Backgammon model; for what we called the oscillator model proper in section 3.7.3 the situation is even simpler since it is possible to show that the hierarchy closes already at the lowest level, yielding an exact autonomous equation for the energy E [167]. This is similar in form to the result of an adiabatic approximation for the Backgammon model (see section 4.5)—which would be exact for the oscillator model—and reads

$$\frac{\partial E}{\partial t} = -E^{3/2} \exp(-C/E) \tag{66}$$

where C is a constant. As a result, the energy $E(t)$ again decays to its ground state value $E = 0$ with an asymptotically logarithmic dependence on time.

4.4. *Mean-field approximations*

In this section we collect some mean-field approaches to the dynamics of KCMs; these are normally based on deriving closed dynamical equations by an appropriate decoupling of correlations.

As an example of *naive* mean-field theory, which neglects all correlations, we paraphrase here the analysis of [217] for the relaxation of the up-spin concentration in the f, d-SFM. As usual, we restrict ourselves to the non-interacting case $J = 0$; a non-zero value of J has negligible effects in the interesting regime of low up-spin concentrations. For Glauber dynamics (30), the spin-flip rates (27) are

$$w(n_i \to 1 - n_i) = \sum_{j_1 \neq \cdots \neq j_f} n_{j_1} \cdots n_{j_f} [(1 - c_{\mathrm{eq}}) n_i + c_{\mathrm{eq}}(1 - n_i)]. \tag{67}$$

Equation (61) then gives for the evolution of the local up-spin concentrations

$$\frac{\partial}{\partial t}\langle n_i\rangle = \langle w(n_i \to 1-n_i)(1-2n_i)\rangle = \sum_{j_1\neq\cdots\neq j_f} \langle n_{j_1}\cdots n_{j_f}[-(1-c_{\rm eq})n_i + c_{\rm eq}(1-n_i)]\rangle. \tag{68}$$

A naive mean-field approximation decouples the average of the spin-product on the right-hand side into single-spin averages. If the system is started in equilibrium, with $\langle n_i\rangle$ uniform across the system, then this will remain the case for all times and one obtains a simple evolution equation for $c = \langle n_i\rangle$

$$\frac{\partial c}{\partial t} \propto c^f (c_{\rm eq} - c). \tag{69}$$

(The proportionality factor is the number of terms in the sum (68), namely $(2d)!/(2d-f)!$.) Linearizing (69) around equilibrium $c = c_{\rm eq}$ then gives an estimate of the relaxation time, $\tau \sim c_{\rm eq}^{-f} \approx \exp(f\beta)$. It is clear, however, that this approximation only takes cooperativity between spins into account very crudely. Accordingly, it fails to predict the superactivated relaxation time increase that occurs in f,d-SFMs for $f \geq 2$; see section 3.1.2. The mean-field treatment can be extended to analyse the relaxation of spatial fluctuations of $\langle n_i\rangle$ [217] but correlation effects due to the kinetic constraints are then still neglected.

More sophisticated mean-field approximations result if some non-trivial correlations are kept. Consider the relaxation of a local up-spin concentration $\langle n_i\rangle$ in the East model, for example. (In equilibrium this relaxation, for a spin that is in the up-state at $t = 0$, also determines the spin autocorrelation function; see the discussion after (114) below.) From the transition rates (31) and the general result (61) one sees that the time evolution of $\langle n_i\rangle$ is coupled to a hierarchy of correlations $\langle n_i n_{i-1}\rangle$, $\langle n_i n_{i-2}\rangle$, $\langle n_i n_{i-1} n_{i-2}\rangle$, etc. [79]. If one truncates by neglecting all correlation functions from a given order onwards, approximations to the autocorrelation function can be obtained by solving the resulting system of linear equations. As explored in other contexts, e.g. the triangular lattice gas [113, 118], such approximations can also be viewed as applications of the projection technique to a space of observables spanned by spin products of a given order, with the memory terms neglected; see section 4.7. Careful selection of the relevant set of observables can significantly improve the results. For example, to calculate the relaxation of a given spin n_i in the East model, Eisinger and Jäckle considered the 'cluster probabilities' of having to the left of n_i a domain of $k-1$ down-spins followed by an up-spin and $m-1$ further spins in arbitrarily specified states. Retaining these probabilities for some fixed cluster length, e.g. $m = 6$, and all integer values $k = 1, 2, \ldots$, they found good fits to simulated relaxation functions down to $c_{\rm eq} = 0.2$. This approximation also revealed an interesting relation to defect-diffusion models, with the clusters obeying an effective diffusion equation with drift towards the spin n_i.

One can try to improve further on such truncation approximations by taking neglected correlations into account through an 'effective field' or 'effective medium'. Taking again the East model as an example, Jäckle and Eisinger [79, 218] proposed the following procedure for approximating the spin autocorrelation function: Suppose the state of spin n_0 was known as a function of time t, and let p be the vector of probabilities for the 2^l configurations of the l spins to the right. Anticipating the notation of section 4.7, the master equation for p can be written as $\partial_t p(t) = L_1^{\rm T} p(t) + n_0(t) L_2^{\rm T} p(t)$ with constant matrices $L_1^{\rm T}$ and $L_2^{\rm T}$; the second term here describes transitions of spin n_1, which are possible only if its left neighbour

is up, i.e. $n_0 = 1$. If one Laplace transforms and approximates the effect of $n_0(t)$ by a frequency-dependent mobility $\Gamma(z)$, this becomes $zp(z) - p(t=0) = L_1^{\mathrm{T}} p(z) + \Gamma(z) L_2^{\mathrm{T}} p(z)$. Solving this for an appropriate initial distribution $p(0)$ the autocorrelation function of spin n_l can be determined; the value of $\Gamma(z)$ can then be deduced from the self-consistency requirement that the same correlation function is obtained for $l = 1$ and $l = 2$. Somewhat surprisingly, the resulting approximation is similar in form to a mode coupling approximation; see (108). The same approach has also been applied to the North-East and $(3, 2)$-Cayley tree models.

4.5. *Adiabatic approximations*

In this section we outline some applications of adiabatic approximations to KCMs. These approximations are based on the assumption that a separation of timescales occurs in the dynamics, allowing a description in terms of separate fast and slow modes. (More generally, a whole hierarchy of sets of modes could occur, all evolving on well-separated timescales.) The key idea is then to assume that the slow modes evolve so gradually that the fast modes can always equilibrate relative to the *instantaneous* configuration of the slow modes. Even if a timescale separation does exist, the model-dependent choice of slow and fast modes is not always obvious. It requires some intuition about the physical mechanisms underlying the occurrence of well-separated timescales; in this sense, a more complete understanding of the validity of adiabatic approximations should ultimately be helpful in clarifying which features of glassy dynamics are universal and which are system-dependent.

We illustrate adiabatic approximations in this section for two models, the East model and the Backgammon model. In the East model, the nature of slow and fast modes is relatively easy to determine [219]. Transitions out of any configuration that contains at least one mobile up-spin will take place with a 'fast' rate of order unity, while transitions out of all other configurations only happen with rates of $\mathcal{O}(c_{\mathrm{eq}})$. For small c_{eq}, i.e. low temperatures T, this gives a natural separation into fast and slow modes. Mathematically, the latter are the occupation probabilities $p(\mathbf{n}, t)$ of all configurations with no mobile up-spins, i.e. with all up-spins surrounded by down-spins, while the fast modes are the remaining $p(\mathbf{n}, t)$. To eliminate the fast modes, one sets their time derivatives in the master equation (23) to zero. This is the adiabatic approximation: fast modes equilibrate in the 'environment' fixed by the instantaneous values of the slow modes. One obtains in this way an effective master equation for the slow degrees of freedom. This should in principle give a description of the dynamics which becomes exact for low temperatures, but because of the large number of fast modes involved it has been explicitly worked out only for very small system sizes [219]. An interesting refinement of this method would be to classify all slow configurations according to the number k (say) of down-spins that need to be flipped up before any of the original up-spins can flip. Since such relaxation processes have an energy barrier of k and so require times of order $\exp(k/T) \sim c_{\mathrm{eq}}^{-k}$ (see also sections 3.1.2 and 5.4.1), configurations with $k = 1$ relax much more quickly than those with $k \geq 2$; within the set of slow modes they are much faster than all others and can therefore again be adiabatically eliminated. This process could in principle be iterated for larger k to give an effective master equation for the dynamics on a hierarchy of increasingly long timescales.

As an aside, we mention briefly a recent analysis of KCMs on hierarchical structures [123, 124] which is similar in spirit. As explained in section 3.4, in these models flips of spins in any given level l are facilitated by spins in level $l - 1$ below.

The simplest adiabatic approximation is that the typical relaxation timescales on the different levels, which increase as one moves up in the hierarchy, are widely separated; for the analysis of level l one can then assume equilibrium in level $l-1$. The resulting equations can model some non-equilibrium effects typical of glassy systems, especially with regards to the effect of cyclic heating and cooling, but are too simple to describe strongly cooperative behaviour.

As a second example application of the adiabatic approximation, we consider the Backgammon model [150, 151]; see section 3.7.2. Here a timescale separation occurs because the probabilities P_k for a randomly chosen box to contain k particles evolve very differently for $k=0$ and $k>0$. $P_0=-E/M$ is the density of empty boxes and increases only very slowly with time. On the other hand, the different configurations in the non-empty boxes are explored rapidly, so that the probabilities P_k $(k>0)$ quickly reach an equilibrium state compatible with the given value of P_0. Consider now the evolution equation (64) for P_0 (see section 4.3), which for $T=0$ reads $\partial P_0/\partial t = P_1(1-P_0)$. The adiabatic approximation replaces P_1 on the right-hand side by the value $P_1=P_1(P_0)$ that it would have in equilibrium at the given P_0; in other words, $P_1(P_0)$ is the value of P_1 in a microcanonical ensemble with energy $E=-MP_0$. Solving the resulting closed equation $\partial P_0/\partial t = P_1(P_0)(1-P_0)$ then gives the exact [153] long-time evolution of $P_0(t)$, as given earlier in (65). The adiabatic approximation thus actually provides an exact description of the asymptotic dynamics for the Backgammon model at $T=0$. Notice that associated with the effective constant-energy (microcanonical) equilibrium ensemble assumed by the adiabatic approximation is a corresponding effective temperature. This illustrates the close connection between adiabatic dynamics and the existence of out-of-equilibrium FDT violations (see sections 2.3 and 5.4.3); a theoretical framework for this connection is described in detail in [22]. Finally, let us note briefly that adiabatic methods have also been applied to oscillator models. We already mentioned in section 3.7.3 that for the oscillator model proper the adiabatic approximation is exact; its disordered analogue, the spherical Sherrington–Kirkpatrick model [165, 166], requires a more sophisticated analysis involving two slow modes.

4.6. *Methods for one-dimensional models*

In one dimension, additional techniques are available for analysing kinetically constrained models. As an example, we describe here an application to the East model [220, 221] of what is variously known as the method of interparticle distribution functions [222], the bag model [223] or the independent interval approximation [224].

Consider a quench at $t=0$ from an equilibrium state at high temperature, with up-spin concentration $\approx 1/2$, to a low temperature T corresponding to $c_{\mathrm{eq}} \approx \exp(-\beta) \ll 1$. The up-spin concentration $c(t)$ will gradually decrease towards c_{eq}, with individual up-spins becoming increasingly widely separated. It therefore makes sense to describe the system in terms of domains. As shown by the vertical lines in $\ldots 1|0001|1|1|01|001|1|1|01|0\ldots$, it is useful to define a domain as consisting of an up-spin and all the down-spins that separate it from the nearest up-spin to the left. The length l of a domain then also gives the distance between the up-spin at its right edge and the nearest up-spin to the left. In equilibrium, the distribution of domain lengths and its average are

$$P_{\mathrm{eq}}(l) = c_{\mathrm{eq}}(1-c_{\mathrm{eq}})^{l-1}, \quad \bar{l}_{\mathrm{eq}} = 1/c_{\mathrm{eq}}. \tag{70}$$

Now for small $c_{\rm eq}$, the equilibrium probability of finding an up-spin within a chain segment of *finite* length l is $\mathcal{O}(lc_{\rm eq})$ and tends to zero for $c_{\rm eq} \to 0$ at fixed l. In this limit the flipping down of up-spins therefore becomes *irreversible* to leading order. The dynamics of the system becomes one of coarsening by coalescence of domains: an up-spin that flips down merges two neighbouring domains into one large domain. During such an irreversible coarsening process, no correlations between the lengths of neighbouring domains can build up if there are none in the initial state. For the present model the equilibrated initial state consists of domains independently distributed according to (70). Therefore an independent interval approximation for the dynamics, defined as neglecting correlations between domains, becomes exact in the low-temperature limit. Even when not exact, the independent interval approximation can give very accurate results, e.g. recently for a 'driven' version of the East model [225].

The coarsening dynamics of the East model is unusual in that it involves a hierarchy of timescales. Consider the typical rate $\Gamma(l)$ at which domains of length l disappear by coalescing with their right neighbours. Because domain coalescence corresponds to the flipping down of up-spins, $\Gamma(l)$ can also be defined as follows. Take an open spin chain of length l, with a 'clamped' up-spin ($n_0 = 1$) added on the left. Starting from the configuration $10\ldots01$, $\Gamma^{-1}(l)$ is the typical time needed to reach the empty configuration $10\ldots00$ where spin n_l has 'relaxed'; the relaxation process can be thought of as a path connecting the two configurations. Call the maximum number of excited spins (up-spins except n_0) encountered along a path its height h. One might think that the relaxation of spin n_l needs to proceed via the configuration $11\ldots1$, giving a path of height l. In fact, the minimal path height $h(l)$ is much lower and given by [220]

$$h(l) = k + 1 \quad \text{for } 2^{k-1} < l \leq 2^k \tag{71}$$

where $k = 0, 1, \ldots$ This result is easily understood for $l = 2^k$ [218, 219]: to relax the 2^k-th spin n_{2^k}, one can first flip up $n_{2^{k-1}}$ and use it as an anchor for relaxing n_{2^k}. The corresponding path is (with $n_{2^{k-1}}$ and n_{2^k} underlined) $1\ldots\underline{0}\ldots\underline{1} \to 1\ldots\underline{1}\ldots\underline{1} \to 1\ldots\underline{1}\ldots\underline{0} \to 1\ldots\underline{0}\ldots\underline{0}$ and reaches height $h(2^k) = h(2^{k-1}) + 1$; the $+1$ arises because the anchor stays up while the spin at a distance 2^{k-1} to its right is relaxed. Continuing recursively, one arrives at $h(2^k) = h(1) + k$; but $h(1) = 1$ because the only path for the relaxation of n_1 is $11 \to 10$. A general proof [220] of (71) can be constructed by showing that the 'longest' configurations that can be reached by flipping up no more than h spins have an up-spin at site $i = 2^k - 1$; see also [226] where bounds on the number of configurations reachable at or below height h are derived.

The result (71) implies that coarsening in the East model proceeds in a hierarchical fashion. The energy barrier for the relaxation of spin n_l is $h(l) - 1$; the -1 comes from the one excited spin (n_l) in the initial configuration. The rate for this relaxation process is $\Gamma(l) = \mathcal{O}(\exp[-(h(l) - 1)/T]) = \mathcal{O}(c_{\rm eq}^{h(l)-1})$. For $c_{\rm eq} \to 0$ the dynamics thus divides into stages distinguished by $k = h(l) - 1 = 0, 1, \ldots$ During stage k, the 'active' domains with lengths $2^{k-1} < l \leq 2^k$ disappear, on a timescale $\mathcal{O}(\Gamma^{-1}(l)) = \mathcal{O}(c_{\rm eq}^{-k})$; different stages can be treated separately because the relevant timescales differ by factors of $1/c_{\rm eq}$. The distribution of inactive domains ($l > 2^k$) changes only because such domains can be created when smaller domains coalesce. Combining this with the (exact) independent interval approximation discussed above, one finds for $l > 2^k$

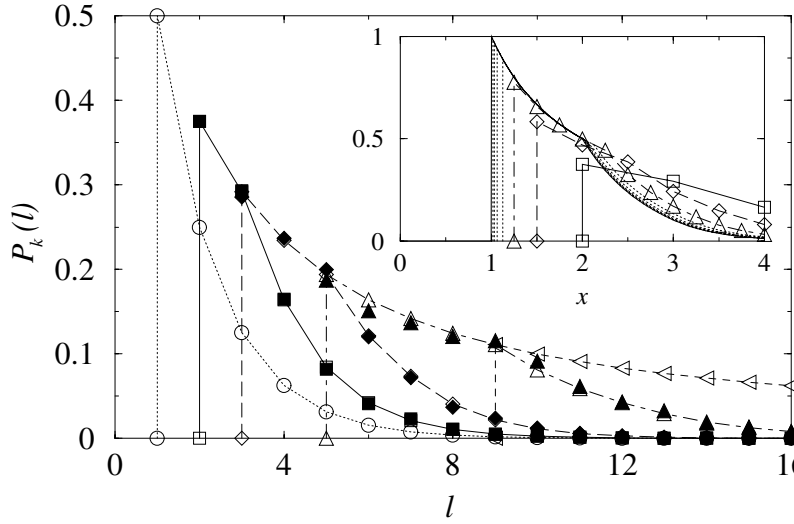

Figure 18. Coarsening in the East model after a quench from the equilibrium state with up-spin concentration $1/2$. Shown are the domain length distributions $P_k(l)$ at the end of the various stages of the low-T coarsening dynamics. Open symbols and lines: theoretical results, for $k = 0$ (◯; initial condition), 1 (□), 2 (◇), 3 (△). Full symbols: simulation results for a chain of length $N = 2^{15}$ and $c_{\rm eq} = 10^{-4}$ ($k = 1, 2$) and $c_{\rm eq} = 10^{-3}$ ($k = 3$). Inset: scaled predictions $2^{k-1}P_k(l = 2^{k-1}x)$ versus. x for $k = 1, \ldots, 8$. Bold line: predicted scaling function. From [220]. Copyright American Physical Society.

$$\frac{\partial}{\partial t}P(l,t) = \sum_{2^{k-1}<l'\leq 2^k} P(l-l',t)\left[-\frac{\partial P(l',t)}{\partial t}\right]. \tag{72}$$

The term in square brackets is the rate at which active domains disappear; $l' \leq 2^k$ because inactive domains do not disappear. This equation can be integrated from the beginning to the end of each stage k, by introducing generating functions and using the fact that all active domains have disappeared at the end of the stage. The end result [220] is an exact expression for the domain length distribution $P(l, t \to \infty)$ at the end of stage k, which we write as $P_{k+1}(l)$, in terms of the distribution $P_k(l)$ at the end of the previous stage. Figure 18 shows the results for the case where $P_0(l)$ is the equilibrium distribution (70) for up-spin concentration $1/2$. Not unexpectedly, a scaling limit is approached for large k: the rescaled distributions $\tilde{\boldsymbol{P}}_k(x) = 2^{k-1}P_k(l)$, with scaled domain size $x = l/2^{k-1}$, converge to a limiting distribution $\tilde{\boldsymbol{P}}(x)$ which is independent of the initial condition and can be calculated explicitly. The average domain length in the scaling limit is given by $\bar{l}_k = 2^{k-1}\bar{x}$, with $\bar{x} = \exp(\gamma) = 1.78\ldots$ where γ is Euler's constant [220]. In the time domain this leads to anomalous coarsening with a temperature-dependent exponent, since stage k is completed on a timescale $t \sim c_{\rm eq}^{-k} \sim \exp(-k/T) \sim \exp[-\ln \bar{l}/(T \ln 2)]$ and thus $\bar{l} \sim t^{T \ln 2}$. (Such anomalous coarsening has also been found in other models of non-equilibrium dynamics, often without detailed balance; see [221] for examples.) By extrapolating the coarsening law to the equilibrium domain length $\bar{l}_{\rm eq} \sim \exp(1/T)$, one then also finds that for $T \to 0$ the dominant divergence of the equilibration time for the East model is $\tau \sim \exp[1/(T^2 \ln 2)]$, i.e. an EITS law (3).

4.7. *Projection and mode-coupling techniques*

Much of the work on the stationary dynamics of KCMs makes use of so-called projection techniques (section 4.7.1), which attempt to isolate relevant slow degrees of freedom from the less relevant fast variables. The latter end up contributing via 'memory functions' and in section 4.7.2 we review the definition of one particular memory function which is regarded as most suitable for the analysis of systems with stochastic dynamics. The mode-coupling approximation itself is discussed in section 4.7.3.

4.7.1. *Projection approach*

The basic ideas of the projection approach are due to Mori [227]; for a modern textbook exposition see, e.g. [228]. The key aim of the formalism is to derive exact dynamical equations for a selected set of 'relevant' variables, with the contributions from the remaining 'irrelevant' variables isolated in a form suitable for further, approximate treatment.

Consider a system governed by Markovian dynamics in continuous time, with a set of S configurations $\mathbf{n}$. All models that we discuss in this review are of this form; for the case of an SFM, for example, $\mathbf{n}$ would be the vector formed of all the spin variables n_i and range over $S = 2^N$ configurations. The basic equation governing the dynamical evolution is thus the master equation (23)

$$\frac{\partial}{\partial t}p(\mathbf{n},t) = \sum_{\mathbf{n}'} w(\mathbf{n}' \to \mathbf{n})p(\mathbf{n}',t) - \sum_{\mathbf{n}''} w(\mathbf{n} \to \mathbf{n}'')p(\mathbf{n},t) = \sum_{\mathbf{n}'} L^{\mathrm{T}}(\mathbf{n},\mathbf{n}')p(\mathbf{n}',t) \quad (73)$$

if one defines the $S \times S$ matrix L (the Liouvillian operator) with elements

$$L(\mathbf{n}',\mathbf{n}) = L^{\mathrm{T}}(\mathbf{n},\mathbf{n}') = w(\mathbf{n}' \to \mathbf{n}) - \delta_{\mathbf{n}',\mathbf{n}} \sum_{\mathbf{n}''} w(\mathbf{n} \to \mathbf{n}''). \quad (74)$$

If $p(\mathbf{n},t)$ is viewed as a time-dependent vector $p(t)$ with S entries, then $\partial p(t)/\partial t = L^{\mathrm{T}}p(t)$ with the formal solution

$$p(t) = \mathrm{e}^{L^{\mathrm{T}}t}p(0). \quad (75)$$

An observable of the system is just a function $a(\mathbf{n})$, which can again be regarded as a vector. It makes sense to define a scalar or inner product on this space of vectors which is not Euclidean but instead reflects the equilibrium correlations between observables,

$$(a,b) \equiv \langle ab \rangle = \sum_{\mathbf{n}} a(\mathbf{n})b(\mathbf{n})p_{\mathrm{eq}}(\mathbf{n}) \quad (76)$$

where $p_{\mathrm{eq}}(\mathbf{n})$ is the equilibrium distribution over configurations. Strictly speaking (76) is a disconnected correlation, and we should subtract $\langle a \rangle \langle b \rangle$ (compare (7)), but for simplicity one assumes that any non-zero equilibrium averages have been subtracted off from all observables, such that $\langle a \rangle = 0$ etc. In terms of the scalar product (76), time-dependent correlation functions take the simple form

$$\begin{aligned} C_{ab}(t) &= \sum_{\mathbf{n}'} b(\mathbf{n}')p(\mathbf{n}',t|\mathbf{n},0)a(\mathbf{n})p_{\mathrm{eq}}(\mathbf{n}) \\ &= \sum_{\mathbf{n}'} \left(\mathrm{e}^{Lt}\right)(\mathbf{n},\mathbf{n}')b(\mathbf{n}')a(\mathbf{n})p_{\mathrm{eq}}(\mathbf{n}) = (a,\mathrm{e}^{Lt}b). \end{aligned} \quad (77)$$

Here $p(\mathbf{n}', t|\mathbf{n}, 0)$ is the probability that the system is in configuration $\mathbf{n}'$ at time t if it was in configuration $\mathbf{n}$ at time 0; from (75) this is the $(\mathbf{n}', \mathbf{n})$-element of the matrix $\exp(L^{\mathrm{T}}t)$, hence the $(\mathbf{n}, \mathbf{n}')$-element of the matrix $\exp(Lt)$. From (77), if one defines for any observable b its value at time t as

$$b(t) = \mathrm{e}^{Lt} b \tag{78}$$

then simply $C_{ab}(t) = (a, b(t))$. Intuitively, the element $b(\mathbf{n}, t)$ of the vector $b(t)$ can be interpreted as the average value of b at time t if the system started off in configuration $\mathbf{n}$ at time $t = 0$.

Now consider a set of 'relevant' observables a_i. For simplicity, assume that they all have unit variance and are uncorrelated in equilibrium, i.e. $(a_i, a_j) = \delta_{ij}$; the generalization to the case of arbitrarily correlated observables will be given below. Each $a_i(t)$ obeys the equation of motion (78); if we Laplace transform to $a_i(z) = \int_0^\infty \mathrm{d}t\, a_i(t) \exp(-zt)$ this can be written as

$$z a_i(z) - a_i = L a_i(z) = L(z - L)^{-1} a_i = (z - L)^{-1} L a_i. \tag{79}$$

The same symbol for $a_i(t)$ and its Laplace transform $a_i(z)$ is used here since the argument makes clear which one is meant; a_i continues to denote the value of the observable at time $t = 0$. The key idea is now to project the equations of motion (79) on to the subspace of observables spanned by the a_i; since the a_i are orthonormal, the appropriate projector acts as

$$Pb = \sum_i a_i (a_i, b). \tag{80}$$

The orthogonal projector is defined as $Q = 1 - P$. P and Q obey the usual relations for projectors, e.g. $P^2 = P$, $Q^2 = Q$, $PQ = QP = 0$. They are also self-adjoint with respect to the inner product, e.g. $(a, Pb) = (Pa, b)$ since both expressions give $\sum_i (a, a_i)(a_i, b)$.

To bring the projected equations into a convenient form, one now writes $(z - L)^{-1} = (z - PL - QL)^{-1}$ in (79) and applies the matrix equality

$$(A - B)^{-1} = (A - B)^{-1} B A^{-1} + A^{-1} \tag{81}$$

to $A = z - QL$, $B = PL$ to get

$$z a_i(z) - a_i = (z - L)^{-1} P L a_i + (z - L)^{-1} P L (z - QL)^{-1} Q L a_i + (z - QL)^{-1} Q L a_i. \tag{82}$$

Carrying out the projections implied by P results in

$$\begin{aligned} z a_i(z) - a_i = {} & \sum_j a_j(z) \Omega_{ji} + \sum_j a_j(z) (a_j, L(z - QL)^{-1} Q L a_i) \\ & + (z - QL)^{-1} Q L a_i \end{aligned} \tag{83}$$

where the rate matrix Ω has elements $\Omega_{jk} = (a_j, L a_k)$. Transforming back to the time domain and using $Q^2 = Q$ to show that $\mathrm{e}^{QLt} Q = \mathrm{e}^{QLQt} Q = Q \mathrm{e}^{QLQt} Q$ results in the desired projected equation of motion,

$$\frac{\partial}{\partial t} a_i(t) = \sum_j a_j(t) \Omega_{ji} + \sum_j \int_0^t \mathrm{d}t'\, a_j(t') M_{ji}(t - t') + r_i(t) \tag{84}$$

Here

$$M_{jk}(t) = (a_j, LQe^{QLQt}QLa_k) \tag{85}$$

is a time-dependent memory matrix (also called a memory kernel) and

$$r_i(t) = e^{QLQt}r_i, \qquad r_i = QLa_i \tag{86}$$

is the so-called random force. Equation (84) is in the form of a generalized Langevin equation. The first term on the right-hand side leads to an exponential decay of the observables towards zero (the matrix Ω_{ki} has only non-positive eigenvalues, because the same is true for L); the second term represents a generalized friction term with the memory kernel $M_{ki}(t)$. The name random force is used for $r_i(t)$ because it is always orthogonal to the space of observables being projected on to: the definition (86) implies $Pr_i(t) = 0$. In particular $(a_j, r_i(t)) = 0$ so that the random forces are uncorrelated with the initial values of all the observables considered. Using this property of the random force, taking a product of (84) with the different a_k also gives the desired equation for the correlation functions $C_{ij}(t) = (a_i, a_j(t))$:

$$\frac{\partial}{\partial t}C_{ki}(t) = \sum_j C_{kj}(t)\Omega_{ji} + \sum_j \int_0^t \mathrm{d}t'\, C_{kj}(t')M_{ji}(t-t') \tag{87}$$

or, in matrix form and after Laplace transform, bearing in mind that the initial condition is $C_{ki}(t=0) = \delta_{ki}$,

$$C(z) = (z - \Omega - M(z))^{-1}. \tag{88}$$

In the case of general observables with arbitrary equilibrium correlations this result generalizes to

$$C(z) = C(zC - \Omega - M(z))^{-1}C \tag{89}$$

where C (in our notation, see after (79)) denotes the correlation matrix at time $t = 0$, whose elements $C_{ij} \equiv C_{ij}(t=0) = (a_i, a_j)$ are the equilibrium correlations.

Importantly, in systems with detailed balance one can show that the memory matrix is the correlation function of the random force. This follows from the fact that for such systems, the operator L is self-adjoint. (The detailed balance condition $w(\mathbf{n}' \to \mathbf{n})p_{\mathrm{eq}}(\mathbf{n}') = w(\mathbf{n} \to \mathbf{n}')p_{\mathrm{eq}}(\mathbf{n})$ implies from (74) that $L(\mathbf{n}', \mathbf{n})p_{\mathrm{eq}}(\mathbf{n}') = L(\mathbf{n}, \mathbf{n}')p_{\mathrm{eq}}(\mathbf{n})$ for all $\mathbf{n}$ and $\mathbf{n}'$; multiplying by $a(\mathbf{n})b(\mathbf{n}')$ and summing over $\mathbf{n}$ and $\mathbf{n}'$ gives the desired result $(La, b) = (a, Lb)$.) Using also the fact that Q is self-adjoint, the definition (85) can thus be written as

$$M_{jk}(t) = (QLa_j, e^{QLQt}QLa_k) = (r_j, r_k(t)). \tag{90}$$

Using similar arguments one also shows that, for systems with detailed balance, the correlation function matrix, frequency matrix and memory function matrix are all symmetric.

The result (90) implies, in particular, that one can treat $M(z)$ in the same way as $C(z)$, expressing it in terms of an appropriate frequency matrix $\Omega_2(z)$ and a new, second-order memory function $M_2(z)$. This gives for the correlation function

$$C(z) = C[zC - \Omega - M(zM - \Omega_2 - M_2(z))^{-1}M]^{-1}C \tag{91}$$

where M is the value of the memory matrix at $t = 0$, $M_{ij} = (QLa_i, QLa_j)$. This approach implicitly tracks the motion of the random forces r_i, and so it is not surprising that the same result for $C(z)$ would be obtained from the first-order memory function if the space of relevant observables was enlarged to include

the a_i as well as the r_i (or, equivalently, the a_i and La_i; either way one projects onto the same space of observables). This process can be iterated to obtain a continued fraction expression for C in terms of memory functions of increasing order [229].

4.7.2. *Irreducible memory function*

The projection formalism, while formally exact, hides all complexities of the dynamics in the memory functions, and one needs to find approximate ways of calculating these in order to make the approach useful. In applications to microscopic models of dense supercooled liquids (systems of classical particles obeying Newton's equations), the relevant 'slow' observables a_i are normally chosen as Fourier modes of the particle number density fluctuations, and the dynamics is deterministic and time-reversible. Approximations (such as mode-coupling, see below) are normally applied to the second-order memory function. The resulting models for the correlation functions have been much studied [16–18] and predict, e.g. dynamical transitions—signalled by the divergence of the longest relaxation time—as external control parameters such as the overall particle density are varied.

For models with stochastic dynamics and detailed balance, it is less obvious which memory function to choose as the starting point for approximations. Above we encountered the first- and second-order memory function; Kawasaki [230, 231] suggested another, so-called irreducible memory function, based on earlier work on the dynamics of colloidal suspensions [232]. The idea is to decompose the operator QLQ that governs the time evolution of the random force into two parts:

$$QLQ = L_0 + L_1. \tag{92}$$

Here L_0 is defined by its action on an arbitrary vector b, as

$$L_0 b = \sum_{ij} QLa_i \Omega^{-1}_{ij} (QLa_j, b) \tag{93}$$

while L_1 is defined by the relation (92). Applying the identity (81) with $A = z - L_1$, $B = L_0$ to the Laplace transform of the expression (90) for the memory matrix then gives

$$M_{jk}(z) = (QLa_j, (z - QLQ)^{-1} L_0 (z - L_1)^{-1} QLa_k) + (QLa_j, (z - L_1)^{-1} QLa_k). \tag{94}$$

Calling the last term the irreducible memory function $M^{\mathrm{irr}}_{jk}(z)$ and using the definition (93), this becomes

$$M_{jk}(z) = \sum_{lm} M_{jl}(z) \Omega^{-1}_{lm} M^{\mathrm{irr}}_{mk}(z) + M^{\mathrm{irr}}_{jk}(z) \tag{95}$$

or in matrix form $M(z) = M^{\mathrm{irr}}(z) + M(z)\Omega^{-1} M^{\mathrm{irr}}(z)$. The first-order memory function can thus be expressed in terms of the irreducible one as $M(z) = M^{\mathrm{irr}}(z)(1 - \Omega^{-1} M^{\mathrm{irr}}(z))^{-1}$, and in the correlation function matrix (89) this gives

$$C(z) = C[zC - \Omega\big(1 - \Omega^{-1} M^{\mathrm{irr}}(z)\big)^{-1}]^{-1} C. \tag{96}$$

A nice physical interpretation of the irreducible memory function was given by Pitts and Andersen [233]. They argue that a system with stochastic dynamics (e.g. a system of colloidal particles with Brownian dynamics, or the much more abstract lattice gases with kinetic constraints) must eventually be derivable from an underlying

system with deterministic, time-reversible dynamics. At long times, the two descriptions should give the same results for correlation functions. This then implies that the irreducible memory function for stochastic dynamics must be proportional to the second-order memory function of the time-reversible description. The argument is based on a comparison of (91), as applied to the time-reversible system, with (96) when applied to the stochastic system. Time-reversibility can be shown to imply that the matrices Ω and Ω_2 in (91) vanish, giving

$$C(z) = C[zC - M(zM - M_2(z))^{-1}M]^{-1}C. \tag{97}$$

For times that are long compared to the microscopic timescales of the deterministic dynamics, the corresponding z can be shown to be small enough for the term zM to be neglected [233]. Agreement with (96) then requires that $M_2(z) = -M\Omega^{-1}M + M\Omega^{-1}M^{\mathrm{irr}}(z)\Omega^{-1}M$. The first term is independent of z and gives a delta-function-like contribution to $M_2(t)$; for longer times, the second term shows that $M_2(t)$ of the deterministic description and $M^{\mathrm{irr}}(t)$ of the stochastic description are related by constant factors as claimed. The upshot of this is that approximations analogous to mode-coupling theory for dense liquids are obtained by applying the mode-coupling approximation to the irreducible memory function of stochastic systems.

4.7.3. *Mode-coupling approximation*

The simplest approximation for the (reducible) memory function is to neglect it. Setting $M(z) = 0$ in (89), the calculation is reduced to the diagonalization of the matrix Ω, and all correlation functions become superpositions of exponentially decaying modes. Effectively this corresponds to a mean-field-like truncation of the hierarchy of correlation functions to just those of the 'relevant variables' retained. This approach can describe some aspects of the slowing down of the dynamics in kinetically constrained systems, but is incapable of predicting, e.g. an incomplete decay of correlation functions which would be expected at a dynamical transition.

An improved—but still uncontrolled—approach is the mode-coupling approximation (MCA). As an illustration, consider the East model. The configuration $\mathbf{n}$ is specified by that of all spins $n_i = 0, 1$, and the matrix elements of the Liouvillian are given by (25) and (31)

$$L(\mathbf{n}', \mathbf{n}) = L^{\mathrm{T}}(\mathbf{n}, \mathbf{n}') = \sum_i n'_{i-1}[c(1-n'_i) + (1-c)n'_i]\left(\delta_{\mathbf{n},F_i\mathbf{n}'} - \delta_{\mathbf{n},\mathbf{n}'}\right). \tag{98}$$

Here we have abbreviated by $c \equiv c_{\mathrm{eq}}$ the equilibrium concentration of up-spins, and F_i is the operator which flips spin i. If we are interested in spin-correlation functions, the relevant observables are the spin fluctuations $\eta_i = [c(1-c)]^{-1/2}(n_i - c)$, normalized such as to obey $C_{ij} = (\eta_i, \eta_j) = \delta_{ij}$. Together with the unit observable e and all different products $\eta_{i_1} \cdots \eta_{i_m}$ $(m = 1, \ldots, N)$ these observables form an orthonormal basis for the space of all observables. In an obvious abuse of notation, products such as $\eta_j\eta_k$ are here understood to be taken componentwise, e.g. $(\eta_j\eta_k)(\mathbf{n}) = \eta_j(\mathbf{n})\eta_k(\mathbf{n})$.

One can now construct the rate and memory matrices. For an arbitrary observable $a(\mathbf{n})$ one has, from (98)

$$(La)(\mathbf{n}) = \sum_i n_{i-1}[c(1-n_i) + (1-c)n_i][a(F_i\mathbf{n}) - a(\mathbf{n})] \tag{99}$$

and applying this to $a = \eta_i$ gives

$$L\eta_i = -c\{\eta_i + [(1-c)/c]^{1/2}\eta_{i-1}\eta_i\}. \tag{100}$$

The rate matrix is $\Omega_{ij} = (\eta_i, L\eta_j) = -c\delta_{i,j}$ since $(\eta_i, \eta_j\eta_k) = 0$. The initial values of the random forces follow as

$$r_i = QL\eta_i = L\eta_i - \sum_j \eta_j(\eta_j, L\eta_i) = -[c(1-c)]^{1/2}\eta_{i-1}\eta_i \tag{101}$$

giving for the reducible memory matrix

$$M_{ij}(t) = c(1-c)(\eta_{i-1}\eta_i, \mathrm{e}^{QLQt}\eta_{j-1}\eta_j) \tag{102}$$

while the expression for $M_{ij}^{\mathrm{irr}}(t)$ is obtained by replacing QLQ with L_1 in the exponent on the right-hand side of (102). The MCA can be applied to either of these functions. It replaces QLQ or L_1 by L, and also assumes that the resulting fourth-order correlation function can be factorized into pairwise contributions like $(\eta_i, \mathrm{e}^{Lt}\eta_j)$. Since the spin–spin correlation functions for the East model are site-diagonal, $C_{kl}(t) = (\eta_k, \mathrm{e}^{Lt}\eta_l) = C(t)\delta_{kl}$ (see section 5.3), the only non-zero contribution to (102) becomes $M_{ij}^{\mathrm{MCA}}(t) = \delta_{ij}M^{\mathrm{MCA}}(t)$ with [218]

$$M^{\mathrm{MCA}}(t) = c(1-c)(\eta_{i-1}, \mathrm{e}^{Lt}\eta_{i-1})(\eta_i, \mathrm{e}^{Lt}\eta_i) = c(1-c)C^2(t). \tag{103}$$

Using this as an approximation for $M_{ij}^{\mathrm{irr}}(t)$, one has from (96), bearing in mind that all matrices involved are diagonal,

$$C(z) = \left(z + \frac{c}{1 + c^{-1}M^{\mathrm{MCA}}(z)}\right)^{-1}. \tag{104}$$

Together with (103) this is a closed MCA equation for $C(t)$, which is equivalent to a model of the glass transition studied in detail by Leutheusser [234, 235]. One can ask, in particular, whether on lowering c a dynamical transition occurs to a non-ergodic state where $C(t)$ no longer decays to zero for $t \to \infty$. If $C(t \to \infty) = q$, then $C(z) \simeq q/z$ and $M^{\mathrm{MCA}}(z) \simeq c(1-c)q^2/z$ for small z. Inserting into (104) and taking $z \to 0$ gives

$$q = \left(1 + \frac{c}{(1-c)q^2}\right)^{-1} \tag{105}$$

or $q/(1-q) = (1-c)q^2/c$. The largest solution in the range $0 \le q \le 1$ gives $C(t \to \infty)$ [17]; it is easily worked out as $q = 1/2 + [1/4 - c/(1-c)]^{1/2}$, yielding a first-order dynamical transition—a discontinuous jump of q, from 0 to 1/2—at $c/(1-c) = 1/4$. Thus, the MCA approximation applied to the irreducible memory function of the East model predicts a spurious dynamical transition at $c = 0.2$ [230]. As expected from the discussion at the end of section 4.7.2, applying the MCA to the *reducible* memory function gives even less reasonable results: Jäckle and co-workers found both for constrained spin models (e.g. the East model [218]) and the triangular lattice gas [118] that unphysical divergences for the correlation functions at long times could occur.

It should be noted that for models with stochastic dynamics, MCAs for second- or higher-order memory functions can never predict a non-ergodic decay of correlation functions to a non-zero value; see e.g. [233, 236, 237]. This can be seen from (91). If $M_2(z)$ is linked via a MCA to $C(z)$, then a non-ergodic state requires that $M_2(z)$ diverge as $\sim 1/z$ for $z \to 0$; but then $C(z) = C(zC + \mathcal{O}(z) - \Omega)^{-1}C$ for small z which has a finite limit for $z \to 0$ rather than the assumed $1/z$ divergence (as

long as Ω is non-zero). For time-reversible dynamics, the situation is different since there $\Omega = 0$; see before (97).

Notice that for more complicated directed models, e.g. the North-East model or Cayley tree models, the random force $r_i = QL\eta_i$ will contain not just second-order products of spin fluctuations, but also higher orders such as $\eta_j\eta_k\eta_l$. For sufficiently simple models [230, 238] the coefficients can be worked out explicitly, and the MCA then gives expressions for the memory functions which also involve higher powers of $C(t)$. If this procedure is too complicated, one can in addition project r_i on to a subspace of observables, e.g. the one spanned by the second-order products $\eta_j\eta_k$ [237]. Finally, we note that in the context of supercooled liquids, *extended* MCAs have been derived [19, 239, 240]. These lead to approximations for the memory matrix of the form $M^{\mathrm{MCA}}(z)[1 + \Delta(z)M^{\mathrm{MCA}}(z)]^{-1}$, where $M^{\mathrm{MCA}}(z)$ is the memory matrix in the conventional MCA, e.g. (103) for the East model, and $\Delta(z)$ is a new memory matrix. The presence of a non-zero $\Delta(z)$ ensures that in extended MCA the memory matrix does not become singular for $z \to 0$ even if $M^{\mathrm{MCA}}(z)$ does, and thus smoothes out the sharp dynamical transitions generally predicted by conventional MCA. The formalism of extended MCA has not yet been adapted for models with stochastic dynamics; nevertheless, approximations of similar form have recently been derived for kinetically constrained models using the diagrammatic approaches reviewed in the next section.

4.8. *Diagrammatic techniques*

Equilibrium correlation functions for kinetically constrained models have also been studied using diagrammatic expansion. In fact, the first theoretical treatment [74] for f, d-SFMs was derived from a diagrammatic expansion. We review here the formulation recently provided by Pitts and Andersen [238] for the East model and other models with directed constraints; a related approach was used for the 1, 1-SFM in [241]. The spin autocorrelation function in the East model is site-diagonal (see section 5.3), and in the notation of section 4.7 can be written as

$$C(t) = (\eta_i, \mathrm{e}^{Lt}\eta_i), \qquad C(z) = (\eta_i, (z - L)^{-1}\eta_i). \tag{106}$$

The Liouvillian is given in (98) and can be written as $L = \sum_i L_i$, with L_i corresponding to spin flips at site i. One can now expand the inverse in (106), and insert decompositions of the identity matrix $1 = \sum_\phi \phi)(\phi$, where ϕ runs over the orthonormal basis vectors of the space of all observables built up from products of the η_j (see after (98)). This gives for the Laplace transform of the spin–spin autocorrelation

$$C(z) = \sum_{k=0}^{\infty} \frac{1}{z^{k+1}} \sum_{i_1 \cdots i_k} \sum_{\phi_1 \cdots \phi_{k-1}} (\eta_i, L_{i_1}\phi_1)(\phi_1, L_{i_2}\phi_2) \cdots (\phi_{k-1}, L_{i_k}\eta_i). \tag{107}$$

Each term in this series can be represented by a diagram; the value associated with each diagram is determined by a product of 'matrix elements' $(\phi, L_j\phi')$, which for the East model are easily worked out explicitly. A closer investigation of the structure of the diagrammatic expansion reveals that the first-order reducible and irreducible memory functions can both be obtained as the sum of appropriately selected subsets of diagrams [238]. If these subseries are summed approximately, expressions for the memory functions result which are, non-trivially, of the same general form as those obtained from a MCA within the projection formalism: the irreducible memory

function $M^{\rm irr}(t)$ becomes a polynomial in $C(t)$. For the East model, for example, the most straightforward approximation yields

$$M^{\rm irr}(t) = c(1-c)C(t). \tag{108}$$

(This result was also obtained by Jäckle and Eisinger [79, 218] using their 'effective medium approximation'.) Compared to (103), the power of $C(t)$ on the right-hand side of (108) is reduced by one, although (103) itself can also be retrieved if a different subset of the diagrams for $M^{\rm irr}(z)$ is summed. For the (3, 2)-Cayley tree model and the North-East model one obtains by the same approach *identical* expressions for the irreducible memory function,

$$M^{\rm irr}(t) = 2c^3(1-c)C(t) + c^2(1-c)^2C^2(t) \tag{109}$$

again containing one power of $C(t)$ less than the results from the MCA used by Kawasaki [230].

For the East model, Pitts and Andersen [238] pushed the analysis even further and showed that a more sophisticated rearrangement of the series for $M^{\rm irr}(z)$ can be used to derive approximations that are of the same form as the extended MCA for supercooled liquids (see section 4.7.3). As expected on general grounds from the structure of extended MCA, these improved approximations avoid the spurious dynamical transitions predicted for the East model by simpler approximations such as (108). A fuller discussion of the results obtained from the diagrammatic expansions will be given later, in section 5.3.

4.9. *Mappings to quantum systems and field theories*

It can be useful to think of the vector space of observables on the space of configurations $\mathbf{n}$ as a quantum mechanical Hilbert space. A useful basis for this Hilbert space are the vectors $|\mathbf{n}\rangle = |n_1 \ldots n_N\rangle$; $|\mathbf{n}\rangle$ corresponds to the observable which is one if each spin i has the specified value n_i, and zero otherwise. The vector describing the probability of being in any given configuration is then written as $|p(t)\rangle = \sum_{\mathbf{n}} p(\mathbf{n}, t)|\mathbf{n}\rangle$, and the master equation (73) becomes

$$\frac{\partial}{\partial t}|p(t)\rangle = -H|p(t)\rangle. \tag{110}$$

The quantum Hamiltonian H here corresponds to the operator denoted $-L^{\rm T}$ in (73); the minus sign is introduced so that the eigenvalues of H are non-negative and its ground states just give the steady states $|p\rangle$ of the system. Notice that the quantum mechanical Hilbert space product is defined so that the configurations $|\mathbf{n}\rangle$ are orthonormal; this is different from (76).

We describe briefly how to construct H, using the East model as an example. One essentially needs to transcribe $L^{\rm T}$ from (98). It is useful to adopt a particle language, with $n_i = 0$ and 1 respectively corresponding to the absence and presence of a particle at site i. It is then natural to define $|0\rangle$, the configuration with $n_1 = \ldots = n_N = 0$, as the vacuum, and obtain other configurations by applying suitable creation operators $b_i^\dagger$ which act as

$$b_i^\dagger|\ldots n_i = 0 \ldots\rangle = |\ldots n_i = 1 \ldots\rangle, \qquad b_i^\dagger|\ldots n_i = 1 \ldots\rangle = 0. \tag{111}$$

The 'Paulion' [242] operators $b_i^\dagger$ and their Hermitian conjugates b_i then commute at different sites, while at the same site they obey anticommutation rules, $\{b_i, b_i\} = \{b_i^\dagger, b_i^\dagger\} = 0$, $\{b_i, b_i^\dagger\} = 1$. The operator $b_i^\dagger b_i$ counts the number of particles at site i in

the usual way, $b_i^\dagger b_i|\mathbf{n}\rangle = n_i|\mathbf{n}\rangle$. Only one more ingredient is needed to write down H: the spin-flip operator F_i from (98) becomes $b_i^\dagger + b_i$ in the quantum version. Thus, the Hamiltonian $H \equiv -L^{\mathrm{T}}$ for the East model is

$$\begin{aligned} H &= -\sum_i b_{i-1}^\dagger b_{i-1}[c(1-b_i^\dagger b_i) + (1-c)b_i^\dagger b_i](b_i^\dagger + b_i - 1) \\ &= \sum_i b_{i-1}^\dagger b_{i-1}[c(b_i-1)b_i^\dagger + (1-c)(b_i^\dagger - 1)b_i] \end{aligned} \tag{112}$$

using the anticommutation relations to simplify the final expression. Conservation of probability is reflected in the fact that $\langle e|H = 0$, where $|e\rangle = \sum_{\mathbf{n}} |\mathbf{n}\rangle = \prod_i (1 + b_i^\dagger)|0\rangle$ is the unit or 'reference' state; this ensures that $\langle e|p(t)\rangle = \sum_{\mathbf{n}} p(\mathbf{n}, t) = 1$ does not change in time. As is typical, the Hamiltonian (112) is non-Hermitian since it is derived purely from a dynamical problem. Since the dynamics obeys detailed balance, however, the similarity transformation $|\mathbf{n}\rangle \to P_{\mathrm{eq}}^{1/2}|\mathbf{n}\rangle$ and $H \to P_{\mathrm{eq}}^{1/2} H P_{\mathrm{eq}}^{-1/2}$ with $P_{\mathrm{eq}} = \sum_{\mathbf{n}} p_{\mathrm{eq}}(\mathbf{n})|\mathbf{n}\rangle\langle\mathbf{n}|$ could be used to transform H to an explicitly Hermitian form.

Physical observables A are functions of the n_i, and therefore correspond to operators which are diagonal in the basis $|\mathbf{n}\rangle$, $A(\mathbf{n}, \mathbf{n}') = \langle \mathbf{n}|A|\mathbf{n}'\rangle = A(\mathbf{n})\delta_{\mathbf{n},\mathbf{n}'}$; their expectation values are given in the quantum formulation by

$$\langle A(t)\rangle = \sum_{\mathbf{n}} A(\mathbf{n}) p(\mathbf{n}, t) = \langle e|A|p(t)\rangle = \langle e|Ae^{-Ht}|p(0)\rangle. \tag{113}$$

Above, we effectively viewed the quantum mechanical Hilbert space as a Fock space, since it is spanned by configurations with any possible value of the total particle number $\sum_i n_i$ between 0 and N. Equivalently, one can think of the Hilbert space as the configuration space of a quantum spin system, with $n_i = (1 + \sigma_i)/2$ and σ_i the eigenvalue of the z-component σ_i^z of a quantum spin operator. The particle creation and annihilation operators then become raising and lowering operators $\sigma_i^\pm = \sigma_i^x \pm i\sigma_i^y$, and the vacuum state is the one with all spins down.

The above idea of mapping classical stochastic dynamical systems on to quantum models was pioneered by Doi [243, 244] for 'bosonic' systems, where many particles can occupy a given site, and later generalized to the 'fermionic' case of at most single occupancy that is relevant to us (see, e.g. [245]). An overview of developments in the field since then and a comprehensive bibliography can be found in [242]. As demonstrated beautifully in recent reviews [195, 246], quantum mappings have proved very powerful in the analysis of many stochastic non-equilibrium systems, particularly where the resulting Hamiltonians are those of known (and sometimes even exactly solvable) quantum systems [247]. They can also form the starting point for field-theoretic path-integral representations [248, 249]. Either from the latter or directly from the real-space (lattice) quantum Hamiltonians, renormalization group methods (see, e.g. [195, 250, 251]) then also become available to study the behaviour at large lengthscales.

For KCMs specifically, however, the benefits of the approach largely remain to be explored. Some use has been made of the formalism (e.g. [100, 215, 217, 237, 241, 252]) but with few extra insights gained that would not also have been available directly from the master equation; and in at least one case the formal manipulations actually obscure rather than clarify the simplifications resulting from detailed balance [237, 252].

4.10. *Mappings to effective models*

The low-temperature dynamics of KCMs can often be understood by means of a mapping to effective models. We already discussed such a mapping for f, d-SFMs with $f = 1$ in section 3.1.2, where we found that the dynamics at low up-spin concentration $c_{\rm eq}$ can be described in terms of the diffusion of defects, in this case isolated up-spins, with an effective diffusion constant $D_{\rm eff} = c_{\rm eq}/2$. Apart from diffusing, up-spins can also 'coalesce': when two of them are only separated by a single down-spin, the latter can flip up and then two of the resulting three up-spins can flip down successively. The reverse process where a single up-spin creates a second one is of course also possible by detailed balance. The effective low-temperature model for the $1, d$-SFMs is thus one of diffusing up-spins which can 'react' according to $A + A \leftrightarrow A$, where A stands for the single species of defect 'particle' in the system. This convenient representation, in which the kinetic constraints no longer appear explicitly, has been exploited, e.g. in [241, 253], and a similar description has been used for a driven version of the 1, 1-SFM [254] (see section 5.7). Much is known about such reaction–diffusion models; see, e.g. [255] for a recent list of references on the $A + A \leftrightarrow A$ model in $d = 1$. We have not specified above the precise ratio of the reaction and diffusion rates, but its value is expected to be unimportant in the relevant regime of small $c_{\rm eq}$ [256].

As explained already in section 3.5, in a lattice version [127] of the topological froth model a similar mapping to an effective model is also useful. At low-temperatures very few defects ($+1, -1$-spins) exist, and it can be argued [127] that the dynamics is dominated by defect pairs—dimers of adjacent $+1, -1$-spins—and isolated defects. Since dimers can diffuse and annihilate with each other or with isolated defects, one thus has again an effective reaction–diffusion model at low temperatures which can be used to understand, e.g. the relaxation of the energy, i.e. the defect concentration, after a quench.

Other effective models for KCMs can be obtained by coarse-graining to a continuum description; this approach has been successfully exploited to describe the properties of lattice gases, e.g. the KA model with and without gravity [257, 258]. One represents the state of the system by a coarse-grained density field $c(z)$ which under the effect of gravity should only depend on height z. Since the lattice gas is non-interacting, the local free energy density is simply $f(c) = T[c \ln c + (1 - c) \ln(1 - c)] + gcz$, with the last term accounting for the effects of gravity. One can now postulate a standard dynamics for the conserved density field, $(\partial/\partial t)c(z) = -\partial J(z)/\partial z$. The current $J(z) = -\Gamma(c(z))\partial\mu(z)/\partial z$ is the product of a local mobility $\Gamma(c)$ and the negative gradient of the chemical potential, which is given by $\mu(z) = \delta F/\delta c(z)$ with $F = \int {\rm d}z f(c(z))$ the total free energy. The model is made glassy only through the choice of the functional form of the mobility $\Gamma(\rho)$. To model the power-law singularity of the diffusion constant seen in simulations of the KA model [88] (see section 3.3.1), this was chosen in [258] as $\Gamma(\rho) = c(1 - c/c_{\rm dyn})^{\phi}$, which tends to zero with an exponent $\phi \approx 3.1$ as the density approaches the dynamical transition at $c_{\rm dyn}$. Being based on the behaviour of the diffusion constant in a system at uniform density c, it is not obvious that this is still a good approximation for the *local* mobility, especially in the interesting high-density region where one may expect pronounced inhomogeneities. Nevertheless, is has been shown to work remarkably well both for the KA model under gravity [258] and without gravity but with particle exchange with a reservoir allowed [257]. We mention in

passing that the dynamics of a related class of models with density-dependent mobilities have recently been analysed in [259, 260].

5. Results

In this section, we give a comprehensive survey of the known results on the dynamics of KCMs, including work on related models where appropriate. We begin in section 5.1 with the question of (effective) irreducibility, which ensures that naive calculations of equilibrium behaviour apply to KCMs. The following sections are arranged to mirror the structure of section 2. In section 5.2 we give results for the typical relaxation timescales of KCMs and their dependence on temperature or, for lattice gases, density; we also evaluate there the evidence for genuine dynamical transitions in KCMs. In section 5.3 we address the stationary dynamics of KCM, which should be relevant for modelling the dynamics around the (metastable) equilibrium of supercooled liquids. Section 5.4 is concerned with out-of-equilibrium dynamics, including nonlinear relaxation after quenches or crunches, hysteresis effects in heating–cooling cycles and two-time correlation and response functions. Dynamical lengthscales in KCMs and the evidence for dynamical heterogeneities are discussed in section 5.5. In section 5.6 we review the applicability of energy landscape paradigms such as configurational entropies and Edwards measures to KCMs. Finally, section 5.7 surveys some recent results on the behaviour of KCMs under external driving, which can be used to model, e.g. tapping experiments in granular media.

Within each subsection, we list results for the various models as far as possible in the order in which they were introduced in section 3. First are f, d-SFMs and their variants with directed constraints; where appropriate, we discuss the models with $f = 1$ separately because of their qualitatively different defect-diffusion dynamics. The next major group of models is formed by the kinetically constrained lattice gases, followed by the models inspired by cellular structures and the triangle and plaquette models obtained by mappings from interacting systems with unconstrained dynamics. Finally, results for related models such as urn, oscillator and needle models are included where appropriate.

5.1. *Irreducibility*

Beginning with **spin-facilitated models** with undirected constraints, let us summarize under which conditions on f the f, d-SFM is effectively irreducible. Formally, this means $p(c, L \to \infty) = 1$ for all $c > 0$; $p(c, L)$ is the probability that a random initial configuration with up-spin concentration c on a lattice of $N = L^d$ spins belongs to the high-temperature partition (see section 3.1.1). In order to understand finite-size effects, it is also useful to define the concentration $c_*(L)$ as the one where $p(c, L) = 1/2$ for given L; effective irreducibility corresponds to $c_*(L \to \infty) = 0$. The irreducibility results quoted below were mostly derived within the context of bootstrap percolation (BP). Recall from section 4.1 that the m-BP process is defined as iteratively removing from a lattice all particles that have fewer than m neighbours. By mapping particles to down-spins and vacancies to up-spins we saw in section 4.1 that if this process leads to an empty lattice, the corresponding configuration in the f, d-SFM belongs to the high-temperature partition, provided that m is chosen as $m = 2d + 1 - f$. As an example, the irreducibility problem for the $3, 3$-SFM corresponds to 4-BP in $d = 3$ dimensions.

As explained in section 4.1, f, d-SFMs with $f > d$ are always strongly reducible; for $f = 1$, on the other hand, it is trivial to see that they are effectively irreducible. Non-trivially, Schonmann [261] was able to prove rigorously that all models with the intermediate values $2 \leq f \leq d$ are also effectively irreducible. Enter [262] had earlier proved the result for the special case of the $2, 2$-SFM, formalizing an earlier unpublished argument due to Straley; Schonmann [261, 263] gave a generalization to BP-like models with more complicated rules. Fredrickson and Andersen [74] had earlier given a non-rigorous argument for irreducibility of the $3, 3$-SFM; Reiter [82] also constructed irreducibility proofs for the $2, 2$-SFM and $3, 3$-SFM.

Numerical investigations of finite-size reducibility effects in SFMs go back at least to Fredrickson and Brawer [85], who studied $p(c, L)$ and $c_*(L)$ in the $2, 2$-SFM. A simple linear extrapolation of $c_*(L)$ versus the inverse linear system size $L^{-1} = N^{-1/2}$ suggested $c_*(L \to \infty) \approx 0.04$, but Fredrickson and Brawer [85] argued that the functional form of this extrapolation was inappropriate since earlier arguments [74] had already suggested $c_*(L \to \infty) = 0$. It was later shown rigorously [207] and confirmed by simulation [264] that for the general $2, d$-SFM, $c_*(L)$ decreases only very slowly with system size, as $c_*(L) \sim 1/(\ln L)^{1/(d-1)}$. For other choices of f, the finite-size effects can be even larger. Enter *et al.* [208] considered the case $f = d$; this is the 'most dangerous' case that is still effectively irreducible, since for $f = d + 1$ and above the models are strongly reducible. For $d = 3$ the finite-size scaling of the critical concentration was predicted to be $c_*(L) \sim 1/\ln(\ln L)$ [208]; compared to $d = 2$ this has an extra ln in the denominator and this pattern continues for higher d, with $c_*(L) \sim 1/\ln[\ln(\ln L)]$ for $d = 4$, etc. This very slow approach of $c_*(L)$ to zero is obviously difficult to verify numerically; for $d = 3$ initial simulations were interpreted in terms of a non-zero $c_*(L \to \infty)$ [201, 204, 265], but later work showed an approach of $c_*(L)$ to zero that is consistent with the predictions [208].

Consider next spin models with **directed kinetic constraints**. For the asymmetric $1, 1$-SFM and its limit case the East model, the same argument as for the (symmetric) $1, 1$-SFM applies; all configurations except those with all spins down belong to the high-temperature partition and reducibility effects are unimportant. For the North-East model [81, 261] it has been shown, via a mapping to directed percolation, that in the thermodynamic limit a configuration will have a finite fraction of permanently frozen spins if its up-spin concentration c is below the critical value $c_* = 0.2942$. (The link to directed percolation arises because a spin will never be flipped up if and only if there is an infinite path starting from the chosen spin that consists of steps towards the North or East and visits only down-spin sites.) For the (a,f)-Cayley tree models in the most strongly constrained case $f = a - 1$, one has a continuous blocking transition at $c_* = (a - 2)/(a - 1)$, below which the fraction of permanently frozen spins grows continuously from zero; this can be shown by using recursion relations for trees of increasing depth (see section 4.1). For $2 \leq f < a - 1$ a blocking transition still exists, but is discontinuous.

Moving on to constrained **lattice gases**, reducibility effects in the KA model were discussed already in the original paper on the model [88]. As mentioned in section 3.3, such effects obviously depend on the parameter m in the model; recall that particles with m or more occupied neighbour sites are not allowed to move. On a cubic lattice $m = 6$ corresponds to an unconstrained system, while the case $m = 3$ is strongly reducible, with any set of eight particles arranged in a cube unable to move. For $m = 4$, KA argued that the model should be effectively irreducible in the thermo-

dynamic limit, as follows. They focused on the 'backbone', comprising all particles which are permanently frozen by other frozen particles, i.e. which remain frozen when all mobile particles are removed (see section 4.1). The backbone can thus be determined by iteratively removing all mobile particles from the lattice. In this process, a particle is removed if it has fewer than $m = 4$ particles as neighbours, and if there is at least one free neighbour site for which this condition would still be true after a jump to that site. Since the first part of this criterion is just the same as BP with $m = 4$, a backbone of permanently frozen particles will remain for densities where 4-BP does not reach the empty lattice configuration. This implies [208] that for particle densities $c \geq 1 - \mathcal{O}(1/\ln(\ln L))$ a backbone will occur with high probability in a system of linear size L; this criterion is just the obvious transformation ($c \to 1 - c$) of the one for irreducibility of the 3, 3-SFM because the latter problem is essentially equivalent to 4-BP. For lower densities one expects the probability of a backbone to occur to be small, and the system to be effectively irreducible. The theoretically expected finite size effects are extremely strong, however: $c \approx 1 - \mathcal{O}(1/\ln(\ln L))$ translates into a *double* exponential divergence $L \sim \exp\{A \exp[B/(1-c)]\}$ of the system sizes required to avoid a backbone at a given density. KA showed by direct simulation that up to densities $c \leq 0.86$ for their $L = 20$ system the probability for a backbone to occur is very small (≈ 0.007; see figure 12 above), and that therefore finite-size reducibility effects on their simulation results should be negligible. (A possible caveat is that there may be particles that are permanently frozen only by *mobile* neighbours, and these would not be counted in the backbone; but simulations by Jäckle and Krönig [113] for the triangular lattice gas suggest that this is a small effect.) For only slightly higher densities ($c = 0.88$ and 0.885), they found that much larger system sizes ($L = 40$ and 50, respectively) were required to avoid backbones; this is at least qualitatively consistent with the theoretically expected strong increase of L with c.

In the KA model with particle exchange allowed at the boundary with a reservoir at some chemical potential, or under the effect of gravity in a simulation box of large height, reducibility effects are greatly reduced compared to the conventional KA model. This is because particles can be removed one by one to the reservoir, or the upper reaches of the simulation box, and then reinserted, so that all configurations that can be 'emptied' in this way are mutually accessible. In some cases this makes the dynamics fully irreducible. A nice illustration is provided by a b.c.c. lattice where particles can move only if they have fewer than $m = 5$ nearest neighbours in their old and new positions [117]; lattice planes can then be successively emptied starting from the top, since every particle has at most four nearest neighbours in the lattice plane underneath (and, due to the lattice structure, none in its own plane). For the conventional KA setup, i.e. a cubic lattice with $m = 4$, it was argued in [110] that configurations up to densities $c = 1 - \mathcal{O}(1/L)$ are mutually accessible. While there are *some* configurations with such densities that can be accessed, accessibility of *typical* configurations should only be possible up to lower densities $c = 1 - \mathcal{O}(1/\ln L)$. This follows from the fact that, in a given lattice plane at the top of the system that is to be emptied, most particles (for c close to 1) have one neighbour in the plane underneath; they can thus be removed only if they have less than three neighbours in the plane. The problem thus reduces to BP on a square lattice with $m = 3$ which—as we know from the equivalence to the irreducibility problem in the 2, 2-SFM—reaches the empty configuration with probability close to one only for $1 - c \sim 1/\ln L$.

For the triangular lattice gas (with two-vacancy assisted hopping), it was shown in [113] that no permanently blocked particles should exist in the thermodynamic limit, at any particle concentration $c < 1$. The argument is quite similar to the irreducibility proofs outlined in section 4.1. It is based on the fact that a hexagonal ring of vacancies can move outwards as long as there is at least one vacancy on each of the six edges surrounding the hexagon. The probability of a local particle configuration with a vacancy hexagon that can grow to arbitrary size can be shown to be non-zero, and so in a thermodynamically large system at least one such local configuration will exist with probability one. A similar argument had earlier been given for the hard-square lattice gas [173] and later refined in [205, 206].

For models inspired by **cellular structures**, we are not aware of any explicit analysis of reducibility effects. However, as explained in section 3.5 these models all have dynamics of the defect-diffusion type. By analogy with $1, d$-SFMs, reducibility effects would therefore be expected to be irrelevant. For the **triangle and plaquette models** of section 3.6 the dynamics is clearly irreducible since it is in one-to-one correspondence with the irreducible (since unconstrained) spin-flip dynamics of the underlying spin system.

Finally, among the other models related to KCMs, only **needle models** are not obviously irreducible. The only case that has been addressed here is that of needles attached at their endpoints to a square (planar) lattice, and with their motion restricted to one side of the lattice plane [194]. Here it easy to see that every configuration can be reached from any other, going via the unentangled state with all needles orthogonal to the plane. The transformation to the unentangled state is achieved by a series of small steps: one first 'stretches' the configuration in the direction perpendicular to the lattice, and then 'cuts back' the increased needle lengths to their original value. The overall effect is a small rotation of all needles which does not cause them to cross, and repeated application eventually leads to the unentangled state. For needles attached to three-dimensional lattices, the irreducibility or otherwise of the dynamics appears to be an open problem.

5.2. *Relaxation timescales and dynamical transitions*

In this section we give results for the typical relaxation timescales of KCMs and their dependence on temperature or, for lattice gases, density; we also evaluate the evidence for dynamical transitions where ergodicity is broken. As explained in section 3.1.1, our criterion for a dynamical transition will be a divergence of an appropriate relaxation time in the thermodynamic limit.

We begin with **spin-facilitated models**. As explained in section 3.1.2, f, d-SFMs with $f = 1$ behave rather differently than those with $f \geq 2$, since relaxation can occur by diffusion of defects (isolated up-spins) through the system. This lack of any significant cooperativity in the dynamics leads to behaviour typical of strong glasses, with relaxation times increasing in an Arrhenius fashion as T is lowered; exemplary results for the 1, 1-SFM are shown in figure 8 above. This expectation was confirmed in a theoretical analysis by Fredrickson and Andersen [74], who used a diagrammatic technique to obtain approximations to the integrated relaxation time of the spin autocorrelation function. A later mean-field theory [217], paraphrased in section 4.4, also predicted the expected Arrhenius dependence of relaxation times. As an aside, we note that Fredrickson and Andersen [74] also investigated SFMs on lattices other than the conventional cubic ones, and found that there defect-diffusion dynamics can also occur for $f \geq 2$. This is the case for, e.g. the SFM on a triangular lattice with

$f = 2$. Here the defects are pairs of neighbouring up-spins. Such a pair can facilitate an up-flip of a neighbouring spin; if then one of the original up-spins flips down, the defect has effectively rotated around one of its endpoints, and by repetition of this process can diffuse across the lattice in a tumbling motion.

More interesting are f, d-SFMs with $f \geq 2$ (on the conventional cubic lattices); we saw in section 3.1.2 that in these models relaxation processes proceed in a strongly cooperative fashion which should lead to a superactivated relaxation timescale increase. For $2, d$-SFMs, for example, the approximate analysis of [74] resulted in an integral equation for the autocorrelation function very similar to typical mode-coupling equations (see section 4.7.3). This predicts a divergence of the relaxation time, and therefore a dynamical transition, at an up-spin concentration of $c_{\mathrm{dyn}} = 1/\{[(3/2)^3 2d(2d-1)]^{1/2} + 1\}$. Fredrickson and Andersen argued that since their approximation was of a mean-field type it should be reasonable at least for larger d. For, e.g. $d = 1$ it is clearly incorrect since the $2, 1$-SFM, being strongly reducible, shows an incomplete decay of the spin autocorrelation function at *any* c. For $d = 2$, the theory fails in the opposite way: later simulations [85, 266] and theoretical arguments [82] strongly suggested that there is no true dynamical transition at any non-zero c. As is typical of MCA-like theories, however, a fit of the relaxation time increase to a power-law behaviour suggests a divergence close to the theoretically predicted value c_{dyn}. For larger spatial dimension, $d = 3$, simulations of the $2, 3$-SFM [266] found agreement with the theory of [74] over a broader range of c, as expected, although again there was no evidence of an actual dynamical transition. Butler and Harrowell [93, 94] also obtained relaxation times for the $2, 2$-SFM from simulations of the persistence function (see section 5.3 below), finding the expected superactivated temperature dependence. The $2, 2$-SFM and $2, 3$-SFM (with slightly modified transition rates) were revisited in later simulations by Graham *et al*. [77, 78], who also studied the $3, 3$-SFM. Their data for the relaxation times—extracted using stretched exponential fits to spin autocorrelations—are shown in figure 9 above. Graham *et al*. fitted their results by a VTF law (2), with a divergence at a non-zero temperature T_0. This provides a good fit over two and a half decades in τ, as does a power-law singularity at non-zero temperature for the $2, 3$-SFM data. However, extrapolations towards an actual divergence are subject to the usual reservations; inspection of figure 9 suggests, for example, that an EITS behaviour with Arrhenius corrections, $\tau \sim \exp(A/T^2 + B/T)$, would also fit the data but not give any divergence at $T > 0$. The absence of such a divergence is also predicted by a recent theoretical treatment [237] of $2, d$-SFMs, using an MCA for the second-order memory function of spin fluctuations to obtain approximate spin autocorrelation functions. This gave a superactivated growth of the relaxation time at low T, whose functional form was not however analysed in detail. Overall, we regard the theories and simulation data on the 'cooperative' SFMs as compatible with the absence of a bona fide dynamical transition at non-zero temperature. However, the theoretical prediction of even the functional form of the temperature dependence of relaxation timescales in these models remains an open problem. (One plausible conjecture on the basis of the growth of dynamical lengthscales is that the divergence of τ for small T is in fact doubly exponential, $\tau \sim \exp[A \exp(1/T)]$; see section 5.5.)

Next we turn to SFMs with **directed kinetic constraints**. The simplest of these is the East model, which as discussed in section 5.1 is effectively irreducible at any non-zero up-spin concentration or, equivalently, non-zero temperature. Already when the model was first proposed [79] it was argued that relaxation timescales should remain

finite for any $T > 0$. This has recently been proved rigorously: the longest relaxation time, obtained as the inverse of the smallest decay rate that one would find by full diagonalization of the master equation, is bounded between $\exp[1/(2T^2 \ln 2)]$ and $\exp[1/(T^2 \ln 2)]$ in the limit of small temperatures [267]. The upper bound in this result is also consistent with the estimate of [220]. The East model therefore exhibits an EITS relaxation time divergence at low temperatures, as anticipated intuitively in section 3.1.2 on the grounds of the cooperative nature of relaxation processes. That relaxation times in the East model must diverge in a superactivated fashion, i.e. more strongly than any power of the inverse up-spin concentration $1/c \approx \exp(\beta)$, had already been shown by Jäckle and coworkers [218, 219]. They used an elegant argument based on the fact that the relaxation necessarily becomes faster if the kinetic constraint on the leftmost spin in a finite chain is lifted. We note briefly that MCA approaches fail rather dramatically for the East model: Kawasaki's [230] application of the MCA to the irreducible memory function, reviewed in section 4.7.3, predicts a spurious dynamical transition at up-spin concentration $c = 0.2$.

Having seen that the 1, 1-SFM with its undirected kinetic constraint shows strong-glass behaviour, while the East model has a much more dramatic relaxation time increase typical of fragile glasses, it is not unexpected that the asymmetric 1, 1-SFM which interpolates between these two extremes shows a fragile-to-strong cross-over on lowering T [83, 84]. Referring to (32) in section 3.1, the East model corresponds to the value $a = 0$ for the interpolating parameter, and displays cooperative relaxation on 'fragile' timescales $\tau \sim \exp(1/T^2 \ln 2)$. For any $a > 0$, however, one has the diffusion of isolated up-spins, which dominates the dynamics of the 1, 1-SFM, as an additional relaxation process. As will be explained shortly, the timescale for the latter is $\tau_{\text{diff}} \sim (1 + a^{-1}) \exp(1/T)$. This increases only in an Arrhenius (strong) fashion so that defect-diffusion, being the faster process, dominates the relaxation at low T. The cross-over occurs where $\tau \approx \tau_{\text{diff}}$; since the prefactor in τ_{diff} becomes large for $a \to 0$, the cross-over shifts to lower temperatures as a decreases. The derivation of the defect-diffusion timescale τ_{diff} is essentially an extension of the analogous argument for the 1, 1-SFM given in section 3.1.2. Consider the rate for diffusion of an isolated up-spin by one step to the right; the rate for a diffusion step to the left is the same from detailed balance. The right neighbour of the up-spin needs to flip up, which from (32) takes place at rate $c_{\text{eq}} \equiv c$. A successful diffusion step is only obtained if the original up-spin then flips down before the new up-spin does; the probability for this is $a/(a + 1)$ since the rates for a down-flip of the original and of the new spin are $a(1 - c)$ and $1 - c$, respectively. This gives the overall rate of $ca/(1 + a)$ for a diffusion step, hence $\tau_{\text{diff}} \sim (1 + a^{-1}) \exp(1/T)$ as anticipated.

To finish off our discussion of SFMs with directed constraints, we now discuss the North-East and Cayley tree models. These differ from all models discussed so far in this section in that they are strongly reducible below some non-zero up-spin concentration c_*; see section 5.1. Since reducibility implies non-ergodicity, these models must therefore show diverging timescales as c approaches c_*. It is in principle possible that a separate, and therefore non-trivial, dynamical transition could occur at some higher c_{dyn}, but numerical studies suggest that this is not the case and that relaxation timescales diverge only at c_* [81]. In the North-East model, simulations for fairly small lattice sizes ($L = 40$) suggest a power-law divergence of the relaxation time as c approaches c_*, with an exponent around 5, but possibly larger for larger lattices [81].

A number of theories have been applied to both the North-East and Cayley tree models and generally do predict dynamical transitions, though at incorrect values of c. For the $(a, a-1)$-Cayley tree, diagrammatic treatments [238], an MCA applied to the irreducible memory function [230] and an effective medium approximation [268] have all been used. The known value of the transition is at $c_{\rm dyn} = c_* = (a-2)/(a-1)$; see section 5.1. The diagrammatic method predicts a higher value, $c_{\rm dyn} = (a-1)/a$ ($= 2/3$ for $a = 3$, compared to the true $c_* = 1/2$). The effective medium approximation gives an even higher estimate, $c_{\rm dyn} = 0.690$ for $a = 3$. Both are somewhat superior to the MCA, which gives a transition at too low a value of c, e.g. $c_{\rm dyn} = 0.4090$ for $a = 3$ [269], and also incorrectly predicts that the fraction of frozen spins jumps discontinuously to a non-zero value below the transition. For the North-East model, all three approaches make exactly the same predictions as for the $(3, 2)$-Cayley tree model with $a = 3$. Thus, neither captures the behaviour observed in numerical simulations [81, 268] and expected from the relation to directed percolation, with a transition at $c_{\rm dyn} = c_* \approx 0.2942$ (see section 5.1) and a non-analytic increase of the fraction q of frozen spins below the transition according to $q \sim (c_* - c)^{0.25 \pm 0.05}$.

We next turn to relaxation timescales in kinetically constrained **lattice gases**. Kob and Andersen, in their original paper on the KA model [88], determined the self-diffusion constant $D_{\rm s}$ as a function of the particle density c; $D_{\rm s}$ was obtained from the long-time limit of the mean-square particle displacements. For densities between $c \approx 0.3$ and $c = 0.86$, they obtained a very good fit to their data with $D_{\rm s} \sim (c_{\rm dyn} - c)^{\phi}$, covering over three decades in $D_{\rm s}$, with $c_{\rm dyn} = 0.881$ and exponent $\phi = 3.1$ (see figure 13 above). This suggests a dynamical transition caused by a divergence of the diffusion timescale $1/D_{\rm s}$ at $c = c_{\rm dyn}$. A singularity of Vogel–Fulcher type ($1/D_{\rm s} \sim \exp[A/(c_{\rm dyn} - c)]$) could be excluded as providing a much worse fit to the data. Relaxation times extracted from equilibrium correlation functions also showed power law divergences at densities very close to $c_{\rm dyn}$. KA argued convincingly that their data were not affected by finite-size effects, and that the extrapolated vanishing of $D_{\rm s}$ at $c = c_{\rm dyn}$ was therefore a genuine dynamical transition. They conceded, however, that simulations closer to or in fact above $c_{\rm dyn}$ would be needed to establish the existence of such a transition more firmly. It is intriguing that the $c_{\rm dyn}$ found by KA is quite close to the density where the (linear) system size L needed to avoid reducibility effects due to permanently frozen particles begins to increase strongly. The theoretical expectation is that L eventually diverges as $L \sim \exp\{A \exp[B/(1-c)]\}$ (see section 5.1), and this very strong increase of a lengthscale might explain the apparent vanishing of the diffusion constant $D_{\rm s}$. In the mathematical limit $L \to \infty$, $D_{\rm s}$ may remain non-zero up to $c < 1$, but its value would be so small and the system sizes required to measure it so unrealistically large that this would be of little physical relevance. Finally, it has been suggested that the power-law singularity of $D_{\rm s}$ might be analogous to critical slowing-down, in which case one would expect the exponent ϕ to be insensitive to the precise nature of the kinetic constraint or the lattice type. Simulations for f.c.c. lattices with $m = 5, 7, 8$ [270], and for the b.c.c. lattice with $m = 5$ [258] support this hypothesis. The underlying reasons for such apparent universality remain poorly understood, however.

For the triangular lattice gas with two-vacancy assisted hopping [113, 118] numerical simulations were performed of both the self and collective diffusion constants (see section 2.2). The self-diffusion constant $D_{\rm s}$ decreases by about four

orders of magnitude as the particle concentration is increased from $c = 0$ to $c = 0.77$; it can be fitted both by a power-law $D_s \sim (c_{dyn} - c)^{\phi}$ and an exponential singularity $D_s \sim \exp[-A/(1-c)]$. Since in the thermodynamic limit no particles are expected to be permanently blocked (see section 5.1), it was argued that the dynamical transition at $c_{dyn} < 1$ predicted by the first fit is spurious [113]. However, this argument effectively assumes that *irreducibility* (absence of permanently blocked particles) rules out a dynamical *ergodicity* breaking transition; as explained in section 3.1.1, this is not an obvious implication. The self-diffusion constant D_s for the triangular lattice gas was also obtained from an approximate calculation of the intermediate self-scattering function (14), using the projection formalism with the memory function set to zero. As explained in section 2.2, the long-time and long-wavelength limit of this quantity determines D_s. The approximation used was too simple to capture the rapid decrease of D_s with increasing c, however, and in fact predicts a non-zero limit for $c \to 1$ [113]. A similar approximation for the collective diffusion constant D predicts $D \sim (1-c)^2$. Extending the set of observables included in the projection technique modifies this to $D \sim (1-c)^3$, but even so the numerically observed decrease of D with c is much more pronounced [118].

Next we consider models inspired by **cellular structures**. As discussed qualitatively in section 3.5, these all exhibit diffusion of appropriate defects, so that one would expect an activated temperature dependence of relaxation times. Indeed, Davison and Sherrington considered the relaxation time τ over which the autocorrelation function of the local deviations $n_i - 6$ from the hexagonal ground state decays to $1/e$ of its initial value [126], and found that it is well fitted by an offset Arrhenius law, $\tau = A + B\exp(C/T)$. Similar behaviour is observed in the lattice analogue of the model [127]. The **plaquette** model also exhibits defect-diffusion and therefore activated relaxation times; see section 3.6. The **triangle** model, on the other hand, displays cooperative relaxation processes similar to those in the East model. As explained in section 5.4.1 below, this leads to an estimate of the relaxation timescale $\tau \sim \exp[T^2/(2\ln 2)]$ [131]. This differs from the result for the East model only through the extra factor of $1/2$ in the exponent, which accounts for the two-dimensional nature of the model.

In models with entropic barriers such as the **Backgammon model** or the **oscillator** model relaxation times remain finite at any non-zero temperature, exhibiting only power law corrections to the dominant Arrhenius behaviour $\tau \sim \beta^n \exp(A\beta)$; here A is a constant and $n = -2$ and $n = 1/2$ in the Backgammon and oscillator models, respectively. Relaxation times to reach the ground state at $T = 0$ do of course diverge with the system size (as 2^N for the Backgammon model [156, 157, 161], or more slowly as N^2 [161] in variants such as model C from [151]), but at $T > 0$ the final energy per box or particle lies above the ground state by a finite amount and so all timescales remain finite.

Finally, we comment on **needle models**. In the model of thin needles attached to an f.c.c. lattice, Renner *et al.* [192] investigated the dependence of the rotational self-diffusion constant D_s on the ratio $l = L/a$ of needle length L and lattice constant a. The measured values could be well fitted by a power-law singularity $D_s \sim (l_{dyn} - l)^{\gamma}$ with $l_{dyn} \approx 2.7$ and $\gamma \approx 4.2$. This would indicate a dynamical transition, though it is difficult to exclude the possibility that measurements around $l \approx l_{dyn}$ would reveal a rounding of the apparent singularity. For a similar model, with needles attached by their endpoints to a cubic lattice, Obukhov *et al.* [194] argued that there was a true dynamical transition at $l_{dyn} \approx 4.5$. Their evidence for this was based on simulations

of the average root-mean-square angular displacements $\theta(t)$ as a function of time. They argued that if there is indeed a transition, then for all l near $l_{\rm dyn}$, $\theta(t)$ should show the same behaviour, up to times that diverge as $l \to l_{\rm dyn}$. The effect of an increase in length (which they implemented approximately by freezing a small fraction of the needles) should therefore be smallest for $l = l_{\rm dyn}$, and their simulations appeared to confirm this. They also interpreted their results as showing that $\theta(t)$ had a finite long-time limit for $l > l_{\rm dyn}$, but again it seems difficult to exclude the alternative interpretation of a cross-over to slow rotational diffusion outside their simulation time window. For smaller lengths $l < l_{\rm dyn}$, Obukhov *et al.* [194] argued phenomenologically that since a needle interacts typically with l^3 others, the relaxation timescale should increase as $\exp(l^3)$, and found some simulation evidence for this. If there is indeed a dynamical transition then this behaviour should cross over to a divergence at $l = l_{\rm dyn}$, but this was not investigated in detail. For the two-dimensional case of needles attached to a square lattice, the simulation data were consistent with the relaxation time behaviour $\tau \sim \exp(l^2)$, and no evidence of a dynamical transition was found.

5.3. *Stationary dynamics*

One of the important questions about KCMs is how good they are at reproducing the characteristic aspects of the supercooled state. We therefore review in this section the results for equilibrium properties of KCMs such as correlation, response and persistence functions.

We begin by defining the relevant quantities for **spin-facilitated models**. Many studies have analysed the spin autocorrelation function, which using $\langle n_i \rangle = c \equiv c_{\rm eq}$ can be written as

$$C(t) = \frac{1}{N} \sum_i \frac{\langle n_i(t) n_i(0) \rangle - c^2}{c(1-c)}. \tag{114}$$

We have multiplied by a constant factor here to normalize the correlation function to $C(0) = 1$. Notice that only the cN spins which are in the up-state $n_i = 1$ at time 0 contribute non-zero averages $\langle n_i(t) n_i(0) \rangle$ in (114); one can therefore also write $C(t) = (\langle n_i(t) \rangle - c)/(1-c)$ where n_i is any spin that is initially up.

The dynamics of the overall up-spin concentration $c(t) = (1/N) \sum_i n_i(t)$ is also often of interest; in equilibrium its average is $\langle c(t) \rangle = c$ for all times. Its normalized equilibrium correlation function is

$$C_{\rm c}(t) = \frac{1}{N} \sum_{ij} \frac{\langle n_i(t) n_j(0) \rangle - c^2}{c(1-c)} \tag{115}$$

and is seen to be a sum of non-local spin correlation functions $\langle n_i(t) n_j(0) \rangle - c^2$. Finally, the persistence function $F(t)$ has also been studied; it measures the fraction of spins which, starting from an equilibrated configuration at time 0, have never flipped up to time t. The integral $\int_0^\infty {\rm d}t\, F(t)$ gives the mean-first passage time, i.e. the average time after which a spin will first flip. The persistence function and mean-first passage times can also be defined separately for spins that were up or down in the starting configuration.

We begin by considering **spin-facilitated models** with **defect-diffusion** dynamics, i.e. f, d-SFMs with $f = 1$. Most work has focused on the $1, 1$-SFM, though there are also a few results for $1, d$-SFMs in $d > 1$ (see below). To get some intuition, we first

recap briefly the discussion in section 3.1.2 of the low-temperature, i.e. small-c, dynamics of the 1, 1-SFM. We saw that up-spins occur as isolated defects, and that these diffuse with an effective diffusion constant $D_{\rm eff} = c/2$. The typical distance between defects is $1/c$, so that the timescale τ on which defects start noticing each other is set by $(2D\tau)^{1/2} = 1/c$, giving $\tau = c^{-3}$ as in (34). The spin autocorrelation function, $C(t) = (\langle n_i(t)\rangle - c)/(1-c)$ for spins with $n_i(0) = 1$, simplifies for small c to $C(t) = \langle n_i(t)\rangle$. It is therefore just the probability that a spin that was up at time 0 is also up at time t. For $t \ll \tau$, where defects are non-interacting random walkers, this is just the return probability of a random walk and therefore

$$C(t) = \int_{-\pi}^{\pi} \frac{{\rm d}q}{2\pi} \exp[-2D_{\rm eff}(1-\cos q)t] \tag{116}$$

which is a function of ct only, with $C(t) = 1 - ct$ for $ct \ll 1$ and $C(t) = (2\pi ct)^{-1/2}$ for $ct \gg 1$. This behaviour should then cross over to a faster decay when t becomes of order $\tau = c^{-3}$ and defects start interacting; in this regime $C(t)$ is already small, of order $(c\tau)^{-1/2} = c$. Interestingly, we see here that the spin relaxation function in the 1, 1-SFM allows three different timescales to be defined: the *instantaneous* time, where $C(t) = 1/{\rm e}$, scales as $c^{-1} \approx \exp(1/T)$. The longest timescale, on which defects begin interacting is $\tau = c^{-3} = \exp(3/T)$. The *integrated* timescale $\int_0^\infty {\rm d}t\, C(t)$, finally, is dominated by the $(ct)^{-1/2}$ tail of $C(t)$ up to times $t \approx \tau$, and therefore scales as $c^{-1/2}\tau^{1/2} = c^{-2} \approx \exp(2/T)$; see figure 8 above. All three timescales show activated behaviour, as anticipated in section 3.1.2. Figure 19 shows that the scaling of $C(t)$ obtained above, i.e. a product of $(ct)^{1/2}$ times a cutoff function on longer timescales t, is qualitatively confirmed by simulations [55].

We now turn to detailed theoretical calculations of the spin autocorrelation function of the 1, 1-SFM. A comprehensive analysis was given in [253]. Calculations

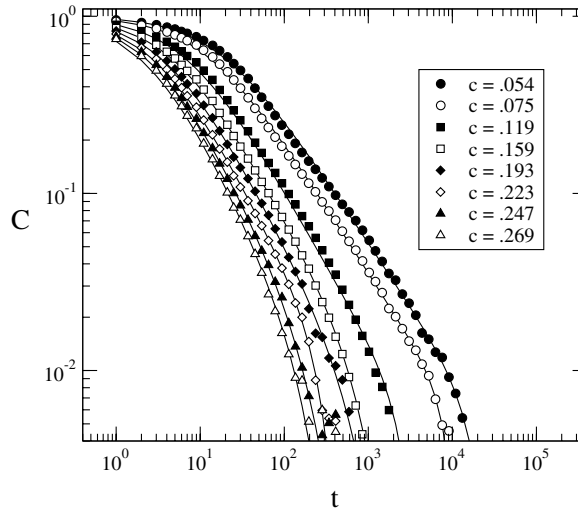

Figure 19. Normalized spin autocorrelation function $C(t)$ in the 1, 1-SFM for up-spin concentrations ranging from $c = 0.269$ down to $c = 0.054$. The solid lines show fits to the form $C(t) = (1 + t/\tau_1)^{-\alpha}\exp(-at^b)$ where τ_1, α, a and b are fitting parameters. As expected from the diffusive nature of the dynamics, the exponent α is close to $1/2$, and τ_1 is of order $1/c$ (see text for details). From [55]. Copyright American Institute of Physics.

were performed within the projection approach, with memory terms set to zero. Three different sets of observables were considered for the projection. The first contained the normalized fluctuations $\eta_i = [c(1-c)]^{-1/2}(n_i - c)$ of local spins around their averages, and their pairwise products; the second included in addition some triple products. The third contained single spin fluctuations as well as the variables $L^n\eta_i$ with $n = 1, \ldots, 5$, which can be motivated via a high-temperature expansion. As expected, the last choice works best for large c (down to $c \approx 0.3$). For lower c, the approximation which includes triple spin products gives the most accurate results and predicts an asymptotic decay of $C(t) \approx (2\pi ct)^{1/2}\exp(-t\sqrt{8c^5})$. For times $c^{-1} \ll t \ll c^{-5/2}$ this gives precisely the square-root decay as expected from the discussion above. A treatment of the effective low-temperature model of diffusing defects gave a similar functional form, but with the exponential cutoff function replaced by $\exp(-\sqrt{8c^2 D_{\mathrm{eff}} t})$. This has the scaling with $c^3 t = t/\tau$ expected on qualitative grounds, but the functional form is not necessarily reliable since it is derived under the assumption that the exponent is still small and defects have just started to interact. Information on the integrated relaxation time, which depends on the long-time behaviour of $C(t)$, could therefore not be deduced from this approach; within the best alternative (three-spin) approximation of [253] it scaled as $c^{-7/4}$, still somewhat below the scaling with c^{-2} expected from the qualitative arguments above. A later analysis of equilibrium correlation functions in the 1, 1-SFM [241] took a different approach based on a spatial coarse-graining of the local up-spin concentrations. To produce small concentration fluctuations, however, the coarse-graining distance must then be of the order $1/c$ or larger, and fluctuations on such lengthscales are no longer related to the spin autocorrelation function in an obvious way.

Interestingly, it turns out that the relaxation of the *overall up-spin concentration* in the 1, 1-SFM, as determined by the correlation function $C_{\mathrm{c}}(t)$ defined in (115), can be calculated exactly in the limit of small c [271, 272]. This is possible because of the mapping of the 1, 1-SFM on to an effective $A + A \leftrightarrow A$ reaction–diffusion model; see section 3.1.2. An exact calculation [271, 272] for the latter results in $C_{\mathrm{c}}(t) = (1 + 2t/\tau)\mathrm{erfc}[(t/\tau)^{1/2}] - 2[t/(\pi\tau)]^{1/2}\exp(-t/\tau)$, with a long-time behaviour of $[\pi(t/\tau)^3]^{-1/2}\exp(-t/\tau)$. The timescale here is $\tau = (2D_{\mathrm{eff}}c^2)^{-1} = c^{-3}$ as before, so that fluctuations in the overall up-spin concentration relax when diffusing up-spins begin to interact (see above). In contrast to the *spin* autocorrelation function, there is no decay on the shorter timescale $\sim 1/c$ for diffusion of individual defects, because the up-spin concentration remains unchanged while up-spins only diffuse but do not interact.

Finally for the 1, 1-SFM, we turn to the persistence function of down-spins, which is fairly straightforward to estimate [241]. Consider a domain of l down-spins bounded by up-spins at $t = 0$. As time increases, the up-spins will have flipped spins in a region of size $\sim\sqrt{2D_{\mathrm{eff}}t}$ around each, so that only around $l - 2\sqrt{2D_{\mathrm{eff}}t}$ persistent down-spins will remain. Since the equilibrium distribution of down-spin domain lengths is $P(l) \approx c\exp(-cl)$ for low c, the persistence function is approximately

$$\sum_{l \geq 2\sqrt{2D_{\mathrm{eff}}t}} \left(l - 2\sqrt{2D_{\mathrm{eff}}t}\right) c\mathrm{e}^{-cl} = \mathrm{e}^{-2c\sqrt{2D_{\mathrm{eff}}t}} \tag{117}$$

and again decays on timescales scaling as $c^{-2}D_{\mathrm{eff}}^{-1} \sim c^{-3} = \tau$.

For the $1, d$-SFM in arbitrary dimension d, with equilibrium up-spin concentration c, it was shown in [214] that $2dc$ is an exact eigenvalue of the Liouvillian, giving the relaxation rate of an appropriately defined staggered magnetization. The authors also found numerically for $d = 1, 2$ that exactly half this rate determines the early stages of the decay of the spin autocorrelation functions in these models, which are well fitted by the simple exponential $C(t) = \exp(-dct)$. This result actually has a simple interpretation for small c, where up-spins are isolated and far from each other. As for the 1, 1-SFM, the spin autocorrelation function is then for short times just the return probability of a random walker in d dimensions with diffusion constant D_{eff}. This is the d-th power of the result (116) for $d = 1$, giving for short times $C(t) = (1 - ct)^d = 1 - dct + \mathcal{O}((ct)^2)$ consistent with the early time scaling found in [214].

Next we consider SFMs with **cooperative dynamics**, i.e. f, d-SFMs with $f \geq 2$. As mentioned already in section 5.2, in their early theoretical work on $2, d$-SFMs Fredrickson and Andersen [73, 74] predicted that the spin autocorrelation function should show a dynamical transition at some up-spin concentration c_{dyn}; an increasingly non-exponential shape of the correlation function was predicted on approaching c_{dyn} from above, while below the correlation function should decay to a non-zero value. Simulations soon after [85], however, showed that this predicted transition is spurious; instead, the spin autocorrelation functions showed stretched exponential decays for low c, with stretching exponents decreasing as c was lowered, and relaxation times increasing in a super-Arrhenius fashion (see section 5.2). Similar results were later reported by Graham *et al*. [77, 78] for the spin autocorrelation function in the 2, 2-SFM, 2, 3-SFM and 3, 3-SFM (with the slight modification that rates for allowed transitions were chosen to be independent of the number of facilitating neighbours). The stretched exponential behaviour sets in at low c and intermediate times; the short time relaxation is exponential. In all cases the stretching exponent b stays between around 0.3 and 0.6 and decreases with c. Fredrickson [273] also studied the autocorrelation function of the total up-spin concentration, $C_{\text{c}}(t)$, and found similar behaviour, but with different stretching exponents which were somewhat closer to 1. Harrowell [274] simulated the *persistence function* in the $2, 2$-SFM and found that at long times it was well fitted by a stretched exponential with a stretching exponent b close to $1/2$, for up-spin concentrations c between around 0.08 and 0.2. Additional evidence of stretching was obtained [275] by analysing the power spectrum of spin fluctuations, i.e. the Fourier transform of the autocorrelation function $C(t)$; see (10) in section 2.2. At high temperatures the spectrum is practically Lorentzian, with a slight broadening because even for $T \to \infty$ the kinetic constraints still act (since $c = 1/2$; constraints only become irrelevant for $c = 1$, corresponding formally to $\beta = -\infty$). At temperatures below $T = 0.5$ the power spectrum showed $1/\omega$-noise in a large band of frequencies; from (11) this corresponds directly to a large frequency range where the dissipative response is approximately constant, and hence to a wide spectrum of relaxation times.

Finally, we mention simulation work [276] on the spin autocorrelation function in the $2, 2$-SFM with a ferromagnetic interaction J included; see (22). Stretched exponential behaviour is again observed, but with parameters (relaxation time and stretching exponent) that depend on J and T only through the equilibrium concentration c of up-spins. This shows that the dynamical behaviour of the model in the glassy regime is largely independent of the precise details of the energy function and instead dominated by the effects of the kinetic constraints.

We now move on to the stationary dynamics of SFMs with **directed constraints**. In these models, it can be shown [268] that the directionality of the constraint implies that all non-local spin correlations $\langle n_i(t)n_j(t)\rangle - c^2$ vanish, so that the spin autocorrelation function (114) and the autocorrelation function (115) of the total up-spin concentration give exactly the same information. The proof is easiest to see in the East model: consider spin n_i and a spin to its right, n_j with $j > i$. Because each spin facilitates spin-flips of only its *right* neighbours, the value of $n_j(0)$ cannot affect the state of $n_i(t)$ at times $t > 0$. Hence $\langle n_i(t)n_j(0)\rangle - c^2 = 0$ for $t > 0$. But in detailed balance systems all correlation matrices are symmetric (see section 4.7.1) and so also $\langle n_j(t)n_i(0)\rangle - c^2 = 0$ for $t > 0$; the two results together imply that all non-local correlations vanish.

For the simplest model with directed constraints, the East model, Jäckle and Eisinger [79, 218] obtained an approximation for the spin autocorrelation function using an effective medium approximation. Effectively the same result was derived by Pitts and Andersen [238] using diagrammatic methods; see (108). The approximation predicts a spurious dynamical transition at an up-spin concentration of $c = 0.5$, with $q = C(t \to \infty)$ increasing smoothly from zero to non-zero values. The MCA derived by Kawasaki [230], on the other hand, gives the relation (103) and, as discussed in section 4.7.3, predicts a transition at $c = 0.2$, with a discontinuous jump of q from 0 to 1/2. Both approximations can therefore only be reasonable at sufficiently large c, or for short times at smaller c; a comparison with numerical simulations [269] shows that the effective medium approximation is generally more accurate in these regimes. Improved approximations of the form of extended MCA [238] avoid the prediction of a spurious dynamical transition at $c > 0$, and are quantitatively more satisfactory over a larger range of times and up-spin concentrations. However, for small c they still predict a decay of $C(t)$ that is too fast and too similar to an exponential compared with numerical simulations. It had been noticed early on [79] that the non-exponential behaviour is well fitted by a stretched exponential only over a limited time range.

Pitts *et al.* [269] also suggested that for low T (i.e. low c) the autocorrelation function of the East model might exhibit scaling behaviour in the form $C(t) = \tilde{C}(t/\tau(T))$ with a diverging timescale $\tau(T)$ for $T \to 0$ and a scaling function $\tilde{C}$ close to a stretched exponential. It seems likely that such scaling will indeed apply in the *asymptotic* long-time regime; from arguments based on links to defect-diffusion models [218], the rigorous work of [267] and results for the out-of-equilibrium behaviour [220] the asymptotic timescale should be $\tau(T) \sim \exp(1/T^2 \ln 2)$, but the asymptotic scaling function is expected to be a simple (not a stretched) exponential, possibly up to power-law factors [218]. However, for times much shorter than $\tau(T)$ it was shown that the correct scaling variable for the initial decay of the autocorrelation function is not $t/\tau(T)$ but rather $\delta = [t/\tau(T)]^{T \ln 2}$ for low T [220, 221], giving very strongly stretched relaxation behaviour. To be compatible with the cross-over to the asymptotic $t/\tau(T)$-scaling, the scaling function of δ would then have to decay to zero at the finite value $\delta = 1$, since $\delta > 1$ gives $t/\tau(T) = \delta^{1/T} \to \infty$ for $T \to 0$ [213]. Buhot and Garrahan [83, 84] gave an alternative derivation of the stretching exponent $T \ln 2$, by considering the persistence function of up-spins. (For the East model, this is essentially identical to the autocorrelation function for $c \to 0$, since once an up-spin has flipped down the probability for it to 'reappear' later in the same place is $\mathcal{O}(c)$.) For the asymmetric 1, 1-SFM with small asymmetry parameter a they found a cross-over in the

persistence function from behaviour typical of the East model ($a = 0$) to that for the 1, 1-SFM, at times around $t \sim (1 + a^{-1})e^{1/T}$ where the diffusion of up-spins enabled by the non-zero value of a becomes significant (see section 5.2).

For the more complicated SFMs with directed constraints, i.e. the North-East model and the $(a, a-1)$-Cayley tree models, most work has focused on predicting the location of the dynamical transitions, which in these models arise from strong reducibility effects below some up-spin concentration c_* (see section 5.2). Beyond this, almost no details on the shape of spin autocorrelation and persistence functions are known.

Let us now consider the equilibrium dynamics of kinetically constrained **lattice gases**. Kob and Andersen [88] simulated the intermediate self-scattering function (14), suitably modified to take account of lattice symmetries (see section 3.3.1). In accord with the original motivation for defining the model, they compared their results primarily to the predictions of MCT as applied to supercooled liquids [16–19]. No plateau at intermediate times was found, in contrast to MCT (see figure 14 above). This was rationalized from the fact that in MCT the decay of correlations to the plateau is caused by particles 'rattling' in their cages; but in the KA model, particles that are caged in were argued to be likely completely immobile, so that rattling is essentially absent and any plateau would be very close to the initial value of the correlator. MCT predicts a power law in time for the decay from the plateau, and in the glassy regime of high densities the simulation results for small wavevectors (large lengthscales) were in accord with this. But the power law exponent was not independent of density as expected from MCT, and for larger wavevectors deviations from power law behaviour appeared. The decay at longer times is predicted to be a stretched exponential by MCT, and the large-wavevector data could be fitted by this, but again with a variable stretching exponent not expected from theory. Overall, Kob and Andersen concluded that the KA model, in spite of having been designed to incorporate the caging effects that MCT should be able to describe, showed surprisingly poor agreement with MCT predictions.

For the triangular lattice gas, the autocorrelation function (114) has been simulated; since in this model $n_i = 0, 1$ represent a hole and a particle, respectively, this is essentially a local density correlation function. Non-exponential time-dependences were found on increasing particle concentration c, but with a functional form more complicated than a simple stretched exponential [118]. The correlation of Fourier-transformed density fluctuations, i.e. the intermediate scattering function (13), shows more structure. In particular, at high particle densities the character of the relaxation changes as a function of the wavevector, from a single decay at small wavevectors (large lengthscales) to a two-stage decay with an intermediate plateau at large wavevectors; see figure 20. (As explained in section 5.5 below, this wavevector-dependence can be interpreted as evidence for dynamical heterogeneity.) An MCA applied to the reducible memory function produced satisfactory fits to the data at low c (< 0.3), but was found to lead to unphysical divergences of the correlation functions for larger c; compare the discussion in section 4.7.2. Contrasting with the results for the KA model, one notices that the triangular lattice gas exhibits two-step relaxation processes while the KA model does not. This may be due to the different correlation functions studied (*self* versus *coherent* intermediate scattering function): although at least from the MCT for supercooled liquids [16–19] one would not expect this to cause qualitative differences, Jäckle [86] hints that also for the triangular lattice gas the self-

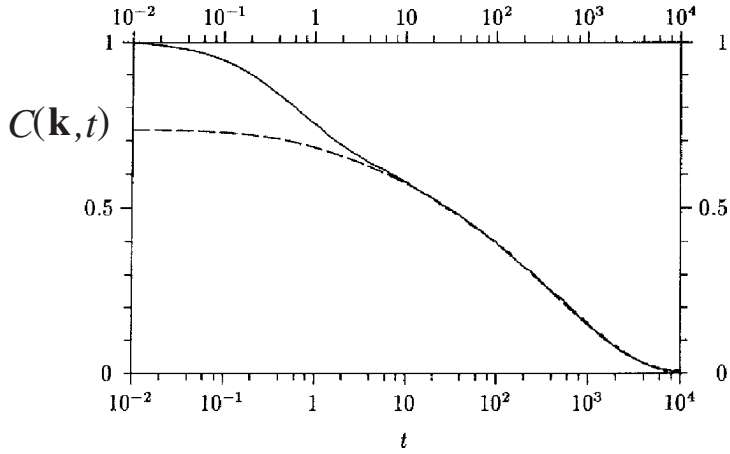

Figure 20. Intermediate scattering function (13) for the triangular lattice gas, for particle concentration $c = 0.7$ and a large wavevector $\mathbf{k}$ corresponding to lengthscales of order the lattice spacing. Notice the two-stage relaxation; the shoulder would be expected to grow into a plateau for even higher c. The dashed line is, up to a multiplicative constant, the fraction of particles that do not hop up between times 0 and t; this is seen to govern the long-time decay of the intermediate scattering function. From [86]. Copyright Institute of Physics Publishing.

intermediate scattering functions do not show two-step relaxations. Another possible explanation might be that the triangular lattice gas has genuinely different dynamics, with wider cages in which particles can 'rattle' while being confined by their neighbours. But it is not obvious from the dynamical rules why this should be the case; a closer comparison between the two models would be desirable to clear up this puzzle.

In the topological, off-lattice version of the **cellular model** (section 3.5), Davison and Sherrington [126] considered the autocorrelation function of the local deviations $n_i - 6$ from the hexagonal ground state. For the lowest $T \approx 0.25$ for which equilibrium can be achieved, this just begins to develop a shoulder, which one expects to broaden into a plateau for lower T. The region around the shoulder could be fitted reasonably well with the prediction of the MCT for supercooled liquids, which gives a power-law decay from a plateau value. The plateau could be more clearly seen in the lattice version of the model [127], with the timescale for the decay from the plateau following an Arrhenius law as expected due to the activated character of the dynamics.

In the model of thin **needles** attached to an f.c.c. lattice, Renner *et al.* [192] investigated equilibrium correlation functions by extensive computer simulations. They used Newtonian dynamics, so that the state of each needle i is characterized by a its orientation, specified by unit vector $\mathbf{u}_i$, and its angular velocity $\boldsymbol{\omega}_i$. The autocorrelation function of the $\mathbf{u}_i$ was found to develop a shoulder for needle lengths (normalized by the lattice constant) of $l = L/a \approx 2.5$. For larger l it failed to decay completely within the simulation time window, with the shoulder developing into a region of very slow decay, roughly linear in $\ln t$. (Less detailed simulations for the same model on a b.c.c. lattice [193] found similar results.) A clearer change in behaviour was seen in a carefully crafted correlation function of the angular

velocities, $\psi(t) = \langle \mathcal{P}_2(\hat{\boldsymbol{\omega}}_i(t) \cdot \hat{\boldsymbol{\omega}}_i(0)) \rangle$, where $\mathcal{P}_2(x) = (3x^2 - 1)/2$ is the second Legendre polynomial and $\hat{\boldsymbol{\omega}}_i$ is the angular velocity normalized to unit length. The attraction of this choice is that it detects whether the needle orientations $\mathbf{u}_i$ explore the whole unit sphere (which means that orientational caging effects are unimportant) or whether they remain close to a particular orientation. In the first case also $\hat{\boldsymbol{\omega}}_i$ explores the whole unit sphere, and $\psi(t)$ decays to 0 for large t. In the second case, $\hat{\boldsymbol{\omega}}_i$—which is always orthogonal to $\mathbf{u}_i$—remains confined to the plane orthogonal to the frozen needle orientation, and decorrelation within this plane gives $\psi(t) = 1/4$ for large t. Consistent with this, $\psi(t)$ was found to develop a plateau at $\psi = 1/4$ for needle lengths above $l \approx 2.7$. The change in behaviour is smooth, and therefore is unlikely to correspond to a true dynamical transition (see section 5.2), but nevertheless takes place over a narrow range of l.

We mention finally that stretched exponential behaviour has also been found in the energy autocorrelation function for a simplified Backgammon model [158] and for the low-T Glauber dynamics of the unconstrained ferromagnetic Ising chain [146, 277, 278], in both cases in an intermediate time window limited by exponential behaviour for early and late times.

5.4. *Out-of-equilibrium dynamics*

In this section we discuss the out-of-equilibrium dynamics of KCMs, which should be relevant for understanding the behaviour of glasses (as opposed to supercooled liquids, which still achieve metastable equilibrium on accessible timescales). We begin with a discussion of nonlinear relaxation after sudden changes in, e.g. temperature (section 5.4.1). Section 5.4.2 reviews results on the behaviour of KCMs under cyclic heating and cooling. In section 5.4.3 we move on to two-time correlation and response functions and effective temperatures defined on the basis of FDT violations out of equilibrium. Finally, section 5.4.4 briefly discusses ways of classifying glassy dynamics in KCMs by comparing the evolution of two independent 'clones' of a system.

5.4.1. *Nonlinear relaxation*

We begin our discussion with **spin-facilitated models**, specifically with $1, d$-SFMs that exhibit defect-diffusion rather than cooperative relaxation processes. In the $1, 1$-SFM, the relaxation of the up-spin concentration $c(t)$ after a quench to low T, and therefore low equilibrium up-spin concentration $c_{\rm eq}$, was studied in [55]. On timescales of order unity, one has effectively zero-temperature dynamics as explained in section 4.3, and $c(t)$ will decay to a plateau value, e.g. $c = (1/2)\mathrm{e}^{-1/2}$ if the system was at $T = \infty$, $c = 1/2$ before the quench. Thereafter, relaxation takes place via the diffusion of isolated up-spins which coalesce when they meet; as long as $c(t) \gg c_{\rm eq}$, the reverse process of one up-spin creating another one is negligible. One thus has a process of diffusive growth of domains of down-spins. The basic rate for this process is set by the effective up-spin diffusion constant $D_{\rm eff} = c_{\rm eq}/2$, giving average domain lengths scaling as $\bar{l} \sim (c_{\rm eq} t)^{1/2}$ (see figure 21) and thus for the up-spin concentration $c(t) \sim 1/\bar{l} \sim (c_{\rm eq} t)^{-1/2}$. This scaling also follows from exact results for the effective low-$c_{\rm eq}$ reaction–diffusion model $A + A \to A$, see, e.g. [272]. Equilibrium is reached when $c = c_{\rm eq}$, giving an equilibration time scaling as $c_{\rm eq}^{-3}$. Notice that this equilibration timescale is of the same order as the longest relaxation time in the final equilibrium state; see section 5.3.

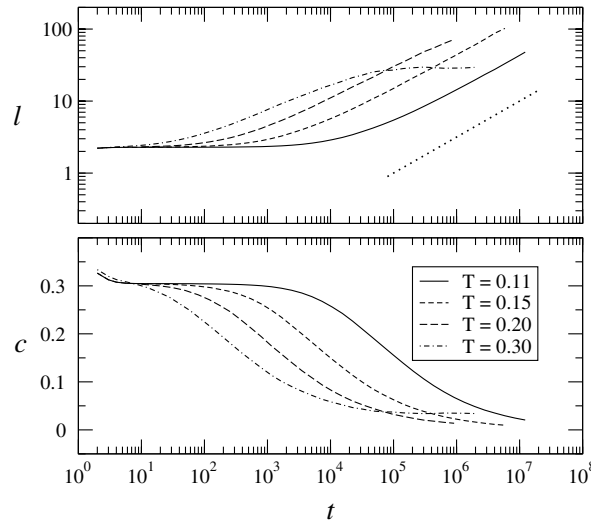

Figure 21. Growth of the average domain length $\bar{l}$ (top) and corresponding decay of the up-spin concentration c (bottom) after a quench in the 1, 1-SFM. Results are given for several temperatures corresponding to equilibrium up-spin concentrations (from top to bottom in the lower plot) $c_{\rm eq} \approx 1.1 \times 10^{-4}, 1.3 \times 10^{-3}, 6.7 \times 10^{-3}, 0.034$. The average domain length grows diffusively as $\bar{l} \sim t^{1/2}$ (dotted straight line in upper plot). From [55]. Copyright American Institute of Physics.

Next we consider SFMs with **cooperative dynamics**. For the 2, 2-SFM, the relaxation of the up-spin concentration after a quench from $c_{\rm eq} = 1$ (all spins-up) was simulated in [85]. Already for final up-spin concentrations $c_{\rm eq}$ around 0.3, the relaxation curves were distinctly non-exponential, and could be fitted by stretched exponentials down to $c_{\rm eq} \approx 0.08$. Fredrickson [273] considered more general changes in $c_{\rm eq}$, both increasing and decreasing. For changes that were not too large, the nonlinearities could be well described by a 'fictive temperature' approach (see, e.g. [7]), which assumes that the instantaneous relaxation time is the equilibrium relaxation time for the *current* up-spin concentration. For quenches to low $c_{\rm eq} \approx 0.1$, Graham *et al*. [77, 78] reported that the short-time relaxation exhibited a shoulder before crossing over into stretched exponential behaviour. Comparing with the discussion of the 1, 1-SFM above, this is as expected. In fact, for even lower T one expects to see a roughly T-independent decay onto a plateau on timescales of order unity, reflecting the flipping down of mobile up-spins that would take place even at $T = 0$, with further decay only on the much larger activated timescale $c_{\rm eq}^{-1} \approx \exp(1/T)$ for up-flips.

Among SFMs with **directed constraints**, the East model is the simplest one. Here, the relaxation of the up-spin concentration $c(t)$ after a quench from high to low T can be understood from the analysis described in section 4.6, which reveals that the dynamics takes place on a hierarchy of timescales of order $c_{\rm eq}^{-k} \approx \exp(k/T)$, with $k = 0, 1, \ldots$ If $c(t)$ is plotted against the scaled time variable $\nu = T \ln t$, then for $T \to 0$ the k-th stage of the dynamics shrinks to the point $\nu = k$. In this limit the results of section 4.6 imply that the average domain length $\bar{l}$ will increase in a 'staircase' fashion, with jumps at integer values of ν. The up-spin concentration $c = 1/\bar{l}$ will therefore also relax in plateaux towards $c_{\rm eq} \ll 1$. At non-zero

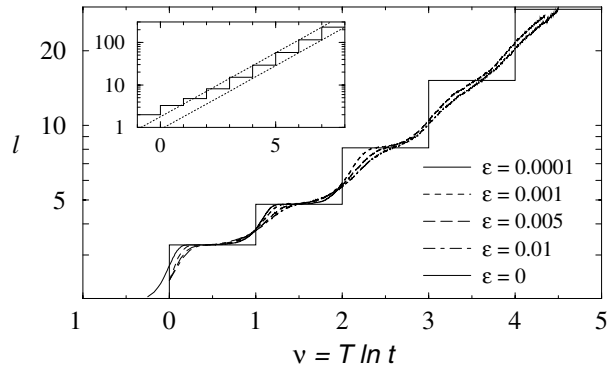

Figure 22. Evolution of average domain length $\bar{l}$ in the East model, after a quench at $t = 0$ from equilibrium at $c = 1/2$ to a small temperature T. Simulation results for four values of $\epsilon = \exp(-1/T) = c_{\rm eq}/(1 - c_{\rm eq})$ are shown, obtained from a single run for a spin chain of length $N = 2^{15}$. Note the scaled logarithmic x-axis, $\nu = T \ln t$. Bold line: theoretical prediction for $T \to 0$. Inset: theory for larger ν, and $\nu \to \infty$ asymptotes. From [220]. Copyright American Physical Society.

temperature the steps between the plateaux will be rounded and cross over into the decay predicted by the anomalous coarsening law, $c = 1/\bar{l} \sim t^{-T \ln 2}$. Figure 22 shows the results of simulations for a range of values of $\epsilon = \exp(1/T) = c_{\rm eq}/(1 - c_{\rm eq})$. Compared to earlier simulations [80], the longer timescales (up to $t = 10^{10}$) reveal the plateaux in $\bar{l}$ versus ν that develop with decreasing T; their values are in good agreement with the predicted theoretical values. In [80], the relaxation of $c(t)$ had also been explored after *upward* quenches, i.e. increases in T of $c_{\rm eq}$. A strong asymmetry in the relaxation functions for upward and downward temperature changes was found; this of course makes sense due to the strong dependence of the relaxation time on the final temperature.

For the asymmetric 1, 1-SFM, which compared to the East model enables facilitation also by right up-spin neighbours but at a rate reduced by the asymmetry parameter a (see (32)), we already mentioned in section 5.2 that, in addition to the cooperative relaxation processes of the East model, relaxation can proceed by up-spin diffusion on the timescale $\tau_{\rm diff} \sim (1 + a^{-1})e^{1/T}$. Buhot and Garrahan [83, 84] argued that the decay of $c(t)$ should therefore cross over for $t \approx \tau_{\rm diff}$ to the diffusive domain growth scaling $(t/\tau_{\rm diff})^{-1/2}$ typical of the 1, 1-SFM. They confirmed this in simulations; as a increases the relaxation of $c(t)$ exhibits fewer and fewer plateaux since the cross-over time $\tau_{\rm diff}$ decreases.

At this point, we briefly interrupt the usual order in which we give results for the different KCMs and discuss the **triangle model** (see section 3.6). The reason is that this model exhibits, somewhat surprisingly, a time- and lengthscale hierarchy very similar to that of the East model. Newman and Moore [130] showed that the relevant configurations for relaxations at low temperatures consist of three up-spins in the corners of equilateral triangles of side length $l = 2^k$. (Recall that the spins we are talking about here are the 'defect spins' $n_i = (1 - \sigma_i\sigma_j\sigma_k)/2 \in \{0, 1\}$, not the spins $\sigma_i = \pm 1$ of the underlying interacting model, and that the allowed transitions are simultaneous flips of the n_i at the corners of elementary *upward* triangles.) For $k = 0$, there is no energy barrier for flipping down the three up-spins. For $k = 1$, the spins can be flipped down by flipping three smaller triangles of unit side length in series, as

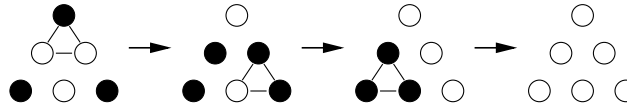

Figure 23. Relaxation pathway in the triangle model. The starting configuration has three defects (up-spins, shown as filled circles) at the corners of an equilateral triangle of side length 2. These can be relaxed by successively flipping the spins in three elementary triangles as shown; the activation barrier is $\Delta E = 1$ since one extra up-spin is created during this process. This procedure can be iterated to larger triangles, e.g. up-spins in the corners of a triangle of size 4 can be relaxed by carrying out the above move sequence in three subtriangles of size 2, with a resulting activation barrier of $\Delta E = 2$. Figure from [130]. Copyright American Physical Society.

shown in figure 23. Since the intermediate state now contains four up-spins, this process has an energy barrier of one. Continuing recursively, one sees that minimum energy path for flipping three up-spins in the corners of a triangle of size $l = 2^k$ is simply k; this is in direct analogy to the relaxation of domains of size $l = 2^k$ in the East model. The associated activation timescales $\tau \sim \exp(k\beta) \approx c_{\rm eq}^{-k}$ again become well separated for low temperatures, and the up-spin concentration $c = \langle n_i \rangle$ after a quench shows the corresponding plateaux [131]. The theory for the East model can be applied to this case and, while no longer exact, provides a good approximation to the observed plateau heights [131]. Smoothing out across the plateaux, the typical distance between up-spins grows as $\bar{l} \sim t^{T \ln 2}$ as in the East model; since $\bar{l}_{\rm eq} \sim \sqrt{c_{\rm eq}} \sim \exp(1/2T)$ in equilibrium, extrapolation of this growth law gives an equilibration time $\tau \sim \exp(1/2T^2 \ln 2)$ differing only by a factor $1/2$ from that for the East model [131]. We had already anticipated this result in section 5.2.

Let us return now to SFMs and consider one of the **variations on SFMs** discussed in section 3.2: the ferromagnetic Glauber Ising chain with the constraint that flips of spins with two up-spin neighbours are forbidden. The coarsening behaviour of this model at $T = 0$ has been studied by simulation and an independent interval approximation combined with a scaling analysis [105]. The kinetic constraint implies that domains of up-spins cannot coalesce, because the final down-spin between them can never be eliminated. Domain walls can therefore be eliminated only by coalescence of *down-spin* domains, giving faster growth $l_-(t) \sim t^{1/2} \ln t$ for the average length of down-spin domains, while up-spin domains coarsen according to the conventional $l_+(t) \sim t^{1/2}$. The up-spin concentration—which in the absence of the kinetic constraint and at $T = 0$ would remain constant in time—therefore decays logarithmically to zero, $c(t) = l_+(t)/[l_-(t) + l_+(t)] \sim 1/\ln t$ and this has been likened [105] to the slow compaction observed in vibrated granular media (see section 2.6).

Next we consider constrained **lattice gases**. As pointed out in section 3.3, in the standard KA model the density c of particles is conserved. Nonlinear density relaxation can therefore only be studied in variants of the model that allow for compaction under gravity or particle exchange with a reservoir. In the KA model with gravity (on a b.c.c. lattice, with $m = 5$) the relaxation of the density was studied from an initial loose packed state of bulk density $c \approx 0.71$, obtained by letting the particles fall from the upper half of the simulation box at $T = 0$ [117]. (The equilibrium state at this temperature, by contrast, has all particles packed at the bottom of the system to their maximum density $c = 1$; see section 5.1 for why this

maximally dense state is accessible in spite of the kinetic constraints.) If one then lets the system evolve at non-zero T, corresponding roughly to excitation by vertical vibration of the container, $c(t)$ increases slowly. Its time-dependence could be well-fitted by an inverse logarithmic law, $c(t) = c_\infty - [c_\infty - c(0)]/[1 + A\ln(t/\tau)]$ which has been used to describe experimental data on granular compaction (see section 2.6). While the equilibrium bulk density $c_{\rm eq}$ is a decreasing function of T, the extrapolated long-time value c_∞ of the density first *increases* with T, goes through a maximum and then decreases before eventually meeting the equilibrium curve. (The meeting point occurs at $1/T \approx 0.04$. Since the lattice units were chosen such that the height difference for a particle hop to a nearest neighbour site in a lattice plane above or below is unity, this temperature corresponds to a 'barometric' excitation height of around 25; this is a substantial fraction of the bulk height of the sample, which was $\approx$100.) The fact that $c_\infty < c_{\rm eq}$ for lower T was interpreted as evidence for a dynamical transition, with the system failing to achieve equilibrium even at very long times. The possibility that a slow increase of $c(t)$ towards $c_{\rm eq}$ would be observed outside the simulation time window is of course difficult to exclude. As an aside, we note that the same model has also been used successfully to study segregation of granular materials under vibration: by allowing some particles to move irrespective of the kinetic constraints, one obtains a model with two particle species. At $T > 0$ the more mobile particles then accumulate at the bottom of the simulation box, since they can fill the holes that remain between the constrained particles [117].

The second variation of the KA model where density relaxation can be investigated does not include gravity but allows particle exchange in a boundary layer that is in contact with a particle reservoir at some chemical potential μ; see section 3.3. A 'crunch' then corresponds to a sudden increase in μ. The relaxation of particle density after such a crunch has been investigated by simulations and within a coarse-grained continuum model (see section 4.10). If the final chemical potential is such that the corresponding equilibrium density $c_{\rm eq}$ is below that of the dynamical transition at $c_{\rm dyn}$ (see section 5.2), the continuum model predicts [258] that the timescale for the relaxation of the density profile to the uniform value $c_{\rm eq}$ is governed by the inverse self-diffusion constant in a homogeneous system, i.e. $\tau \sim 1/D_{\rm s} \sim (c_{\rm dyn} - c_{\rm eq})^{-\phi}$ with $\phi \approx 3.1$. As $c_{\rm eq}$ approaches $c_{\rm dyn}$, this timescale diverges. For crunches to higher chemical potentials, the continuum model predicts that the density profile relaxes towards the maximum achievable density $c_{\rm dyn}$ with a power-law time-dependence $\sim t^{-1/\phi}$ [257], and numerical simulations are consistent with this [110, 257].

The two ideas of including gravity and allowing particle exchange with a reservoir have also been combined; the boundary layer for particle exchange is then assumed to be at the top of the system. Density relaxations are somewhat more complicated to predict in this situation because of the non-trivial vertical density profile. The typical relaxation time was predicted to diverge when the equilibrium density of the lowest, densest layer approaches $c_{\rm dyn}$, but with an exponent $\phi - 2$ that is smaller than ϕ [258]. For higher reservoir chemical potentials, a section at the bottom of the density profile relaxes to $c_{\rm dyn}$ for long times; the time-dependence for this relaxation was found from both an asymptotic solution of the continuum model and numerical simulations as a power law, $t^{-1/(\phi-1)}$.

We now turn to models inspired by **cellular structures**; see section 3.5. In the topological froth model, glassy behaviour is seen in the relaxation of the energy (which is proportional to the number of defects). Starting from two different initial

configurations, one strongly disordered and one perfectly ordered, the initial configuration is remembered at low T even for the longest accessible simulation times [125]. The time evolution of the energy relaxation from a high-temperature, disordered state was studied in more detail for the lattice version of the model [127] and showed the two-step form expected for activated dynamics, with a nearly T-independent decay to a plateau on timescales of order unity, and the remaining decay taking place only on activated (Arrhenius) timescales. From the effective low-temperature model for this system (see sections 3.5 and 4.10) one deduces that the short-time evolution is dominated by diffusion of defect dimers and dimer–antidimer annihilation $A + B \to \varnothing$; the dynamics on longer, activated timescales arises instead from the diffusion of isolated defects and defect-antidefect annihilation, giving again $A + B \to \varnothing$. This leads to the prediction of $t^{-1/2}$-scaling for both the short- and long-time decays, which is in good agreement with simulations [127].

Finally, for models with entropic barriers such as the **Backgammon** and **oscillator** models, we already saw in section 4.3 that the energy relaxes logarithmically slowly after a quench [149–153]. This behaviour persists for all times if the final temperature is zero; at non-zero temperature it is observed only at intermediate times smaller than the longest relaxation time. For the zeta urn model [159, 162] with a random initial configuration, one finds both at criticality and in the condensed regime that the occupancies $P_k(t)$ show scaling behaviour, becoming functions of the single scaling variable $kt^{-1/2}$ when both k and t are large.

5.4.2. *Heating–cooling cycles*

In this section we review the behaviour of KCMs under cyclic variations of temperature (or density etc). As explained in section 2.1, such heating–cooling cycles in real glasses show strong hysteresis effects. These demonstrate that, as soon as a supercooled liquid falls out of equilibrium because its relaxation times are too large to keep pace with the external heating and cooling, it develops a strong memory of its temperature history.

To recap briefly the discussion in section 2.1, on cooling the energy E departs from the equilibrium line at some cooling-rate dependent T_g; for lower temperatures, the decrease in energy with temperature T is much reduced and the value of the specific heat therefore drops around T_g. When the system is heated back up, the energy increases slowly enough with T to cross *below* the equilibrium line, rejoining it by a steep increase only at a higher temperature; this increase manifests itself as a peak in the specific heat. (Notice that we use the term specific heat here to refer to the temperature-derivative of the energy; in equilibrium, the specific heat is also related to the amplitude of energy fluctuations but out of equilibrium this is not the case.)

Many KCMs exhibit the above effects; by way of illustration we show in figure 24 typical cooling–heating cycles in the Backgammon model [149, 150]. While the temperature evolution of the energy during the cooling process is easy to understand in terms of the effective freezing of the slow degrees of freedom of the system, the behaviour on reheating is less intuitively obvious. We therefore now sketch an analysis of this phenomenon due to Brey and Prados, who applied the concept of a 'normal curve' for the heating process to a number of simple models. The normal curve in general exists for any irreducible Markov process with time-dependent transition rates. It gives the long-time behaviour of the time-dependent probability distribution over configurations, independently of initial conditions, and is the

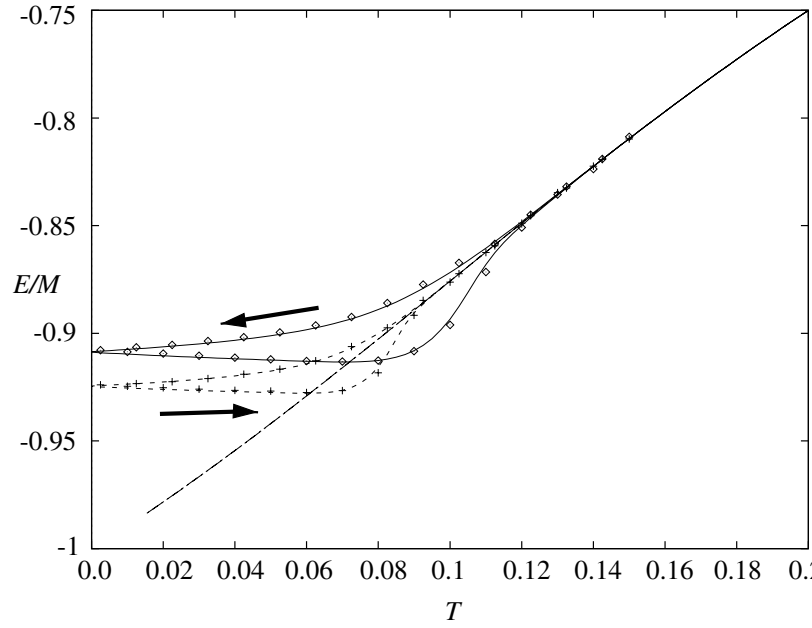

Figure 24. Heating–cooling cycles in the Backgammon model at two different cooling rates. For the lower cooling rate (dashed) the system follows the equilibrium relation between E and T to lower temperatures. From [150].

analogue of the unique stationary distribution for irreducible Markov processes with constant transition rates [278, 279]. For cooling processes the dynamics becomes reducible in the limit $T = 0$, even in models without kinetic constraints, and so a normal curve does not exist; for the heating case, however, there is no such restriction. Brey *et al*. [277, 280] studied in detail the ferromagnetic Ising chain with Glauber dynamics. (A similar analysis can be performed [124] for the models with hierarchical kinetic constraints described in section 3.4.) They showed that the energy during a heating process from $T = 0$ can be decomposed into two contributions, $E(T) = E_{\mathrm{N}}(T) + E_{\mathrm{p}}(T)$. The first term is the normal curve for heating, constructed with equilibrium at $T = 0$ as the starting configuration. The second term describes the correction due to the preceding cooling protocol by which $T = 0$ was reached, and vanishes in the limit of infinitely slow cooling. Brey *et al*. proved that the normal curve stays *below* the equilibrium curve $E_{\mathrm{eq}}(T)$ and coincides with it only at $T = 0$ and $T = \infty$. On the other hand, in a realistic cooling schedule one does not reach equilibrium at $T = 0$, so that $E_{\mathrm{p}}(T \approx 0)$ is positive and the total energy $E(T)$ is above the equilibrium curve at low T. As T is increased and the normal curve drops increasingly below the equilibrium curve, the two effects eventually cancel and this causes the crossing of $E(T)$ below the equilibrium curve.

The effects of cyclical heating and cooling have been studied in a number of KCMs; we already referred to the Backgammon model above. As far as **spin-facilitated models** are concerned, Graham *et al*. [77, 78] studied in detail the behaviour of the specific heat in temperature cycles for the $2,2$-SFM, $2,3$-SFM and $3,3$-SFM. Starting from a glassy configuration obtained by quenching to low T, a sharp peak in the specific heat was observed on heating, and a much broader peak

at lower temperatures on cooling; as explained at the beginning of this section, this agrees qualitatively with experimental observations on glasses.

In the context of **lattice gases**, the analogues of cooling runs were studied for the grand canonical KA model, where particle exchange with a reservoir is allowed in a boundary layer (see section 3.3). The evolution of the inverse particle density $1/c$ was simulated in slow compression runs, implemented by decreasing the inverse chemical potential $1/\mu$ at a constant rate [110]. The inverses are chosen here to emphasize the analogy with energy and temperature in glasses; small $1/\mu$ corresponds to low T, and small $1/c$ to the glassy regime of low energy. Similarly to cooling experiments in real glasses, $1/c$ begins to deviate from the equilibrium curve $1/c = 1 + e^{-\mu}$ (see (35)) later and later as the compression rate is reduced. Given that the KA model has an at least effective dynamical transition at $c_{\mathrm{dyn}} = 0.881$ (see section 5.2), where the timescale for self-diffusion appears to diverge, one would expect that c_{dyn} is the density that is reached in very slow compression experiments. The results are compatible with this [110]; see figure 15 above. Increasing and decreasing $1/\mu$ in analogy to heating–cooling cycles also leads to the expected hysteresis in $1/c$, with lower values of $1/c$ found in the decompression phase that is analogous to reheating.

Finally, simulations of cooling runs have been carried out in several other KCMs. In the **triangle model**, annealing runs with an exponential cooling schedule, $T(t) = T_0 \exp(-\gamma t)$ were performed, and showed the expected deviations from the equilibrium relationship between defect concentration c and temperature T when inverse cooling rates and relaxation times became comparable [130]. In the topological model of **cellular structures**, cooling experiments [126] found that even for slow cooling rates the system falls out of equilibrium at sufficiently low temperatures where relaxation timescales become very long ($T \approx 0.2$), and similar behaviour is observed in the lattice variant [127].

5.4.3. *Two-time correlation and response, and effective temperatures*

As explained in section 2.3, systems such as glasses which do not equilibrate on experimentally accessible timescales show *ageing*, which means that their properties depend on the 'waiting time' t_{w} that has elapsed since they were prepared by, for example, a quench. The time-evolution of one-time quantities such as up-spin concentration or particle density, discussed in section 5.4.1, already testifies to this. Often ageing effects can persist, however, even when the relaxation of one-time quantities has become so slow that their values are already effectively constant. One then needs to consider two-time quantities such as correlations and response functions. Since the system is out of equilibrium, these generically violate FDT, and it has been suggested that the FDT violation factor $X(t, t_{\mathrm{w}})$ defined by (18) can be used to define an effective temperature $T_{\mathrm{eff}} = T/X$.

We begin our discussion with **spin-facilitated models**. As in section 5.3, let us review briefly the definitions of the two-time quantities most frequently studied in these models. The two-time spin autocorrelation function is, in a natural generalization of (114),

$$C(t, t_{\mathrm{w}}) = \frac{1}{N} \sum_i [\langle n_i(t) n_i(t_{\mathrm{w}}) \rangle - \langle n_i(t) \rangle \langle n_i(t_{\mathrm{w}}) \rangle]. \tag{118}$$

No normalizing factors have been introduced here, since the normalization of two-time quantities is a somewhat subtle issue; see section 2.3. Comparing with (16), it is

easy to see that $C(t, t_w)$ is (apart from a factor of N) the two-time correlation function of a 'random staggered magnetization' $\phi = (1/N)\sum_i \epsilon_i n_i$, with the signs $\epsilon_i = \pm 1$ chosen randomly for each i [281]. Imposing the constraint $\sum_i \epsilon_i = 0$ simplifies matters by making $\langle \phi(t) \rangle = 0$ for all t. The associated response function is obtained by adding a term $-Nh\phi$ to the energy function E; if the field is increased from zero to a small constant value h at time t_w, then the normalized change in ϕ, $\langle \phi(t) \rangle / h$, gives the two-time step response function $\chi(t, t_w)$ for $t > t_w$. As emphasized in section 2.3, in an out-of-equilibrium situation two-time correlation and response are non-trivial functions of their two time arguments, whereas in equilibrium they depend only on $t - t_w$.

As in the case of stationary dynamics, one may also be interested in the two-time correlations of the overall up-spin concentration; by analogy with (115), but again without normalization, this is

$$C_c(t, t_w) = \frac{1}{N} \sum_{ij} [\langle n_i(t) n_j(t_w) \rangle - \langle n_i(t) \rangle \langle n_j(t_w) \rangle]. \tag{119}$$

The corresponding perturbation in the energy function, which defines the response $\chi_c(t, t_w)$, is $-Nhc = -h\sum_i n_i$. For the standard SFMs where $E = \sum_i n_i$, this effectively changes temperature from T to $T/(1-h) = T + hT + \cdots$, so that $\chi_c(t, t_w)$ can also be thought of as measuring the response of the up-spin concentration to small temperature changes.

After these preliminary definitions we turn to results for SFMs with undirected constraints. All the work on two-time quantities that we are aware of has focused on $1, d$-SFMs with their defect-diffusion dynamics. Simulations in $d = 1, 2$ considered a quench from $T = \infty$ ($c_{eq} = 1/2$) to small T and c_{eq} and measured the spin correlation function $C(t, t_w)$, normalized by the equal-time value at the earlier time, $C(t_w, t_w)$ [214]. A strong dependence on t_w was observed for waiting times of order unity, while in the regime $1 \ll t_w \ll c_{eq}^{-1}$ the effect of t_w was negligible. This makes sense in light of the discussion in section 5.4.1. For times of order unity the system evolves through the flipping-down of mobile up-spins; as emphasized in section 4.3, in this regime one expects the exactly solvable $T = 0$ dynamics to correctly predict the dynamics, and this was indeed found in [214]. Further evolution of the system requires diffusion of isolated up-spins, and so only takes place once t_w becomes of order $1/D_{eff} \sim c_{eq}^{-1}$. Even for t_w of this order and larger, however, simulations showed ageing effects on $C(t, t_w)$ to be rather weak [55, 214]. For the $1, 1$-SFM, one might expect that in this time regime, where the model exhibits growing domains of down-spins, the two-time correlations should collapse when plotted as a function of the ratio of typical domain lengths at the early and late times, $\bar{l}(t_w)/\bar{l}(t) \approx c(t)/c(t_w)$. The simulations of [55, 282] did not show this, but the values of t_w accessed may not have been large enough to see the expected scaling.

In the $1, 1$-SFM, the response function $\chi(t, t_w)$ conjugate to the spin autocorrelation is found to be non-monotonic as a function of the later time t [46, 55, 282]. This may appear surprising, but a nice intuitive justification for this behaviour was given in [46], for the regime of times long compared to the initial fast relaxation processes (see above). For low up-spin concentrations $c(t)$, up-spins are far apart, as they would be in equilibrium if c_{eq} is small. Since only up-spins and their neighbours are mobile and can therefore contribute to the response, $\chi(t, t_w)$ should be proportional to $[c(t)/c_{eq}]\chi_{eq}(t - t_w)$, where $\chi_{eq}(t - t_w)$ is the equilibrium response at the final

temperature after the quench. This form fits simulation data very well [46]; the non-monotonicity arises since $\chi(t, t_w)$ is a product of two factors, one ($c(t)$) decreasing with t and one ($\chi_{eq}(t - t_w)$) increasing. The behaviour of the autocorrelation function can be rationalized with a similar approach. Intriguingly, these scaling relations suggest that $C(t, t_w)$ and $\chi(t, t_w)$ are related by the trivial *equilibrium* FDT, even though, e.g. the up-spin concentration $c(t)$ is still far above its equilibrium value c_{eq}. Simulation results indeed showed that a plot of $T\chi(t, t_w)$ versus $C(t, t) - C(t, t_w)$ (see section 2.3) gives a straight line of slope one through the origin [46]. Earlier attempts [55] at FDT plots using the disconnected correlation function $(1/4)\langle(2n_i(t_w) - 1)(2n_i(t) - 1)\rangle$, chosen in such a way as to be automatically normalized to unity at $t = t_w$, had produced rather counter-intuitive non-monotonic relations between response and correlation.

An interesting twist to the apparently trivial FDT relations in the out-of-equilibrium dynamics of the 1, 1-SFM is provided by recent work on defect (domain-wall) dynamics in the ferromagnetic Ising chain with unconstrained Glauber dynamics [145]. The dynamics of these defects is rather similar to those in the 1, 1-SFM, except that rather than coalesce they annihilate when they meet. Indeed, appropriate scaling plots of domain-wall autocorrelation and response functions look rather similar to those in [46], and the FDT plot becomes a straight line at long times. This suggests again that the FDT violation factor is $X(t, t_w) = 1$ and equilibrium FDT holds. However, when plotted, e.g. against t/t_w, one finds that $X(t, t_w)$ is a non-trivial function and generically < 1. This apparent paradox is resolved by noticing that significant FDT violations only occur on timescales $t - t_w$ of order t_w, where the autocorrelation function has already decayed to such a small fraction of its equal-time value that FDT violations are not visible either in the FDT plot or the scaling collapse. A detailed investigation of $X(t, t_w)$ for the 1, 1-SFM for similar effects in the regime $t - t_w \sim t_w$ should therefore be worthwhile.

We finish off our discussion of the 1, 1-SFM by briefly mentioning results for the response $\chi_c(t, t_w)$ of the up-spin concentration to small temperature changes [214]. As is typical of activated dynamics, this response function is actually negative, and much larger in absolute value than the equilibrium response. The apparently counter-intuitive negative sign can be understood by considering, e.g. a small decrease in T: this slows down the relaxation of $c(t)$ to lower values, giving *larger* values of $c(t)$ rather than smaller ones as in equilibrium.

Next we turn to SFMs with **directed constraints**, in particular the East model. The two-time spin autocorrelation function $C(t, t_w)$ and corresponding response $\chi(t, t_w)$ were simulated in [55]. Because of the hierarchy of well-separated timescales that dominates the out-of-equilibrium dynamics (see section 4.6), $C(t, t_w)$ exhibits plateaux, and a naive plot against t/t_w does not give a reasonable collapse of the curves. On the other hand, plotting $C(t, t_w)/C(t_w, t_w)$ against the domain length ratios $\bar{l}(t_w)/\bar{l}(t) = c(t)/c(t_w)$ gave good scaling collapse, as expected from the coarsening character of the out-of-equilibrium dynamics at low T. In fact, since in the limit $T \to 0$ domains simply coalesce irreversibly, one would predict $C(t, t_w) = c(t)[1 - c(t_w)]$ and thus $C(t, t_w)/C(t_w, t_w) = c(t)/c(t_w)$, and this is compatible with the data of [55].

The response function $\chi(t, t_w)$ was found to be monotonic in t for the East model, in contrast to the results for the 1, 1-SFM; this may be because the much slower decrease in time of $c(t)$ is not sufficient to produce noticeably non-monotonic behaviour. FDT plots were also considered in [55], but have to be regarded with

caution since they were constructed using a disconnected correlator as for the 1, 1-SFM. They consisted to a rough approximation of two straight line segments, but with no obvious limit plot being approached for long times; the FDT violation factor X in the non-equilibrium sector became rather small (≈ 0.1) for low temperatures. This is not inconsistent with the coarsening character of the model, which in $d > 1$ would be expected to give $X = 0$ (see section 2.3 and [283]). Since the East model is $d = 1$-dimensional, however, this comparison is not conclusive.

At this point we consider the **triangle model**, because of the similarities of its out-of-equilibrium dynamics to that of the East model. Interestingly, the response function $\chi_c(t, t_w)$ of the up-spin concentration of the 'defect spins' $n_i = (1 - \sigma_i\sigma_j\sigma_k)/2$ was found to be non-monotonic in t [131], and led to corresponding non-monotonic FDT plots. The origin of this behaviour can be understood from the plateaux in the evolution of $c(t)$, which occur between the relaxation timescales $\tau_k \sim \exp(k/T)$. The perturbation conjugate to c is essentially an increase in temperature, which reduces the τ_k but leaves the heights of the plateaux in $c(t)$ unaffected. The response is therefore largest around the transitions between the plateaux, and small in between. Garrahan and Newman [131] argued that this argument should also apply to the *local* response function $\chi(t, t_w)$, and conjectured on this basis that $\chi(t, t_w)$ in the *East model* should also exhibit non-monotonic behaviour, at lower temperatures than those simulated in [55]. Notice that in the triangle model, because of its derivation via a mapping from a system of interacting spins $\sigma_i = \pm 1$ (see section 3.6), there are further correlation and response functions that one can consider [130, 131]. One intriguing observation is that the two-time autocorrelation function of the σ_i (rather than the n_i) seems to scale neither with t/t_w, nor with the ratio of typical distances between defects $\bar{l}(t_w)/\bar{l}(t)$; the reasons for this are not presently understood [131].

We next review results on two-time quantities in constrained **lattice gases**. As explained in section 5.4.1, one needs to consider the recent variations on the KA model that include gravity or a particle reservoir to study these out-of-equilibrium quantities. As an analogue of two-time correlation functions, the average squared particle displacement $B(t, t_w) = \langle [\mathbf{r}_a(t) - \mathbf{r}_a(t_w)]^2 \rangle$ has been studied; the corresponding response function that would be related via FDT in equilibrium is obtained by applying a random force to each particle and measuring the displacement in the direction of the force. In the grand canonical KA-model, ageing effects on $B(t, t_w)$ were studied after a crunch, i.e. an increase of the chemical potential μ to a point where the equilibrium density c_{eq} would be above the critical value c_{dyn} [110, 257, 284]. (Since particle exchange only acts in the boundary plane, this increase of chemical potential is performed slowly, rather than near-instantaneously as in a conventional temperature quench, to avoid inhomogeneities across the sample.) For large t_w, it was found that $B(t, t_w)$ becomes to a good approximation a function of the scaled time difference $(t - t_w)/t_w$ and increases roughly logarithmically, indicating very slow anomalous diffusion. A qualitative explanation for this is provided [257] by supposing that $B(t, t_w) \sim \int_{t_w}^{t} \mathrm{d}t' \, D_s(t')$, with $D_s(t')$ a time-dependent self-diffusion constant which depends on density according to $D_s(t) \sim (c_{dyn} - c(t))^{\phi}$. Since, as described in section 5.4.1, the density approaches the critical value as $c_{dyn} - c(t) \sim t^{-1/\phi}$ this gives $D_s(t) \sim t^{-1}$ and thus directly the observed logarithmic increase $B(t, t_w) \sim \ln(t/t_w)$ of the particle displacements. Remarkably, an FDT plot of the conjugate response versus $B(t, t_w)$ was of a simple 'mean field' form (see section 2.3), consisting of two approximately straight line

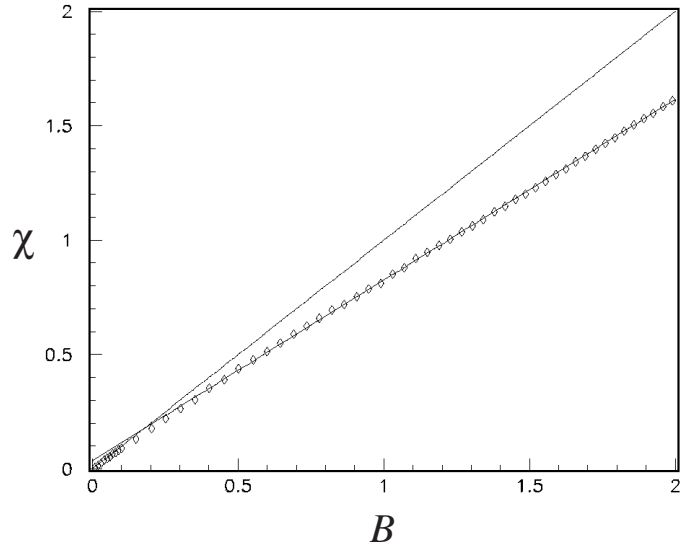

Figure 25. Out-of-equilibrium FDT plot for the grand canonical KA model: simulation results for waiting time $t_w = 10^5$ after a 'crunch' to chemical potential $\mu = 2.2$. Symbols show a parametric plot, obtained by varying the final time t, of the two-time response (of particle displacements to random forces) against the corresponding two-time correlation (mean-square particle displacement $B(t, t_w)$). The plot initially follows equilibrium FDT, indicated by the line through the origin, but then crosses over on to a second straight line with slope smaller by an FDT violation factor of $X \approx 0.79$. From [284].

segments [284]; this is shown in figure 25. The FDT violation factor was $X \approx 0.79$ in the non-equilibrium sector (though its dependence on t_w does not appear to have been investigated), and it was later shown that this value can be understood from an appropriately defined Edwards measure; see section 5.6. Similar FDT results were also found for compaction under gravity at constant number of particles [285].

As mentioned in section 5.4.1, the KA model connected to a particle reservoir has also been considered when subject to gravity, with the contact layer with the reservoir at the top of the system. For sufficiently high reservoir chemical potential μ, the system develops a dense zone at the bottom where the particle density slowly approaches the critical value c_{dyn}. Using a continuum model, it was argued [258]—in accord with simulation [285]—that in this dense zone the mean-square particle displacement scales as $B(t, t_w) \sim t_w^{-1/(\phi-1)} - t^{-1/(\phi-1)}$, where $\phi \approx 3.1$ is the exponent for the divergence of the inverse self-diffusion constant at the critical density. Intriguingly, the exponents here are *negative*, implying that for $t \to \infty$ the displacement saturates to a constant value (which itself tends to zero for $t_w \to \infty$). Notice also that, in contrast to the case without gravity discussed above, the ageing here is not 'simple', i.e. $B(t, t_w)$ is not a function of the scaled time difference $(t - t_w)/t_w$ alone.

Moving on to KCMs inspired by **cellular structures**, Aste and Sherrington [125] studied the two-time *persistence* function in the topological froth model, defined as the fraction of cells that have not been involved in any moves between t_w and t. While for high temperatures this is t_w-independent and decays exponentially with $t - t_w$, for low temperatures ($T < 1$) simulations show ageing effects. These can be

qualitatively understood [125] from the fact that most moves are due to the diffusion of pairs of pentagonal and heptagonal cells, whose concentration decreases with t_w. The two-time correlation function for local deviations from the hexagonal ground state configuration, $\langle (n_i(t) - 6)(n_i(t_w) - 6)\rangle$, along with the conjugate response function, was simulated in [126]. This correlation function decays to a plateau within times $t - t_w$ of order unity, while the remaining decay takes place on timescales growing with t_w. The response function is non-monotonic in t at fixed t_w. This can be understood by arguments similar to those for the 1, 1-SFM above; the decay in the response at long times again arises from the decrease in the number of defects that drive the dynamics, which in this case are pairs of 5- and 7-sided cells. The behaviour of the lattice version of the model is qualitatively similar [127]. Interestingly, however, if response and correlation are normalized properly (see section 2.3) by the equal time correlator at the *later* time t, the resulting FDT plot becomes the trivial equilibrium one [128]. The physical reasons for this remain to be understood.

Of the models that arise via a mapping from underlying interacting spin systems with unconstrained dynamics we have already dealt with the triangle model above. Two-time quantities in the **plaquette model** have recently been considered in [46], focusing on the correlation and response functions for the defect spins $n_i = (1 - \sigma_i\sigma_j\sigma_k\sigma_l)/2$ (see section 3.6). Recall that the elementary transitions between configurations are simultaneous flips of four of the n_i in the corners of an elementary lattice square. This implies in particular that pairs of n.n. defects $n_i = 1$ can diffuse unidirectionally—pairs in the x-direction can diffuse along the y-direction and vice versa—and pairs of defects in diagonally opposite corners of lattice squares can oscillate. Both of these processes are fast, taking place on timescales of order one since they involve no change of the energy $E = \sum_i n_i$, and determine the behaviour of $C(t, t_w)$ and $\chi(t, t_w)$ for $t - t_w$ of order unity. On longer timescales, diffusion of isolated defects takes over. This proceeds by an isolated defect creating a freely diffusing defect pair, which must then be absorbed by another isolated defect. The activation energy for creating the pair is $\Delta E = 2$, and the overall timescale for this process scales as $\exp(2/T)/c(t)$; the factor $1/c(t)$ gives the typical probability that the defect-pair will indeed be absorbed by a *different* isolated defect, rather than the original one. On the basis of these considerations, good scaling collapse of response and correlation functions in the two different time-regimes could be obtained [46]. Remarkably, an FDT plot of $T\chi(t, t_w)$ versus $C(t, t) - C(t, t_w)$ gave data collapse on to a master plot for a range of different t and t_w, and consisted of two straight line segments. Buhot and Garrahan [46] gave a plausible argument for the location of the breakpoint between these two segments, but the value of the FDT violation factor X in the non-equilibrium sector remains to be understood.

Let us finally turn to models related to KCMs, beginning with **urn models**. For the Backgammon model different types of correlation functions have been considered. In the original paper on the Backgammon model [149], the energy–energy correlation function was simulated at $T = 0$, finding simple ageing scaling with $(t - t_w)/t_w$. These results were later confirmed by numerical integration of the exact master equation solution in [152] and by asymptotic expansion techniques [153, 155] which showed the existence of subdominant logarithmic corrections to the simple scaling. The energy–energy autocorrelation function does not show the existence of a fast relaxation process analogous to the β-relaxation in supercooled liquids and glasses. Such a separate fast process does appear, however, in the autocorrelation

function $C(t, t_w)$ of the local number of particles per box. This correlation function and its associated response was considered in [154], using a numerical integration of a truncated hierarchy of dynamical equations; a detailed analytical solution was subsequently given by Godrèche and Luck [160]. The main findings are that, for large t_w, $C(t, t_w)$ develops a pronounced plateau, as does the corresponding response; the long-time decay from this plateau again shows simple ageing scaling. The FDT violation factor $X(t, t_w)$ when plotted against $C(t, t_w)$ for fixed large t_w is well approximated by a piecewise constant function, equal to one for values of $C(t, t_w)$ above the (t_w-dependent) plateau and to a smaller value for smaller C. This second, non-trivial value of X tends to one logarithmically as $1 - \text{const}/\ln^2 t_w$, however, so that there is no non-trivial limit plot; also, X does not correspond to a ratio between the actual temperature T and the temperature defining the effective equilibrium state found in the adiabatic analysis of the dynamics (see section 4.5).

For the zeta-urn model [162] the FDT violation factor $X(t, t_w)$ is found to become asymptotically a non-trivial function of the ratio t/t_w. Of interest is particularly the limit X_∞ obtained for $t/t_w \to \infty$, which is related to universal amplitude ratios in critical dynamics. Along the critical line in the phase diagram of the urn model (see section 3.7.2) one finds that $4/5 < X_\infty < 1$. This contrasts with analogous results for ferromagnetic Ising models at criticality (see, e.g. [138]) where $0 < X_\infty < 1/2$, and is more similar to the Backgammon model where $X(t, t_w) \to 1$ in the limit of large t.

For the **oscillator model** (see section 3.7.3), it is natural to consider the two-time autocorrelation function of the oscillator positions x_i, and the corresponding response. One finds [167, 169] that these display simple scaling with logarithmic corrections: defining $g(s) = s(\ln s)^{3/2}$, one has $C(t, t_w) = g(t_w)/g(t)$ for the correlation and $R(t, t_w) = -\partial\chi(t, t_w)/\partial t_w = g(t_w)/[tg(t)]$ for the impulse response. The effective temperature derived via the FDT violation can easily be computed and gives the equipartition result $T_{\text{eff}} = 2E(t)$ in the long-time limit; the simplicity of this result has no counterpart in any of the other models.

5.4.4. *Coarsening versus glassiness*

We conclude this section with a brief discussion of an interesting quantity for characterizing the qualitative nature of out-of-equilibrium dynamics. This is the overlap between two 'clones' of a system evolving under different realizations of the stochastic noise in the dynamics. Specifically, one imagines that the system has aged until t_w and is in configuration $\mathbf{n}^{(1)}(t_w)$. One then makes a copy $\mathbf{n}^{(2)}(t_w) = \mathbf{n}^{(1)}(t_w)$ and lets the two clones evolve independently for $t > t_w$. The quantity of interest, introduced in the context of the spherical SK model [44] and analysed in detail in [286], is then the 'clone overlap'

$$Q_{t_w}(t) = \frac{1}{N}\sum_i [\langle n_i^{(1)}(t) n_i^{(2)}(t)\rangle - \langle n_i^{(1)}(t)\rangle\langle n_i^{(2)}(t)\rangle]. \tag{120}$$

The averages are both over the configuration at the starting time t_w and over the subsequent stochastic evolution; only the former couples the two clones. The decay of $Q_{t_w}(t)$ tells one how fast the clones separate in configuration space as they evolve, and is to be compared with the two-time correlation function $C(t, t_w)$ defined in (118), which measures how much each clone has decorrelated from its configuration at time t_w. In equilibrium, because of detailed balance, the forward evolution by

time $\Delta t = t - t_w$ of one clone is equivalent to backward evolution by the same time, so that

$$Q_{t_w}(t_w + \Delta t) = C(t_w + 2\Delta t, t_w). \tag{121}$$

Both quantities are of course functions of Δt only because of TTI; for exponentially decaying correlation functions (121) gives $Q_{t_w}(t_w + \Delta t) \propto C^2(t_w + \Delta t, t_w)$.

Barrat *et al.* [286] proposed the name 'type I' for systems for which $Q_{t_w}(t)$ remains large while $C(t, t_w)$ decays to zero. Intuitively, this corresponds to the system 'falling down a gutter' in configuration space, where the two clones remain similar even though they have moved far from their starting point at t_w. A number of coarsening systems display this behaviour, with in fact $S_\infty = \lim_{t_w\to\infty} \lim_{t\to\infty} Q_{t_w}(t) > 0$ while the analogous limit for $C(t, t_w)$ vanishes. The intuitive reason for this is that on large lengthscales and at low T most coarsening models behave essentially deterministically [144]—with the ferromagnetic Ising chain with Glauber dynamics an obvious exception—so that the two clones stay closely correlated in their evolution while moving far from their configuration at time t_w. In 'type II' systems, on the other hand, Q and C decay on the same timescale, and this can be interpreted as true 'glassy' evolution resulting from a rugged energy landscape in which the two clones quickly begin to follow different routes.

Only a few studies exist of the clone overlap in KCMs. One reason for this is that the limiting quantity S_∞ is not useful for KCMs: barring dynamical ergodicity breaking, the system will eventually equilibrate to its trivial Boltzmann distribution and the clones then decorrelate, giving $Q_{t_w}(t \to \infty) = 0$ and hence $S_\infty = 0$. (In an infinitely large coarsening system, on the other hand, S_∞ can be non-zero since equilibrium is never reached.) One therefore has to look at finite times and consider whether $Q_{t_w}(t)$ decays more slowly (type I) or on the same timescale (type II) as $C(t, t_w)$.

One-dimensional spin-facilitated models were studied in [55]. Numerical results for the East model showed plateaux in the t-dependence of $Q_{t_w}(t)$ where Q was larger than expected from the equilibrium relation (121), indicating a resemblance to coarsening (type I) systems. For the 1, 1-SFM, on the other hand, the equilibrium relation (121) was found to be valid to a good approximation, showing that Q and C decay on the same timescale and the dynamics is therefore of type II. Similar type II behaviour has also been observed for the lattice model of the topological froth [127] and a disordered version in $d = 3$ of the plaquette model [132]. Results for the evolution of the grand canonical KA model [112] after a crunch to large reservoir chemical potential likewise suggest type II behaviour: even though the particle density c approaches the value $c_{\rm dyn}$ where the (effective) dynamical transition takes place, $Q_{t_w}(t)$ always tends to zero as $t \to \infty$. A direct comparison with $C(t, t_w)$ would however be needed to make this argument more conclusive.

The implications of these results for KCMs in general remain unclear: the fact that the limiting quantity S_∞ cannot be used makes a clear-cut distinction into type I and II dynamics on the basis of the clone overlap difficult. One possibility would be to look at the so-called anomaly in the two-time response function $\chi(t, t_w)$ conjugate to $C(t, t_w)$. This anomaly can be defined as $A(\Delta t) = \chi(\Delta t, 0) - \lim_{t_w\to\infty} \chi(t_w + \Delta t, t_w)$ and measures the difference in step response between an ageing system and an equilibrium system. Barrat *et al.* [286] suggested that type I (coarsening) and II (glassy) dynamics should correspond respectively to a zero and non-zero long-time value $A(\Delta t \to \infty)$ of the anomaly. Studying the behaviour of

$A(\Delta t)$ for KCMs could therefore help to clarify whether a classification into coarsening versus glassy behaviour is meaningful for these models.

5.5. *Dynamical lengthscales, cooperativity and heterogeneities*

As explained in section 2.5, an important question in glassy dynamics is whether the increase in relaxation timescales is linked to a growth in a dynamical lengthscale. Such a lengthscale could arise from cooperativity in the dynamics; if the dynamics is spatially heterogeneous, then the size of the heterogeneities (i.e. the size of regions within which the dynamics is approximately homogeneous) also defines a length. In this section we report on the various attempts in the literature at defining dynamical lengthscales for KCMs. Notice that the absence of a growing *static* (equilibrium) lengthscale is trivial in KCMs, since equilibrium correlations are ruled out by the non-interacting energy functions used.

We begin the discussion with **spin-facilitated models**. A first category of lengthscale definitions is based on irreducibility considerations: as we saw in sections 4.1 and 5.1, at low temperatures KCMs are effectively irreducible only for systems above a given size. We call such lengthscales 'irreducibility lengths'; they have also been referred to as percolation lengths because of the link to bootstrap percolation, e.g. in [75, 76], or cooperativity lengths [81, 173, 205, 287, 288]. Consider for example an f, d-SFM. As discussed in section 4.1, one can define the probability $p(c, L)$ that a randomly chosen equilibrium configuration in a system of linear size L belongs to the high-temperature partition; this means that the all-up spin configuration can be reached by a series of transitions respecting the kinetic constraints. A characteristic, c-dependent irreducibility length $L_*(c)$ can then be defined as that L for which $p(c, L)$ has a given value, say $p(c, L) = 1/2$ [173, 205, 287]. This is just the inverse function of the critical concentration $c_*(L)$ defined in section 4.1. $L_*(c)$ could also be obtained as the inverse function of a somewhat differently defined critical concentration, $c_*(L) = \int_0^1 \mathrm{d}c\, c[\mathrm{d}p(c, L)/\mathrm{d}c]$ [75]. However, since the derivative $\mathrm{d}p/\mathrm{d}c$ is non-negligible only in the narrow c-range where $p(c, L)$ increases steeply from 0 to 1 (compare figure 6 above), the two definitions are essentially identical. Closely related is the definition of an irreducibility lengthscale proposed in [81]: instead of measuring the probability that a randomly chosen configuration belongs to the high-temperature partition, let $f(c, L)$ be the average fraction of down-spins that remain after all mobile spins have been flipped up iteratively. Setting $f(c, 0) = 1$, one can define $q(c, L) = f(c, L-1) - f(c, L)$, the probability that a down-spin remains immobile for system size $L-1$ but not for size L. If (as is the case for, e.g. the 2, 2-SFM) the system is effectively irreducible, then $f(c, L \to \infty) = 0$ for any $c > 0$ and thus $\sum_{L=1}^{\infty} q(c, L) = 1$. An average lengthscale can then be defined as $\sum_L Lq(c, L)$ [81]. Whatever method is used, one typically finds irreducibility lengths that diverge very quickly as temperature is lowered. For the 2, 2-SFM, for example, the critical up-spin concentration for effective irreducibility decreases only logarithmically with system size, $c_*(L) \sim 1/\ln L$; see section 5.1. This gives $L_*(c) \sim \exp(A/c)$ or, with $c \approx \exp(-1/T)$, a *doubly* exponential divergence $L_*(T) \sim \exp[A \exp(1/T)]$ of the irreducibility length as the temperature is decreased. Irreducibility lengths can also be defined for models with directed kinetic constraints, e.g. the North-East model and the $(3, 2)$-Cayley tree, and then diverge at the up-spin concentration c_* below which even infinite systems are strongly reducible [81].

More local approaches to defining an irreducibility length have also been proposed, e.g. by Sappelt and Jäckle [288]. They defined the length $l(i, \mathbf{n})$, for a

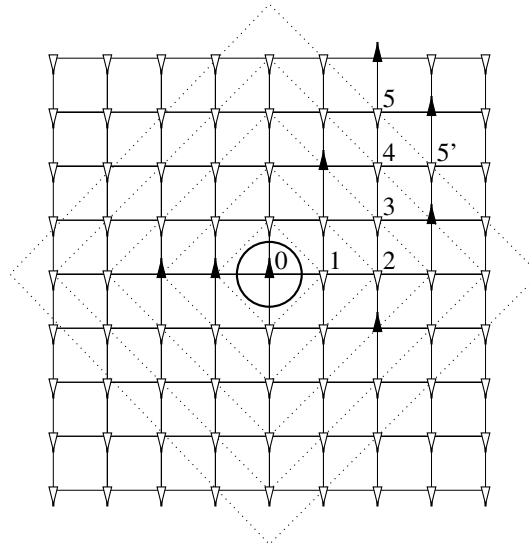

Figure 26. Definition of local irreducibility (or cooperativity) length in the $2,2$-SFM, for the circled spin in the centre. Dotted lines show n.n. shells around this spin. If the spins in the first n.n. shell are held fixed, the centre spin cannot be flipped. The same is true if the spins in the second shell are held fixed while other spins are allowed to move. Continuing outwards, only once spins in the fifth n.n. shell are allowed to flip can the centre spin be flipped down, by the spin-flip sequence 5 (or $5'$) $\to 4 \to 3 \to 2 \to 1 \to 0$. The cooperativity length is therefore $l = 5$.

given spin i and configuration $\mathbf{n}$, as the size (measured in number of n.n. shells) of the smallest region around spin i within which other spins have to be flipped to make the spin mobile. Figure 26 shows an example for the $2,2$-SFM. The spin in the centre of the configuration shown has $l(i,\mathbf{n}) = 5$ because in order to make it mobile one needs to flip some spins in the fifth n.n. shell, but none that are further away. In addition to an average lengthscale, which is comparable to the global irreducibility lengths defined earlier, this method yields a whole distribution of lengthscales. Sappelt and Jäckle [288] found that it had two distinct maxima, one for small l (in fact at $l = 1$) and a second broad one around the average value of l. The spatial distribution of $l(i,\mathbf{n})$ should also be able to give insights into the origin of dynamical heterogeneities, but has not to our knowledge been analysed.

The above definitions of irreducibility lengths all share the feature that they take the dynamics of KCMs into account only through the presence or absence of kinetic constraints: they measure how big a system (or a region where motion is allowed) needs to be for all or most spins to become mobile *eventually*, but do not consider what the timescales required would be. It is therefore not immediately obvious whether and how these lengthscales are related to typical relaxation times in KCMs. Possible connections have nevertheless been investigated; e.g. for the $f,2$-SFM with $f = 1.5, 2, 3$ (the last case being strongly reducible) typical relaxation times were found to increase roughly exponentially with the average of the local irreducibility length $l(i,\mathbf{n})$ defined above [97]. In the $2,2$-SFM, Nakanishi and Takano [75] also found a stronger-than-power-law timescale increase with the irreducibility length $L_*(c)$, albeit using an unconventional definition of relaxation time as the *longest*—as

opposed to typical, e.g. integrated—relaxation time for up-spin concentration fluctuations.

Definitions of lengthscales closely related to irreducibility lengths but now accounting for the timescales involved in relaxation have also been proposed. Schulz and Schulz [289] analysed cooperativity in the 2, 2-SFM by randomly selecting a lattice site and then running the dynamics, allowing spin flips only in increasingly large regions around the chosen spin. The smallest region within which a relaxation of the spin occurred within some (long) fixed *time interval* was then defined as the spin's cooperatively rearranging region. The size of this region is clearly a dynamical analogue of the quantity $l(i, \mathbf{n})$ discussed above, and in fact at least as large as the latter. As expected, the size distribution of the cooperative regions broadened towards larger values as T was lowered [289]. It could be fitted with two exponentials, corresponding to small and large regions in broad qualitative agreement with the results of [288] described above; with decreasing T the fraction of large regions as well as their average size increased, the latter in a superactivated fashion.

Among other possible tools for defining dynamical lengthscales, non-local dynamical correlations are obvious candidates. For the 2, 2-SFM, Fredrickson and Brawer [85] numerically simulated equilibrium correlations between different spins, $\langle n_i(0)n_j(t)\rangle - c^2$. These decay to zero for $t \to \infty$, but are also zero at $t = 0$ since different spins are uncorrelated in equilibrium. Fredrickson and Brawer [85] found that the onset of non-zero dynamical correlations was fast, while their decay was much slower and took place on the same timescale as the decay of the spin autocorrelation function. Interestingly, they also observed that dynamical correlations were significant only within a relatively short spatial range, e.g. of order five lattice spacings even for the relatively small up-spin concentration of $c \approx 0.08$.

Next we review studies of dynamical heterogeneities, which have again mainly focused on the 2, 2-SFM. In an early study [275] the fluctuations of the up-spin concentration were analysed. In a large system, these should be Gaussian, but for the small systems ($L = 16, \ldots, 32$) simulated in [275] non-Gaussian fluctuations were detected in a number of higher-order time correlation functions, suggesting non-trivial spatial correlations due to cooperative dynamics.

A more direct analysis of heterogeneities in the 2, 2-SFM was given by Butler and Harrowell [93]. They started the system from a random equilibrium configuration and then recorded for each spin how often it flipped within a time interval t. Obviously (if the system is large enough for reducibility effects to be negligible) then all spins should eventually flip infinitely often as $t \to \infty$. However, Butler and Harrowell found long-lived regions of spins that did not flip even for very long times t, implying pronounced dynamical heterogeneity; see figure 27. The remaining sites of the lattice, i.e. those containing mobile spins, they classified as either active or inactive depending on whether these spins were able to make the surrounding spins mobile on the timescales t considered. The long-time relaxation is dominated by this 'propagation of mobility' from the active sites, while inactive sites occur as islands of mobile spins confined by immobile down-spins and do not contribute significantly to the relaxation except at short times. The typical distance ξ between active sites then provides an intuitively appealing lengthscale characterizing the heterogeneity of the dynamics. It is, however, difficult to make the definition of an active site precise; in their simulations, Butler and Harrowell [93] chose as active sites those spins which were mobile at time $t = 0$ and whose eight surrounding spins had all flipped after some suitably chosen time interval. (This time interval must be neither too short—

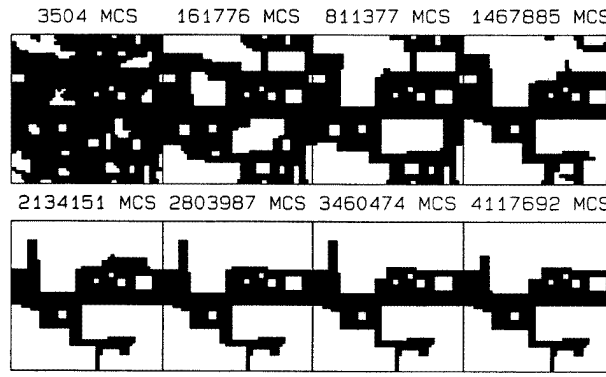

Figure 27. Dynamical heterogeneities in the 2, 2-SFM. Starting from an equilibrium configuration at up-spin configuration $c_{eq} \approx 0.083$ the plots show, for a series of increasing times (measured in Monte Carlo steps, MCS), as black those spins which have never flipped. The lower four plots in particular demonstrate the existence of very long-lived regions of frozen spins. From [93]. Copyright American Institute of Physics.

otherwise no sites would be classified as active—nor so long that inactive sites are counted because mobility from active sites has already been propagated toward them.) Butler *et al.* found a convincing power-law relationship between the relaxation timescale—measured by the mean-first passage time, i.e. the integral of the persistence function—and the distance between active sites, $\tau \sim \xi^{\delta}$ with exponent $\delta \approx 7.6$ over six decades in τ. This fit to the observed dependence of τ on T (or c) is better than one based on the Adam–Gibbs relation [85]; see section 5.6. Butler and Harrowell also estimated ξ, or rather the concentration $1/\xi^2$ of active sites, theoretically and found good agreement with the simulated values [93]. Intriguingly, however, their calculation turns out to be very similar to that of the concentration of nucleating sites occurring in irreducibility proofs for the 2, 2-SFM (section 4.1). This suggests that ξ should be related to the irreducibility length $L_*(c)$, and in fact Butler and Harrowell speculate that these two lengths might diverge in a similar fashion as $c \to 0$. If this is so, then using $L_*(c) \sim \exp(A/c)$ and the power-law relating τ with $\xi \sim L_*$ one would predict $\tau \sim \exp(A'/c)$ for small c, corresponding to an extremely strong, doubly exponential increase $\tau \sim \exp[A' \exp(1/T)]$ of the relaxation time with temperature. However, the simulation results were obtained in the regime where the lengthscales are still small, with, e.g. $\xi \approx 7$ for the lowest $c \approx 0.08$ in qualitative agreement with the correlation function results of [85] described above.

In a companion paper, Butler and Harrowell also considered a more direct operational definition of a dynamical lengthscale for the 2, 2-SFM [94]. This is obtained by adding free surfaces to the 2, 2-SFM and defining the cooperativity length as the lengthscale over which deviations from bulk relaxation behaviour are observed. The free surfaces are implemented by adding two rows of facilitating up-spins on opposite boundaries of the square lattice, while maintaining periodic boundary conditions in the other direction. The persistence time of spins near the surface is small—and shows a simple Arrhenius dependence on temperature—but grows to the bulk value in the layers further from the surface. Pinned surfaces consisting of down-spins, on the other hand, give persistence times that *decrease* into the bulk. The distance from the surface at which bulk behaviour is reached defines a

dynamical lengthscale and, encouragingly, turns out to be similar for free and pinned surfaces. It increases by a factor of three while the persistence time increases by four orders of magnitude; again, a power-law relationship $\tau \sim \xi^{\delta}$ was observed with $7.0 < \delta < 7.6$ [290]. Extrapolating naively, Butler and Harrowell [94] then also estimated that the typical relaxation time increases of $\sim 10^{12}$ observed on supercooling glass-forming liquids would correspond to a growth of the cooperativity length by a relatively modest factor of around $3^3 \approx 30$.

In a later study, Foley and Harrowell [290] further analysed dynamical heterogeneities in the 2, 2-SFM by measuring the spatial correlations of the first passage times averaged over different regions of the lattice. (For a visualization of the local, unaveraged first passage times see also [274]; a more recent study of kinetic structures in SFMs is [291].) Starting from an equilibrium configuration, they measured for each spin i the time τ_i at which it first flips. They then defined, for any given region of linear size l, the average of the τ_i in that region as $\tau(l)$, and considered the moments

$$m_q(l) = \frac{\langle [\tau(l) - \tau]^q \rangle}{\langle [\tau(1) - \tau]^q \rangle}. \tag{122}$$

Here the averages are over all regions of size $l \times l$ in the numerator, and over all regions of size 1×1, i.e. all lattice sites, in the denominator; $\tau = \langle \tau(1) \rangle = \langle \tau(l) \rangle$ is the average first passage (or first flip) time for the whole lattice. The moments $m_q(l)$ thus measure the fluctuations in the average first passage time of regions of size l, scaled so that $m_q(l) \approx 1$ corresponds to times τ_i which are fully correlated within regions of size l. The decrease of $m_q(l)$ with l can thus be used to define a correlation length ξ_q, for which Foley and Harrowell found two main results [290]. First, it is not possible to identify a single such lengthscale since the value of ξ_q depends significantly on the order q of the moment considered; this could suggest a multifractal structure of the spatial correlations in the dynamics. Secondly, they again observed a power-law relation between timescales and dynamical lengthscales, $\tau \sim \xi_2^{\delta}$, though with an exponent $\delta \approx 12$ that is rather larger than for the lengthscales derived from the concentration of actives sites.

More recently, the ratio Q [68] of the lifetime of heterogeneous regions to their local relaxation time has also been measured, in a modified version of the 2, 2-SFM where multi-state spins are used to model orientational degrees of freedom. Q can be determined from an appropriately generalized persistence function, and was found to be of order unity [292]. This could in fact have been expected on the basis of the results of Butler and Harrowell [93, 94] for the 2, 2-SFM: the timescales for propagation of mobility, which limits the lifetime of heterogeneities, are of the same order as typical relaxation timescales. At present it therefore seems that SFMs cannot model the values of $Q \gg 1$ observed in some recent experiments (see section 2.5).

Finally, we mention a very recent approach to the study of heterogeneities in SFMs, proposed by Garrahan and Chandler [293]. They map the non-equilibrium trajectories of a system on a d-dimensional lattice onto the statics of a $(d+1)$-dimensional spin system. This space-time view provides an interesting geometrical framework for understanding dynamical heterogeneities. For example, since in the 1, 1-SFM and the East model spatial domains of down-spins can only be 'invaded' from their left (or, for the 1, 1-SFM, right) boundary, their two-dimensional space-time representations always give closed regions, separated by interfaces formed by

up-spins. Since only neighbours of up-spins are mobile, this shows geometrically that mobile sites will 'follow each other around', in interesting correspondence with simulation results for Lennard-Jones systems [60, 61].

Garrahan and Chandler [293] also studied dynamical heterogeneities in the 1, 1-SFM and East model quantitatively, by considering the time-averaged magnetizations $m_i(t) = (1/t)\int_0^t \mathrm{d}t' \, [2n_i(t') - 1]$. Slow spins that do not flip have the maximal value ($= 1$) of the 'heterogeneity' $m_i^2(t)$, while fast spins give lower values. For $t \to 0$ and $t \to \infty$ there are no spatial correlations between the $m_i^2(t)$, but at intermediate t of the order of typical relaxation times, non-trivial spatial structure can appear. This can then be used to define a lengthscale for dynamical heterogeneities, which increases slowly with decreasing temperature T [293]. The k-dependence of the structure factor (Fourier transform) $S(k)$ associated with the correlations $\langle m_i^2(t) m_j^2(t)\rangle - \langle m_i^2(t)\rangle\langle m_j^2(t)\rangle$ also shows non-trivial features; e.g. in the East model, the hierarchical nature of relaxation processes leads to space-time regions of up-spins with a fractal structure, giving a power-law decrease $S(k) \sim k^{-\ln 3/\ln 2}$ for intermediate k.

Next we review studies of dynamical lengthscales and heterogeneities in **constrained lattice gases**. An irreducibility length can be defined if, instead of the fraction $f(c, L)$ of permanently immobile spins in SFMs, one considers the fraction of particles in the backbone (see section 4.1; recall that the backbone contains all particles that are permanently frozen in place due to the presence of other such particles). For the triangular lattice gas [113], simulation results showed a growth of this length for particle concentration $c \to 1$ that could be fitted by an exponential divergence $\sim \exp[-\mathrm{const}/(1-c)]$. Following earlier work on the hard-square lattice gas [173, 205], Jäckle and Krönig then compared this timescale-independent definition of a lengthscale with dynamical quantities, by measuring the diffusive displacements of particles in finite-size lattices [113]. Strong deviations from the limiting behaviour for large systems were found, e.g. up to $L = 15$ at particle concentration $c = 0.7$; this length is of similar order of magnitude as the irreducibility length $L_* \approx 8$ for this c. The finite-size effects on diffusion are already visible for small particle displacements, and thus genuinely due to cooperative dynamics rather than the trivial upper limit on displacements imposed by the finite lattice. Similar size effects appear in correlation functions measured on lattice strips of finite width [115], both for translational motion and for orientational degrees of freedom in the appropriately extended model (see section 3.3). Intriguingly, it was observed in [173] (for the hard-square lattice gas) that the irreducibility length L_* is substantially larger than the distance over which particles need to diffuse before the mean-square displacement becomes linear in t. This shows that the irreducibility length is a rather subtle measure of the cooperative nature of the dynamics, and cannot simply be thought of as the size of a cage within which particles are trapped until they can diffuse freely.

Jäckle and Krönig [118] further studied dynamical heterogeneities in the triangular lattice gas by considering non-local dynamical correlations, as measured via the dynamic structure factor (13). As explained in section 2.2, the latter should decay as $\exp(-D\mathbf{k}^2 t)$ for long times and small wavevectors $\mathbf{k}$, reflecting the diffusive nature of the dynamics; D is the collective diffusion constant. For larger $\mathbf{k}$, the observed long-time decay rates will deviate from $D\mathbf{k}^2$. The onset of these deviations at wavevectors of length k_c (say) then defines a lengthscale $1/k_c$ below which the

dynamics is heterogeneous; this was found in [118] to increase with c, but the precise form of this dependence was not analysed.

Very recently, heterogeneities in the KA-model have also been studied [294]. Motivated by results for mean-field spin glasses [295–297], the fourth-order correlation function

$$C_4(t) = \frac{1}{Nc^2(1-c)^2} \sum_{ij} \big(\langle n_i(t) n_i(0) n_j(t) n_j(0) \rangle - \langle n_i(t) n_i(0) \rangle \langle n_j(t) n_j(0) \rangle \big) \qquad (123)$$

was simulated. This can also be written as the scaled variance $C_4(t) = N(\langle q^2(t) \rangle - \langle q(t) \rangle^2)$ of the 'overlap' between configurations a time t apart,

$$q(t) = \frac{1}{Nc(1-c)} \sum_i \big(n_i(t) n_i(0) - c^2 \big). \qquad (124)$$

By definition, $q(0) = 1$ and thus $C_4(0) = 0$. As t increases, $q(t)$ will decay, approaching $q(t \to \infty) = 0$ for times long enough for the system to have lost all memory of its initial configuration. However, for particle concentrations c close to the (at least effective) dynamical transition $c_{\mathrm{dyn}} = 0.88$ in the KA model, one would suspect that the system remains trapped near its initial configuration for a long time. This will give a non-zero value of $q(t)$ which will also fluctuate strongly between dynamical histories started off at different initial configurations $n_i(0)$, leading to a large value of $C_4(t)$. Consistent with this, it was found in [294] that the simulated $C_4(t)$ exhibited a maximum at finite t, before decaying again as the system finally loses memory of its initial configuration.† The maximum becomes higher and shifts to larger t as c is increased towards c_{dyn}, reflecting the fact that the system is trapped more strongly, and for longer times, at higher c. Similar results have been found in frustrated lattice gases [299] and Lennard-Jones glasses in $d = 2$ dimensions [300]. In the spherical p-spin glass, a rough analogue of $C_4(t)$ can be shown to have a maximum which actually diverges as the dynamical transition of this mean-field model is approached; this is related to the divergence of an appropriately defined static spin-glass susceptibility below the transition [295–297] and suggests a corresponding diverging lengthscale. In the KA model, the definition (123) of $C_4(t)$ as a sum over all pairs of lattice sites likewise suggests that the observed increase in the maximum value of $C_4(t)$ reflects a growing lengthscale over which the dynamics is heterogeneous because configurations remain dynamically correlated. How this length is related to others defined, e.g. for the triangular lattice gas (see above) is not obvious, and a closer investigation of this issue would seem worthwhile. A wavevector-dependent generalization of $C_4(t)$, obtained by including a factor $\exp[\mathrm{i}\mathbf{k} \cdot (\mathbf{r}_i - \mathbf{r}_j)]$ in the definition (123), could be helpful in defining the lengthscale for dynamical heterogeneities more precisely. Such a quantity would be closely related to the structure factor of dynamical heterogeneities considered by Garrahan and Chandler [293]. This can be seen from the fact that, e.g. the fourth-order contribution to their correlation $\langle m_i^2(t) m_j^2(t) \rangle - \langle m_i^2(t) \rangle \langle m_j^2(t) \rangle$ is proportional to

† In the simulations of [294] it appears that, at least for the smaller values of c investigated, $C_4(t)$ decays to values below unity for $t \to \infty$. On the other hand, from the definitions (123) and (124) one calculates, using the fact that $n_i(0)$ and $n_i(t \to \infty)$ are uncorrelated equilibrium configurations, that $C_4(t \to \infty) = 1$. The origin of this discrepancy is unclear to us. However, more recent simulations confirm the theoretical expectation $C_4(t \to \infty) = 1$ (J. J. Arenzon, private communication), also in inhomogeneous systems as long as one focuses on approximately homogeneous subregions [298].

$\int_0^t \mathrm{d}t_1\,\mathrm{d}t_2\,\mathrm{d}t_3\,\mathrm{d}t_4\,(\langle n_i(t_1)n_i(t_2)n_j(t_3)n_j(t_4)\rangle - \langle n_i(t_1)n_i(t_2)\rangle\langle n_j(t_3)n_j(t_4)\rangle)$, which one would expect to behave qualitatively similarly to the terms under the sum in (123).

5.6. *Energy landscape paradigms*

In this section we review studies investigating the application of energy landscape paradigms such as configurational entropies and Edwards measures (see section 2.4) to KCMs.

The usefulness of the **Stillinger–Weber configurational entropy** was studied in [55] for the East model and the 1, 1-SFM. It was argued that the SW entropy is not relevant for understanding glassy effects in these models. The key observation is that all reasonable definitions of a SW-like configurational entropy are independent of the asymmetry parameter a which interpolates between the two models (see (32)), while the actual dynamics varies dramatically between the limits of $a = 0$ (East model) and $a = 1$ (1, 1-SFM). The natural definition of an inherent structure (IS) is as a configuration that is frozen at $T = 0$ (see section 2.4); in such a configuration, all up-spins are isolated. The number of such configurations with a given up-spin concentration or equivalently energy e_{IS} is easily counted [55] and its logarithm gives the configurational entropy $Ns_{\mathrm{c}}(e_{\mathrm{IS}})$, shown in figure 28. (The configurational entropy for the triangle model can be obtained by similar reasoning [131].) One might hope that a configurational entropy calculated over inherent structures of a given *free energy* f, rather than *energy* e_{IS}, may have better properties; but in the low-temperature regime $f \approx e_{\mathrm{IS}}$ since entropic contributions from the size of the basins around each IS are negligible, and so no significant differences are expected. As an alternative, it might be interesting to study the timescale-dependent definition of a

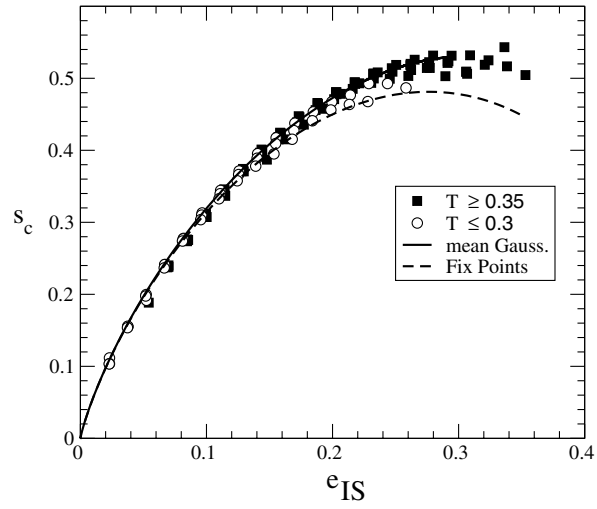

Figure 28. Stillinger–Weber configurational entropy in the 1, 1-SFM for a chain of 64 spins. The lower curve gives the result from a direct count of configurations which are frozen at $T = 0$, and the symbols are estimates derived from the actual dynamics at different temperatures (assuming that the free energy of the inherent structures is independent of their energy e_{IS}). The upper curve is obtained by an approximation based on integrating the temperature dependence of the average value of e_{IS}. From [55]. Copyright American Institute of Physics.

configurational entropy over metastable states proposed by Biroli and Kurchan [56] (see section 2.4). For this one would anticipate clear differences between the 1, 1-SFM and the East model, arising from the fact that in the latter there is a whole hierarchy of well-separated timescales on which metastable states could be defined.

The applicability of the Adam–Gibbs [37] relation $\tau \sim \exp(\text{const}/Ts)$ between typical relaxation times τ and the thermodynamic entropy s has also been investigated for KCMs. Underlying this relation is the assumption that there is a connection between a lengthscale characterizing cooperative dynamics and the (inverse of the) thermodynamic entropy s. Sappelt and Jäckle argued that such a connection cannot exist in general, and certainly not in KCMs [288]. This is most obvious in models such as the North-East model or the (3, 2)-Cayley tree: at the up-spin concentration c_* where these models become strongly reducible, the irreducibility length L_* diverges (see section 5.5) while the entropy per spin, $s = -c \ln c - (1-c)\ln(1-c)$, is a smooth function of c. Even in other KCMs, the divergence of an appropriately defined cooperativity length for $c \to 0$ is much more pronounced than the weak logarithmic divergence of the entropy [288]. Even though the foundations of the Adam–Gibbs relation are therefore uncertain in KCMs, Fredrickson and Brawer found that for the 2, 2-SFM the relation holds to a reasonable accuracy over a range of around six decades in the relaxation time [85], while for the 2, 3-SFM it appears to be violated [28]. As explained in section 5.5, however, Butler and Harrowell [93] later showed that there were small but systematic deviations from Adam–Gibbs even for the 2, 2-SFM, and that the temperature dependence of τ is better rationalized by a power-law link to an appropriately defined lengthscale.

In the last few years, the applicability of **Edwards measures** to the description of glassy dynamics in KCMs has received growing attention. (This includes work on KCMs driven into non-equilibrium stationary states by external forcing, which is discussed in section 5.7 below.) For SFMs, one needs to decide which configurations to regard as 'blocked'. A natural definition is to use again configurations where no spins can move at $T = 0$, i.e. which contain no mobile up-spins; these are identical to the inherent structures in SFMs discussed above. The Edwards measure is then a uniform measure over the subset of these configurations with the desired values for specified observables such as the energy. For the 1, 1-SFM and the East model, as well as the interpolating asymmetric model, a recent analysis of the $T = 0$ dynamics [109] shows that the results are not well described by averages over an Edwards measure constrained to have the correct up-spin concentration. Spin–spin correlations, for example, fall off super-exponentially in the final configurations actually reached by the $T = 0$ dynamics whereas a flat average over blocked configurations gives an exponential decay.

More successful is the application of Edwards measures to constrained lattice gases; here the definition of the blocked configurations to be included in the Edwards measure is straightforward. In the grand canonical version of the KA model, where particle exchange with a reservoir is allowed, it was shown in [301, 302] that the FDT violations observed after an increase of the chemical potential into the non-equilibrium region (see section 5.4.3) were well predicted by an appropriate Edwards measure. Specifically, the effective temperature deduced from the slope of the out-of-equilibrium part of the FDT plot (figure 25) agrees numerically with that found from the entropy of blocked configurations, evaluated at the density $c(t_w)$ reached during the ageing process. The structure factor, i.e. the spatial correlations of density

fluctuations which develop during ageing—but are absent in equilibrium—was likewise well predicted by the Edwards measure approach.

The geometrical organization of the blocked configurations which the Edwards measure focuses on has recently also been investigated [294]. The authors generated blocked configurations by an annealing process in the number of mobile particles. They then moved a randomly chosen particle to a different location, ran the dynamics of the KA model from this starting configuration and monitored whether the system became blocked again after a few transitions or whether it remained substantially unblocked, with many particles being mobilized. They found that the 'unblocking probability' is high at low densities, but tends to zero at the density of the (effective) dynamical transition, $c_{\rm dyn} \approx 0.88$. Above this density, blocked configurations are therefore stable with probability one. Measurements of the overlaps between these configurations showed that at all densities there are blocked configurations arbitrarily close to other blocked configurations. This contrasts with results for mean-field spin glasses (e.g. p-spin spherical models), where in the regime corresponding to high density there is a minimum distance between the analogues of blocked configurations [294]. This observation suggests that the geometrical organization underlying glassy dynamics in KCMs is rather different from that in mean-field models, and clearly deserves further investigation.

5.7. *Driven stationary states*

In this final results section we review recent work on KCMs in out-of-equilibrium stationary states generated by external driving. Much of this research is motivated by attempts to understand the behaviour of granular materials under steady tapping or vibration.

We begin again with **spin-facilitated models** and their variants. The effects of driving by repeated excitation or 'tapping' have been studied in, for example, the $1,1$-SFM [303]. A tap corresponds to evolution at non-zero temperature T for some short time interval $t_{\rm tap}$, after which the system is allowed to relax fully under zero temperature dynamics. A possible motivation for this dynamics comes from granular media; one regards the chain of spins as a crosssection through a granular medium, with up- and down-spins corresponding to low- and high-density regions or holes and particles, respectively. The tap typically generates up-spins (holes) while the subsequent zero-temperature relaxation can only flip spins down, thus filling holes with particles. The kinetic constraint of the $1,1$-SFM imposes the restriction that isolated holes cannot be filled. Using the fact that the zero-temperature dynamical equations of the $1,1$-SFM can be exactly closed [214, 215], the dynamics of the joint tapping and relaxation process can be solved to lowest order in $t_{\rm tap}$ and $\exp(-1/T)$, and a logarithmic decay of the particle density $1-c$ is found over a wide time interval [303]. This behaviour is reminiscent of that found in parking-lot models and other adsorbtion–desorbtion models [216]. The response of the particle density to sudden changes in tapping intensity also displays interesting memory effects [304, 305] but these are not specific to tapping dynamics and occur even in e.g. the Glauber Ising chain [306]. Hysteresis effects from cyclic variations of the tapping intensity have likewise been investigated [307]. Further work on the tapped $1,1$-SFM showed that in the limit of short or weak taps, an effective master equation can be used to describe the evolution of the system from tap to tap, without needing to consider the intermediate excited states generated by the tapping [254]. The steady state of the resulting model can be described by an Edwards measure at the appropriate up-spin

concentration, where all metastable or frozen configurations—those in which only isolated up-spins occur—contribute with equal probability [254].

The effects of different kinds of tapping dynamics in the 1, 1-SFM were further investigated in [308], where the analysis was also extended to the East model. A 'tap' was either a single Monte Carlo sweep of the system at some $T > 0$ (this corresponds to a fixed tap duration of $t_{\text{tap}} = 1$), or a random flip applied to each spin independently with some probability $p < 1/2$; in between taps the system relaxes again at zero-temperature. Thermal and random tapping as defined in this way gave quite different results, e.g. in terms of the magnetization reached in the stationary state. These differences persisted even for small tapping intensity (T or $p \to 0$). A flat Edwards measure over frozen configurations with the correct up-spin concentration was found to describe other aspects of the stationary state, such as the distribution of domain lengths, only for thermal tapping at moderate intensity—consistent with the results of [254]—while systematic deviations occurred for random tapping.

Recently, a driven version of the East model has also been proposed that is motivated by *rheological* considerations [225]: 'soft' glasses such as dense emulsions and colloidal suspensions can be driven into non-equilibrium steady states by shear flow [72]. A modified version of the East model with three-state spins was used, but the third state turned out to be irrelevant for the qualitative behaviour. The 'rheological' driving was implemented by adding *unconstrained* up-flips from $n_i = 0$ to $n_i = 1$ to the model, at a rate $\dot{\gamma}$ which can loosely be thought of as the shear rate. This modification breaks detailed balance. One may expect, however, that the stationary state reached after a long time should be similar to that obtained after ageing (without shear) for a time $t_{\text{w}} \sim 1/\dot{\gamma}$. The steady state under shear can be worked out using the same domain picture as for the ageing case; see section 4.6. An independent interval approximation again needs to be made, though in the driven case it is not clear whether this becomes exact for $T \to 0$ as it does in the ageing case. The theory nevertheless provides a good description of simulation results. There is also the expected close (though not perfect) match between the domain length distributions for the ageing and sheared cases when t_{w} and $\dot{\gamma}$ are related by $t_{\text{w}} = 1/\dot{\gamma}$ [225].

In the Glauber Ising chain with 'falling' dynamics (only energy-decreasing moves are allowed) driven by random taps, Lefèvre and Dean [106] calculated a number of observables (energy fluctuations, correlation functions and domain size distributions) exactly within the Edwards measure and observed very good agreement with numerical simulations. As an aside, we note that for the same 'tapping and falling' dynamics in ferromagnets on random graphs of fixed connectivity $r > 2$ ($r = 2$ gives the Ising chain), Dean and Lefèvre [107] found in simulations a first-order phase transition in the stationary behaviour. For p below some threshold p_{c}, the energy E in the stationary state equalled the ground state energy, jumping by a finite amount to some $E^* = E(p_{\text{c}} + 0)$ as p crosses the threshold. This was interpreted in terms of a change in behaviour of the Edwards entropy $S(E)$: in an approximate calculation $S(E)$ is concave above E^* and therefore gives, in a thermodynamic formalism, locally stable states of energies $E > E^*$, while for $E < E_*$ the entropy $S(E)$ is convex so that states with these energies are unstable.

Finally, driven steady states have also been studied in the context of the **KA model** connected to two reservoirs at unequal chemical potential μ [309]. The difference in chemical potentials sets up a particle current between the two reservoirs, and a non-trivial density profile which can be well reproduced using a continuum

model (see section 4.10). An interesting feature is that the system may show 'negative resistance': if the particle densities of the two reservoirs are both increased by the same factor, the current may decrease. This occurs because the decrease in mobility with increasing density can overwhelm the increase in the density difference which drives the current.

6. Conclusions and outlook

In this review we have discussed the glassy dynamics of kinetically constrained models (KCMs). Their characteristic feature is that they have trivial, normally non-interacting, equilibrium behaviour. The existence of slow glassy dynamics can thus be studied without any 'interference' from an underlying equilibrium phase transition. A further advantage of KCMs is that they introduce explicitly, via constraints on the allowed transitions between configurations, the cooperative character of the dynamics whose origin in more realistic glass models we do not yet fully understand. In our discussion of KCMs we have included spin-facilitated Ising models (SFMs) and their variants; constrained lattice gases; models inspired by cellular structures; the triangle and plaquette models obtained via mappings from interacting systems without constraints; and finally related models such as urn, oscillator, tiling and needle models. We now summarize the results and assess how good KCMs are at modelling glassy dynamics in physical systems such as structural glasses. Avenues for future research are also discussed.

Broadly speaking, KCMs fall into two classes. The first one contains the $1, d$-SFMs, the cellular models and the plaquette model, all of which can be analysed in terms of appropriately defined defects that diffuse and react which each other. Typical relaxation timescales show an activated temperature dependence, so that these KCMs model 'strong' glasses. The reaction–diffusion picture provides a fairly full understanding of the dynamics both in and out of equilibrium, including, e.g. the shape of correlation and response functions. Some open questions remain, however, especially with regard to fluctuation–dissipation theorem (FDT) violations and the description of out-of-equilibrium dynamics in terms of an effective temperature. Urn and oscillator models also fall into the category of 'strong glass' KCMs, but due to their lack of spatial structure require different conceptual tools to understand the dynamics, in particular the notion of entropic barriers which slow down the dynamics at low temperatures.

The second class of KCMs contains all remaining models, in particular the constrained lattice gases and SFMs with directed constraints or with facilitation by $f > 1$ spins. These show genuinely cooperative dynamics which cannot be broken down into the motion of localized defects. Their relaxation times diverge in a superactivated fashion as temperature decreases, so that they model 'fragile' glasses. The cooperative nature of the dynamics means that these models are much less well understood than the defect-diffusion KCMs. It also implies that **reducibility** effects become a serious concern. While arguments developed, e.g. for bootstrap percolation show that in the thermodynamic limit most models become effectively irreducible in the sense that almost all configurations are dynamically accessible, the system sizes required can be extremely large in the glassy regime (low up-spin concentrations for SFMs, or high particle concentrations for lattice gases).

Related though distinct is the question of **dynamical transitions** where ergodicity is broken because of diverging relaxation timescales. The only cooperative KCM for

which strong evidence for such a transition exists is the KA lattice gas, in which relaxation times appear to diverge when the particle concentration approaches $c_{\mathrm{dyn}} \approx 0.88$. Even here finite size effects are difficult to exclude, however, since around this concentration reducibility effects also become strong for the system sizes that are accessible in numerical simulations. In the absence of analytical arguments the existence of a dynamical transition is therefore likely to remain conjectural. However, from a more pragmatic point of view the more important question is *why* relaxation times diverge as quickly as they do around $c = c_{\mathrm{dyn}}$, not whether they are truly infinite or finite but extremely large at higher densities. This remains an essentially open issue, as does the origin of the conjectured universality in the timescale divergence near c_{dyn}. In SFMs, the 'fragile' timescale divergence with decreasing temperature T also remains poorly understood, except for the simplest cases such as the East model where an EITS law $\tau \sim \exp(A/T^2)$ has been found.

Closely related are the issues of **heterogeneous dynamics** and **dynamical lengthscales**. KCMs are ideal for the study of these effects, having only trivial static correlations so that all effects are directly due to the dynamics. Direct evidence for dynamical heterogeneities has been found in the 2, 2-SFM and more recently also in the East model. There has also been some success in identifying dynamical lengthscales and relating these to the observed relaxation times. But more needs to be done, both at the analytical and the numerical level, to identify an unambiguously defined cooperativity length and understand how its growth affects the dynamics. This is particularly important now that much more data on heterogeneities in experimental systems are becoming available.

Many of the cooperative KCMs are found in simulations to have stretched exponential **relaxation functions at equilibrium**. A quantitative theoretical understanding of these effects remains to be achieved, again with the possible exception of the East model where there are at least plausible conjectures for the stretching behaviour at low temperatures. Mode-coupling approximations, the most successful of which are based on approximations to the irreducible memory functions, generally perform rather badly, predicting, e.g. spurious dynamical transitions. Recent diagrammatic expansions offer some improvements, giving results formally analogous to those of the extended mode-coupling theory for supercooled liquids, but still predict relaxations which are too close to exponential deep in the glassy regime. A better understanding of the physical nature of these approximation techniques will be essential for progress in this direction. Adiabatic approximations, by contrast, are based directly on a physically intuitive separation into fast and slow degrees of freedom and have been used with some success in the analysis of cooperative KCMs. A clear example of this is the East model, where the timescale separation (involving in fact a whole hierarchy of widely separated times) becomes exact in the low-temperature limit and gives a fairly full understanding of the out-of-equilibrium behaviour after a deep quench. Further exploration of such techniques both for KCMs and more general glass models should therefore be fruitful.

For cooperative KCMs in general our understanding of the **out-of-equilibrium dynamics** is still only at the beginning. While some general qualitative features such as apparent freezing in cooling runs and hysteresis in heating–cooling cycles are well understood, more complex effects such as the behaviour of two-time correlation and response functions still present puzzles. There is no simple picture as yet of the observed FDT violations, for example: in the KA lattice gas and the plaquette model, simple mean field-like FDT plots consisting to a good approximation of two

straight lines are observed, while other KCMs show more complex behaviour including non-monotonic FDT relations. The robustness of these results to the choice of observable, the existence of a well-defined effective temperature T_{eff} and its connection to an appropriately defined configurational entropy also remain to be clarified. The KA model is the most encouraging in this sense: the T_{eff} from an appropriate FDT plot agrees with that derived from an effective equilibrium description in terms of a flat 'Edwards measure' over blocked configurations. In other models, however, no such simple correspondence is found and much work remains to be done to understand these results in a wider context.

Finally, KCMs without detailed balance are also beginning to be explored. We touched on these when discussing stationary states reached by **external driving** which can model the tapping of granular materials or shear flow of 'soft' glassy materials. Recent work has focused on the suitability of Edwards measures for describing the resulting stationary states, but a coherent picture is yet to emerge. More generally, the similarities in the phenomenology of granular materials (which are effectively at temperature $T = 0$) and 'thermal' glasses suggest that detailed balance is not a key ingredient in glassy dynamics. One may for example expect that slowly driven and ageing systems behave in similar way, and for a driven version of the East model this has indeed been confirmed. Future work on new KCMs without detailed balance will no doubt deepen our understanding of driven glassy systems.

Overall, we believe that the simplicity of KCMs and their ability to combine slow dynamics with trivial equilibrium behaviour make them prime candidates for further progress in the issues at the heart of current research in glassy dynamics.

Acknowledgements

We are grateful to all our collaborators, much of whose work has been described in this review, including Luis Bonilla, Andrea Crisanti, Martin Evans, Suzanne Fielding, Silvio Franz, Adan Garriga, Luca Leuzzi, Peter Mayer and Paco Padilla. We are also indebted to many other colleagues, too numerous to mention, for enlightening discussions on many of the topics covered in this review. Particular thanks are due to all participants in the SPHINX workshop on *Glassy Behaviour of Kinetically Constrained Models* held in Barcelona in March 2001, for an exciting and productive meeting. PS acknowledges financial support through Nuffield grant NAL/00361/G. FR has been supported by the Spanish Ministerio de Ciencia y Tecnología Grant BFM2001-3525.

List of abbreviations

b.c.c.	body-centred cubic
BP	bootstrap percolation
EITS	exponential inverse-temperature square
f.c.c.	face-centred cubuc
FDT	fluctuation–dissipation theorem
IS	inherent structure
KA	Kob–Andersen
KCM	kinetically constrained model
KWW	Kohlrausch–Williams–Watts
MCA	mode-coupling approximation
MCT	mode-coupling theory

n.n. nearest neighbour
SFM spin-facilitated model
(f, d-SFM: spin-facilitated model on d-dimensional lattice with f facilitating spins)
SW Stillinger–Weber
TTI time-translation invariance
VTF Vogel–Tamman–Fulcher

References

[1] Goldstein, M., and Simha, R. editors, 1976, *The Glass Transition and the Nature of the Glassy State*, volume 279 (New York: New York Academy of Science).
[2] O'Reilly, J. M., and Goldstein, M. editors, 1981, *Structure and Mobility in Molecular and Atomic Glasses*, volume 371 (New York: New York Academy of Science).
[3] Donth, E. J., 1981, *Glaszustand* (Berlin: Akademie).
[4] Brawer, S. A., 1983, *Relaxation in Viscous Liquids and Glasses* (New York: American Ceramic Society).
[5] Parthasarathy, R., Rao, K. J., and Rao. C. N. R., 1983, *Chem. Soc. Rev.*, **12,** 361–385.
[6] Angell, C. A., and Goldstein, M. editors. 1986, *Dynamic Aspects of Structural Change in Liquids and Glasses*, volume 484 (New York: New York Academy of Science).
[7] Scherer, G. W., 1986, *Relaxation in Glass and Composites* (New York: Wiley).
[8] Angell, C. A., 1995, *Science*, **267,** 1924–1935.
[9] Greer, A. L., 1995, *Science*, **267,** 1947–1953.
[10] Hodge, I. M., 1995, *Science*, **267**, 1945–1947.
[11] Frick, B., and Richter, D., 1995, *Science*, **267,** 1939–1945.
[12] Stillinger, F. H., 1995, *Science*, **267,** 1935–1939.
[13] Ediger, M. D., Angell, C. A., and Nagel, S. R., 1996, *J. Phys. Chem.*, **100,** 13200–13212.
[14] Proceedings of Trieste workshop on unifying concepts in glassy physics, 1999, *J. Phys. Cond. Matt.*, **12,** 6295–6682.
[15] Debenedetti, P. G., 1996, *Metastable Liquids: Concepts and Principles* (Princeton University Press).
[16] Bengtzelius, U., Götze, W., and Sjolander, A., 1984, *J. Phys.* C, **17,** 5915–5934.
[17] Götze, W., 1991, Aspects of structural glass transitions. In J. P. Hansen, D. Levesque, and J. Zinn-Justin, editors, *Liquids, Freezing and Glass Transition* (Amsterdam: North-Holland), pp. 287–503.
[18] Götze, W, and Sjögren, L., 1992, *Rep. Prog. Phys.*, **55,** 241–376.
[19] Götze, W., and Sjögren, 1995, *Transp. Theory Stat. Phys.*, **24,** 801–53.
[20] Jäckle, J., 1986, *Rep. Prog. Phys.*, **49,** 171–231.
[21] Struik, L. C. E., 1978, *Physical Aging in Amorphous Polymers and other Materials* (Houston: Elsevier).
[22] Crisanti, A., and Ritort, R., 2002, Violation of the fluctuation-dissipation theorem in aging systems: basic notions and the numerical evidence. Preprint cond-mat/0212490.
[23] Bouchaud, J. P., Cugliandolo, L. F., Kurchan, J., and Mézard, M., 1998, Out of equilibrium dynamics in spin-glasses and other glassy systems. In A. P. Young, editor, *Spin Glasses and Random Fields* (Singapore: World Scientific), pp. 161–223.
[24] Cugliandolo, L. F., 2002, Dynamics of glassy systems. Preprint cond-mat/0210312, to appear as Les Houches lecture notes.
[25] Ediger, M. D., 2000, *Annu. Rev. Phys. Chem.*, **51,** 99–128.
[26] Sillescu, H., 1999, *J. Non-Cryst. Solids*, **243,** 81–108.
[27] Debenedetti, P. G., and Stillinger, F. H., 2001, *Nature*, **410,** 259–267.
[28] Fredrickson, G. H., 1988, *Ann. Rev. Phys. Chem.*, **39,** 149–180.

[29] Palmer, R. G., 1989, Models for slow relaxation in glassy systems. In H Takayama, editor, *Cooperative Dynamics in Complex Physical Systems*, volume 43 of *Springer Series in Synergetics* (Heidelberg: Springer), pp. 118–127.
[30] Proceedings of Barcelona workshop on glassy dynamics in kinetically constrained models, 2002, *J. Phys. Cond. Matt.*, **14,** 1381–1696.
[31] Vogel, H., 1921, *Phys. Z.*, **22,** 645.
[32] Fulcher, G. S., 1925, *J. Am. Ceram. Soc.*, **77,** 3701.
[33] Tamman, G., and Hesse, W., 1926, *Z. Anorg. Allgem. Chem.*, **156,** 245.
[34] Anderson, P. W., 1979, Lectures on amorphous systems. In R. Balian, R. Maynard, and G. Toulouse, editors, *Les Houches, Session XXXI: Ill-Condensed Matter* (Amsterdam: North-Holland), Chapter 3, pp. 159–261.
[35] Bässler, H., 1987, *Phys. Rev. Lett.*, **58,** 767–770.
[36] Richert, R., and Bässler, H., 1990, *J. Phys. Cond. Matt.*, **2,** 2273–2288.
[37] Adam, G., and Gibbs, J. H., 1965, *J. Chem. Phys.*, **43,** 139–146.
[38] Tool, A. Q., 1946, *J. Am. Ceram. Soc.*, **29,** 240.
[39] Cugliandolo, L. F., Kurchan, J., and Peliti, L., 1997, *Phys. Rev.* E, **55,** 3898–3914.
[40] Reichl, L. E., 1980, *A Modern Course in Statistical Physics* (Austin: University of Texas Press).
[41] Kohlrausch, R., 1854, *Ann. Phys (Leipzig)*, **91,** 179.
[42] Cugliandolo, L. F., and Kurchan, J., 1993, *Phys. Rev. Lett.*, **71,** 173–176.
[43] Cugliandolo, L. F., and Kurchan, J., 1994, *J. Phys.* A, **27,** 5749–5772.
[44] Cugliandolo, L. F., and Dean, D. S., 1995, *J. Phys.* A, **28,** 4213–4234.
[45] Sollich, P., Fielding, S., and Mayer, P., 2002, *J. Phys. Cond. Matt.*, **14,** 1683–1696.
[46] Buhot, A., and Garrahan, J. P., 2002, *Phys. Rev. Lett.*, **88,** 225702.
[47] Goldstein, M., 1976, *J. Chem. Phys.*, **64,** 4767.
[48] Stillinger, F. H., and Weber, T. A., 1982, *Phys. Rev.* A, **25,** 978–989.
[49] Stillinger, F. H., 1995, *Phys. Rev.* E, **52,** 4685–4690.
[50] Kob, W., Sciortino, F., and Tartaglia, P., 2000, *Europhys. Lett.*, **49,** 590–596.
[51] Gibbs, J. H., and DiMarzio, E. A., 1958, *J. Chem. Phys.*, **28,** 373–383.
[52] Marinari, E., Crisanti, A., Ritort, F., and Rocco, A., 2001, A new method to compute the configurational entropy of glassy systems. Preprint cond-mat/0105391.
[53] Franz, S., and Virasoro, M. A., 2000, *J. Phys.* A, **33,** 891–905.
[54] Biroli, G., and Monasson, R., 2000, *Europhys. Lett.*, **50,** 155–161.
[55] Crisanti, A., Ritort, F., Rocco, A., and Sellitto, M., 2000, *J. Chem. Phys.*, **113,** 10615–10634.
[56] Biroli, G., and Kurchan, J., 2001, *Phys. Rev.* E, **64,** 016101.
[57] Crisanti, A., and Ritort, F., 2001, A real-space description of the glass transition based on heterogeneities and entropy barriers. Preprint condmat/0102104.
[58] Crisanti, A., and Ritort, F., 2002, *Phil. Mag.* B, **82,** 143–149.
[59] Edwards, S. F., and Oakeshott, R. B. S., 1989, *Physica* A, **157,** 1080–1090.
[60] Donati, C., Douglas, J. F., Kob, W., Plimpton, S. J., Poole, P. H., and Glotzer, S. C., 1998, *Phys. Rev. Lett.*, **80,** 2338–2341.
[61] Donati, C., Glotzer, S. C., Poole, P. H., Kob, W., and Plimpton, S. J., 1999, *Phys. Rev.* E, **60,** 3107–3119.
[62] Weeks, E. R., Crocker, J. C., Levitt, A. C., Schofield, A., and Weitz, D. A., 2000, *Science*, **287,** 627–631.
[63] Heuer, A., Wilhem, M., Zimmermann, H., and Spiess, H. W., 1995, *Phys. Rev. Lett.*, **75,** 2851–2854.
[64] Tracht, U., Wilhem, M., Heuer, A., Feng, H., Schmidt-Rohr, K., and Spiess, H. W., 1998, *Phys. Rev. Lett.*, **81,** 2727–2730.
[65] Inoue, T., Cicerone, M. T., and Ediger, M. D., 1995, *Macromolecules*, **28,** 3425–3433.
[66] Cicerone, M. T., and Ediger, M. D., 1995, *J. Chem. Phys.*, **103,** 5684–5692.
[67] Schiener, B., Böhmer, R., Loidl, A., and Chamberlin, R. V., 1996, *Science*, **274,** 752–754.
[68] Heuer, A., 1997, *Phys. Rev.* E, **56,** 730–740.
[69] Deschenes, L. A., and Van den Bout, D. A., 2001, *Science*, **292,** 255–258.
[70] Liu, A. J., and Nagel, S. R., 1998, *Nature*, **396,** 21–22.

[71] Jaeger, H. M., Nagel, S. R., and Behringer, R. P., 1996, *Rev. Mod. Phys.*, **68,** 1259–1273.
[72] Liu, A. J., and Nagel, S. R. (eds), 2001, *Jamming and Rheology: Constrained Dynamics on Microscopic and Macroscopic Scales* (London: Taylor and Francis).
[73] Fredrickson, G. H., and Andersen, H. C., 1984, *Phys. Rev. Lett.*, **53,** 1244–1247.
[74] Fredrickson, G. H., and Andersen, H. C., 1985, *J. Chem. Phys.*, **83,** 5822–5831.
[75] Nakanishi, H., and Takano, H., 1986, *Phys. Lett.* A, **115,** 117–121.
[76] Nakanishi, H., and Takano, H., 1986, *Phys. Lett.* A, **118,** 415–418.
[77] Graham, I. S., Piché, L., and Grant, M., 1993, *J. Phys. Cond. Matt.*, **5,** 6491–6496.
[78] Graham, I. S., Piché, L., and Grant, M., 1997, *Phys. Rev.* E, **55,** 2132–2144.
[79] Jäckle, J., and Eisinger, S., 1991, *Zeitschr. Phys.* B, **84,** 115–124.
[80] Muñoz, M. A., Gabrielli, A., Inaoka, H., and Pietronero, L., 1998, *Phys. Rev.* E, **57,** 4354–4360.
[81] Reiter, J., Mauch, F., and Jäckle, J., 1992, *Physica* A, **184,** 458–476.
[82] Reiter, J., 1991, *J. Chem. Phys.*, **95,** 544–554.
[83] Buhot A., and Garrahan, J. P., 2001, *Phys. Rev.* E, **64,** 021505.
[84] Buhot A., and Garrahan, J. P., 2002, *J. Phys. Cond. Matt.*, **14,** 1499–1507.
[85] Fredrickson, G. H., and Brawer, S. A., 1986, *J. Chem. Phys.*, **84,** 3351–3366.
[86] Jäckle, J., 2002, *J. Phys. Cond. Matt.*, **14,** 1423–1436.
[87] Palmer, R. G., 1982, *Adv. Phys.*, **31,** 669–735.
[88] Kob, W., and Andersen, H. C., 1993, *Phys. Rev.* E, **48,** 4364–4377.
[89] Glarum, S. H., 1960, *J. Chem. Phys.*, **33,** 639–643.
[90] Bordewijk, P., 1975, *Chem. Phys. Lett.*, **32,** 592–595.
[91] Shlesinger, M. F., and Montroll, E. W., 1984, *Proc. Nat. Acad. Sci. USA*, **81,** 1280–1283.
[92] Bendler, J. T., and Shlesinger, M. F., 1987, *J. Molecular Liquids*, **36,** 37–46.
[93] Butler, S., and Harrowell., P., 1991, *J. Chem. Phys.*, **95,** 4454–4465.
[94] Butler, S., and Harrowell, P., 1991, *J. Chem. Phys.*, **95,** 4466–4470.
[95] Pigorsch, C., Kimball, J. C., and Frisch, H. L., 1999, *Phys. Rev.* E, **59,** 3196–3201.
[96] Schulz, M., and Donth, E., 1994, *J. Non-Cryst. Solids*, **168,** 186–194.
[97] Willart, J. F., Tetaert, M., and Descamps, M., 1999, *J. Phys.* A, **32,** 8429–8436.
[98] Schulz, B., Schulz, M., and Trimper, S., 1998, *Phys. Rev.* E, **58,** 3368–3371.
[99] Schulz, M., and Reineker, P., 1993, *Phys. Rev.* B, **48,** 9369–9373.
[100] Pigorsch, C., Schulz, M., and Trimper, S., 1999, *Int. J. Mod. Phys.* B, **13,** 1379–1396.
[101] Cornell, S. J., Kaski, K., and Stinchcombe, R. B., 1991, *Phys. Rev.* B, **44,** 2263–12274.
[102] Skinner, J. L., 1983, *J. Chem. Phys.*, **79,** 1955–1964.
[103] Spohn, H., 1989, *Commun. Math. Phys.*, **125,** 3–12.
[104] Budimir, J., and Skinner, J. L., 1985, *J. Chem. Phys.*, **82,** 5232–5241.
[105] Majumdar, S. N., Dean, D. S., and Grassberger, P., 2001, *Phys. Rev. Lett.*, **86,** 2301–2304.
[106] Lefèvre, A., and Dean, D. S., 2001, *J. Phys.* A, **34,** L213–L220.
[107] Dean, D. S., and Lefèvre, A., 2001, *Phys. Rev. Lett.*, **86,** 5639–5642.
[108] Prados, A., and Brey, J. J., 2001, *J. Phys.* A, **34,** L453–L459.
[109] De Smedt, D., Godrèche, C., and Luck, J. M., 2002, *Eur. Phys. J.* B, **27,** 363–380.
[110] Kurchan, J., Peliti, L., and Sellitto, M., 1997, *Europhys. Lett.*, **39,** 365–370.
[111] Padilla, F. G., and Ritort, F., 1997, *J. Phys.* A, **30,** 7089–7114.
[112] Sellitto, M., 2002, *J. Phys. Cond. Matt.*, **14,** 1455–1472.
[113] Jäckle, J., and Krönig, A., 1994, *J. Phys. Cond. Matt.*, **6,** 7633–7653.
[114] Jäckle, M., 1997, *Progress of Theoretical Physics Supplement*, **126,** 53–60.
[115] Donati, C., and Jäckle, J., 1996, *J. Phys. Cond. Matt.*, **8,** 2733–2740.
[116] Artz, S., Schulz, M., and Trimper, S., 1998, *Physics Letters* A, **244,** 271–276.
[117] Sellitto, M., and Arenzon, J. J., 2000, *Phys. Rev.* E, **62,** 7793–7796.
[118] Krönig, A., and Jäckle, J., 1994, *J. Phys. Cond. Matt.*, **6,** 7655–7672.
[119] Palmer, R. G., Stein, D. L., Abrahams, E., and Anderson, P. W., 1984, *Phys. Rev. Lett.*, **53,** 958–961.
[120] Ogielski, A. T., and Stein, D. L., 1985, *Phys. Rev. Lett.*, **55,** 1634–1637.

[121] Palmer, R. G., Stein, D. L., Abrahams, E., and Anderson, P. W., 1985, *Phys. Rev. Lett.*, **54,** 365.
[122] Zwanzig, R., 1985, *Phys. Rev. Lett.*, **54,** 364.
[123] Brey, J. J., and Prados, A., 2001, *Phys. Rev.* E, **63,** 021108.
[124] Prados, A., and Brey, J. J., 2001, *Phys. Rev.* E, **64,** 041505.
[125] Aste, T., and Sherrington, D., 1999, *J. Phys.* A, **32,** 7049–7056.
[126] Davison, L., and Sherrington, D., 2000, *J. Phys.* A, **33,** 8615–8625.
[127] Davison, L., Sherrington, D., Garrahan, J. P., and Buhot, A., 2001, *J. Phys.* A, **34,** 5147–5182.
[128] Sherrington, D., Davison, L., Buhot, A., and Garrahan, J. P., 2002, *J. Phys. Cond. Matt.*, **14,** 1673–1682.
[129] Garrahan, J. P., 2002, *J. Phys. Cond. Matt.*, **14,** 1571–1579.
[130] Newman, M. E. J., and Moore, C., 1999, *Phys. Rev.* E, **60,** 5068–5072.
[131] Garrahan, J. P., and Newman, M. E. J., 2000, *Phys. Rev.* E, **62,** 7670–7678.
[132] Alvarez, D., Franz, S., and Ritort, F., 1996, *Phys. Rev.* B, **54,** 9756–9764.
[133] Lipowski, A., 1997, *J. Phys.* A, **30,** 7365–7373.
[134] Lipowski, A., and Johnston, D., 2000, *J. Phys.* A, **33,** 4451–4460.
[135] Lipowski, A., and Johnston, D., 2000, *Phys. Rev.* E, **61,** 6375–6382.
[136] Lipowski, A., Johnston, D., and Espriu, D., 2000, *Phys. Rev.* E, **62,** 3404–3410.
[137] Dimopoulos, P., Espriu, D., Jane, E., and Prats, A., 2002, *Phys. Rev.* E, **66,** 056112.
[138] Godrèche, C., and Luck, J. M., 2002, *J. Phys. Cond. Matt.*, **14,** 1589–1599.
[139] Glauber, R. J., 1963, *J. Math. Phys.*, **4,** 294.
[140] Felderhof, B. U., 1971, *Rep. Math. Phys.*, **1,** 215–234.
[141] Prados, A., Brey, J. J., and Sánchez-Rey, B., 1997, *Europhys. Lett.*, **40,** 13–18.
[142] Godrèche, C., and Luck, J. M., 2000, *J. Phys.* A, **33,** 1151–1170.
[143] Lippiello, E., and Zannetti, E., 2000, *Phys. Rev.* E, **61,** 3369–3374.
[144] Bray, A. J., 1994, *Adv. Phys.*, **43,** 357–459.
[145] Mayer, P., Berthier, L., Garrahan, J. P., and Sollich, P., 2002, Fluctuation–dissipation relations in the non-equilibrium critical dynamics of Ising models (submitted for publication).
[146] Brey, J. J., and Prados, A., 1996, *Phys. Rev.* E, **53**(1 PtA), 458–464.
[147] Godrèche, C., and Luck, J. M., 2000, *J. Phys.* A, **33,** 9141–9164.
[148] Ehrenfest, P., and Ehrenfest, T., 1990, *The Conceptual Foundations of the Statistical Approach to Mechanics* (New York: Dover).
[149] Ritort, F., 1995, *Phys. Rev. Lett.*, **75,** 1190–1193.
[150] Franz, S., and Ritort, F., 1995, *Europhys. Lett.*, **31,** 507–512.
[151] Godrèche, C., Bouchaud, J. P., and Mézard, M., 1995, *J. Phys.* A, **28,** L603–L611.
[152] Franz, S., and Ritort, F., 1996, *J. Stat. Phys.*, **85,** 131–150.
[153] Godrèche, C., and Luck, J. M., 1996, *J. Phys.* A, **29,** 1915–1928.
[154] Franz, S., and Ritort, F., 1997, *J. Phys.* A, **30,** L359–L365.
[155] Godrèche, C., and Luck, J. M., 1997, *J. Phys.* A, **30,** 6245–6272.
[156] Lipowski, A., 1997, *J. Phys.* A, **30,** L91–L94.
[157] Murthy, K. P. N., and Kehr, K. W., 1997, *J. Phys.* A, **30,** 6671–6677.
[158] Prados, A., Brey, J. J., and Sánchez-Rey, B., 1997, *Phys. Rev.* B, **55,** 6343–6355.
[159] Drouffe, J. M, Godreche, C., and Camia, F., 1998, *J. Phys.* A, **31,** L19–L25.
[160] Godrèche, C., and Luck, J. M., 1999, *J. Phys.* A, **32,** 6033–6054.
[161] Arora, D., Bhatia, D. P., and Prasad, M. A., 1999, *Phys. Rev.* E, **60,** 145–148.
[162] Godrèche, C., and Luck, J. M., 2001, *Eur. Phys. J.* B, **23,** 473–486.
[163] Godrèche, C., and Luck, J. M., 2002, *J. Phys. Cond. Matt.*, **14,** 1601–1615.
[164] Leuzzi, L., and Ritort, F., 2002, *Phys. Rev.* E, **65,** 056125.
[165] Bonilla, L. L., Padilla, F. G., Parisi, G., and Ritort, F., 1996, *Europhys. Lett.*, **34,** 159–164.
[166] Bonilla, L. L., Padilla, F. G., Parisi, G., and Ritort, F., 1996, *Phys. Rev.* B, **54,** 4170–4182.
[167] Bonilla, L. L., Padilla, F. G., and Ritort, F., 1998, *Physica* A, **250,** 315–326.
[168] Garriga, A., 2002, *J. Phys. Cond. Matt.*, **14,** 1581–1588.
[169] Nieuwenhuizen, T. M., 2000, *Phys. Rev.* E, **61,** 267–292.

[170] Leuzzi, L., and Nieuwenhuizen, T. M., 2001, *Phys. Rev.* E, **64,** 011508.
[171] Leuzzi, L., and Nieuwenhuizen, T. M., 2001, *Phys. Rev.* E, **64,** 066125.
[172] Leuzzi, L., and Nieuwenhuizen, T. M., 2002, *J. Phys. Cond. Matt.*, **14,** 1637–1649.
[173] Ertel, W., Froböse, K., and Jäckle, J., 1988, *J. Chem. Phys.*, **88,** 5027–5034.
[174] Ajay, and Palmer, R. G., 1990, *J. Phys.* A, **23,** 2139–2145.
[175] Stillinger, F. H., and Weber, T. A., 1986, *Ann. N.Y. Acad. Sci.*, **484,** 1–12.
[176] Weber, T. A., Fredrickson, G. H., and Stillinger, F. H., 1986, *Phys. Rev.* B, **34,** 7641–7651.
[177] Bhattacharjee, S. M., and Helfand, E., 1987, *Phys. Rev.* A, **36,** 3332–3339.
[178] Weber, T. A., and Stillinger, F. H., 1987, *Phys. Rev.* B, **36,** 7043–7050.
[179] Bhattacharjee, S. M., 1989, *Phys. Rev.* A, **40,** 7424–7426.
[180] Rao, S. S., and Bhattacharjee, S. M., 1992, *Phys. Rev.* A, **45,** 670–674.
[181] Widom, M., 1993, *Phys. Rev. Lett.*, **70,** 2094–2097.
[182] Kalugin, P. A., 1994, *J. Phys.* A, **27,** 3599–3614.
[183] Jaric, M. V., and Johnson, S. L., 1996, *Phys. Lett.* A, **219,** 238–242.
[184] Degier, J., and Nienhuis, B., 1996, *Phys. Rev. Lett.*, **76,** 2918–2921.
[185] Kalugin, P. A., 1997, *J. Phys.* A, **30,** 7077–7087.
[186] Leuzzi, L., and Parisi, G., 2000, *J. Phys.* A, **33,** 4215–4225.
[187] Frenkel, D., and Maguire, J. F., 1981, *Phys. Rev. Lett.*, **47,** 1025–1028.
[188] Frenkel, D., and Maguire, J. F., 1983, *Mol. Phys.*, **49,** 503–541.
[189] Edwards, S. F., and Evans, K. E., 1982, *J. Chem. Soc. Faraday Trans. II*, **78,** 113–121.
[190] Edwards, S. F., and Vilgis, T., 1986, *Phys. Scr.*, T**13,** 7–16.
[191] Onsager, O., 1949, *Ann. N.Y. Acad. Sci.*, **51,** 627.
[192] Renner, C., Löwen, H., and Barrat, J. L., 1995, *Phys. Rev.* E, **52,** 5091–5099.
[193] Jimenez-Ruiz, M., Criado, A., Bermejo, F. J., Cuello, G. J., Trouw, F. R., Fernandez-Perea, R., Löwen, H., Cabrillo, C., and Fischer, H. E., 2002, *J. Phys. Cond. Matt.*, **14,** 1509–1521.
[194] Obukhov, S., Kobzev, D., Perchak, D., and Rubinstein, M., 1997, *J. Phys.* I, **7,** 563–568.
[195] Stinchcombe, R., 2001, *Adv. Phys.*, **50,** 431–496.
[196] Trimper, S., 1999, *Int. J. Mod. Phys.* B, **13,** 2637–2644.
[197] Halpern, V., 1999, *J. Phys. Cond. Matt.*, **11,** L575–L579.
[198] Halpern, V., 2000, *J. Phys. Cond. Matt.*, **12,** 4303–4311.
[199] Schulz, M., and Reineker, P., 1995, *Phys. Rev.* B, **52,** 4131–4137.
[200] Gonçalves, L. L., De Haro, M. L., and Tagüeña-Martìnez, J., 2001, *Phys. Rev.* E, **63,** 026114.
[201] Adler, J., and Aharony, A., 1988, *J. Phys.* A, **21,** 1387–1404.
[202] Chalupa, J., Leath, P. L., and Reich, G. R., 1979, *J. Phys.*C, **12,** L31–L35.
[203] Adler, J., *Physica* A, **171,** 453–470.
[204] Kogut, P. M., and Leath, P. L., 1981, *J. Phys.* C, **14,** 3187–3194.
[205] Jäckle, J., Froböse, K., and Knödler, D., 1991, *J. Stat. Phys.*, **63,** 249–260.
[206] Jäckle, J., Froböse, K., and Knödler, D., 1991, *J. Stat. Phys.*, **65,** 415–416.
[207] Aizenman, M., and Lebowitz, J. L., 1988, *J. Phys.* A, **21,** 3801–3813.
[208] van Enter, A. C. D., Adler, J., and Duarte, J. A. M. S., 1990, *J. Stat. Phys.*, **60,** 323–332.
[209] Binder, K., 1995, *The Monte Carlo Method in Condensed Matter Physics* (second, corrected and updated edition) (Berlin: Springer).
[210] Newman, M. E. J., and Barkema, G. T., 1999, *Monte Carlo Methods in Statistical Physics* (Oxford University Press).
[211] Landau, D. P., and Binder, K., 2000, *A Guide to Monte Carlo Simulation in Statistical Physics* (Cambridge University Press).
[212] Bortz, A. B., Kalos, M. H., and Lebowitz, J. L., 1975, *J. Comp. Phys.*, **17,** 10.
[213] Sollich, P., and Evans, M. R., Glassy dynamics in the East model (submitted for publication).
[214] Follana, E., and Ritort, F., 1996, *Phys. Rev.* B, **54,** 930–937.
[215] Schulz, M., and Trimper, S., 1997, *Int. J. Mod. Phys.* B, **11,** 2927–2940.
[216] Evans, J. W., 1993, *Rev. Mod. Phys.*, **65,** 1281–1329.

[217] Schulz, M., and Trimper, S., 1998, *Phys. Rev.* E, **57,** 6398–6404.
[218] Eisinger, S., and Jäckle, J., 1993, *J. Stat. Phys.*, **73,** 643–670.
[219] Mauch, F., and Jäckle, J., 1999, *Physica* A, **262,** 98–117.
[220] Sollich, P., and Evans, M. R., 1999, *Phys. Rev. Lett.*, **83,** 3238–3241.
[221] Evans, M. R., 2002, *J. Phys. Cond. Matt.*, **14,** 1397–1422.
[222] Doering, C. R., and ben-Avraham, D., 1988, *Phys. Rev.* A, **38,** 3035–3042.
[223] Derrida, B., Godrèche, C., and Yekutieli, I., 1991, *Phys. Rev.* A, **44,** 6241–6251.
[224] Krapivsky, P. L., and Ben-Naim, E., 1997, *Phys. Rev.* E, **56,** 3788–3798.
[225] Fielding, S. M., 2002, *Phys. Rev.* E, **66,** 016103.
[226] Chung, F., Diaconis, P., and Graham, R., 2001, *Adv. Appl. Math.*, **27,** 192–206.
[227] Mori, H., 1965, *Prog. Theor. Phys.*, **33,** 423.
[228] Hansen, J. P., and McDonald, I. R., 1986, *Theory of Simple Liquids* (2nd ed.) (London: Academic Press).
[229] Mori, H., 1965, *Prog. Theor. Phys.*, **34,** 399.
[230] Kawasaki, K., 1995, *Physica* A, **215,** 61–74.
[231] Kawasaki, K., 1997, *J. Stat. Phys.*, **87,** 981–988
[232] Cichocki, B., and Hess, W., 1987, *Physica* A, **141,** 475–488.
[233] Pitts, S. J., and Andersen, H. C., 2000, *J. Chem. Phys.*, **113,** 3945–3950.
[234] Leutheusser, E., 1984, *Phys. Rev.* A, **29,** 2765–2773.
[235] Leutheusser, E., 1984, *Z. Phys. B-Cond. Matt.*, **55,** 235–240.
[236] Löwen, H., Hansen, J. P., and Roux, J. N., 1991, *Phys. Rev.* A, **44,** 1169–1181.
[237] Einax, M., and Schulz, M., 2001, *J. Chem. Phys.*, **115,** 2282–2296.
[238] Pitts, S. J., and Andersen, H. C., 2001, *J. Chem. Phys.*, **114,** 1101–1114.
[239] Sjögren, L., 1980, *Phys. Rev.* A, **22,** 2866–2882.
[240] Götze, W., and Sjögren, L., 1987, *Zeitschr. Phys.* B, **65,** 415–427.
[241] Schulz, M., and Trimper, S., 1999, *J. Stat. Phys.*, **94,** 173–201.
[242] Mattis, D. C., and Glasser, M. L., 1998, *Rev. Mod. Phys.*, **70,** 979–1001.
[243] Doi, M., 1976, *J. Phys.* A, **9,** 1465–1477.
[244] Doi, M., 1976, *J. Phys.* A, **9,** 1479–1495.
[245] Grassberger, P., and Scheunert, M., 1980, *Fortschritte Phys.-Prog. Phys.*, **28,** 547–578.
[246] Stinchcombe, R. B., 2002, *J. Phys. Cond. Matt.*, **14,** 1473–1487.
[247] Alcaraz, F. C., Droz, M., Henkel, M., and Rittenberg, V., 1994, *Ann. Phys.*, **230,** 250–302.
[248] Peliti, L., 1985, *J. Phys.-Paris*, **46,** 1469–1483.
[249] Lee, B. P., and Cardy, J., 1995, *J. Stat. Phys.*, **80,** 971–1007.
[250] Hu, B., 1982, *Phys. Rep.*, **91,** 233–295.
[251] Hooyberghs, J., and Vanderzande, C., 2000, *J. Phys.* A, **33,** 907–919.
[252] Schulz, M., and Trimper, S., 2002, *J. Phys. Cond. Matt.*, **14,** 1437–1453.
[253] Reiter, J., and Jäckle, J., 1995, *Physica* A, **215,** 311–330.
[254] Brey, J. J., Prados, A., and Sánchez-Rey, B., 2000, *Physica* A, **275,** 310–324.
[255] ben-Avraham, D., 1998, *Phys. Rev. Lett.*, **81,** 4756–4759.
[256] Zhong, D. X., and ben-Avraham, D., 1995, *J. Phys.* A, **28,** 33–44.
[257] Peliti, L., and Sellitto, M., 1998, *J. Phys.* IV, **8,** 49–56.
[258] Levin, Y., Arenzon, J. J., and Sellitto, M., 2001, *Europhys. Lett.*, **55,** 767–773.
[259] Corberi, F., Nicodemi, M., Piccioni, M., and Coniglio, A., 1999, *Phys. Rev. Lett.*, **83,** 5054–5057.
[260] Corberi, F., Nicodemi, M., Piccioni, M., and Coniglio, A., 2001, *Phys. Rev.* E, **63,** 031106.
[261] Schonmann, R. H., 1992, *Ann. Probab.*, **20,** 174–193.
[262] van Enter, A. C. D., 1987, *J. Stat. Phys.*, **48,** 943–945.
[263] Schonmann, R. H., 1990, *J. Stat. Phys.*, **58,** 1239–1244.
[264] Adler, J., Stauffer, D., and Aharony, A., 1989, *J. Phys.* A, **22,** L297–L301.
[265] Manna, S. S., Stauffer, D., and Heermann, D. W., 1989, *Physica* A, **162,** 20–26.
[266] Leutheusser, E., and De Raedt, H., 1986, *Solid State Commun.*, **57,** 457–458.
[267] Aldous, D., and Diaconis, P., 2002, *J. Stat. Phys.*, **107,** 945–975.
[268] Jäckle, J., and Sappelt, D., 1993, *Physica* A, **192,** 691–707.
[269] Pitts, S. J., Young, T., and Andersen, H. C., 2000, *J. Chem. Phys.*, **113,** 8671–8679.

[270] Imparato, A., and Peliti, L., 2000, *Phys. Lett.* A, **269,** 154–157.
[271] Burschka, M. A., Doering, C. R., and ben-Avraham, D., 1989, *Phys. Rev. Lett.*, **63,** 700–703.
[272] ben-Avraham, D., Burschka, M. A., and Doering, C. R., 1990, *J. Stat. Phys.*, **60,** 695–728.
[273] Fredrickson, G. H., 1986, *Ann. N.Y. Acad. Sci.*, **484,** 185–205.
[274] Harrowell, P., 1993, *Phys. Rev.* E, **48,** 4359–4363.
[275] Alers, G. B., Weissman, M. B., Kinzig, A., and Israeloff, N., 1987, *Phys. Rev.* B, **36,** 8429–8434.
[276] Zheng, B., Schulz, M., and Trimper, S., 1999, *Phys. Rev.* B, **59,** 6717–6721.
[277] Brey, J. J., Prados, A., and Ruiz-Montero, M. J., 1994, *J. Non-Cryst. Solids*, **172,** 371–377.
[278] Brey, J. J., and Prados, A., 1993, *Physica* A, **197,** 569–582.
[279] Brey, J. J., and Prados, A., 1996, *Phys. Rev.* B, **47,** 1541–1545.
[280] Brey, J. J., and Prados, A., 1994, *Phys. Rev.* B, **49,** 984–997.
[281] Barrat, A., 1998, *Phys. Rev.* E, **57,** 3629–3632.
[282] Crisanti, A., Ritort, F., Rocco, A., and Sellitto, M., 2002, *J. Phys. Cond. Matt.*, **14,** 1523–1537.
[283] Corberi, F., Lippiello, E., and Zannetti, M., 2001, *Phys. Rev.* E, **63,** 061506.
[284] Sellitto, M., 1998, *Eur. Phys. J.* B, **4,** 135–138.
[285] Sellitto, M., 2001, *Phys. Rev.* E, **63,** 060301.
[286] Barrat, A., Burioni, R., and Mézard, M., 1996, *J. Phys.* A, **29,** 1311–1330.
[287] Froböse, K., 1989, *J. Stat. Phys.*, **55,** 1285–1292.
[288] Sappelt, D., and Jäckle, J., 1993, *J. Phys.* A, **26,** 7325–7341 (with errata, *ibid.* **27,** 2237 and **30,** 3739).
[289] Schulz, M, and Schulz, B., 1998, *Phys. Rev.* B, **58,** 8178–8181.
[290] Foley, M., and Harrowell, P., 1993, *J. Chem. Phys.*, **98,** 5069–5073.
[291] Kahle, S., Schulz, M., and Donth, E., 1998, *J. Non-Cryst. Solids*, **238,** 234–243.
[292] Heuer, A., Tracht, U., and Spiess, H. W., 1997, *J. Chem. Phys.*, **107,** 3813–3820.
[293] Garrahan, J. P., and Chandler, D., 2002, *Phys. Rev. Lett.*, **89,** 035704.
[294] Franz, S., Mulet, R., and Parisi, G., 2002, *Phys. Rev.* E, **65,** 021506.
[295] Donati, C., Franz, S., Glotzer, S. C., and Parisi, G., 2002, *J. Non-Cryst. Solids*, **307,** 215–224.
[296] Franz, S., Donati, C., Parisi, G., and Glotzer, S. C., 1999, *Philos. Mag.* B, **79,** 1827–1831.
[297] Franz, S., and Parisi, G., 2000, *J. Phys. Cond. Matt.*, **12,** 6335–6342.
[298] Arenzon, J. J., Levin, Y., and Sellitto, M., 2003, Slow dynamics under gravity: a nonlinear diffusion model. Preprint cond-mat/0301454.
[299] Fierro, A., De Candia, A., and Coniglio, A., 2002, *J. Phys. Cond. Matt.*, **14,** 1549–1556.
[300] Melcuk, A. I., Ramos, R. A., Gould, H., Klein, W., and Mountain, R. D., 1995, *Phys. Rev. Lett.*, **75,** 2522–2525.
[301] Barrat, A., Kurchan, J., Loreto, V., and Sellitto, M., 2000, *Phys. Rev. Lett.*, **85,** 5034–5037.
[302] Barrat, A., Kurchan, J., Loreto, V., and Sellitto, M., 2001, *Phys. Rev.* E, **63,** 051301.
[303] Brey, J. J., Prados, A., and Sánchez-Rey, B., 1999, *Phys. Rev.* E, **60,** 5685–5692.
[304] Brey, J. J., and Prados, A., 2001, *Phys. Rev.* E, **63,** 061301.
[305] Brey, J. J., and Prados, A., 2002, *J. Phys. Cond. Matt.*, **14,** 1489–1498.
[306] Brey, J. J., and Prados, A., 2002, *Europhys. Lett.*, **57**, 171–177.
[307] Prados, J., Brey, J. J., and Sánchez-Rey, B., 2000, *Physica* A, **284,** 277–298.
[308] Berg, J., Franz, S., and Sellitto, M., 2002, *Eur. Phys. J.* B, **26,** 349–356.
[309] Sellitto, M., 2002, *Phys. Rev.* E, **65,** 020101.